

Selected Abstracts from Pharmacology 2022

Posters, Tuesday 13th September

Poster presentations—Molecular and cellular

P025 | NanoBiT/BRET assessment of eGFP-WNT-3A binding to FZD₇ in SW480 cells under endogenous promotion

Pawel Kozielowicz¹; Lukas Grätz¹; Joanna Sajkowska-Kozielowicz¹; Stefanie Moser²; Gary Davidson²; Gunnar Schulte¹

¹Karolinska Institutet; ²Karlsruhe Institute of Technology

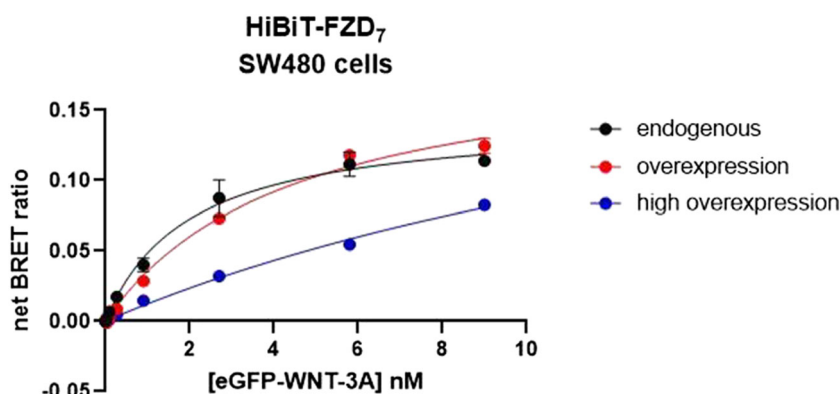
Introduction/Background & aims: The 10 mammalian Frizzleds (FZD₁₋₁₀) are G protein-coupled receptors (GPCRs) which, together with Smoothed (SMO), constitute the class F of GPCRs. The 19 WNT lipoglycoproteins are the ligands of FZDs, and they interact with the extracellular cysteine-rich domain (CRD) of the receptor. Our previous analysis of all 10 human FZD paralogues revealed differences in the profile of eGFP-WNT-3A binding [1]. Here, using CRISPR-Cas9 genome editing and NanoBiT/BRET, we studied WNT-3A/FZD₇ pharmacology. We investigated WNT-3A-induced internalisation of endogenous FZD₇. Moreover, we studied eGFP-WNT-3A kinetics and saturation binding to FZD₇ in a pathophysiologically relevant model of SW480, cells which typify colorectal carcinoma. We aimed to evaluate how ligand–receptor binding affinity changes with different receptor amounts. Additionally, the usage of HiBiT-LgBiT and CRISPR-Cas9 system allows quantification of membranous FZD₇ molecules in a living SW480 cell.

Method/Summary of work: HEK293F cells were used to prepare eGFP-WNT-3A conditioned medium with afamin. sgRNA and donor template to insert a N-terminal HiBiT-tag onto endogenous FZD₇ in SW480 were designed with IDT. We used 10 ng of HiBiT-FZD₇ plasmid DNA for overexpression and 100 ng of HiBiT-FZD₇ plasmid DNA for high overexpression conditions (per well in a 96-well plate). Data presented in this study come from at least five individual experiments, each performed typically in duplicates. The fitting models were selected based on an extra-sum-of-squares F-test ($P < .05$). Binding affinity values are presented as a best-fit K_D with SEM.

Results/Discussion: We detected WNT-3A-induced FZD₇ internalisation that presented itself with different kinetics depending on the receptor levels. Next, in the kinetic binding experiments, we detected significant changes in eGFP-WNT-3A kinetic binding affinity between endogenous, overexpressed and highly-overexpressed FZD₇ (0.38 nM vs. 2.37 nM vs. 3.78 nM). In the saturation binding assays, the reported saturation binding affinity values were determined from nonlinear regression curves showing saturable binding for endogenous and overexpressed, and nearly saturable binding for highly overexpressed cells (Figure 1). These K_D were calculated as follows: 1.98 nM for endogenous, 4.48 nM for overexpressed and 20.75 nM for highly overexpressed FZD₇ in SW480 cells. Moreover, we estimated the number of FZD₇ in a living SW480 cell and compared these numbers with overexpressed and highly overexpressed systems.

Conclusion(s): We have demonstrated that by employing NanoBiT technology, fluorescent WNT and the NanoBiT/BRET binding method, we were able to obtain pharmacological quantification of WNT-3A/FZD₇ interactions in live SW480 cells. Importantly, our data indicate that increasing amounts of FZD₇ lead to an artificial reduction in WNT-3A affinity, underlining the need of studying WNT-FZD binding under endogenous conditions.

FIGURE 1 Saturation binding (3 hours of incubation) of eGFP-WNT-3A to HiBiT-FZD₇ expressed at different levels in SW480 cells. Ligand binding affinity decreases with increasing amounts of receptors. Data are presented as mean \pm SEM from five individual experiments



REFERENCE(S)

1. Kozielewicz P, Shekhani R, Moser S, Bowin CF, Wesslowski J, Davidson G, Schulte G. (2021). Quantitative profiling of WNT-3A binding to all human frizzled paralogues in HEK293 cells by NanoBIT/BRET assessments. *ACS Pharmacol. Transl. Sci.* 2021, 4, 3, 1235–1245

P027 | The role of Connexin 43 in proliferation and migration of mouse pulmonary arterial fibroblasts

Saad Wali^{1,2}; Kathryn Wilson¹; David Welsh¹; Simon Kennedy^{2*}; Yvonne Dempsey^{1*}

¹Department of Biological and Biomedical Sciences, School of Health and Life Sciences, Glasgow Caledonian; ²School Of Cardiovascular & Metabolic Health, College of Medical, Veterinary & Life Sciences, University of Glasgow

(* Authors contributed equally)

Introduction/Background & aims: Connexin 43 (Cx43) is involved in cellular communication and regulation of both the systemic and pulmonary vasculature. Pulmonary arterial fibroblasts are involved in pulmonary vascular remodelling which is characteristic of pulmonary arterial hypertension (PAH). Previous work has shown that Cx43 may be important in the pathophysiology of PAH. Here, we assess the role of Cx43 in proliferation and migration of mouse pulmonary arterial fibroblasts (MPAFs), using both mice heterozygous for Cx43 (Cx43^{+/-} mice) and pharmacological inhibition of Cx43.

Method/Summary of work: Both wildtype (WT) and Cx43^{+/-} littermate mice (C57BL/6 background, 2–4 months old) were used. Mice

were euthanised by intraperitoneal injection of pentobarbital sodium (700 mg/kg) containing lidocaine (20 mg/ml). Primary MPAFs were obtained from the main and branch pulmonary arteries and grown in Dulbecco's modification of Eagle's medium (DMEM) supplemented with 10% foetal bovine serum (FBS) plus 100 µg/ml primocin and 2 mM L-glutamine. Cells were pretreated with ^{37,43}Gap27 (300 µM; an inhibitor of Cx37 and Cx43) before being placed in normoxic or hypoxic (5% O₂) conditions for 24 h. Proliferation of MPAFs was assessed using an automated cell counter, while migration of MPAFs was assessed using a scratch assay.

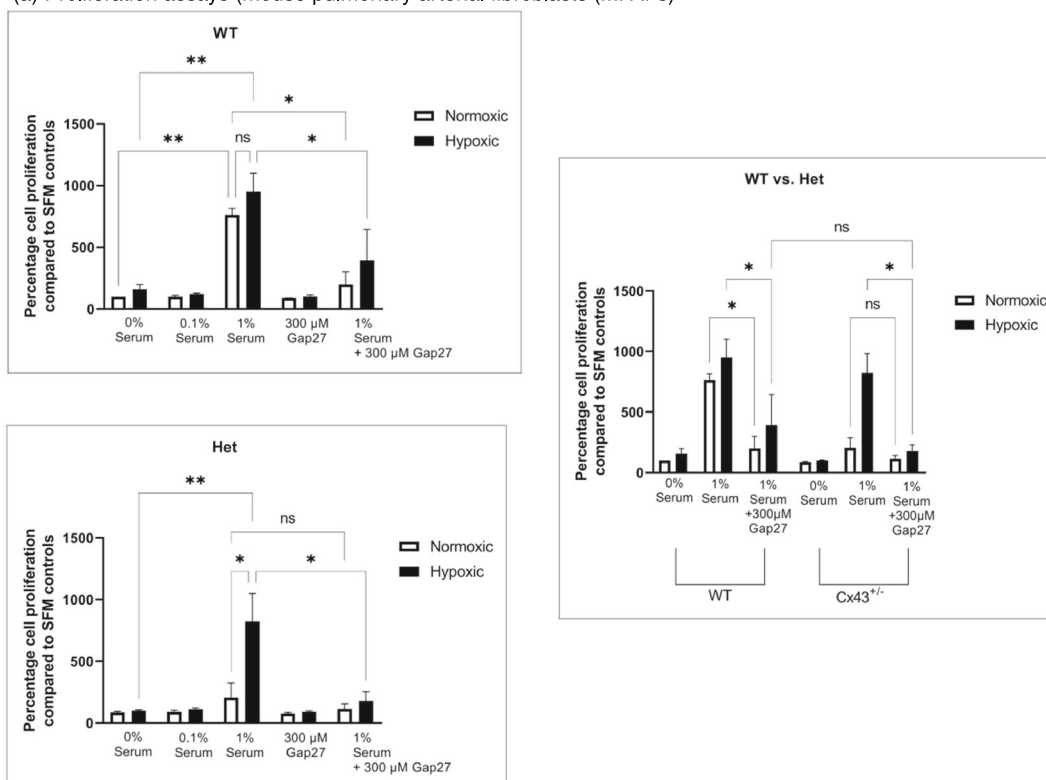
Results/Discussion: MPAFs derived from Cx43^{+/-} mice had a reduced proliferative and migratory response to serum under normoxic conditions compared with WT MPAFs. However, proliferation and migration under hypoxic conditions was similar between WT and Cx43^{+/-} MPAFs. Addition of ^{37,43}Gap27 to Cx43^{+/-} MPAFs was necessary to reduce proliferation and migration under hypoxic conditions.

Conclusion(s): This study has shown that Cx43 plays a role in proliferation and migration of mouse pulmonary arterial fibroblasts. The partial reduction in Cx43 protein found in Cx43^{+/-} mice was sufficient to reduce proliferation and migration under normoxic but not hypoxic conditions. Pharmacological inhibition of Cx43 was required to inhibit proliferation and migration of MPAFs under hypoxic conditions.

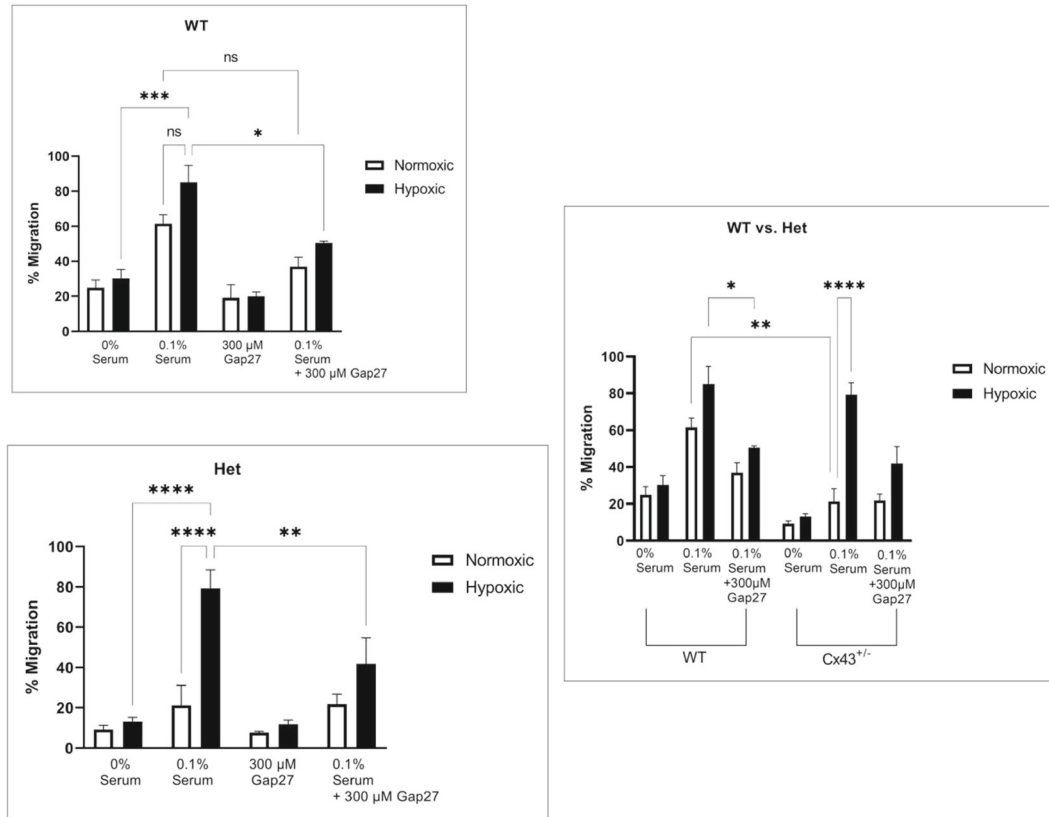
REFERENCE(S)

1. Htet M, Nally JE, Martin PE, Dempsey Y. New insights into pulmonary hypertension: A role for Connexin-mediated Signalling. *International Journal of Molecular Sciences* 2021 29;23(1):379. <https://doi.org/10.3390/ijms23010379>. PMID: 35008804; PMCID: PMC8745497.

(a) Proliferation assays (mouse pulmonary arterial fibroblasts (MPAFs))



(b) Migration assays (mouse pulmonary arterial fibroblasts (MPAFs))



P028 | Mechanism of action of phosphodiesterase type 5 inhibitors in preventing human myofibroblast transformation

Sophie Harding¹; Marcus Ilg²; Alice Laphorn¹; David Ralph³; Selim Celtek¹

¹Anglia Ruskin University; ²Anglia Ruskin Univeristy; ³University College London Hospital

Introduction/Background & aims: Peyronie's disease (PD) is a fibrotic disorder of the penis, where a fibrous plaque forms in the tunica albuginea (TA). This can lead to pain, curvature and erectile dysfunction, and currently, effective treatments are limited to surgery and collagenase injection. Transformation of fibroblasts to myofibroblasts has been recognised as a key event in the pathophysiology of PD. Previous work has shown that phosphodiesterase type 5 inhibitors (PDE5i) and selective oestrogen receptor modulators (SERMs) can prevent myofibroblast transformation in vitro and prevent development of PD in vivo, while their combination shows a synergistic effect [1]. This study aimed to decipher the mechanism of action of PDE5i.

Method/Summary of work: Primary fibroblasts were isolated and cultured from the TA of patients who were operated for PD. In-cell ELISA (ICE) assay was used to measure the transformation of the

primary fibroblasts to myofibroblasts by measuring α -smooth muscle actin expression in response to TGF- β 1 (10 ng/ml). Concentration response curves of PDE5i and vardenafil in the presence and absence of pharmacological inhibitors were generated to determine components involved in the PDE5i mechanism of action. Data were derived from three replicates from three patients and are presented as mean \pm SEM and analysed using unpaired Students' t test.

Results/Discussion: The ICE assay was validated using a TGF- β 1 receptor inhibitor (SB-505124) which inhibited TGF- β 1-myofibroblast transformation with an IC50 of $0.29 \pm 0.07 \mu\text{M}$. Vardenafil, a PDE5i, inhibited TGF- β 1-induced myofibroblast transformation with an IC50 of $27.31 \pm 8.81 \mu\text{M}$. Protein kinase G inhibitor (KT5823; $1 \mu\text{M}$) did not affect inhibition of transformation by vardenafil. cAMP analogue 8-Br-cAMP and PDE3 inhibitor cilostamide prevented TGF- β 1-induced myofibroblast transformation with IC50 values of 6.88 ± 14.29 and $14.05 \pm 1.63 \mu\text{M}$, respectively. cGMP analogue 8-pCPT-cGMP, which does not inhibit PDE3, did not affect TGF- β 1-induced myofibroblast transformation. Inhibitory effect of vardenafil was significantly reduced in the presence of a protein kinase A inhibitor (KT5720; $1 \mu\text{M}$).

Conclusion(s): These results suggest that PDE5i prevents TGF- β 1-induced transformation of myofibroblasts not through PKG but through the PDE3/cAMP/PKA pathway. PDE5i likely increases cGMP concentrations which then inhibit PDE3. This results in the accumulation of cAMP which activates protein kinase A.

REFERENCE(S)

1. Ilg, M.M., Mateus, M., Stebbeds et al. Antifibrotic synergy between phosphodiesterase type 5 inhibitors and selective oestrogen receptor modulators in Peyronie's disease models. *European Urology*. 2019;75(2): 329–340.

P029 | Exploring the structural basis of protease activated receptor 4 (PAR4) protein interactions by proteomic analysis

Marco Bonfanti; Lisa Van Den Driest; Gwyn Gould; Margaret Rose Cunningham

University of Strathclyde

Introduction/Background & aims: Protease activated receptor 4 (PAR4) is a G-protein coupled receptor (GPCR), which becomes activated by proteolytic cleavage of its N-terminus¹. The main proteases activating PAR4 are thrombin and cathepsin G, highlighting the role of the receptor in thrombosis and inflammation. For this reason, the receptor has been extensively studied in platelets. Just recently, the involvement of PAR4 has begun to be studied in other clinical scenarios, such as obesity. On the extreme end of PAR4 C tail (S³⁸¹ SLLQ), there may be a potential short linear motif (SLiM) resembling a PDZ binding motif. PDZ proteins are a family of proteins that can recognise this motif and engage with the receptor to regulate GPCR localisation, trafficking and signalling². In this study, we sought to characterise the network of PAR4 interacting partners and investigate how removal of this region affects PAR4-protein interaction.

Method/Summary of work: Stable isotope labelling of amino acids in cell culture (SILAC) proteomics was performed in metabolically labelled HEK293 cells transiently transfected with YFP, WT PAR4-YFP or PAR4_ΔSLLQ-YFP. Following GFP-trap affinity purification (Chromotek), transfected samples were pooled (1:1:1) prior to tryptic digestion and Orbitrap mass spectrometry (LC MS/MS) processing ($n = 5$). Datasets were filtered, and network analysis was performed to assess enrichment. PANTHER was used to explore the gene ontology (GO) and Reactome used to explore biomolecular pathways. Volcano plotting was then performed to determine differential regulation of interacting partners between WT PAR4-YFP or PAR4_ΔSLLQ-YFP datasets.

Results/Discussion: Out of the 10,380 proteins identified across the datasets, only 577 exceeded the threshold of a 95% confidence interval. A total of 304 proteins from this list were common to those expressed in the human heart [1]. Volcano plot analysis demonstrated that KTN1, RPL15, DDOST, RDX and RPL37A were down-regulated, while and SLC25A3, RPL24, ATP5PB, PSMC4, XPO1 and WDR36 were up-regulated. Network analysis revealed clusters of mitochondrial and ribosomal proteins with GO analysis highlighting the role of these proteins in cellular and metabolic processes with predominant molecular functions being binding and catalytic activity. Reactome analysis revealed how the proteins found in these datasets were mainly involved in translation, metabolism of amino acids, mitochondrial calcium ion transport and cellular responses to stress.

Conclusion(s): No PDZ containing proteins were found to be related to the proposed SLiM region. Nevertheless, PAR4-associated protein clusters expressed in mitochondria with roles in cell metabolism will be further characterised in the laboratory. Future work will also include exploring the roles of these protein clusters in cardiac and adipose cells.

REFERENCE(S)

1. French, S. L. & Hamilton, J. R. Protease-activated receptor 4: From structure to function and back again. *British Journal of Pharmacology* vol. 173 2952–2965 (2016).
2. Romero, G., Von Zastrow, M. & Friedman, P. A. Role of PDZ proteins in regulating trafficking, signaling, and function of GPCRs: Means, motif, and opportunity. *Advances in Pharmacology* 62, 279–314 (2011).
3. Karlsson, M. et al. A single-cell type transcriptomics map of human tissues. *Science Advances* 7, (2021).

P030 | Ameliorative effects of aqueous fraction of *Chlorophytum alismifolium* against diabetic nephropathy in murine model: The involvement of KIM-1 and aldose reductase

Abdulkhakim Abubakar¹; Khadija Isa¹; Abdulazeez Jimoh²; Abdullahi Nazifi³; Highab Muhammad⁴; Rabi Danraka²; Nura Bello²; Maryam Salaudeen²; Ibrahim Yunusa²; Idris Maje²; Ezzeldin Abdurahman²

¹Ahmadu Bello University, Zaria, Nigeria; ²Ahmadu Bello University Zaria, Zaria, Nigeria; ³Bayero University, Kano, Nigeria; ⁴Federal University Dutse, Dutse, Nigeria

Introduction/Background & aims: Diabetes mellitus (DM) is a leading cause of hospitalisation, morbidity and mortality globally [1]. The use of *Chlorophytum alismifolium* tuber extract in the management of DM and its complications is well documented [2]. This study focused on the role of AFCA in mitigating kidney injury molecule-1 (KIM-1) and aldose reductase (AR) in hyperglycaemic rats.

Method/Summary of work: The studies were conducted with the approval of the Ahmadu Bello University Committee on Animal Use and Care (ABUCAUC) with the Ethical Approval Number: ABUCAUC/2020/31. Ethics and regulations governing the care and use of experimental animals as contained in 'Principles of laboratory animal care' published by the National Institute of Health (NIH Publication No. 85–23, revised, 1996) were also considered. Chemical profiling using GC–MS and acute toxicity studies were conducted on AFCA. Hyperglycaemia was induced in rats using alloxan, and the serum KIM-1 and AR were evaluated using ELISA after the administration of AFCA at the doses of 150, 300 and 600 mg/kg. Statistical significance was established using ANOVA followed by Bonferroni's post hoc test.

Results/Discussion: GC–MS revealed the presence of 2 (3H) naphthalenone, isothiazole and isoxazolidine derivatives, while the LD₅₀ was estimated to be >5000 mg/kg. AFCA at all the doses significantly ($p < .05$) reduced the serum concentrations of KIM-1 and AR in hyperglycaemic rats. Kidney injury molecule-1 (KIM-1) and

Aldose reductase (AR) are important biomarkers of renal function which are elevated in nephropathy [3,4]. In this study, administration of AFCA down-regulated the levels of serum KIM-1 and AR, and it may play a crucial role in averting damage in diabetic kidney disease. Isothiazole is the most prominent compound found in AFCA which has previously been reported to elicit aldose reductase inhibitory activity and thereby ameliorating nephropathy [5].

Conclusion(s): The aqueous fraction of *Chlorophytum alismifolium* attenuated diabetic nephropathy through the reduction in serum KIM-1 and AR levels in hyperglycaemic rats.

REFERENCE(S)

1. Hursh, B. E., Ronsley, R., Islam, N., Mammen, C., & Panagiopoulou, C. (2017). Acute kidney injury in children with type 1 diabetes hospitalized for diabetic ketoacidosis. *JAMA Pediatrics*, 171(5), e170020.
2. Abubakar, A., Nazifi, A.B., Maje, I.M., Tanko, Y., Anuka, J.A. and Abdurahman, E.M. (2021a). Antihyperglycaemic activity of ethylacetate extract of *Chlorophytum alismifolium* in type 2 diabetes. The involvement of peroxisome proliferator activated receptor- γ and dipeptidyl peptidase-4. *Journal of Integrative Medicine*, 19 (1), 78–84.
3. Lopez-Giacoman S, Madero M (2015) Biomarkers in chronic kidney disease, from kidney function to kidney damage. *World Journal of Nephrology*, 4(1):57–73.

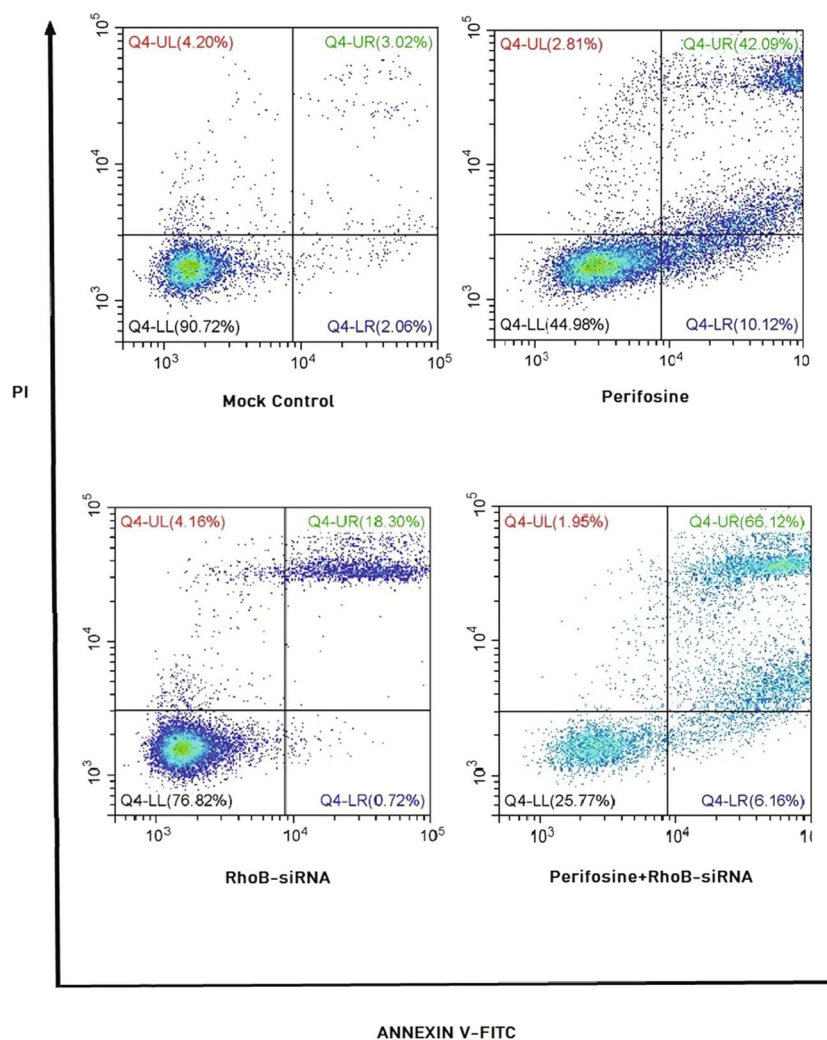
P031 | Effect of RhoB depletion on the sensitivity of nonsmall-cell lung cancer (NSCLC) cells to Akt inhibition in vitro

Nurullah Akgün; Zekai Halıcı

Ataturk University

Introduction/Background & aims: Increasing the effectiveness and reliability of the Akt inhibition method used in the treatment of lung cancer may pave the way for a more favourable use of this method in the future. To reveal the existence of a mechanism that can control and regulate the efficacy of Akt inhibition, we focused on the GTPase, RhoB, which has been classified as both a tumour suppressor and an oncogene in several studies [1]. Based on this dual effect, we aimed to evaluate the possible role of RhoB in the regulation of Akt inhibition in NSCLC.

Method/Summary of work: All stages of the study were performed on the nonsmall cell lung cancer cell line A549. Small interfering rna (siRNA)-mediated RhoB knockdown was carried out and also combined with perifosine (Akt inhibitor) treatment. Cells were seeded in



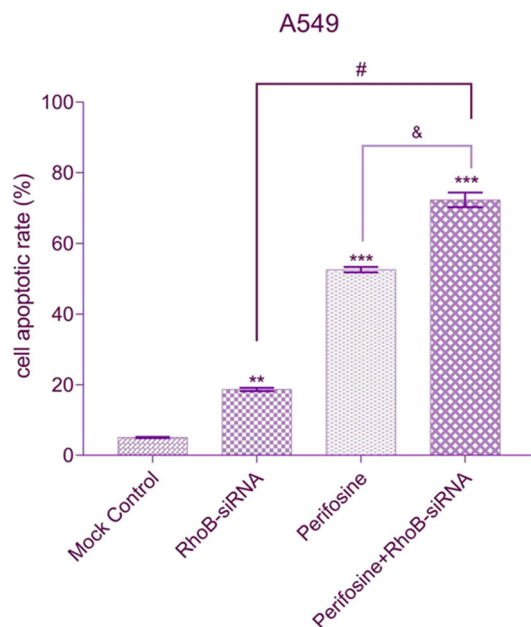


FIGURE 1 RhoB depletion enhances the sensitivity of NSCLC cells to Perifosine in vitro. Apoptosis in A549 cells in each group as analysed by flow cytometry. Mock control: Cells transfected with transfection reagent without siRNA; Perifosine: Cells treated with perifosine alone; RhoB-siRNA: Cells transfected with RhoB-siRNA; Perifosine+RhoB-siRNA: Cells transfected with RhoB-siRNA and treated with perifosine. ** $P < .01$ compared with mock control; *** $P < .001$ compared with mock control; # $P < .05$ Perifosine vs. RhoB-siRNA; & $P < .05$ Perifosine+RhoB-siRNA versus perifosine. All statistical significance was determined using both a Student's *t* test and one-way ANOVA followed by Dunnett's post hoc test. Data represent mean \pm standard deviation (SD). Three independent experiments were repeated thrice ($n = 3$).

6-well plates and cultured for 24 h. They transfected with 100 nM of RhoB-siRNA in accordance with the instructions of the Lipofectamine RNAiMAX transfection reagent. After 6 h of transfection, the cells were treated with perifosine. About 10 μ M of perifosine was used as IC_{50} value for 72 h exposure [2]. Cell death/apoptosis was determined by flow cytometry.

Results/Discussion: To investigate the effects of RhoB on antitumour efficacy of Akt inhibition in NSCLC cells, we knocked down RhoB in A549 cells using siRNA. Annexin V and PI double staining results revealed that RhoB knockdown plus with perifosine significantly increased the apoptotic rate according to perifosine alone and RhoB-siRNA alone (Figure 1).

Conclusion(s): Increasing the response and reliability to therapy targeted to the Akt pathway remains a major clinical challenge today. In the present study, we found that knockdown of RhoB enhanced Akt inhibition-induced apoptosis in A549 cells. Thus, this study opens a new door that RhoB expression level may have a critical role in the regulation of Akt inhibition in NSCLC.

REFERENCE(S)

- Ju JA, Gilkes DM. RhoB: Team oncogene or team tumor suppressor?. *Genes (Basel)* 2018;9(2):67. Published 2018 Jan 30. <https://doi.org/10.3390/genes9020067>
- Dasmahapatra GP, Didolkar P, Alley MC, Ghosh S, Sausville EA, Roy KK. In vitro combination treatment with perifosine and UCN-01 demonstrates synergism against prostate (PC-3) and lung (A549) epithelial adenocarcinoma cell lines. *Clinical Cancer Research* 2004 Aug 1; 10(15):5242-5252.

P032 | β -arrestin2 conformational changes are induced by μ -opioid receptor activation

Owen Underwood¹; Raphael Haider²; J. Robert Lane¹; Stephen Briddon¹; Carsten Hoffmann²; Meritxell Canals¹

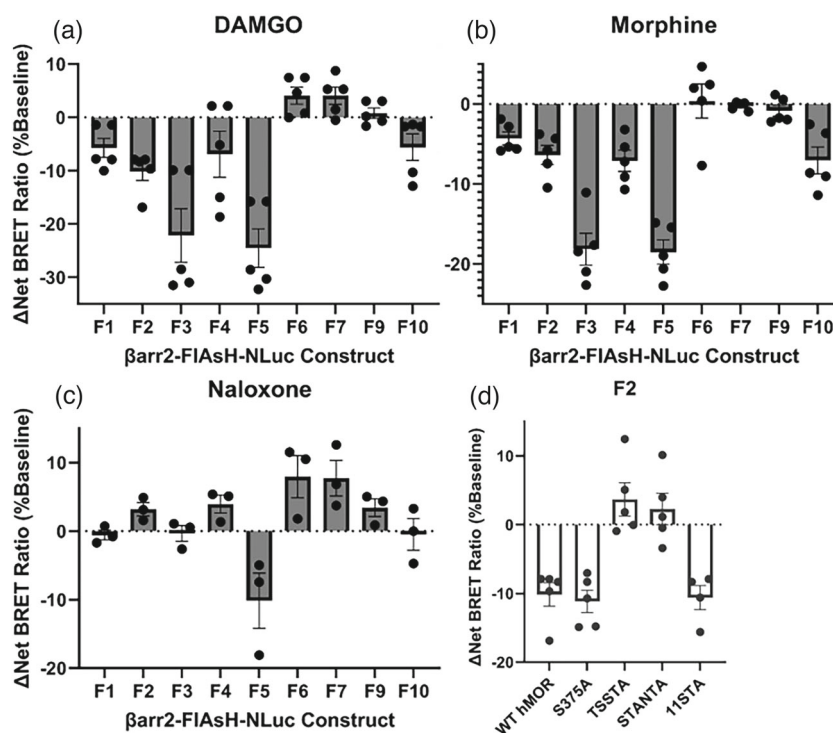
¹University of Nottingham; ²Jena University Hospital

Introduction/Background & aims: Mechanisms by which opioids cause limiting side effects such as respiratory depression are still cause for debate. β -arrestin2 (β arr2) has been suggested to participate in signal transduction of these effects; however, recent evidence suggests otherwise. However, it is clear that different opioid agonists display a broad range of efficacies for recruiting β arr2 and receptor internalisation. β arr2 conformation upon receptor activation has a strong influence on its signalling capabilities and is highly dependent on receptor phosphorylation [1]. Here, we investigated the ability of μ -opioid receptor (MOR) agonists and MOR phosphomutants to induce differential conformational changes of β arr2 using newly developed intramolecular biosensors.

Method/Summary of work: Intramolecular bioluminescence resonance energy transfer (BRET) β arr2 biosensors were developed in the Hoffmann lab^[2] in which, β arr2 is tagged with a C-terminal nanoluciferase (NLuc) and a Fluorescein Arsenical Hairpin (FIAsH) moiety in defined positions within the β arr2 sequence. HEK293T cells were transfected with the β arr2-FIAsH-NLuc constructs alongside GRK2, as well as either WT MOR or MOR with mutations (S/T to A) at C-tail phosphosites. Cells were FIAsH-labelled^[2] and treated with furimazine (5 μ M) and opioid ligands (1 and 10 μ M). Bioluminescence and fluorescence were read at 475 ± 30 and 535 ± 30 nm, respectively, using a PHERAstar FSX, 10 min postligand addition. Data were exported through MARS and analysed in GraphPad Prism V8. Net BRET ratio was calculated by subtracting measured BRET emission of F0, a β arr2-NLuc construct with no FIAsH binding motif.

Results/Discussion: Data suggests β arr2-FIAsH-NLuc constructs form differential conformational states upon activation of the μ -opioid receptor, and in some sensors, this is independent of ligand efficacy (Representative graphs shown fig. a, b, c). Upon similar experiments with MOR phosphomutants and a single ligand, DAMGO, differential conformational states were exhibited with each phosphomutant (Representative graphs shown fig. d).

Conclusion(s): We conclude that β arr2 forms phosphorylation-dependent conformational states, dictated by activating ligand.



REFERENCE(S)

1. Chen Q, Perry NA, Vishnivetskiy SA, et al. Structural basis of arrestin-3 activation and signaling. *Nature Communications* 2017;8(1):1427.
2. Nuber S, Zabel U, Lorenz K, et al. β-Arrestin biosensors reveal a rapid, receptor-dependent activation/deactivation cycle. *Nature* 2016; 531(7596):661–664.

P033 | Discovery and characterisation of novel antagonists of orphan receptor GPR84

Yueming Li; Laura Jenkins; Sara Marsango; Graeme Milligan

University of Glasgow

Introduction/Background & aims: GPR84 is an ‘orphan’ Gi-coupled receptor which is expressed in a variety of immune cells such as monocytes, macrophages and neutrophils [1]. In response to proinflammatory changes, the GPR84 transcript and protein level are up-regulated which suggests that blocking this receptor might be a potential treatment to inflammatory related diseases such as ulcerative colitis and idiopathic pulmonary fibrosis [2,3]. The widely available high affinity GPR84 antagonist, GLPG1205, failed in clinical trials in ulcerative colitis, and the clinical trials in patients with idiopathic pulmonary fibrosis were completed in September 2021 [2]. These studies indicate that finding novel antagonists for GPR84 is essential for better understanding the therapeutic potential to block this receptor in a range of conditions and potentially discover new medicines.

After initial screening, several compounds were found to be able to block GPR84. Among them, compound 271 structure in Figure 1) was able to fully block the activation of human GPR84 stimulated by

2-HTP in [³⁵S]GTPγS binding assay and was able to block mouse GPR84. Therefore, pharmacological characterisation of compound 271 was further studied.

Method/Summary of work: [³⁵S]GTPγS incorporation assay is the main assay used in this research topic. Stable cell lines made from Flp-In T-REx 293 cells were used to prepare membrane protein. In experiments designed to assess inhibition of agonist stimulation, prepared membrane proteins were preincubated with antagonists for 15 min at room temperature before adding agonists. The reaction was initiated by addition of [³⁵S]GTPγS (50 nCi per reaction) with 1 μM GDP and incubated at 30°C for 60 min. The reaction was terminated by ice-cold PBS using a UniFilter FilterMate Harvester. MicroScint-20 was added to dried filters, and [³⁵S]GTPγS binding was quantified by liquid scintillation spectroscopy [2].

Results/Discussion

Conclusion(s): Compound 271 is a potent antagonist of 2-HTP of both human and mouse GPR84, and it is able to fully block the

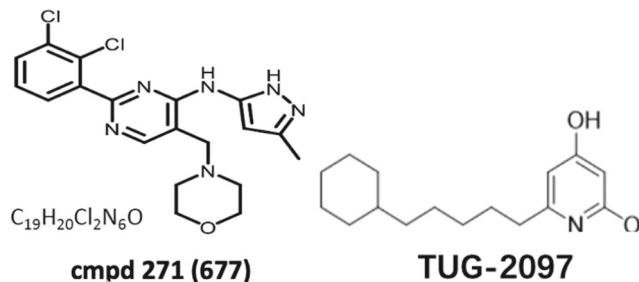


FIGURE 1 Chemical structure of antagonist compound 271 and agonist compound TUG-2097

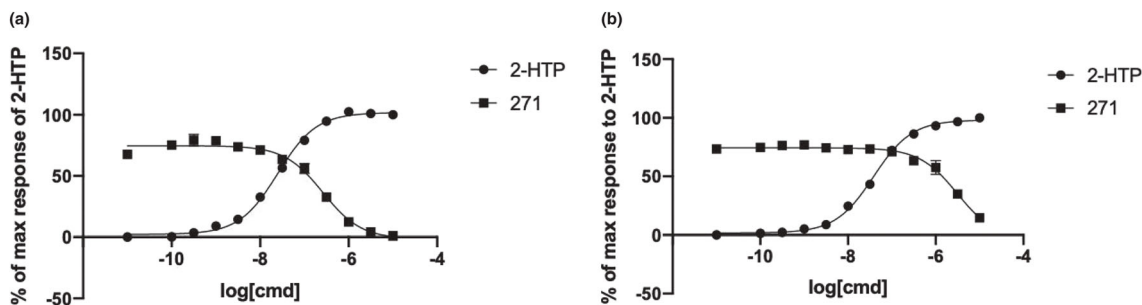


FIGURE 2 Compound 271 is a potent antagonist of both human and mouse GPR84 with the activation with 2-HTP. Ability of different concentrations of compound 271 to block the activation of GPR84 agonist 2-HTP was assessed in [³⁵S]GTPγS binding assay with Flp-In TREX 293 cells expressing the (a) human GPR84-Gα₁₂ fusion protein or (b) mouse GPR84-Gα₁₂ fusion protein.

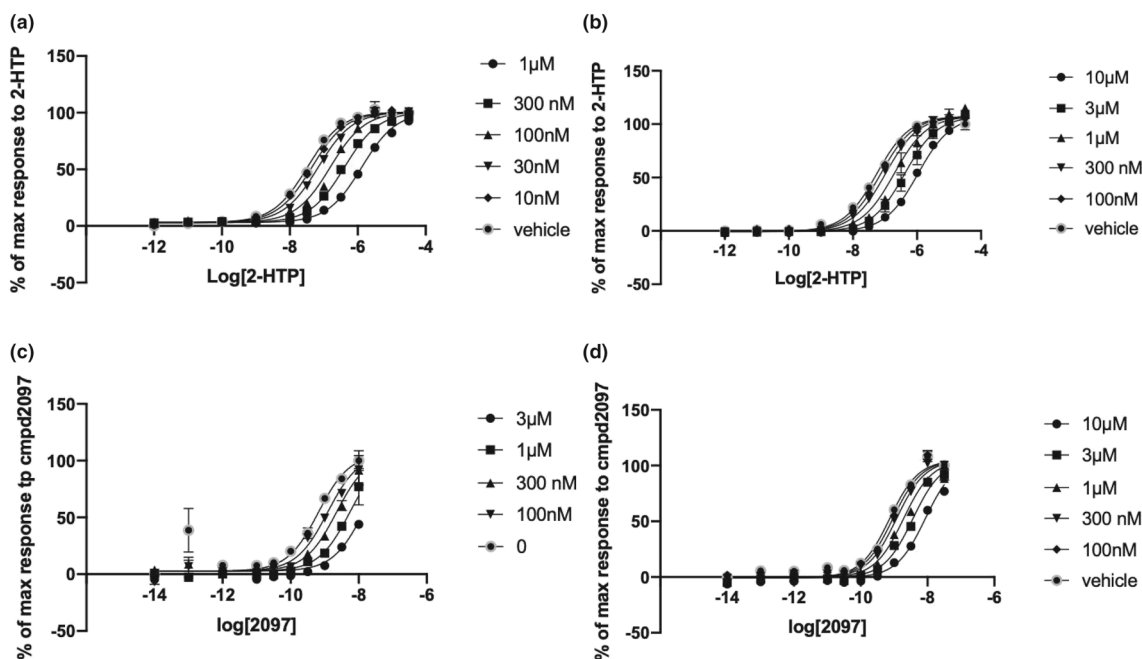


FIGURE 3 Compound 271 is a competitive antagonist at human and mouse GPR84. Ability of different concentrations of compound 271 to alter the concentration–response curve of (a, b) 2-HTP and (c, d) compound 2097 in [³⁵S]GTPγS binding assay with membranes of Flp-In TREX 293 cells induced to stably express (a, c) human GPR84 Gα₁₂ protein or (b, d) mouse GPR84-Gα₁₂ protein.

activation of human GPR84 stimulated by 2-HTP. Compound 271 is competitive orthosteric antagonists at human and mouse GPR84 with the activation of orthosteric agonists.

REFERENCE(S)

- Marsango S, Barki N, Jenkins L, Tobin AB, Milligan G. Therapeutic validation of an orphan G protein-coupled receptor: The case of GPR84. *British Journal of Pharmacology*. 2020. <https://doi.org/10.1111/bph.15248>
- Jenkins L, Marsango S, Mancini S, et al. Discovery and characterization of novel antagonists of the proinflammatory orphan receptor GPR84. *ACS Pharmacology & Translational Science*. 2021;4(5):1598–1613. <https://doi.org/10.1021/acspsci.1c00151>
- Marsango S, Ward RJ, Jenkins L, et al. Selective phosphorylation of threonine residues defines GPR84-arrestin interactions of biased ligands. *Journal of Biological Chemistry*. 2022;101932. <https://doi.org/10.1016/j.jbc.2022.101932>

P034 | Exploring the signalling bias and efficacy of carfentanil

Nokomis Ramos-Gonzalez¹; Sam Groom²; Katy Sutcliffe¹; Sukhvinder Bancroft¹; Chris Bailey²; Richard Sessions¹; Graeme Henderson¹; Eamonn Kelly¹

¹University of Bristol; ²University of Bath

Introduction/Background & aims: Fentanyl is a synthetic μ opioid receptor agonist that displays high potency. Fentanyl has many structural analogues (referred to as fentanyls) including carfentanil. Fentanyl-related overdose deaths are increasing rapidly in the US [1]. We have previously identified carfentanil as a β-arrestin-biased ligand, we now explore carfentanil's agonist intrinsic efficacy by decreasing receptor

reserve as well as carfentanil's unique molecular interactions with the μ opioid receptor using molecular dynamics simulations (MDs).

Method/Summary of work: Concentration–response curves for agonist-induced G protein activation or β -arrestin 2 recruitment to the μ opioid receptor were generated using BRET. HEK293 cells were transiently transfected with 3 μ g human μ opioid receptor-Renilla luciferase II and β -arrestin 2-GFP or 3 μ g $G\alpha i1$ -Renilla luciferase II and GFP10-G γ 2 and 3 μ g HA- μ opioid receptor. Cells were pre-incubated with agonists for 2 or 10 min for the G-protein and β -arrestin 2 assays, respectively. To decrease receptor reserve, cells were pretreated with irreversible antagonist β -FNA for 1 h to plating, which was then washed out with PBS. The resulting concentration–response curves were analysed using the Furchgott method to determine K_A , K_A/EC_{50} ratios and to construct occupancy curves [2].

Carfentanil was docked in the inactive-state MOPr (PDB: 4DKL) [3] using the Bristol university docking engine (BUDE). About 1 μ s MDs were generated using AMBER.

Results/Discussion: Decreasing the μ opioid receptor reserve revealed that for G protein activation (Figure 1a,c,e), DAMGO is a highly efficacious agonist, while carfentanil and fentanyl signalled with equivalent agonist intrinsic efficacy that was somewhat lower than that of DAMGO. This indicates that carfentanil's high potency for G protein activation is mainly due to its high affinity for μ opioid receptor. For β -arrestin 2 recruitment (Figure 1b,d,f), carfentanil displayed higher agonist intrinsic efficacy than DAMGO or fentanyl, in line with its β -arrestin bias.

We have also explored the molecular interaction of carfentanil with μ opioid receptor using MDs and have determined two potential binding poses for carfentanil (Figure 1g,h). Residues tyrosine128^{2.64} or isoleucine296^{6.51} interact with carfentanil's 4-carbomethoxy in its opposing orientations; this 4-carbomethoxy group is of interest as it determines carfentanil's structural difference from fentanyl. We have run *in silico* mutagenesis and are currently carrying out *in vitro* mutagenesis on these residues to determine if they are responsible for carfentanil's β -arrestin 2 bias.

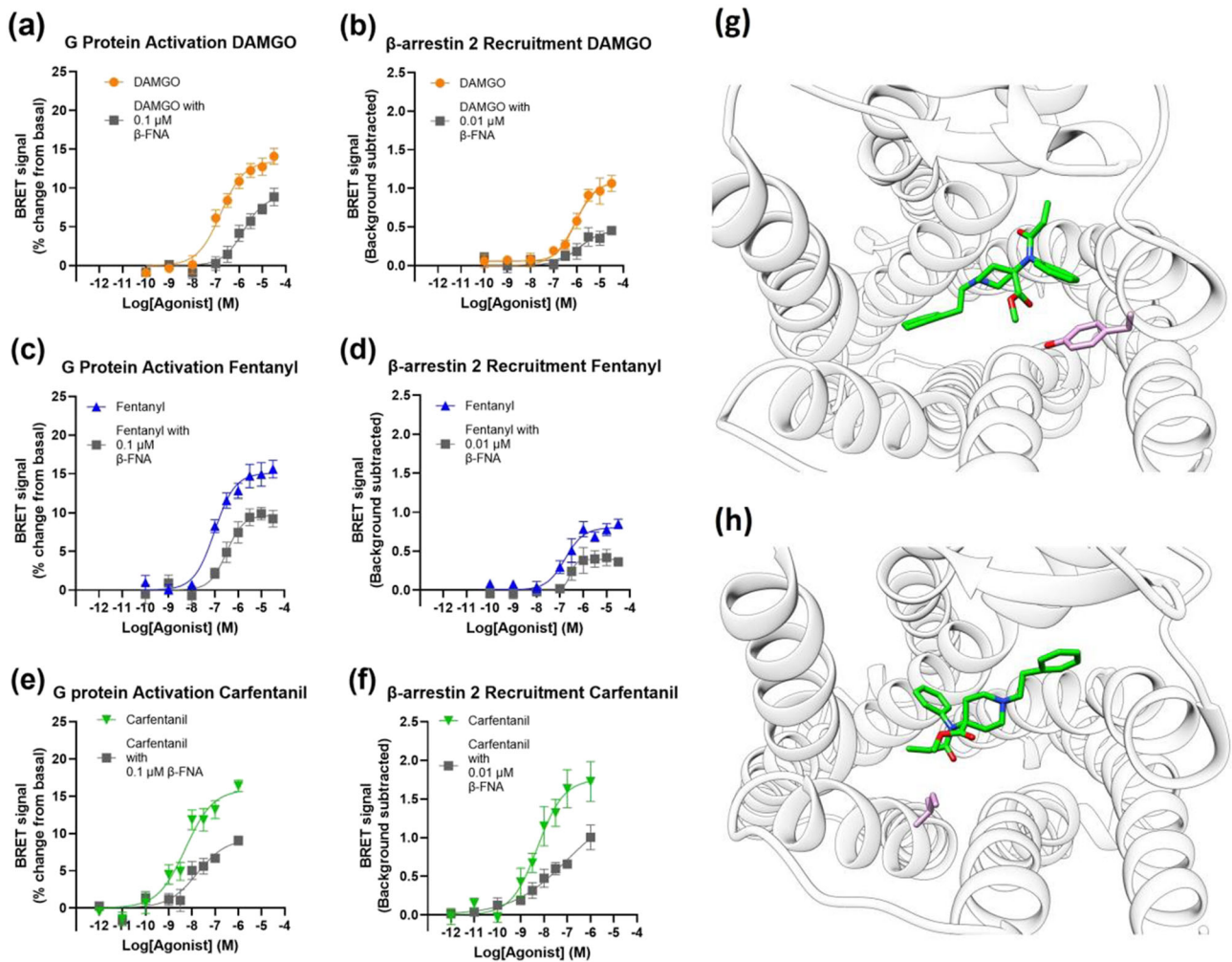


FIGURE 1 Concentration response curves for G protein activation (a, c, e) and β -arrestin-2 recruitment (b, d, f), measured by BRET, for DAMGO, fentanyl and carfentanil in the presence and absence of irreversible antagonist β -FNA. $n = 5$; points are mean \pm SEM; all experiments were carried out in duplicate. (g, h) Images showing the two potential binding poses of carfentanil (green). Residues of interest tyrosine128^{2.64} or isoleucine296^{6.51} are highlighted in pink. Images show the final frame from 1 μ s MD simulation.

Conclusion(s): Carfentanil's lower agonist intrinsic efficacy for the G protein activation pathway indicates that its high potency is determined principally by its high affinity. Carfentanil's high agonist intrinsic efficacy for the β -arrestin 2 pathway is in line with our previous work showing that carfentanil displays β -arrestin 2 bias. Carfentanil's bias may result from specific interactions within the μ opioid receptor binding pocket, as carfentanil has an additional 4-carbomethoxy group, when compared with fentanyl. Carfentanil's interaction with tyrosine128^{2.64} or isoleucine296^{6.51} may allow it to stabilise a β -arrestin 2 biased conformation of the receptor, and we have begun to explore this using *in silico* and *in vitro* mutagenesis.

REFERENCE(S)

1. Jannetto, P. J., Helander, A., Garg, U., Janis, G. C., Goldberger, B., & Ketha, H. (2019). The fentanyl epidemic and evolution of fentanyl analogs in the United States and the European Union. *Clinical Chemistry*, 65(2), 242–253.
2. Morey T.E., Belardinelli L. & Dennis D.M. (1998). Validation of Furchgott's method to determine agonist-dependent A1-adenosine receptor reserve in Guinea-pig atrium. *British Journal of Pharmacology*. 123, 1425–1433
3. Manglik A., Kruse A.C., Kobilka T.S., Thian F.S., Mathiesen J.M., Sunahara R.K., Pardo L., Weis W.I., Kobilka B.K. & Granier S. (2012). Crystal structure of the μ -opioid receptor bound to a morphinan antagonist. *Nature* 485:321–325.

P035 | Using 3D printing to investigate the nature of membrane protein–lipid interactions

Callum Brien; John Simms

Aston University

Introduction/Background & aims: The lipid composition of the cell membrane is fluid and changes with cell type. Distinct sets of lipids are shown to modulate the conformational transition of GPCRs from inactive to active states via allosteric and nonspecific bulk interactions. We have designed and assembled a 3D printed micro-/macro-physiological device for the study of Glucagon Like Peptide 1 Receptor (GLP-1R). This device can be used to culture cells in a controlled environment and investigate the effects of varying external conditions on GPCR signalling.

Method/Summary of work: The 3D printed device was constructed using Polyethylene Terephthalate G Copolyester (PETG), a noncytotoxic, FDA approved engineering resin. The device was then used in conjunction with a 3D printed peristaltic pump to administer a controlled rate of media flow. Using MTT assays, we established that HEK293T cells cultured on PETG had increased survival rates in comparison with other 3D printer polymers. By coating PETG with poly-l-lysine or dopamine, we saw a further increase in cell survival. HEK293T cells expressing the GLP-1R were cultured within the device under a range of controlled external conditions and scaffolds. The effect on receptor function of altering stress via flow rate was then determined by functional assays.

Results/Discussion: GLP-1R transfected HEK293T cells cultured on PETG coated with dopamine and given a constant flow of media had increased peak cAMP signalling time in comparison with cells on PETG without dopamine. MTT assays of cells on PETG with dopamine also showed increased rates of survival compared with untreated PETG. Using the allosteric agonist Compound 2 and orthosteric ligand GLP-1, the functional activity of HEK293T GLP-1R was measured. Cells cultured on PETG with dopamine that were given Compound 2, and GLP-1 showed an increase in cAMP signalling when given flow vs no flow.

Conclusion(s): We have developed a macro-physiological platform for the study of GPCRs in a controlled, adjustable environment. Altering the overall bulk properties of the membrane with fluid flow increased maximal cAMP stimulation, suggesting that this shifts the receptors conformational equilibrium towards the active state. These results provide a basis for further investigations into the underlying mechanisms behind these changes.

P036 | Pharmacological characterisation of a novel IL-1 β -mediated early induction of noncanonical NF- κ B signalling in human endothelial cells

Rachel Craig; Robin Plevin; Kathryn McIntosh; Ashley McCulloch; Christopher West; Simon Mackay; Andrew Paul

Beatson Institute

Introduction/Background & aims: Nuclear factor Kappa B (NF- κ B) is a family of transcription factors linked to several disease states including cancer and cardiovascular disease. Two distinct pathways, the canonical and noncanonical, are activated by different cytokines with IL-1 β considered a regulator of canonical signalling while LIGHT (TNFS14) is associated with the noncanonical arm. The noncanonical pathway is distinguished by its slow kinetics, reliant on stabilisation of NF- κ B-inducing kinase (NIK) and activation of IKK α to induce p100 processing and p52 NF- κ B nuclear translocation [1]. Here a novel pathway has been identified showing IL-1 β induction of early noncanonical NF- κ B signalling.

Method/Summary of work: Western blotting was used to characterise phosphorylation of NF κ B2 (p-p100), formation of NF κ B2 p100/p52 and p52 nuclear translocation. Selective kinase inhibitors were also examined. ELISA was used to measure CXCL12 production. Protein expression was quantified by densitometry and statistical significance determined using ANOVA and Dunnet's multiple comparisons test.

Results/Discussion: In human umbilical vein endothelial cells, a time-dependent increase in p-p100 was observed upon stimulation with IL-1 β (10 ng/ml) with maximum phosphorylation as early as 30 min (fold stimulation: 22.93 \pm 4.885 [$P < .01$, $n = 4$]). IL-1 β also increased nuclear p52 over a similar time course (fold stimulation: 38.01 \pm 8.907 ($P < .05$, $n = 5$)) suggesting activation of the noncanonical pathway. Pretreatment with a novel IKK α inhibitor SU1261, developed in-house, caused a concentration-dependent decrease in IL-1 β stimulated p100 phosphorylation and p52 nuclear translocation, whereas inhibitors targeted at NIK

(CW15337), ERK (PD184352) or JNK (SP600125) had no significant effect. This contrasts with LIGHT (100 ng/ml) which stimulated p100 phosphorylation with a significant delay (fold stimulation: 24.03 ± 4.108 [$P > .001$, $n = 5$]). This response was found to be sensitive to both NIK and IKK α inhibition. SU1261 caused a concentration-dependent decrease in both IL-1 β (fold stimulation: IL-1 β [24 h] = 14 ± 0.1794 , IL-1 β + SU1261 = 0.8557 ± 0.4445) and LIGHT (fold stimulation: LIGHT [48 h] = 2.081 ± 0.1794 , LIGHT + SU1261 = 0.2448 ± 0.1224)-induced CXCL12 production.

Conclusion(s): Here a novel pathway has been discovered, characterised by early induction of p100 phosphorylation and p52 nuclear translocation without a need for cytoplasmic p52 formation. Further, it appears that NIK is redundant, while IKK α is partially required. The specific manner of early p52 nuclear translocation remains to be determined alongside the contribution this plays to normal physiological functioning.

REFERENCE(S)

1. Sun SC. The non-canonical NF-kappaB pathway in immunity and inflammation. *Nature Reviews. Immunology* 2017;17(9):545–558 <https://doi.org/10.1038/nri.2017.52> [published Online First: 2017/06/06].

P037 | Involvement of sphingosine kinase 1/sphingosine-1-phosphate in inducible nitric oxide synthase expression and NO production by IL-1 β -treated 3T3-L1 adipocytes

Ibrahim Aljaezi; Yazeed Alshuweishi; Simon Kennedy; Kenneth Watterson

University of glasgow

Introduction/Background & aims: Obesity is a major global health problem and an important risk factor for insulin resistance and cardiovascular diseases. Obesity is characterised by chronic inflammation in adipose tissue depots, and upregulation of inducible nitric oxide synthase (iNOS) could be a key link between obesity and the risk of cardiovascular diseases. More research is therefore needed to uncover the molecular mechanism of iNOS upregulation under inflammatory conditions in adipose tissue.

Sphingosine kinase (SphK1) is a key enzyme responsible for phosphorylating sphingosine into sphingosine-1-phosphate (S1P), and it has been shown that SphK1/S1P contributes to iNOS expression and NO production in a number of cells [1,2]. The objective of the present study was to investigate the role of SphK1 and S1P receptors in modulating the expression of iNOS and NO production in adipocytes exposed to an inflammatory stimulus.

Method/Summary of work: The 3T3-L1 preadipocytes were differentiated into mature adipocytes. Mature adipocytes were stimulated with IL-1 β (10 ng/ml for 24 h) to mimic inflammatory conditions and to study the effect on iNOS expression and NO production. SphK1 protein expression and mRNA were studied in stimulated adipocytes at different time points by Western blotting and PCR.

To investigate the involvement of the SphK1/S1P system in iNOS and NO production, stimulated adipocytes were pretreated with a sphingosine kinase 1 inhibitor; PF543 (100 nM for 24h) or S1PR₁₋₃ antagonists W146 (an S1PR₁ antagonist), JTE013 (an S1PR₂ antagonist) and CAY (an S1PR₃ antagonist) (all at 10 μ M for 24 h). iNOS protein expression was then determined using Western blotting, and NO production in the supernatant was measured using a Sievers 280 analyser. Data are expressed as mean \pm SEM; statistical analysis was carried out by one way ANOVA.

Results/Discussion: IL-1 β up-regulated iNOS and NO production in 3T3-L1 adipocytes and also increased SphK1 mRNA and protein expression in 3 T3-L1 adipocytes. PF543 treatment decreased iNOS protein expression, and NO production (iNOS expression and NO production were reduced by $\approx 30\%$ in IL-1 β treated control cells with PF543, compared with IL-1 β treated control cells $p < .05$, $n = 3$). All three of the S1PR₁₋₃ antagonists significantly suppressed iNOS expression in stimulated adipocytes ($p < .05$, $n = 3$). However, only the S1PR₂ antagonist (JTE013) attenuated NO productions (NO production was 100 pmole/mg in IL-1 β treated control cells versus 56 pmole/mg with JTE013 $p < .05$, $n = 3$).

Conclusion(s): Inflammatory stimulation with IL-1 β up-regulates iNOS and NO production as well as SphK1 in 3 T3-L1 adipocytes. IL-1 β requires SphK1/S1PRs to induce iNOS expression and NO production, which is most likely mediated by the S1P₂ receptor. These results have importance in increasing our understanding of inflammatory mechanisms in adipose tissue.

REFERENCE(S)

1. Nayak D, Huo Y, Kwang WXT, et al. Sphingosine kinase 1 regulates the expression of proinflammatory cytokines and nitric oxide in activated microglia. *Neuroscience* 2010;166:132–144.
2. Lv M, Li S, Jiang Y, Zhang W. The Sphk1/SIP pathway regulates angiogenesis via NOS/NO synthesis following cerebral ischemia-reperfusion. *CNS Neuroscience & Therapeutics*. 2020;2019;26:538–548.

P038 | Concentration-dependent cholinergic responses in the novel *in vivo* research animal *Lumbriculus variegatus*

Julanta Carriere; Craig Dickson; Aidan Seeley

Swansea University

Introduction/Background & aims: *Lumbriculus variegatus*, more commonly known as the Californian Blackworm, is a species of aquatic worm which has potential as a novel *in vivo* pharmacology research animal [1]. Cholinergic signalling is highly conserved in animals, and signalling can be excitatory, inhibitory or modulatory depending on the receptor and cell type [2]. Here we report that *L. variegatus* is responsive to the canonical agonist, acetylcholine and the agonist, nicotine and that these effects can be inhibited by the nicotinic acetylcholine receptor (nAChR) antagonist, mecamylamine.

L. variegatus displays two stereotypical behaviours when stimulated. Stimulation of the posterior region elicits helical swimming, whereas stimulation of the anterior region results in body retraction and reversal [3]. Previously, rapid-image collection has been used to measure unstimulated, free locomotion of *L. variegatus* [1].

Here we demonstrate the concentration-dependent effects of acetylcholine and nicotine on *L. variegatus* stereotypical movements and free, unstimulated, locomotor activity and that administration of nicotinic receptor antagonists can decrease these effects.

Method/Summary of work: Stereotypical movements were recorded following tactile stimulation of anterior and posterior regions before acetylcholine or nicotine exposure, after 10-min exposure to acetylcholine (0–100 mM) or nicotine (0–1 mM) and 10 min and 24 h after removal of drug compounds and subsequent incubation in pondwater. The antagonism of these responses was determined by pretreatment with mecamlamine (0.01–10 mM) before stereotypical movements were quantified. Unstimulated free locomotion was measured by rapid image collection of *L. variegatus* under the same conditions. Statistical significance was determined by paired *t* tests or a two-way ANOVA.

Results/Discussion: Exposure to 25 mM acetylcholine significantly inhibited body reversal ($p < .05$, $n = 8$) and helical swimming ($p < .01$, $n = 8$) but had no effect on free, unstimulated, movement ($p > .05$, $n = 8$). Exposure to 0.1 mM nicotine significantly inhibited body reversal ($p < .05$, $n = 8$) and helical swimming ($p < .01$, $n = 8$). Additionally, free locomotion was inhibited by $91.0 \pm 2.4\%$ ($p < .0001$, $n = 8$). Inhibition of body reversal could be prevented by exposure to mecamlamine (0.01–5 mM) with levels indistinguishable from pre-exposure conditions ($p > .05$, $n = 6$). However, the ability of *L. variegatus* to perform helical swimming stereotypical movements remained significantly inhibited ($p < .05$, $n = 6$) in the presence of nicotine after mecamlamine exposure.

Conclusion(s): This work demonstrates the concentration-dependent effects of acetylcholine and nicotine, and inhibition of these effects by the nAChR antagonist mecamlamine on *L. variegatus* behaviours highlights the wider potential utility of *L. variegatus* for pharmacological research.

REFERENCE(S)

1. Seeley, A. *et al.* (2021) *Lumbriculus variegatus*: A novel organism for in vivo pharmacology education. *Res. Perspect*; 9:e00853. <https://doi.org/10.1002/prp2.853>
2. Treinin & Jin. (2021) Cholinergic transmission in *elegans*: Functions, diversity, and maturation of ACh-activated ion channels. *Journal of Neurochemistry*; 158(6):1274–1291. <https://doi.org/10.1111/jnc.15164>
3. Ding, J., Drewes, C.D. & Hsu, W.H. (2001) Behavioral effects of ivermectin in a freshwater oligochaete, *Lumbriculus variegatus*. *Environmental Toxicology and Chemistry*; 20(7): 1584–1590. <https://doi.org/10.1002/etc.5620200724>

P039 | Serotonergic responses in the novel in vivo research animal *Lumbriculus variegatus*

Max Shepherd; Henriette Leser; Romessa Mahmood; Aidan Seeley
Swansea University

Introduction/Background & aims: *Caenorhabditis elegans* uses serotonin as a neurotransmitter to regulate locomotion [1], and the study of other invertebrate models may provide model systems with the potential to make important contributions to the study of serotonin signalling. *Lumbriculus variegatus*, more commonly known as the Californian Blackworm, is a species of aquatic worm which has potential as a novel *in vivo* pharmacology research animal [2]. Here we report that *L. variegatus* is responsive to exogenous serotonin and the selective-serotonin reuptake inhibitor, fluoxetine. Moreover, we demonstrate the presence of endogenous serotonin within this novel organism.

Behaviour quantification of *L. variegatus* can be achieved through rapid image collection to measure unstimulated locomotion of *L. variegatus* and stimulated locomotion by stimulation of the posterior region, promoting helical swimming or stimulation of the anterior region, resulting in body retraction and reversal [2].

Here we demonstrate the concentration-dependent effects of serotonin and fluoxetine on *L. variegatus* stereotypical movements and free, unstimulated, locomotor activity and the presence of endogenous serotonin within *L. variegatus* by SDS-PAGE and Western Blot analysis.

Method/Summary of work: Stereotypical movements were recorded following tactile stimulation of anterior and posterior regions before serotonin or fluoxetine exposure, after 10-min exposure to serotonin (0–2 mM) or fluoxetine (0–500 μ M) and 10 min and 24 h after removal of drug compounds and subsequent incubation in pondwater. Unstimulated free locomotion was measured by rapid image collection of *L. variegatus* under the same conditions. Expression of endogenous serotonin was determined by snap freezing *L. variegatus* at -80°C , lysis in RIPA buffer, subjecting samples to SDS-PAGE and Western Blot analysis. Statistical significance was determined by paired *t* tests or a two-way ANOVA.

Results/Discussion: Exposure to ≥ 0.25 mM serotonin significantly inhibited both body reversal and helical swimming ($p < .05$, $n = 8$). About 24 h after serotonin exposure, a significant difference was observed for both stereotypical movements in *L. variegatus* exposed to ≥ 0.1 mM ($p < .05$, $n = 8$). Conversely, the free, unstimulated movement was unaffected by serotonin exposure, and *L. variegatus* movement was indistinguishable from pre-exposure conditions ($p > .05$, $n = 8$).

Moreover, exposure to fluoxetine resulted in inhibition of both movements at ≥ 250 μ M ($p < .05$, $n = 8$) with effects persisting 24 h ($p < .05$, $n = 8$). Free locomotion was similarly acutely affected by ≥ 250 μ M fluoxetine ($p < .05$, $n = 8$) with inhibitory effects persisting 24 h of exposure to fluoxetine and then subsequent incubation in drug-free pondwater. Endogenous expression of serotonin in *L. variegatus* was confirmed by Western Blot analysis.

Conclusion(s): This work demonstrates the concentration-dependent effects of serotonin and fluoxetine on behavioural responses and confirms endogenous serotonin in *L. variegatus* which highlights the wider potential utility of *L. variegatus* for pharmacological research.

REFERENCE(S)

1. Gurel *et al.* (2012) Receptors and other signaling proteins required for serotonin control of locomotion in *Caenorhabditis elegans*. *Genetics*; 192(4): 1359–1371. <https://doi.org/10.1534/genetics.112.142125>

2. Seeley, A. *et al.* (2021) *Lumbriculus variegatus*: A novel organism for in vivo pharmacology education. *Res. Perspect*; 9:e00853. <https://doi.org/10.1002/prp2.853>

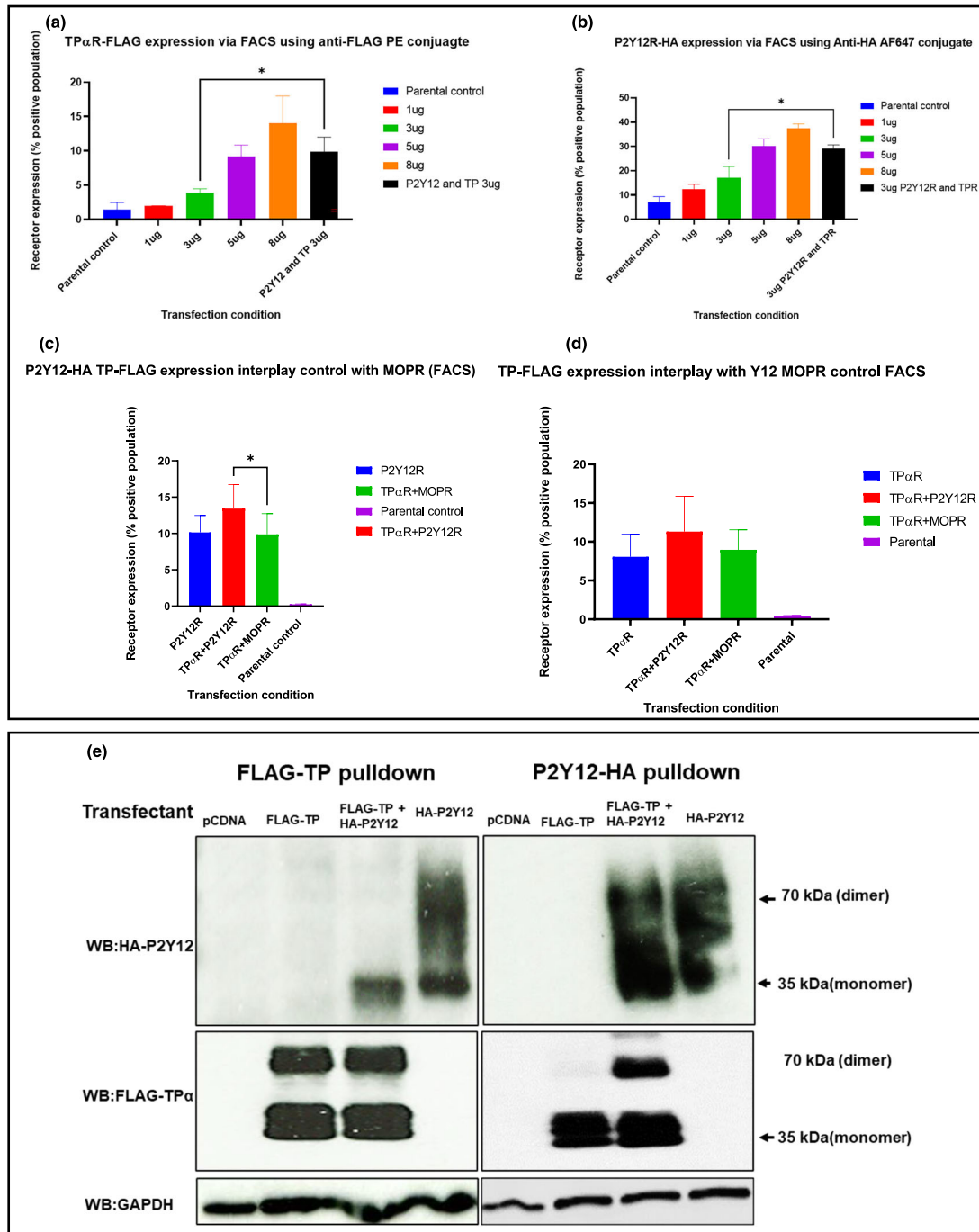
P040 | Ticagrelor enhances platelet TP receptor surface expression in patients due to P2Y12/TP dimerization

Michael Keith¹; Lawrence Hutchinson¹; Jawad Khalil²; Stuart Mundell¹

¹University of Bristol; ²University of Leeds

Introduction/Background & aims: Dual antiplatelet therapy (DAPT) targeting both TP receptor ligand production and P2Y12 receptor activation is standard following percutaneous coronary intervention (PCI) in coronary artery disease patients. Trial data remain inconclusive but suggest redundancy of aspirin in the presence of strong P2Y12 inhibitors such as ticagrelor or prasugrel. Here we explore potential interplay between the Gαq-coupled TP and Gαi-coupled P2Y12 receptor pathways.

Method/Summary of work: P2Y12-HA and TP-FLAG receptor expression was assessed by flow cytometry in HEK293T cells transiently transfected with 3 μg of receptor unless otherwise stated. P2Y12R-HA and TP-FLAG were labelled using anti-HA AF647 and anti-FLAG PE



conjugated antibodies, respectively. μ OR-HA was used in place of P2Y12-HA as G α i-coupled GPCR interplay control. Receptor-receptor interactions were assessed via co-immunoprecipitation and performed using HEK293T cell lysates, previously transiently transfected with 3 μ g of receptor and pulled down using monoclonal Anti-HA and anti-FLAG agarose bead conjugates and run-on Western blot. Receptor-receptor interactions were determined by using the reciprocal epitope antibody on cell lysates expressing both receptors.

Results/Discussion: Longitudinal comparisons of platelet responses from patients at the end of DAPT revealed significant reduction in U46619-induced, TP-mediated calcium flux in the presence of ticagrelor plus aspirin, compared with aspirin alone. However, patient ticagrelor treatment was associated with a significant increase in both P2Y12 and, unexpectedly, TP platelet surface expression as assessed by flow cytometry. This was recapitulated *ex vivo* using healthy donor platelets and further explored through co-expression of tagged P2Y12 and TP α in HEK293T cells where enhanced surface expression of each receptor was observed, compared with single receptor transfectants. This appeared specific, since no such enhancement was seen upon substitution of P2Y12 with the similarly G α i-coupled μ OR. Finally, tagged, overexpressed P2Y12 and TP receptors were demonstrated to interact in reciprocal co-immunoprecipitation experiments indicating that they can dimerize.

Conclusion(s): Together, these data suggest cotrafficking and direct receptor-receptor interaction of P2Y12, and TP receptors can be modulated through inhibition of P2Y12 by ticagrelor. These data further highlight the complex relationship between P2Y12/TP receptor biology and help inform the debate on whether the rationale for DAPT is sound or whether P2Y12R antagonist monotherapy could provide greater clinical benefits in patients with acute coronary syndromes.

P041 | NRAS contributes to drug-resistant acute myeloid leukaemia

Fiona M. Healy; Vanessa Marensi; John F. Woolley;

David J. MacEwan

University of Liverpool

Introduction/Background & aims: Acute myeloid leukaemia (AML) is the most common adult leukaemia and has poor prognosis. Patients often relapse following front-line cytarabine + anthracycline chemotherapy and haematopoietic stem cell transplant. Therefore, targeted therapies are emerging for inclusion into treatment regimens, including against myeloid-specific FLT3. However, therapeutic resistance remains an issue and has been attributed to NRAS mutations. Here, we present protein overexpression and CRISPR-Cas9 data to explain the extent to which NRAS contributes to a FLT-3 inhibitor resistant phenotype, using drug resistance models previously generated in our lab.

Method/Summary of work: Previously developed FLT3-inhibitor-resistant MOLM-13 and MV4-11 cell lines (MOLM-13-DR and

MV4-11-DR) were lentivirally transduced to overexpress wild-type and mutated NRAS. Transfection was used to deliver CRISPR-Cas9 components to knock-out NRAS in HEK293T and overexpress NRAS in HeLa. Common NRAS mutational hotspots were Sanger sequenced. Drug sensitivity was studied up to 72 h posttreatment with 0–10 μ M quizartinib, gilteritinib, cytarabine or trametinib using Annexin V/Propidium iodide staining, quantified by flow cytometry. Proliferation was determined by cell counting, up to 96 h. Signalling alterations were determined via Western blotting.

Results/Discussion: Overexpression of various NRAS states conferred a growth advantage relative to control cells, with G12D overexpression exhibiting greatest proliferative capacity (followed by wild type then Q61K over-expression). Previously generated MOLM-13-DR cells developed a homozygous NRAS Q61L mutation, while MV4-11-DR developed a heterozygous NRAS G12D mutation. Overexpression of mutated NRAS (Q61K) in parental MOLM-13 and MV4-11 cells conferred decreased sensitivity to FLT3-inhibitors gilteritinib and quizartinib, as well as cytarabine, though remained more sensitive to these drugs than the DR cells. MOLM-13-NRAS-Q61K-overexpressing cells were less sensitive to inhibition of downstream Ras signalling (targeting MEK with trametinib), versus parental and DR cells. MOLM-13-NRAS-Q61K overexpressing cells showed increased proliferation, relative to parental and DR cells. Preliminary work showed reduced ERK activation in MV4-11-Q61K-overexpressing cells and in HEK293T, CRISPR-Cas9-mediated NRAS knockout increased ERK phosphorylation.

Conclusion(s): NRAS mutations somewhat contribute to a FLT3-inhibitor-resistant phenotype, by conferring a growth advantage. Preliminary work suggests potential alterations in ERK pathway signalling in the presence of NRAS mutations. Further work will use CRISPR-Cas9-edited DR cells, which we have already engineered, to mutate key NRAS mutations occurring only in DR cells back to wild type. These will be analysed using assays described here, and RNA-Seq, to understand the impact of individual mutations. Overall, this work shows that NRAS contributes to a drug-resistant phenotype and could ultimately help ascertain to what extent its mutational status can predict patient response to FLT3-inhibition, with potential for treatment stratification.

P042 | Evaluating cannabinoid receptors as a therapeutic target for uveal melanoma

Marzia Pendino¹; Sandra Garcia Mulero²; Rebeca Sanz Pamplona²; Simone Marcone³; Fiona O'Connell³; Jacintha O'Sullivan³; Josep Piulats⁴; Brendan Kennedy¹

¹University College Dublin; ²Oncology Data Analytics Program (ICO-IDIBELL), Hospitalet de Llobregat, Barcelona, Spain; ³Trinity Translational Medicine Institute, Department of Surgery, Trinity College Dublin, St. James's Hospital, Dublin, Ireland; ⁴Medical Oncology Department, Catalan Institute of Cancer (ICO), Hospitalet de Llobregat, Barcelona, Spain

Introduction/Background & aims: This research evaluates the disease relevance of cannabinoid receptors in uveal melanoma (UM) patient samples and the therapeutic potential of synthetic cannabinoids in UM cell lines. UM is a rare cancer but the most common intraocular malignancy in adults that arises from melanocytes within the uveal tract. Unfortunately, up to 50% of patients develop liver metastases that rapidly progress to mortality. There is no standard of care for metastatic UM.

Method/Summary of work: Cannabinoid receptor gene expression in 80 primary UM samples within The Cancer Genome Atlas was analysed for association with disease-free and overall survival. Gene set variation analysis enriched for molecular functions and biological pathways linked to high or low cannabinoid receptor expression. *In vitro* assays utilised Mel285 and OMM2.5 human UM cell lines derived from a tumour of the eye and a liver metastasis, respectively. Cell viability was examined at 96 h after treatment with the synthetic cannabinoid HU210 by measuring metabolic activity. Colony formation assays assessed long-term UM cell proliferation. Multiplex ELISA determined the secreted levels of 54 inflammatory factors at 4 and 24 h after treatment with HU-210 in the OMM2.5 cell line. Western Blot analysed expression of CB₁. Proteomic profiling of OMM2.5 treated with 20 µM HU-210 for 4, 8 and 24 h was performed by mass spectrometry.

Results/Discussion: Kaplan–Meier survival curves demonstrate a significant correlation between high CB₁ expression and disease-free survival in UM patients. The CB₁/CB₂ agonist HU-210 results in a dose-dependent reduction in Mel 285 and OMM2.5 viability with 20 µM H-U210 reducing cell viability by around 80%, $p < 0.0001$. In contrast, 150 µM of the more selective CB₂ agonist JWH133 was required to significantly reduce viability by 80%, $p = .0001$ in both UM cell lines. About 1 µM rimonabant hydrochloride and 1 µM SR144528, CB₁ and CB₂ selective antagonists, respectively, were the maximum tolerated concentrations not affecting cell viability. About 20 µM HU210 results in a reduction of long-term proliferation of clones in both UM cell lines. Western blot analysis confirmed expression of CB₁ in Mel285, Mel290, OMM2.5 cells. About 200 proteins were significantly altered as revealed by proteome profiling of OMM2.5 after 24 h treatment with 20 µM HU-210.

Conclusion(s): Significant correlations occur between high CB₁ expression and disease-free survival in UM patients. HU210 reduces viability and clone proliferation of UM cell lines. The effects of HU210 on UM cells are linked to modulating inflammatory pathways. Future directions are to evaluate the roles of CB₁ and CB₂ receptors using antagonists in viability, proliferation assays and validation of proteomic profiling.

REFERENCE(S)

1. Kaliki S, Shields CL. Uveal melanoma: Relatively rare but deadly cancer. *Eye (London, England)* 2017;31(2):241–257.
2. Virgili G, Gatta G, Ciccolallo L, Capocaccia R, Biggeri A, Crocetti E, et al. Incidence of uveal melanoma in Europe. *Ophthalmology* 2007; 114(12):2309–15.e2.
3. Weis E, Shah CP, Lajous M, et al The association between host susceptibility factors and uveal melanoma a meta-analysis

P043 | Nrf2 as an emerging therapeutic target in metastatic melanoma

Emily Hobson; Jonathan Cowan; Maria O'Connell

University of East Anglia

Introduction/Background & aims: Metastatic melanoma is an aggressive form of skin cancer that is often resistant to treatment and results in poor patient outcomes. The transcription factor Nrf2 is a key mediator of oxidative stress that regulates numerous genes involved in redox balance and detoxification, such as the phase II detoxification enzyme NQO1 (NAD(P)H dehydrogenase quinone 1). In cancer, high Nrf2 expression promotes tumourigenesis and chemoresistance [1] and is linked with poor prognosis in many cancer types, such as in melanoma [2]. Hence, Nrf2 may be a useful therapeutic target in melanoma. Here, Nrf2 expression was studied in melanoma cell lines, and Nrf2 inhibitors were screened for their effects on cell proliferation, Nrf2 expression and NQO1 activity.

Method/Summary of work: Nrf2 protein expression was measured via western blot analysis of primary melanocytes and M202, A375, SK-MEL-5, M308, UACC-1273, A2058, Mel501, Colo829, M263 and SK-MEL-28 melanoma cell lines. Basal NQO1 mRNA expression was quantified via real-time quantitative PCR (RT-qPCR), with GAPDH as a normalising control. M202 cells were incubated with 10 pM to 100 µM Nrf2 inhibitors (brusatol, luteolin, ML385, retinoic acid, triptolide, trigonelline hydrochloride and clobetasol propionate) for 72 h, and cell proliferation was measured via MTS assay. IC₅₀ values were calculated using Graphpad Prism 8. NQO1 activity was measured via an enzymatic assay [3], after incubation with 20 µM Nrf2 inhibitors for 20 h. For each assay, experiments were performed in triplicate for 3 separate experiments ($n = 3$), and statistical significance was determined via one-way ANOVA with post hoc Dunnett's test ($P < .05$).

Results/Discussion: Nrf2 protein and NQO1 mRNA expression were consistently higher in melanoma cells than in melanocytes, with the highest expression in M202, UACC-1273, A2058 and M263 cells ($n = 3$). Of the Nrf2 inhibitors, triptolide and brusatol had the greatest antiproliferative effects (IC₅₀ values of 28 and 120 nM, respectively) and significantly suppressed Nrf2 expression and NQO1 activity (10.6% and 48.2% vehicle control, respectively, $P < .0001$, $n = 3$). While ML385, trigonelline hydrochloride and clobetasol propionate did not affect cell proliferation, they did significantly decrease Nrf2 expression and NQO1 activity (57.2%, 61.6% and 64.6% vehicle control, respectively, $P < .001$, $n = 3$).

Conclusion(s): We observed that Nrf2 and NQO1 expression were higher in melanoma cells than in normal melanocytes. Although several Nrf2 inhibitors are reported in the literature, the natural products brusatol and triptolide had the greatest effects in high-Nrf2 expressing melanoma cells. Brusatol has off-target effects; however, triptolide may have potential use in metastatic melanoma treatment.

REFERENCE(S)

1. Wu, S., Lu, H. and Bai, Y., 2019. Nrf2 in cancers: A double-edged sword. *Cancer Medicine*, 8(5), pp. 2252–2267.
2. Carpenter, E., Becker, A. and Indra, A., 2022. NRF2 and key transcriptional targets in melanoma redox manipulation. *Cancers*, 14(6), p. 1531.
3. Prochaska, H. and Santamaria, A., 1988. Direct measurement of NAD(P)H:Quinone reductase from cells cultured in microtiter wells: A screening assay for anticarcinogenic enzyme inducers. *Analytical Biochemistry*, 169(2), pp. 328–336.

P044 | TNF- α modulates MMP-9 expression and its type IV collagenase activity in HaCaT cells

Emeka Ogiji

University of Liverpool

Introduction/Background & aims: Severe cutaneous adverse drug reactions (SCARs) are disease entities that present majorly as severe blistering skin rashes characterised by widespread keratinocyte injury and epidermal detachment with associated mucous and systemic involvement. Stevens–Johnson syndrome/toxic epidermal necrolysis (SJS/TEN) is among the most severe forms of SCARs.

MMP-9 has been shown to be highly expressed in the skin samples of SJS/TEN patients which is suggestive that it plays a role in the epidermal detachment seen in the disease. We aimed to develop an *in vitro* zymography assay that could elucidate the role of MMP-9 in the necrolysis that occurs in SJS/TEN and explore if MMP-9 could be targeted for SJS/TEN diagnostics and therapeutics.

Method/Summary of work: HaCaTs were on glass coverslips in 24-well culture plate or in 96-well plates in serum-free Dulbecco's modified eagles' medium for 24 h and treated with TNF- α +/- etanercept and JNJ0966 (a selective MMP9 inhibitor). *In vitro* zymography involved permeabilisation and embedding in 1% low gelling temperature agarose in with 1 μ g/ml DAPI, and 100 μ g/ml DQ collagen IV fluorescein conjugate was applied to each of the wells of 96-well plate in their respective treatment groups. Type IV collagenase activity was visualised after 18 h by fluorescence microscopy. Collagenase activity of HaCaTs cultured in 96-well plates was quantified by plate reader at 395 nm excitation, 509 nm emission.

Results/Discussion: Our results show that cells treated with TNF- α + etanercept or JNJ0966 had significantly less collagenase activity (depicted by green fluorescence) compared with the positive control (TNF- α alone). The mean fluorescence intensity for cells incubated with TNF- α alone was 21.0. In contrast, the intensity was reduced to 13.0 in those treated with TNF- α + JNJ0966.

Also, the absorbance from the cells treated with TNF- α + etanercept or JNJ0966 were lower than that in cells treated with TNF- α alone ($p = .05$). The mean (+/-sd) absorbance (indicative of GFP activity) for the group TNF- α alone normalised to control was 1.2 ± 0.5 which was statistically significant on *t* test when compared with the absorbance of the control which was $1.0 (\pm 0.5)$.

Furthermore, the absorbance of group TNF- α + etanercept was 47.7% lower than that of the control ($p = .08$).

Conclusion(s): Our data suggest that TNF- α modulates MMP-9 expression in HaCaTs and that this expression could be negated by its inhibitors such as etanercept. Furthermore, type IV collagenase activity is inhibited by MMP9-selective inhibitors (JNJ0966). MMP-9 inhibition is a putative treatment for SJS/TEN. Furthermore, *in vitro* zymography could be a potential tool for screening putative therapies for abrogating MMP9 expression.

P045 | Increased hepatic dicarbonyl stress decreases expression of the drug metabolising enzymes cytochrome (CYP) p450 3A4 and carboxylesterase 1

Meriem Tinhinane Maandi; Jon Gunnarsson Mabley;
Soulef Chahinez Maandi

University of Brighton

Introduction/Background & aims: Type 2 diabetes mellitus (T2DM) has been linked to hepatic complications including impairment of drug metabolising enzyme activity, which may alter hepatic xenobiotic metabolism capacity. Hyperglycaemia-mediated increase in methylglyoxal levels and the resulting dicarbonyl stress plays a key role in diabetic complications and cellular dysfunction. However, the potential impact of dicarbonyl stress on drug metabolising enzymes has yet to be elucidated. Therefore, the aim of this study was to analyse the effect of dicarbonyl stress induced via glyoxalase I inhibition on the expression of phase I (cytochrome (CYP) P450 3A4) and phase II (carboxylesterase 1 [CES1]) metabolising enzymes.

Method/Summary of work: The human hepatoma cell line HepG2 was treated with 20 μ M S-p-Bromobenzylglutathione cyclopentyl diester (BBGC), a glyoxalase I inhibitor, to induce dicarbonyl stress via increased intracellular methylglyoxal levels. HepG2 cells were treated with BBGC for 24 h before measuring CYP3A4, CES1 and Interleukin (IL)-8 mRNA levels and protein expression. Nuclear factor kappa B (NF- κ B) expression and translocation was analysed, using immunocytochemistry, after treating the cells with BBGC for 4 h. Data are expressed as mean (or $2[-\Delta\Delta Ct]$ for mRNA expression) \pm SEM from $n = 5-6$ independent experiments. Statistically significant differences were determined using one-way ANOVA with Bonferroni post hoc test or a Student's *t* test.

Results/Discussion: Increased dicarbonyl stress significantly ($p < .01$) decreased mRNA expression of both CYP3A4 (0.67 ± 0.052) and CES1 (0.6 ± 0.096), and this was associated with a decrease in protein expression. Dicarbonyl stress also had a proinflammatory effect significantly increasing both IL-8 mRNA expression (2.64 ± 0.23 , $p < .05$) and secretion (from 2.3 ± 0.18 to 5.33 ± 0.43 μ g/ μ g of protein $p < .01$), coupled with an increased expression and translocation of NF- κ B ($146.7 \pm 2.51\%$, $p < .05$).

Conclusion(s): In the present study, hepatocytes exposed to increased dicarbonyl stress directly impaired the expression of both Phase I and Phase II drug metabolising enzymes. The increased NF- κ B activation and inflammation observed following increased dicarbonyl stress may be mediating the effects on both CES 1 and CYP3A4 expression. Dicarbonyl stress through increased hepatocyte methylglyoxal levels in diabetics may impact drug clearance and drug availability in these patients, which could potentially impede the efficacy of their therapeutic management.

P046 | Investigation of phosphorylation in free fatty acid receptor 4 with a novel phospho site-specific antiserum

Zhaoyang Dong; Laura Jenkins; Natasja Barki; Graeme Milligan; Andrew Tobin

University of Glasgow

Introduction/Background & aims: Free fatty acid receptor 4 (FFA4) is a G protein-coupled receptor activated by long chain fatty acids and is a therapeutic target in conditions including insulin resistance and type 2 diabetes. Phosphorylation of human FFA4 in response to the synthetic agonist TUG-891 occurs at five residues clustered in the

intracellular C-terminal tail (Thr³⁴⁷, Thr³⁴⁹, Ser³⁵⁰, Ser³⁵⁷ and Ser³⁶⁰) [1]. Here, we characterise an antiserum designed to identify FFA4 phosphorylation at Thr³⁴⁷.

Method/Summary of work: Flp-In T-REx 293 cells harbouring human FFA4 were induced to express the receptor construct by overnight treatment with doxycycline (100 ng/ml). In various experiments, cells were then treated with the FFA4 agonist TUG-891 (10 μ M, 5 min). In some studies, samples that were then enriched using GFP trap were exposed to Lambda Protein Phosphatase (3 h, 30°C) to eliminate phosphorylation. Following SDS-PAGE on NuPAGE, Bis-Tris 4-12 gels and immunoblotting antisera to Thr³⁴⁷ FFA4 or GFP were used as primary reagents.

Results/Discussion: Without exposure to TUG-891, anti-Thr³⁴⁷ FFA4 failed to identify the receptor construct (Figures 1 and 2), whereas anti-GFP identified a series of polypeptides clustering at 65 and 130 kDa (Figures 1 and 2). Addition of TUG-891 resulted in clear identification of each these group of polypeptides by anti-Thr³⁴⁷ FFA4 (Figures 1 and 2) without effecting recognition by anti-GFP (Figures 1 and 2). The identification of FFA4-eYFP by anti-Thr³⁴⁷ FFA4 clearly reflected phosphorylation of the receptor as this was no longer observed after treatment with Lambda Protein Phosphatase (Figure 2), which again did not alter protein recognition by anti-GFP (Figure 2).

Conclusion(s): We demonstrate that anti-Thr³⁴⁷ FFA4 is an effective antiserum to show that TUG-891 promotes phosphorylation of this residue.

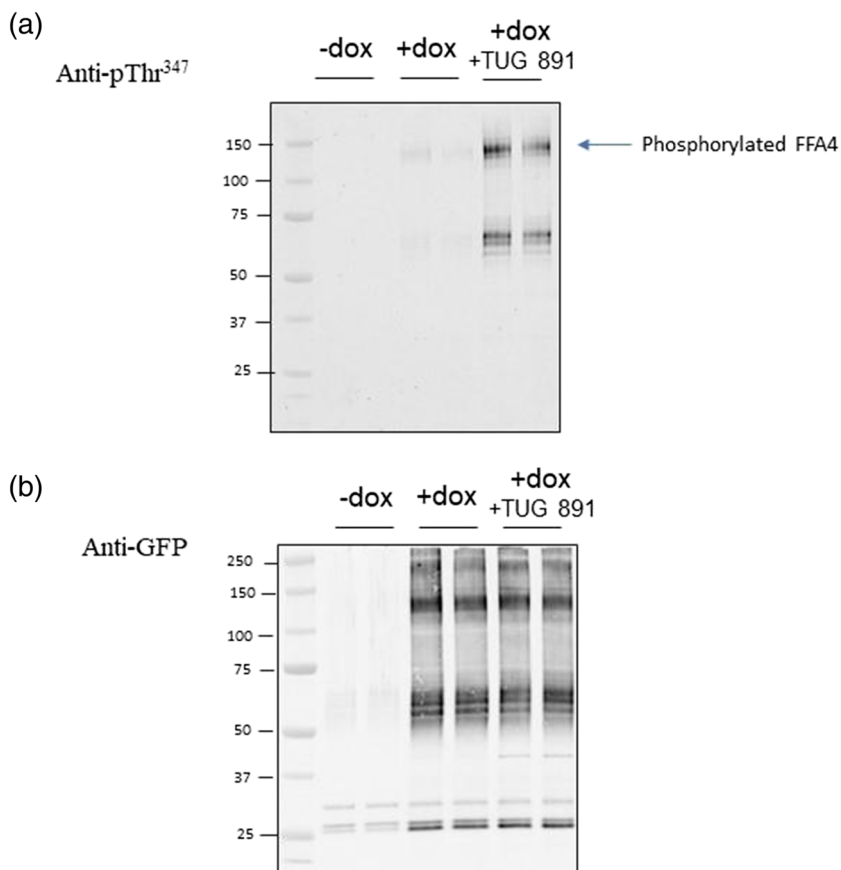


FIGURE 1 TUG-891 induces phosphorylation of Thr³⁴⁷ of hFFA4-eYFP when expressed in Flp-In TREx 293 cells. Flp-In TREx 293 cell harbouring hFFA4-eYFP were induced (+dox) or not (-dox) to express the receptor construct. Where noted, TUG-891 (10 μ M) was added for 5 min. After resolution by SDS-PAGE, samples were immunoblotted with an anti-PThr³⁴⁷ hFFA4 antiserum (a) or with anti-GFP (b). A representative experiment is shown.

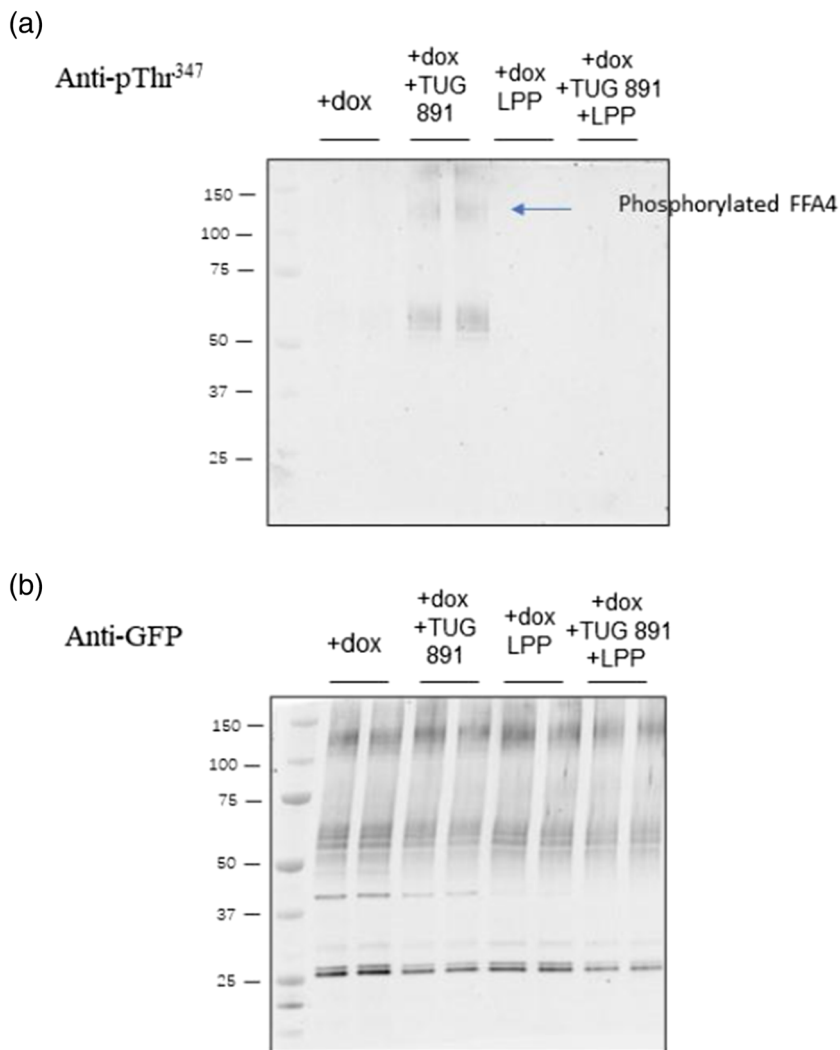


FIGURE 2 The anti-PThr³⁴⁷ hFFA4 antiserum identified only the phosphorylated receptor. Flp-In TREx 293 cells were induced to express hFFA4-eYFP as in Figure 1. Where noted, UG-891 (10 μ M) was added for 5 min. The receptor construct was enriched using GFP-trap, and where noted, samples were treated with Lambda Protein Phosphatase (30°C for 3 h) to fully remove phosphates. After resolution by SDS-PAGE, samples were immunoblotted with an anti-PThr³⁴⁷ hFFA4 antiserum (a) or with anti-GFP. A representative experiment is shown.

REFERENCE(S)

1. A. J. Butcher et al, "Concomitant action of structural elements and receptor phosphorylation determines Arrestin-3 interaction with the Free fatty acid receptor FFA4," *The Journal of Biological Chemistry*, vol. 289, (26), pp. 18451–18465, 2014.

P047 | Enhancing therapeutic approaches for non-small cell lung cancer

Marlene Muscat; Anthony Fenech; Vanessa Petroni Magri

University of Malta

Introduction/Background & aims: Non-small cell lung cancer (NSCLC) is one of the commonest malignancies worldwide and exhibits a 5-year survival rate of only 15%. About 40% of cases are adenocarcinoma, of which 26%–29% exhibit epidermal growth factor receptor (EGFR) mutations which make pharmacological management more difficult. The treatment of choice is surgery, but chemotherapy or targeted therapies may be used in advanced stages. Various drugs targeting EGFR mutant tumours exist; however, resistance commonly

occurs. Therefore, new therapeutic approaches are needed to combat this resistance.

The aim of this project is to investigate the efficacy of tyrosine kinase inhibitors (TKIs) on in vitro models of EGFR mutated NSCLC cells, with a view of eventually combining each drug with a translationally controlled tumour protein (TCTP) antisense oligonucleotide (ASO), and study the TKI effects on TCTP-knockdown EGFR-mutant NSCLC.

Method/Summary of work: The use of TKIs gefitinib and afatinib on HCC827 cells and the effect of afatinib on H1975 cells has been investigated. Cells were seeded in 96-well plates at densities which were experimentally predetermined to avoid the establishment of overconfluent cultures. Cells were exposed to each drug independently at concentrations ranging from 0–25 μ M, for 24, 48 and 72 h and were incubated under standard conditions. Cell viability was measured using PrestoBlue[®] assays, and the data were expressed as a percentage of vehicle-treated cells.

Results/Discussion: Afatinib produced a viability loss of \geq 30% in HCC827 cells at concentrations of around 1.5–2 nM and 80% loss at \sim 4 nM after 72 h. This cytotoxic activity increased to 94% cell loss from 2.5 μ M upwards. H1975 cells exhibited a viability loss of \geq 30%

at 0.05 μM afatinib and 80% at 0.5 μM , and this loss increased to over 90% at concentrations $\geq 5 \mu\text{M}$ after 72 h. With respect to gefitinib, 30% loss in HCC827 cell viability was achieved at $< 10 \text{ nM}$ and 80% loss was achieved at concentrations of 80 nM after 72 h. A high cytotoxicity of 90% or more was maintained from 10 μM upwards. Gefitinib activity on H1975 cells is currently being evaluated.

Conclusion(s): These experiments established concentration and time-response profiles for two TKIs on EGFR-mutant NSCLC cells. HCC827 demonstrated a higher sensitivity to TKIs than H1975. The effects of these drugs will be studied following ASO-mediated TCTP knockdown, using viability assays, gene and protein-expression endpoints. This will determine whether prior TCTP knockdown can be used to increase the cytotoxic activity of these drugs at low concentrations.

P048 | Investigating proteinase activated receptor-4 (PAR4)-dependant cofilin signalling pathways in MEG01 cells

Ryan Shearer; Margaret Cunningham

University of Strathclyde

Introduction/Background & aims: The role of proteinase activated receptor-4 (PAR4) in platelet shape change and stable thrombus formation has now been well-established [1], with efficient cytoskeletal remodelling required to facilitate these events [2]. Through the use of proteomics, combining affinity purification of PAR4 coupled with mass spectrometry, a modified quantitative stable-isotope labelling of amino acids in cell culture (SILAC) strategy was employed to determine potential PAR4 interacting partners. Analysis revealed cofilin, an actin-modulating protein family member, as a high confidence interacting protein of PAR4; therefore, the aim of this project was to characterise cofilin signalling pathways downstream of PAR4 activation.

Method/Summary of work: A megakaryoblastic cell line (MEG-01), which natively expresses PAR4, was used in this study, with receptor activation determined using the PAR4 selective activating peptide (PAR4-AP, 0-300 μM AYPGKF-NH₂). PAR1-dependant cofilin pathways were also studied using selective PAR1-AP (0-100 μM TFLLR-NH₂), with further investigation to assess thrombin-dependant cofilin activity when both receptors are activated (1 U/ml, 0-120 min). Samples were then prepared for assessment of phosphorylated Cofilin (p-Cofilin) and total (t-cofilin) expression using Western blot and indirect immunofluorescence.

Results/Discussion: Stimulation of MEG01 cells with Thrombin (1 U/ml) and AYPGKF-NH₂ (300 μM) lead to an increase in cofilin phosphorylation to a peak of 15 min. For thrombin (mean 1.5-fold over control $p < .05$, n5) and for AYPGKF-NH₂ (mean 1.36-fold increase over control $p = \text{ns}$, n5) detected by western blot. Stimulation of MEG01 cells with TFLLR (100 μM) resulted in no change in phosphorylation state of cofilin over the time course (mean at 15 min was 1.01-fold increase over control $p = \text{ns}$, n5). Additionally, stimulation of MEG01 cells with Thrombin (1 and 3 U/ml) and AYPGKF-NH₂

(300 μM) at 15 min showed significant increases in p-Cofilin levels quantified with confocal microscopy ($p > .0001$) (n3 with a minimum of 24 cells per replicate). Interestingly, stimulation of MEG01 cells with TFLRR-NH₂ led to a modest though still significant increase in p-Cofilin levels quantified by confocal microscopy ($P > .01$) (n3).

Conclusion(s): The data from our research have yielded promising results in that activation of PAR4 leads to increased p-Cofilin levels in MEG01 cells. RhoA/ROCK signalling has recently been demonstrated in this cells type [3]. Results have also shown that these effects are primarily mediated via activation of PAR4 and not PAR1 through the use of PAR specific agonists. The effects that PAR1 and PAR4 activation has on cofilin in other cell contexts still needs to be investigated.

REFERENCE(S)

1. French, S.L., and Hamilton, J.R. (2016). Protease-activated receptor 4: From structure to function and back again. *British Journal of Pharmacology* 173: 2952-2965.
2. Heo, Y., Jeon, H., and Namkung, W. (2022). PAR4-mediated PI3K/Akt and RhoA/ROCK signaling pathways are essential for thrombin-induced morphological changes in MEG-01 cells. *International Journal of Molecular Sciences* 23: 1-15.
3. Heo, Y., Jeon, H., and Namkung, W. (2022). PAR4-mediated PI3K/Akt and RhoA/ROCK signaling pathways are essential for thrombin-induced morphological changes in MEG-01 cells. *International Journal of Molecular Sciences* 23: 1-15.

P049 | A comparison of the mutational landscapes between FLT3 tyrosine kinase inhibitor-resistant and parental AML cells based on whole transcriptomic sequencing

Nisa Nur Goktas

University of Liverpool

Introduction/Background & aims: As sequencing technology has become more accessible, genetic mutations in acute myeloid leukaemia (AML) have begun to be illuminated, paving the way for precision medicine approaches to treating patients with more effective drugs and fewer toxic effects [1]. In this regard, to evaluate the characteristics of genetic mutations and the effect of treatment with a gene-specific tyrosine kinase, gene mutation profiles in two different cell lines (MV4-11 and MOLM-13) with and without drug resistance were examined using next-generation sequencing technologies.

Method/Summary of work: The total RNA was extracted and prepared from MV4-11 parental cells, MV4-11 quizartinib (a selective FMS-like tyrosine kinase 3 [FLT3] inhibitor) drug-resistant cells, MOLM-13 parental cells and MOLM-13 quizartinib drug-resistant cells. After quality control tests were performed, high-quality samples were sent to Novogene Co., LTD to construct cDNA (complementary DNA) library and mRNA (messenger RNA) sequencing. According to the manufacturer's protocol, paired-end sequencing was conducted with a NovaSeq 6000 platform. RNA-sequencing reads were provided by the company as compressed raw data. Then, computational data

TABLE 1 High-impact variants in MOLM-13 and MV4-11 cell lines (VAF: Variant allele frequency)

	MOLM-13	MV4-11
Parental cells	FLT3 C:1775-1795dup (VAF: 44.59%)	FLT3 C:1772-1801dup (VAF: 54.75%)
Quizartinib (FLT3 tyrosine kinase inhibitor) drug-resistant cells	DNMT3A R882C (VAF: 52.16%), NRAS Q61L (VAF: 100%), NPM1 c:860-863dup (VAF: 32.78%)	NRAS G12D (VAF: 72.69%), NPM1 c:847-685dup (VAF: 66.67%)

analysis was performed to investigate variant alterations caused by TKI (tyrosine kinase inhibitor) drug resistance, including SNV (single nucleotide variant) and ITD (internal tandem duplication) abnormalities.

Results/Discussion: Low-quality bases were removed, and the *P*-value was adjusted to 0.05 or below. Following the detection and filtering of variations, it was determined that there were some significant changes that were thought to be related with a poor prognosis in AML. As TKI-resistant cells were compared with parental ones, it was found that some mutations that play a role in poor prognosis emerged, while others disappeared. Whereas mutations in the NRAS-Q61L and DNMT3A-R882C point mutations were detected in the quizartinib resistant MOLM-13, these mutations were not observed in the parental MOLM-13. Similarly, the NRAS-G12D mutation was found in the treated MV4-11, while it was not detected in the untreated MV4-11.

In addition, FLT3-ITDs associated with poor prognosis were detected in parental MOLM-13 and MV4-11 but not in those quizartinib-resistant cells.

Conclusion(s): We found that FLT3-ITDs disappeared following quizartinib treatment, and quizartinib caused significant mutational changes observed in NRAS and DNMT3A genes. The examination of these variations will make an essential contribution to developing genetic basis clinical decisions.

REFERENCE(S)

- Döhner H, Wei AH, Löwenberg B. Towards precision medicine for AML. *Nature Reviews Clinical Oncology*. 2021;18(9):577–590. <https://doi.org/10.1038/s41571-021-00509-w>

P050 | Phosphate-mediated inhibition of calcium-sensing receptor expressed endogenously in the thyroidal TT cell line

Khaleda Alghamdi¹; Donald Ward²; Arthur Conigrave³; Hee-chang Mun³

¹University of Manchester; ²The University of Manchester; ³The University of Sydney

Introduction/Background & aims: The calcium-sensing receptor (CaS) is the key controller of parathyroid hormone (PTH) secretion and extracellular calcium homeostasis. Hyperphosphataemia increases PTH secretion and is associated with secondary hyperparathyroidism (SHPT). We reported recently that inorganic phosphate (Pi), and sulphate, can attenuate CaS activity directly (in CaS-transfected HEK-293 cells), and Pi can increase PTH secretion rapidly from human and murine parathyroid cells [1]. To investigate this further, a thyroid parafollicular C-cell model, TT cells, which express CaS endogenously, were employed.

Method/Summary of work: TT cells, which exhibit CaS-induced calcitonin (CT) secretion, were assayed by epifluorescence intracellular Ca²⁺ imaging and CT assay (with a gastrin-releasing peptide [GRP]-induced CT control). CT levels were analysed using an Immulite 2000 autoanalyser at Royal Prince Alfred Hospital, Camperdown, Australia.

Results/Discussion: When co-stimulated with the CaS-activating calcimimetic R568 (1 μM) and CaS agonist spermine (1 mM), TT cells exhibited classic CaS-induced Ca²⁺ mobilisation, which the Gq/11-specific inhibitor YM-254890 largely abolished (−93 ± 8%; *n* = 4). Similar CaS-induced responses were inhibited by increasing the buffer Pi concentration from 0.8 mM (physiological) to a pathophysiological 2 mM (−33 ± 4%; *P* < .001; *n* = 4). In contrast, raising Pi concentration was without effect on carbachol-induced Ca²⁺ mobilisation (acting via muscarinic receptors; *n* = 3). Finally, 1.2 mM sulphate (high) elicited a similar CaS inhibition as for Pi (−28 ± 16%; *P* < .05; *n* = 4; vs. physiological 0.3 mM sulphate).

Then regarding CT secretion, we observed time-dependent release that was stimulated maximally 15- to 20-fold by increasing Ca²⁺ concentration from 0.5–3.0 mM (EC₅₀ ~ 1.5 mM; *n* = 4). Inorganic Pi (0.8–3.0 mM) inhibited CT release in a noncompetitive manner, with 3 mM Pi almost abolishing CT release at all Ca²⁺ concentrations tested (*n* = 4). Even raising Pi concentration from 0.8–1.4 mM (representing the physiological range) elicited an ~50% reduction in CT release. In contrast, 2 mM Pi had no effect on 1 μM GRP-stimulated CT release (*n* = 6). Sulphate was also a noncompetitive inhibitor of CT release but was less potent than Pi.

Conclusion(s): These results further support the idea that the CaS is a mineral sensor, at which Pi acts directly as a noncompetitive antagonist to limit CaS-induced reductions in PTH secretion. Further, Pi may also limit CaS-induced CT secretion when its serum concentration is raised. Together, our studies provide important new information regarding the physiological control of PTH and CT secretion and the pathophysiology of SHPT.

REFERENCE(S)

- Centeno PP et al. (2019) Phosphate acts directly on the calcium-sensing receptor to stimulate parathyroid hormone secretion. *Nature Communications* 10:4693.

P051 | Characterising the signal transduction pathway of mGlu₅ to determine the role of receptor phosphorylation

Bethany Strellis¹; Liangpu Wei¹; Louis Dwomoh¹; Sophie Bradley²; Brian Hudson¹

¹University of Glasgow; ²Sosei Heptares

Introduction/Background & aims: The type 5 metabotropic glutamate receptor (mGlu₅) is a G protein-coupled receptor (GPCR) primarily located postsynaptically on excitatory neurons and has been linked to schizophrenia, Alzheimer's disease, Fragile X syndrome and addiction [1]. Upon activation, mGlu₅ signals through the Gq protein resulting in downstream activation of multiple kinases, in turn shaping receptor signalling and regulatory processes through phosphorylation. To elucidate the currently unclear physiological role of mGlu₅ phosphorylation as seen in learning and memory events, we aimed to dissect the signalling pathways lying downstream of G protein versus phosphorylation dependent transduction.

Method/Summary of work: To investigate the role of mGlu₅ phosphorylation, a phosphodeficient mutant mGlu₅ receptor construct was generated (mGlu₅-PD), in which all the serine residues in the C terminus were mutated to alanine. To record the Gq protein-coupled transduction pathway, Flp-In™ T-REx 293 stable cell lines expressing either wildtype or mGlu₅-PD receptor were used in IP1 accumulation assays and calcium mobilisation assays following stimulation with the endogenous agonist glutamate. A BRET-based β-arrestin-2 recruitment assay was performed by transfecting mGlu₅, nano-luciferase-tagged β-arrestin-2 and mNeonGreen with a CAAX membrane tag into HEK293 cell lines. Receptor internalisation measurement was carried out by transfecting nano-luciferase-tagged receptor and mNeonGreen with a FYVE endosome tag into HEK293 cells and recording the BRET signal in a 1-h time course using a PheraStar.

Results/Discussion: Wildtype and mGlu₅-PD receptor produced similar signal windows in a calcium assay (139.3% ± 22.06 maximum response compared with 100.0% of wildtype; *n* = 7 performed in triplicate, *P* > .05) and IP1 accumulation assay (137.6% ± 136.1 compared with 100.0% produced by wildtype; *n* = 4 performed in quadruplicate, *P* > .05). However, mGlu₅-PD did appear to reduce ligand-independent signalling in the IP1 assay; the basal IP1 levels in mGlu₅-PD cell lines were reduced by 51.63% compared with the basal levels observed in wildtype (*P* = .0054). The phosphodeficient receptor reduced β-arrestin-2 recruitment by 52.04% compared with wildtype (*n* = 4 performed in triplicate, *P* > .05), and the receptor internalisation was reduced by 66.40% compared with wildtype (*n* = 2 performed in triplicate, *P* > .05).

Conclusion(s): We confirm that the mGlu₅ receptor is directly phosphorylated, with individual phosphorylation sites on the C terminus playing a role in receptor internalisation, β-arrestin-2 recruitment and some modulation of ligand independent signalling through the G protein-coupled pathway.

REFERENCE(S)

1. Bodzeta A, Scheeffals N, MacGillavry H. Membrane trafficking and positioning of mGluRs at presynaptic and postsynaptic sites of excitatory synapses. *Neuropharmacology* 2021;200:108799. <https://doi.org/10.1016/j.neuropharm.2021.108799>

P053 | Exploration of GPCR signalling using nanobody-ligand conjugates with tunable affinity

Shivani Sachdev; Shivani Sachdev; Brendan Creemer; Ross Cheloha
National Institutes of Health, National Institute of Diabetes, Digestive, and Kidney Diseases (NIDDK)

Introduction/Background & aims: While GPCRs are considered a well-established collection of targets, recent technological advances to dissect the molecular mechanisms of GPCR function have revealed new paradigms of receptor activation and signalling. Still, many GPCR-targeted ligands lack selectivity for a single receptor subtype. Antibodies (Abs) can overcome challenges in selectivity; however, developing GPCR-targeted Abs remains challenging and is often unsuccessful. Here, we present a new type of antibody conjugate consisting of single domain antibody fragments (nanobodies, Nb) linked to ligands that bind to GPCRs. We apply this nanobody-epitope pair to characterise the role of ligand affinity in signalling at the parathyroid hormone receptor-1 (PTH1R).

Method/Summary of work: Nb/peptides-ligand conjugates were prepared through a combination of recombinant protein expression, enzymatic labelling, and azide-alkyne click chemistry¹. The activity of Nb/peptide-ligand conjugates was assessed for cAMP production (GloSensor), and translocation of β-arrestin 1 and 2 (ebBRET) in HEK cells stably transfected with either PTHR1 or PTHR1-variants.

Results/Discussion: We found that conjugation of weakly active ligands for PTHR1 to nanobodies that recognise the specific binding site in the receptor potentiates their potency by 10- to 1000-fold as evaluated in the GloSensor assay for cAMP detection. We also assessed the current series of Nb/peptide conjugates in a cAMP 'washout' assay. Results revealed that Nb/peptide conjugates induced prolonged cAMP responses upon ligand washout (EC₅₀ = 0.13 nM) relative to an analogue of a human PTHR1 drug PTH1-11 (EC₅₀ 423 nM). In a BRET assay to monitor arrestin translocation, we observed a robust increase in signal upon treatment with PTH1-34 that plateaued after ~20 min, consistent with β-arrestin recruitment to the plasma membrane. In contrast, Nb/peptide-ligand conjugates displayed markedly impaired recruitment of β-arrestin compared with PTH1-34 (EC₅₀ 3.8 nM) or PTH1-11 (EC₅₀ 10.3 nM). These findings show that Nb/peptide-ligand conjugates stimulate G protein-dependent production of cAMP at the plasma membrane but not β-arrestin recruitment to PTHR1 and subsequent generation of cAMP at endosomes.

Conclusion(s): The platform described here provides a new approach for generating ligands for the highly specific activation of GPCRs. Modulation of peptide epitope structure allows tuning of receptor

affinity without alteration of ligand pharmacophore, enabling investigation of connections between affinity and signalling (potency, efficacy, duration of action, ligand bias, spatial bias). Efforts to extend this platform to other GPCRs are underway.

REFERENCE(S)

- Cheloha, R.W., Fischer, F.A., Woodham, A.W., Daley, E., Suminski, N., Gardella, T.J. and Ploegh, H.L., 2020. Improved GPCR ligands from nanobody tethering. *Nature Communications*, 11(1), pp. 1–11.

P054 | Investigation into the expression and constitutive activity of GPR35

Tezz Quon; Brian Hudson; Graeme Milligan

University of Glasgow

Introduction/Background & aims: GPR35 is an orphan G-protein coupled receptor expressed in a wide range of tissues, with a growing interest as a potential therapeutic target[1]. A lack of reliable anti-GPR35 antibodies has made it difficult to investigate the expression profile of GPR35 at the protein level. Here we use HA tagged mouse GPR35 and human GPR35 knock-in transgenic mice to visualise the expression of GPR35. We also show GPR35 to have G-protein activation pathway specific constitutive activity with increasing receptor expression levels using BRET biosensors.

Method/Summary of work: Tissue or organoids isolated from transgenic knock-in mice containing C-terminally HA tagged mouse GPR35 or human GPR35a were fixed, embedded in paraffin and sectioned before staining with an anti-HA antibody (Roche, 3F10) and imaged on a confocal microscope.

Constitutive activity of GPR35 was assessed by transiently transfecting biosensors including a modified Nano Luciferase $G\alpha_{13}$ TRUPATH^[2] biosensor and a BRET-based arrestin-3 bystander biosensor

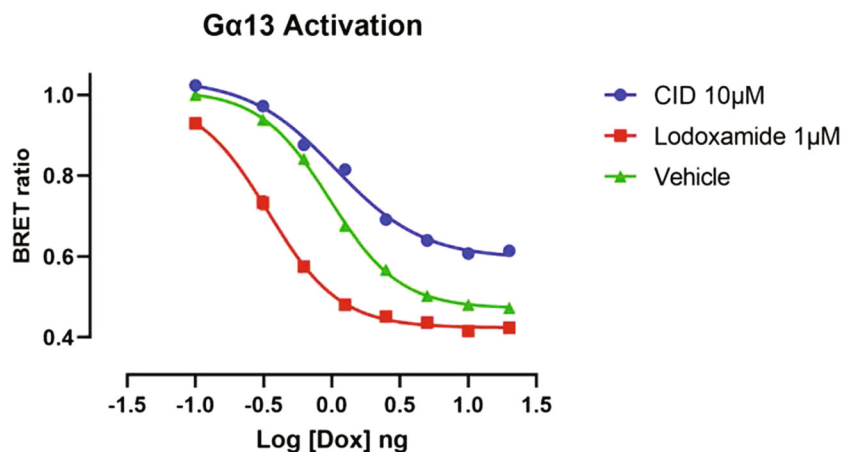
into DOX inducible Flp-In HEK293 cells stably transfected with hGPR35a. Expression was induced with different concentrations of DOX overnight. The $G\alpha_{13}$ sensor activation results in a decrease in the BRET ratio, while the arrestin sensor results in an increase in the BRET ratio.

Results/Discussion: GPR35 expression was detected in a range of tissues and cell types including crypts cells in the gut, most strongly in the colon, and in immune cells in Peyer patches, colon patches and spleen cells, along with a subset of dorsal root ganglion neurons. Increasing expression levels of hGPR35a resulted in a range of constitutive activity, with DOX at 0.625 ng/ml giving the greatest agonist induced response (~70% of vehicle BRET ratio) with minimal antagonist (CID-2745687) response. In higher DOX of 5–100 ng/ml, a strong activation was observed with vehicle alone (~50% of the value of no DOX). Here CID-2745687 showed a greater response (~130% of vehicle), though was unable to counter the entire receptor mediated ligand-independent response compared with no DOX. Constitutive activity was not seen in the arrestin-3 sensor nor any loss of agonist mediated response at higher expression.

Conclusion(s): GPR35 is expressed in a wide range of tissues and is often seen at low levels, even in cell types where function has been shown. The high constitutive activity at $G\alpha_{13}$ activation here, with most ligand mediated response lost at higher expression levels, suggests that low receptor expression may be required for endogenous agonist mediated GPR35 $G\alpha_{13}$ activation.

REFERENCE(S)

- Quon T, Lin LC, Ganguly A, Tobin AB, Milligan G. Therapeutic opportunities and challenges in targeting the orphan G protein-coupled receptor GPR35. *ACS Pharmacol Transl Sci*. 2020;3(5):801–812. <https://doi.org/10.1021/acspsci.0c00079>
- Olsen RHJ, Diberto JF, English JG, et al. TRUPATH, an open-source biosensor platform for interrogating the GPCR transducerome. *Nature Chemical Biology* 2020. <https://doi.org/10.1038/s41589-020-0535-8>



Poster presentations—Neuropharmacology

P055 | The small-molecule FPR2/ALX agonist, quin-C1, increased the viability of human SH-SY5Y neuroblastoma via MTT assay but not NRU and can induce neurite outgrowth

Sheree Smith; Nathaniel Milton; Andrew Paterson

Leeds Beckett University

Introduction/Background & aims: Quin-C1, a substituted quinazolinone, has been described in the literature as a low molecular weight, potent and selective agonist of FPR2/ALX. It has a reported EC50 of 15 nM in transfected HeLa cells via reporter assay [1]. The formyl-

peptide receptors (FPRs) belong to a family of seven α -helical transmembrane G protein-coupled receptors (GPCR). In humans, three subtypes of FPR have been identified (FPR1, FPR2/ALX and FPR3). Immunocytochemistry has revealed expression of FPR2/ALX in the central and peripheral nervous system, and a growing body of literature exists for the role of FPRs in neurogenesis and neuronal differentiation, providing evidence for a broader physiological function of FPRs [2]. We hypothesised that quin-C1 would induce a dose-dependent reduction in viability and induce neurite outgrowth in human SH-SY5Y neuroblastoma cells.

Method/Summary of work: Agonist: 0–1 μ M quin-C1 was prepared in serum-free media with a final solvent concentration of 1% DMSO.

Viability assays: Human SH-SY5Y neuroblastoma was seeded at a density of 300,000 cells/ml and exposed to 0–1 μ M quin-C1 for 24 h. The MTT assay and NRU assay protocols are available at [3].

Differentiation assay: Human SH-SY5Y neuroblastoma were seeded at a density of 400,000 cells/ml and exposed to 0–1 μ M quin-C1 for

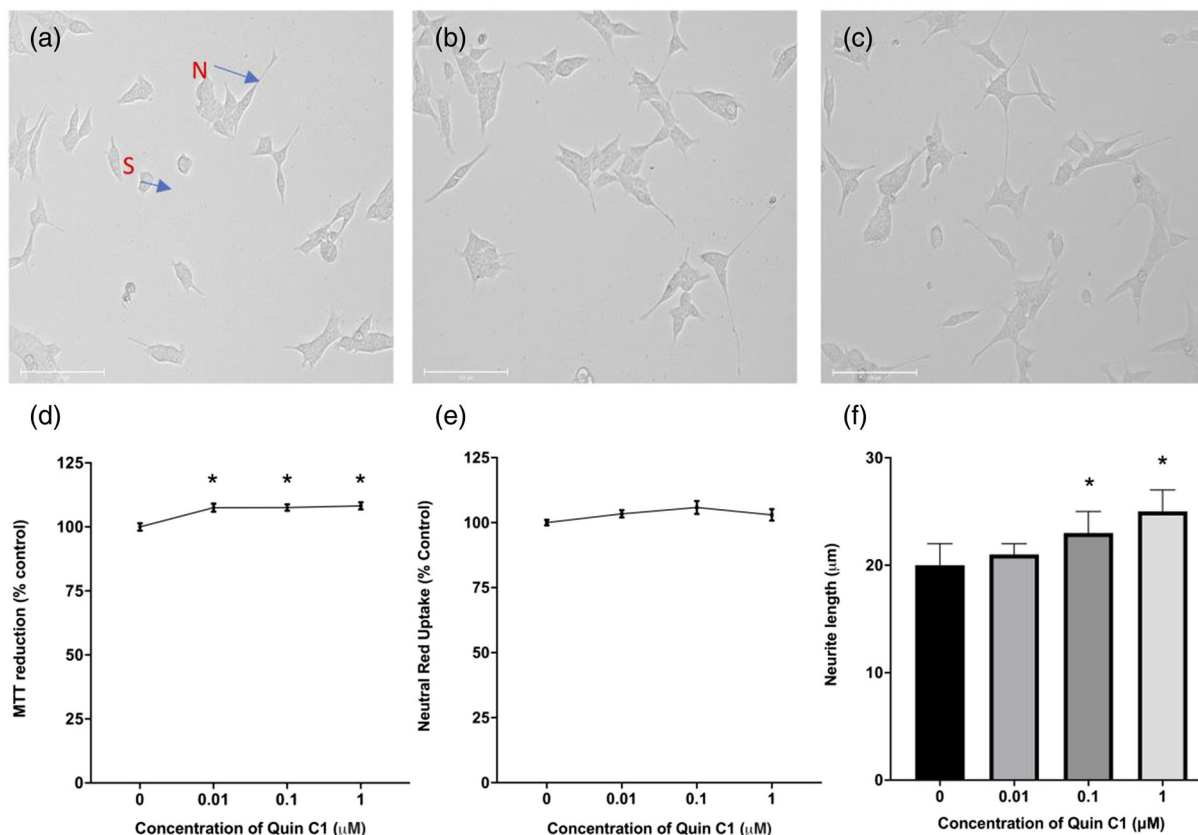


FIGURE 1 (a–c). Images of SH-SY5Y neuroblastoma following 48 h incubation with (a) 0 μ M quin-C1 (negative control) with N representing N-type (neuronal) morphology and S representing S-type (epithelial) morphology, (b) 1 μ M quin-C1, (c) 20 μ M 2,4-DNP (positive control). Magnification = \times 200, scale bar = 125 μ m. (d, e) Percentage viability of SH-SY5Y human neuroblastoma cells following 24 h exposure to 0–1 μ M quin-C1 (d) as determined by MTT assay ($n = 18$). $P < .05$ was considered significant. * represents statistical significance, * $P \leq .05$. (e) As determined by NRU assay ($n = 18$), no statistical significance was found. Values represent mean \pm SEM. Statistical analysis was performed via Brown-Forsythe ANOVA test with Dunnett's T3 multiple comparisons *post hoc* test. Statistical analysis was compared with (0 μ M quin-C1). (f) Bar graph of the effect of 0–1 μ M of quin-C1 for SH-SY5Y neuroblastoma, after 48 h of exposure. Bars represent the median with 95% confidence interval. Statistical analysis was performed via one-way ANOVA with the Kruskal-Wallis *post hoc* test. statistical analysis was compared with negative control (0 μ M quin-C1). A total of 48 random images were analysed per concentration, from three independent experiments. $P < .05$ was considered significant. * represents statistical significance, * $P \leq .05$.

48 h. All quantitative analyses were performed using Fiji open-source software package, version 2.1.0/1.53. Cells were analysed for morphological characterisation and neurite outgrowth.

Results/Discussion: Neurite length measurements were determined for 0 μ M quin-C1 (Figure 1a) and 1 μ M quin-C1 (Figure 1b) and compared with a positive control for neurite outgrowth (20 μ M 2,4-DNP; Figure 1c). Results showed increased viability of human SH-SY5Y; neuroblastoma was observed following exposure to 0.1–1 μ M of quin-C1 via MTT assay (Figure 1D) but not NRU assay (Figure 1e). Quin-C1 also increased neurite length in a dose-dependent manner (Figure 1f).

Conclusion(s): The results suggest that FPR2/ALX may be involved in neuronal differentiation and neurite outgrowth. The differences between the MTT and NRU viability assays suggest that there was not actually a change in viability but rather a change in mitochondrial activity associated with the differentiation. Previous studies have suggested neuronal roles for FPR ligands [2]. From our results, it suggests that FPR2/ALX may pose a novel target in neurogenesis. In particular, the small molecule compound, quin-C1, could be of therapeutic use, if capable of crossing the blood–brain barrier. Further research is required.

REFERENCE(S)

- Zhou C, Zhang S, Nanamori M, et al. Pharmacological characterization of a novel nonpeptide antagonist for formyl peptide receptor-like 1. *Molecular Pharmacology* 2007;72(4):976–983.
- Cussell P, Gomez Escalada M, Milton N, Paterson A. The N-formyl peptide receptors: Contemporary roles in neuronal function and dysfunction. *Neural Regeneration Research*. 2020;15(7):1191–1198.
- Kamiloglu S, Sari G, Ozdal T, Capanoglu E. Guidelines for cell viability assays. *Food Frontiers*. 2020;1(3):332–349.

P056 | Extended kappa opioid receptor antagonism following prolonged release depot buprenorphine injection in rats

Nairong Liu; Jan Melichar; Stephen Husbands; Chris Bailey; Sarah Bailey

University of Bath

Introduction/Background & aims: Recently, a prolonged release depot formulation of buprenorphine, Bupival[®], has been approved in Europe for the treatment of opioid dependence [1]. Melichar and

colleagues have shown that clinically, this prolonged release depot buprenorphine (DEP-BUP), provided as weekly/monthly depot injection, provides reduction in craving and anxiety symptoms in opioid-dependent patients [2]. Buprenorphine is a partial mu opioid receptor (MOP) agonist and a kappa opioid receptor (KOP) antagonist and at higher concentrations is an antagonist at the delta opioid receptor and a partial agonist at the opioid receptor like 1 (ORL1) receptor [3]. We have investigated the duration of KOP antagonism following DEP-BUP administration or acute buprenorphine administration in rats.

Method/Summary of work: Adult male and female Sprague–Dawley rats (8–11 weeks) were used. The warm water (50°C) tail withdrawal assay was used to assess the response to the KOP agonist spiradoline (20 mg/kg, subcutaneously). Rats were habituated to handling and randomly assigned to treatment groups. All rats were injected with the MOP antagonist clocinnamox (CCAM, 4 mg/kg in 6.7% ethanol/saline, intraperitoneally) on day 0. Twenty-four hours later, baseline latency was tested, and rats were injected with saline (0.9% w/v), buprenorphine 0.45 mg/kg, DEP-BUP (once weekly preparation 32 mg/0.64 ml supplied by Camurus, diluted 1:1 with vehicle, administered 0.4 ml/g body weight to produce a depot that achieves blood levels equivalent to 0.45 mg/kg acute administration) or placebo vehicle (all treatments subcutaneously). The response to spiradoline was assessed 1 and 20 h later. Antinociception was calculated as percentage maximum possible effect (% MPE) = (test latency-control latency)/(20s-control latency) \times 100. Values reported are mean \pm sem ($n = 5$ per group), and the effect of time on the treatment response is determined using paired *t* tests.

Results/Discussion: Acute administration of buprenorphine (0.45 mg/kg) significantly blocked the antinociceptive effects of spiradoline after 1 h, but not 20 h, in both male and female rats (Table 1). For DEP-BUP, the response to spiradoline was attenuated at both 1 and 20 h.

Conclusion(s): DEP-BUP displayed extended KOP antagonist activity against spiradoline in both male and female rats. We are investigating whether there is prolonged KOP antagonism at longer treatment durations. KOP antagonism has been proposed as an anxiolytic therapeutic strategy [3], and further studies will be conducted to assess the behavioural impact of DEP-BUP in rodents.

REFERENCE(S)

- Vorspan F, Hjelmstrom P, Simon N, et al. What place for prolonged-release buprenorphine depot-formulation Bupival(R) in the treatment arsenal of opioid dependence? Insights from the French experience on

TABLE 1 Antinociceptive response to spiradoline (20 mg/kg) in rats pretreated with acute buprenorphine (BUP) or saline and prolonged release depot formulation of buprenorphine (DEP-BUP) or vehicle (**P* < .025 versus 1 h timepoint within treatment group)

% MPE (sem)	Acute administration				Depot administration			
	Saline		BUP		Vehicle		DEP-BUP	
	1 h	20 h	1 h	20 h	1 h	20 h	1 h	20 h
Female	39.0 (10.2)	33.4 (2.8)	8.0 (1.7)	39.5* (9.4)	33.2 (7.2)	41.5 (12.9)	9.3 (3.3)	3.0 (3.7)
Male	30.1 (6.8)	44.5 (14.5)	6.1 (2.2)	46.6* (9.2)	34.8 (9.4)	26.9 (14.7)	11.4 (2.5)	10.2 (8.4)

neurotransmitter, dopamine, also inhibited stereotypical movements ($p = .0078$, $n = 8$), with effects indistinguishable from pre-exposure conditions 24 h after exposure ($p > .05$, $n = 8$). The same effects were observed with free locomotion, which was inhibited by $22.1 \pm 10.0\%$ ($p = .0002$, $n = 8$) but were readily reversible 24 h after exposure ($p > .05$, $n = 8$).

Conclusion(s): We provide proof-of-concept utilisation of *L. variegatus* for the study of neurophysiology. Analogous to *Caenorhabditis elegans* and *Drosophila melanogaster*, *L. variegatus* could provide significant advances in medicines development and broader biomedical science studies.

REFERENCE(S)

1. Seeley, A. et al. (2021) *Lumbriculus variegatus*: A novel organism for in vivo pharmacology education. *Res. Perspect*; 9:e00853. <https://doi.org/10.1002/prp2.853>

Poster presentations—Toxicology

P061 | The effects of acute and chronic ethanol exposure in the novel *in vivo* research organism, *Lumbriculus variegatus*

Romessa Mahmood; Elis Roome; Kwang Lee; Aidan Seeley

Swansea University

Introduction/Background & aims: Ethanol produces dose-dependent motor impairment in man and in other animals, including rodents, *Drosophila* and *C. elegans* [1]. Previously, we have demonstrated that *Lumbriculus variegatus*, a species of aquatic worm, demonstrates concentration-dependent behavioural changes when exposed to ethanol [2].

Here we demonstrate that ethanol produces rapid inhibition of *L. variegatus* free, unstimulated, locomotor activity and that acute and chronic exposure to ethanol does not affect these behavioural changes but does result in significant changes to *L. variegatus* body size.

Method/Summary of work: Unstimulated free locomotion was measured following exposure to ethanol (0–500 mM) by rapid image collection of *L. variegatus*. The effect of repeated acute exposure to ethanol was tested by exposing *L. variegatus* to 500 mM ethanol three times at 10 min intervals spaced 30 min apart and collecting images. The effects of ethanol (0–500 mM) on locomotion were also observed in ethanol naïve *L. variegatus* or *L. variegatus* exposed to 100 mM ethanol for ≥ 21 days. *L. variegatus* size was determined by ImageJ analysis following the acquisition of a single image of individual worms. Statistical significance was determined by paired t tests or a two-way ANOVA.

Results/Discussion: After 2 min of exposure to ethanol, *L. variegatus* free locomotion was significantly inhibited free locomotion by 35.6

$\pm 6.5\%$ at 250 mM ($p = .02$, $n = 11$) and $33.1 \pm 8.7\%$ at 500 mM ($p = .03$, $n = 11$). These effects plateaued after 4 min of exposure to 250 mM ($p = .003$, $n = 11$) and 500 mM ethanol ($p = .002$, $n = 11$). Repeated acute exposure to 500 mM resulted in a significant decrease in *L. variegatus* free locomotion ($p < .0001$, $n = 12$), but there was no significant difference to *L. variegatus* movement between exposures ($p > .05$, $n = 12$).

Following exposure to 100 mM ethanol continuously for ≥ 21 days, chronically exposed *L. variegatus* demonstrated no significant difference in response to ethanol (0–500 mM) compared with ethanol naïve *L. variegatus* ($p > .05$, $n = 9$). However, a significant size increase was observed in chronically exposed *L. variegatus* compared with their ethanol naïve counterparts ($p < .01$, $n = 6$).

Conclusion(s): This work demonstrates the concentration-dependent effects of ethanol on *L. variegatus* behaviour and that ethanol tolerance is not induced in this mode, which highlights the wider potential utility of *L. variegatus* for ethanol research.

REFERENCE(S)

1. Wallace, M.J. et al. (2007) Acute functional tolerance to ethanol mediated by protein kinase C ϵ . *Npp*; 32: 127–136. <https://doi.org/10.1038/sj.npp.1301059>
2. Mathur, S.N. et al. (2021) Concentration-dependent behavioural effects of ethanol in the novel *in vivo* model, *Lumbriculus variegatus*. *Journal de Pharmacologie* 178:4923–5006. <https://doi.org/10.1111/bph.15648>.

P062 | Development of an LC–MS/MS method for the detection of snake venom toxins in human plasma

Anné Lerner; Carine Smith; Carine Marks; Nicolaas Mare Vlok; Tracy Ann Kellermann

Stellenbosch University

Introduction/Background & aims: Snakebite envenomation significantly threatens human health due to the effects induced by the venom toxins. Snakes responsible for the envenomation are rarely positively identified, and there are no rapid methods/diagnostics available for conclusive identification of the causative species. The aim of the study was to develop an LC–MS/MS method for the species-specific detection of snake venom toxins from human plasma.

Method/Summary of work: An epidemiological study on the incidence of snakebite in South Africa as reported to Poisons Information Helpline of Western Cape (PIHWC) was performed to provide rationale for the analytical study. Analytical methodology relied on various proteomic and pharmacological techniques. These included compositional analysis and identification of species-specific venom toxins by high resolution (HR) LC–MS/MS and fractionation of *Naja nivea* venom by size exclusion chromatography. Venom fractions were screened for toxicity using a zebrafish model, utilising DanioVision for phenotypic screening and behavioural tracking of the larvae.

Thereafter, a triple quadrupole LC–MS/MS method was developed containing species-specific toxins.

Results/Discussion: Analysis of PIHWC call data revealed that in 43.73% of the recorded snakebite cases, the causative snake species were unidentified. The snake species *Naja nivea*, *Bitis arietans* and *Bitis atropos* species were identified as most medically significant in South Africa and consequently included in the study. This study identified the species predominantly responsible for snakebites from PIHWC call data and highlighted a need for a diagnostic to identify the species responsible for envenomation. Venom from *N. nivea* was chosen as the species for fractionation after common peptides from inter-region venom were identified as unique to the species. Behavioural changes in larvae were observed after exposure to sublethal concentrations of *N. nivea* venom fractions. Significant ($p < .0001$) changes in larval behaviour were observed in two treatment groups compared with the control. Using the transitions generated during HR-LC–MS/MS analysis, MRM's were created and imported onto the triple quadrupole LC–MS. It was shown that using a combination of conventional HR-MS (with database/library searches) and triple quadrupole MS, a method could be created that identified species-specific venom peptides from human plasma to aid diagnosis. Two *N. nivea* cytotoxins were positively identified from human plasma by LC–MS/MS.

Conclusion(s): This is a proof of concept for future work that will include the development of a lateral flow assay to detect venom from envenomed plasma that is cost-effective to produce, aids in defining diagnosis and importantly serves victims of snakebite envenomation in rural communities.

P064 | Glycolytic switching: An early indicator for drug-specific T-cell activation

Joshua Gardner¹; Sean Hammond²; Catherine Betts³; Amy Chadwick¹; Dean Naisbitt¹

¹University of Liverpool; ²Apconix; ³AstraZeneca

Introduction/Background & aims: Drug hypersensitivity reactions can be immune-mediated with T-cells implicated in the activation of adaptive responses arising from exposure to therapeutic compounds. Antigen presentation evokes T-cell activation, and recent studies have demonstrated that ensuing T-cell effector functions are dependent on glycolysis [1]. In this study, the glycolytic activity of vancomycin-specific T-cell clones (TCCs), for which pathways of T-cell activation have been previously characterised via proliferation and cytokine release assays [2], was assessed for dose-dependent, drug-specific and cross-reactive energetic responses with structurally related glycopeptide antibiotics such as teicoplanin. Additionally, glycolytic parameters of TCCs were characterised for responses to

phytohaemagglutinin (PHA) and anti-CD3 activating antibodies to determine fuel usage upon nonspecific and T-cell receptor mediated activation.

Method/Summary of work: Vancomycin-responsive TCCs were generated *in vitro* via serial dilution using peripheral blood mononuclear cells from a combination of hypersensitive patients and healthy volunteers and were confirmed as compound-responsive through proliferation responses measured by thymidine incorporation. The Seahorse XFe⁹⁶ Analyser was used to measure energetic parameters relevant to T-cell activation, namely, the extracellular acidification rate (ECAR) as an indicator of glycolytic function. In addition, to correlate the bioenergetic characteristics of T-cell activation with *in vitro* assays, cytokine release (IFN- γ) in response to stimulation with model compounds and glycopeptide antibiotics was profiled by enzyme-linked immunospot (ELISpot) assay.

Results/Discussion: PHA-induced nonspecific T-cell activation and TCR stimulation using anti-CD3 were characterised by immediate augmentation of ECAR. Mitochondrial stress assays revealed that mitochondrial function remained unchanged following treatment with model stimulants, suggesting a flux towards a glycolytic state accommodates energetic requirements. Activation of vancomycin-reactive TCCs was found to be a highly glycolytic process in which acute drug injection induced a dose-dependent glycolytic shift which was observed to be drug-specific following treatment with structurally unrelated compounds such as carbamazepine, concordant with conventional proliferative and cytokine-based readouts. Interestingly, cross-reactivity between structurally similar glycopeptide antibiotics was detected when analysing energetic responses in populations of TCCs absent cross-reactive potential when considering proliferative and cytokine readouts. In this case, TCCs with prior specificity for vancomycin were also found to exhibit glycolytic switching after exposure to teicoplanin, for which T-cell responses have also been implicated within the pathogenesis of immune-mediated adverse drug reactions [3]. Notably, glycolytic activation of TCC was observed to be HLA restricted, as exposure to HLA-DR blockade attenuated the glycolytic flux with TCCs remaining in quiescent state.

Conclusion(s): In summary, these studies demonstrate the utility of bioenergetic analysis within the functional characterisation of T-cells involved in hypersensitivity reactions.

REFERENCE(S)

- Gubser, P.M., et al., *Rapid effector function of memory CD8(+) T cells requires an immediate-early glycolytic switch*. *Nature Immunology*, 2013. 14(10): p. 1064-+.
- Ogese, M.O., et al., *Deciphering adverse drug reactions: In vitro priming and characterization of vancomycin-specific T-cells from healthy donors expressing HLA-A*32:01*. *Toxicological Sciences*, 2021.
- Gardner, J., et al., *Characterization of teicoplanin-specific T-cells from drug naïve donors expressing HLA-A*32:01*. *Chemical Research in Toxicology*, 2022. 35(2): p. 199–202.

P066 | Dexamethasone and amodiaquine exhibit ocular adverse effects in larval zebrafish

Qi Lu; Alison Reynolds

University College Dublin

Introduction/Background & aims: Dexamethasone is a glucocorticoid used for the treatment of various inflammatory conditions including bacterial infections and endocrine disorders. Amodiaquine and hydroxychloroquine are 4-aminoquinolines used as antimalarials. Previous clinic studies showed that these drugs will cause ocular adverse effects in humans.

The purpose of this study was to determine whether dexamethasone/amodiaquine/hydroxychloroquine adversely affect eye development and visual behaviour in larval stages using zebrafish as a model organism.

Method/Summary of work: Wild type (Tübingen) zebrafish were treated at 1 day postfertilisation (dpf) by immersion for 96 h with dexamethasone (0.01, 0.1, 1, 10, 50, 100, 150, 250 and 1000 μM), amodiaquine (10, 25, 50, 75 and 100 μM) and hydroxychloroquine (125, 250, 500, 1000, 2000 and 4000 μM). At five dpf, survival numbers were recorded, and LD_{50} was calculated. Larvae were characterised for gross morphology, and visual behaviour was analysed using optokinetic response test. Data were analysed by GraphPad Prism.

Results/Discussion: The LD_{50} of dexamethasone was determined at 216 μM and for amodiaquine as 19.11 μM . Dexamethasone caused phenotypic changes to zebrafish which exhibit smaller eyes, shorter body length, mildly curved tails, loss of swim bladders and necrosis in the yolk area compared with vehicle controls. Amodiaquine-treated zebrafish larvae often fail to hatch from their chorions and exhibit shorter body length, severely curved tails, loss of swim bladders and necrosis in the yolk area. In terms of visual behaviour, both dexamethasone and amodiaquine displayed a dose-dependent reduction in visual behaviour. Dexamethasone-treated larvae (150 μM) have a 45.2% reduction in number of saccades ($p < .05$ vs. vehicle), whereas amodiaquine-treated larvae (10 μM) have a 25.8% reduction in number of saccades ($p < .05$ vs. vehicle). Hydroxychloroquine did not exhibit an effect on zebrafish morphology or visual behaviour.

Conclusion(s): This study shows that dexamethasone and amodiaquine cause visual impairment in zebrafish, as seen by a reduction in visual behaviour tests and also teratogenic phenotypes in the eyes.

TABLE 1 Morphological properties of different treated-zebrafish

Group	Eye		Body length	Curved tail	Swim bladder	Necrosis
	Major axis	Minor axis				
Dexamethasone (150 μM)	314.788 μm	189.11 μm^*	3283.78 μm^*	√	×	√
Vehicle 0.75%DMSO	350.97 μm	243.05 μm	3808.7 μm	×	√	×
Amodiaquine (10 μM)	318.14 μm	220.83 μm	3166.17 μm^*	√	×	√
Vehicle 1%DMSO	320.12 μm	202.88 μm	3451.22 μm	×	√	×

Note: Ten larvae in each group were captured by light microscopy. *T* test was used to analyse data by Graphpad Prism.

* $p < .05$ versus vehicle.

REFERENCE(S)

1. Mahon N, Slater K, O'Brien J, Alvarez Y, Reynolds A, Kennedy B. Discovery and development of the quinib series of ocular drugs. *Journal of Ocular Pharmacology and Therapeutics*. 2022;38(1):33–42. <https://doi.org/10.1089/jop.2021.0074>

P068 | Investigating the ability of HepaRG cells to recapitulate drug-induced mitochondrial dysfunction following extended dosing with antibiotics

Robyn Kiy; Amy Chadwick

University of Liverpool

Introduction/Background & aims: Macrolide antibiotics inhibit bacterial protein synthesis. Structural similarities between bacterial and mitochondrial ribosomes mean macrolides may inhibit mitochondrial protein synthesis, a hypothesis consistent with clinical adverse events. However, literature describing the mechanisms of macrolide-induced hepatotoxicity is limited; assumptions are based on drugs with similar mechanisms of action, including known mitotoxicant linezolid. Mitochondrial inhibition may be a class effect with significant implications for novel compounds, so elucidating toxicity mechanisms is essential.

HepaRG represents a physiologically relevant alternative to primary hepatocytes. They enable extended dosing studies *in vitro*, as once fully differentiated, they can be maintained for 28 days. We aimed to assess the utility of HepaRG for recapitulating clinically relevant macrolide-induced mitochondrial dysfunction using model compound linezolid.

Method/Summary of work: HepaRG cells were dosed with linezolid (1.2–100.0 μM) for 4–28 days, and mitochondrial composition and function were regularly assessed at twice-weekly timepoints. Western blots probing for mitochondrial ribosome-translated mitochondrial proteins and cytoplasmic ribosome-translated mitochondrial proteins were performed alongside qPCR, in order to quantify mitochondrial proteins and DNA respectively. Additionally, acute metabolic switch assays were conducted in order to assess the direct impact of linezolid on the electron transport chain [1]. Finally, seahorse respirometry was used to investigate the effects of linezolid treatment on various bioenergetic parameters. Western blot, qPCR and acute metabolic switch assays were conducted in triplicate, and seahorse respirometry was conducted in duplicate, with three separate assays performed in each case. Statistical significance was determined using ANOVA followed by Tukey's post hoc test.

Results/Discussion: Western blot showed significant concentration- and time-dependent decreases in mitochondrially encoded proteins after 21 or 28 days of 11.1 μM linezolid ($P < .05$ and $P < .0001$, respectively). No decrease in mitochondrial DNA (mtDNA) copy number was observed, implying that the linezolid-induced protein loss occurs at the level of translation. However, this reduction in mitochondrial protein did not translate to impaired mitochondrial function. In fact, 7 days of treatment with 100 μM linezolid significantly increased spare respiratory capacity and decreased glycolytic index relative to vehicle control ($P < .001$ and $P < .05$, respectively).

Conclusion(s): We have demonstrated that clinically relevant linezolid exposure inhibits mitochondrial protein synthesis. However, in HepaRG, this does not cause impaired mitochondrial respiration. This has important implications, highlighting the fact that mitochondria are complex organelles able to initiate a multitude of compensatory mechanisms, and exemplifies the limitations of *in vitro* models common in early drug screening stages.

REFERENCE(S)

1. Kamalian L, Douglas O, Jolly CE, Snoeys J, Simic D, Monshouwer M, Williams DP, Park BK, Chadwick AE. Acute metabolic switch assay using glucose/galactose medium in HepaRG cells to detect mitochondrial toxicity. *Current Protocols in Toxicology* 2019;80(1):e76. <https://doi.org/10.1002/cptx.76>. Epub 2019 May 6. PMID: 31058461.

Oral communications, Tuesday 13th September

Oral communications—Molecular and cellular

OC001 | The role of $\text{PGF}_{2\alpha}$ in the development of labour and how FP antagonists could prevent preterm birth

Isabel Hamshaw¹; Richard Stark¹; Mohammad T. Alam²; Emma S. Lucas¹; Gregory D. Ferguson³; Isabel Hamshaw¹

¹University of Warwick; ²United Arab Emirates University; ³Ferring Research Institute Inc

Introduction/Background & aims: Every year, 14.9 million babies are born preterm, accounting for 11.1% of live deliveries. Preterm birth (PTB) is the leading cause of infant morbidity and mortality; however, there are currently no licenced tocolytics that prevent PTB [1]. **Aim:** The aim of this study is to investigate the role of the FP agonist, $\text{PGF}_{2\alpha}$ and four FP antagonists (Table 1) in a SV40 T-Ag immortalised myometrial cell line (MYLA). **Hypothesis:** $\text{PGF}_{2\alpha}$ will stimulate a pro-labour phenotype in MYLA cells that can be inhibited with FP antagonists.

Method/Summary of work: Ca^{2+} assay: MYLA cells were preloaded with Calbryte™ 520 AM, then treated under continuous flow with 300 pM to 10 μM of $\text{PGF}_{2\alpha}$ or 300 pM to 10 μM FP antagonist + 1 μM $\text{PGF}_{2\alpha}$. Intracellular Ca^{2+} release was measured in relation to the number of oscillations per second (Hz) per concentration. **RNA-Sequencing:** Total RNA was isolated from MYLA cells at 7 time points (1, 3, 6, 9, 12, 24, and 48 hours). Illumina TruSeq RNA libraries were prepared and sequenced using NextSeq. Observed changes in mRNA transcripts were verified by RT-qPCR. **Data Analysis:** All data are mean \pm SEM, $n = 3$, analysed using One-Way ANOVA with post hoc Dunnett's multiple comparison test using RStudio and GraphPad Prism 9.

Results/Discussion: FP antagonist pIC_{50} values are reported in Figure 1. There were >2500 statistically significant ($p < .05$) differentially expressed genes when MYLA cells were treated with $\text{PGF}_{2\alpha}$ including 141 pro-labour genes, for example, *OXTR*, *IL-6* and *IL-8*. $\text{PGF}_{2\alpha}$ stimulated the development of a smooth-muscle phenotype with statistically significant increases in *CALD1* ($p < .0001$), *LMOD1* ($p < .05$) and *MYLK* ($p < .0001$). RT-qPCR validated these results and determined that the most potent FP antagonist, N6, suppressed expression of the pro-labour gene *OXTR* ($p < .01$) and the smooth muscle marker *MYLK* ($p < .0001$) (Figure 2).

Conclusion(s): The four FP antagonists are ranked as follows: N6, N0, N1 and N4 from most to least potent. $\text{PGF}_{2\alpha}$ stimulates the development of both a pro-labour and a smooth muscle phenotype which is inhibited by N6.

REFERENCE(S)

1. Miyazaki C, Moreno Garcia R, Ota E, Swa T, Oladapo OT, Mori R. Tocolysis for inhibiting preterm birth in extremely preterm birth, multiple gestations and in growth-restricted fetuses: A systematic review and meta-analysis. *Reproductive Health* 2016;13(1):1–12.

TABLE 1 FP antagonists. All solvated in DMSO to a stock concentration of 10 mM

Chemical name	Text reference
5-(6-bromo-3-methyl-2-(pyrrolidin-1-yl) quinoline-4-carboxamido)-4-(2-chlorophenyl) pentanoic acid	N0
3-amino-1-((5-chloro-1-isobutyl-1H-indazol-7-yl) methyl)-1H-indazole-5-carboxylic acid	N1
(S)-3-((1,1'-biphenyl)-4-ylsulfonyl)-N-((S)-1-(4-fluorophenyl)-3-hydroxypropyl) thiazolidine-2-carboxamide	N4
5-(6-bromo-3-methyl-2-phenylquinoline-4-carboxamido)-4-(2-chlorophenyl) pentanoic acid	N6

Note: Stocks were diluted to 1 μM using DMEM-F12 media for RNA-sequencing or 300 pM to 10 μM for Ca^{2+} assays using modified Krebs-TES buffer (composition [mM]: NaCl, 133; KCl, 4.7; glucose, 11.1; MgSO_4 , 1.2; KH_2PO_4 , 1.2; TES, 10; $\text{CaCl}_2 \cdot \text{H}_2\text{O}$, 2.5; pH 7.4).

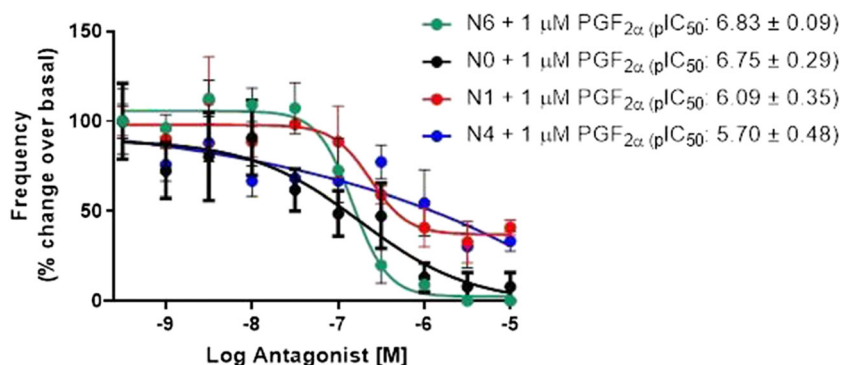


FIGURE 1 Ability of four FP antagonists to inhibit PGF_{2α}-stimulated Ca²⁺ oscillations in MYLA cells. Inhibition of 1 μM PGF_{2α}-stimulated intracellular Ca²⁺ oscillations by 300 pM to 10 μM FP antagonist. Data are mean ± SEM, *n* = 3 independent experiments and expressed as % change over basal.

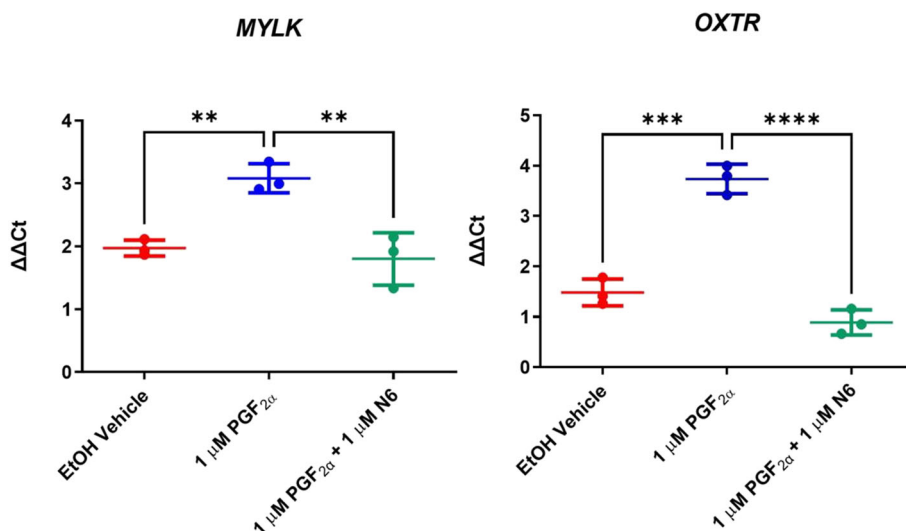


FIGURE 2 Expression of OXTR and MYLK in MYLA immortalised myometrial cells after 48 hours treatment with vehicle, PGF_{2α} or N6. Cells were stimulated for 48 h with EtOH vehicle, 1 μM PGF_{2α} or 1 μM PGF_{2α} and 1 μM N638093. MYLK was used as smooth muscle cell markers and OXTR due to its association with progression of labour. Data are expressed as fold change (ΔΔCt). Data are mean ± SEM, *n* = 3, analysed using one-way ANOVA and post hoc Dunnett's multiple comparison test (***P* < .01, ****P* < .001 and *****P* < .0001)

OC003 | Dual pancreatic adrenergic and dopaminergic signalling as a therapeutic target of bromocriptine

Despoina Aslanoglou¹; Susanne Bertera²; Marta Sanchez-Soto³; Benjamin Free³; Rob Lane⁴; Laura Friggeri⁵; Jens Meier⁵; David Sibley³; Rita Bottino⁶; Peter McCormick⁷; Zachary Freyberg⁸

¹Queen Mary university of London; ²Allegheny Health Network; ³NIH/NINDS; ⁴University of Nottingham; ⁵Vanderbilt University; ⁶Imagine Pharma Inc; ⁷Queen Mary University of London; ⁸University of Pittsburgh

Introduction/Background & aims: The dopaminergic agonist bromocriptine is FDA-approved for type 2 diabetes due to its ability to improve dysglycemia. Although bromocriptine's actions were mainly attributed to stimulation of dopamine D2 receptors (D2R) in the brain, the exact mechanism responsible for its metabolic benefits remains unknown. We previously showed the key roles of DA D2-like receptors in pancreatic β-cell insulin secretion [1]. We recently demonstrated the functional significance of the pancreatic dopaminergic/adrenergic signalling interplay in the regulation of both insulin and

glucagon secretion from mouse and human islets [2]. Here, we aimed to investigate a new mechanism for bromocriptine's metabolic actions via D2R and adrenergic α_{2A} receptor (α_{2A}-AR) signalling in pancreatic α- and β-cells.

Method/Summary of work: A high-throughput homogeneous time-resolved fluorescence resonance energy transfer (HTRF) assay was used to measure secreted glucagon and insulin from mouse and human islets. A novel optical method, nanoBRET, was used to determine recruitment of G-proteins and β-arrestin1 and 2 to receptors. Radioligand binding with [³H]-RX821002 was used to measure α_{2A}-adrenoceptor binding by dopaminergic ligands. HPLC measured catecholamine secretion from islets. Computational modelling using ROSETTA LIGAND docking predicted binding of bromocriptine to D2R and α_{2A}-AR.

Results/Discussion: Bromocriptine acts on β-cells to reduce glucose stimulated insulin secretion (GSIS) in a concentration-dependent manner, in mouse islets (IC₅₀ = 15.8 ± 0.3 nM) and in rat-derived INS1-E cells (IC₅₀ = 14 ± 0.1 nM). Reduced GSIS was due to bromocriptine's combined actions via D2R and α_{2A}-AR. Bromocriptine displaced [³H]-RX821002, confirming binding to endogenous INS1-E α_{2A}-AR (K_i = 28.1 ± 0.1 nM). NanoBRET showed that bromocriptine is a Gα_o/z-biased agonist at α_{2A}-AR, while no recruitment of β-arrestins

p100 phosphorylation in response to both IL-1b and $LT_{\alpha_1b_2}$. In contrast, pre-incubation with a NIK inhibitor, CW15337, had no effect; however, the response to $LT_{\alpha_1b_2}$ was significantly reduced. IL-1b also stimulated a rapid induction of CXCL12 reporter activity. IKK α knock-down reduced IL-1b induced reporter activity by approx. 50% (IL-1b + IKK α = 50.74% \pm 5.94%, $n = 3$). Pretreatment with SU1261 resulted in a concentration-dependent inhibition of CXCL12 with an IC_{50} value of 0.42 μ M ($n = 5$). Induction of CXCL12 mRNA levels was also studied (fold stimulation: IL-1b 8 h = 5.33 \pm 0.83, IL-1b + siRNA IKK α = 2.07 \pm 0.40, $P < .05$, IL-1b + SU1261 = 1.62 \pm 0.53, $P < .001$; $n = 3$).

Conclusion(s): Taken together, these results point to a novel kinetically distinct mode of regulation of noncanonical NF κ B signalling linked to CXCL12 induction which is IKK α dependent but NIK independent and mediated by traditional canonical activating ligands such as IL-1b.

REFERENCE(S)

1. Sun, S.C., *The non-canonical NF-kappaB pathway in immunity and inflammation*. *Nature Reviews. Immunology*, 2017. 17(9): p. 545–558.
2. Gamble, C., et al., *Inhibitory kappa B kinases as targets for pharmacological regulation*. *British Journal of Pharmacology*, 2012. 165(4): p. 802–819.

OC005 | The C-terminal region of the GLP-1 and GIP receptors is not the key determinant for their differential arrestin recruitment

Suleiman Al-Sabah; Bashaier Al-Zaid; Charles Ezemuzie
Kuwait University

Introduction/Background & aims: Glucagon-like peptide-1 (GLP-1) and glucose-dependent insulinotropic polypeptide (GIP) are important regulators of metabolism and mediate the incretin effect. This glucose-dependent potentiation of insulin secretion is severely impaired in patients with type-2 diabetes mellitus. While pharmacological doses of GLP-1 can overcome this impairment, the same is not true for GIP. The reasons for this are unclear; however, differences in the signalling profiles of the GLP-1 and GIP receptors (GLP-1R and GIPR) may contribute. GLP-1R and GIPR are closely related members of the secretin class of G protein-coupled receptors but while GIPR predominately couples to Gs, GLP-1R can also couple to Gq. GLP-1R is a robust recruiter of arrestin, whereas arrestin recruitment to GIPR is relatively poor [1]. The aim of this study was to identify the role of the C-terminal region of the two receptors in their differing signalling behaviour.

Method/Summary of work: Chimeric receptors, where the C-terminal region of one receptor was replaced with that of the other, were generated using Gibson assembly (Figure 1a,b). The resulting receptors (GLP-1/GIPR and GIP/GLP-1R) were labelled at their C-termini with nanoluciferase (Nluc) for bioluminescence resonance energy transfer (BRET)-based Venus-mGs recruitment assays and super yellow fluorescent protein 2 (SYFP2) for arrestin3-Nluc assays. HEK-293 cells were transiently transfected with receptor and effector protein, and dose-dependent recruitment of Venus-mGs or arrestin3-Nluc was observed using BRET. Data (mean \pm S.E. M) were from at least three experiments and expressed as fold change from basal. Statistical significance ($P \leq .05$) was determined using ANOVA.

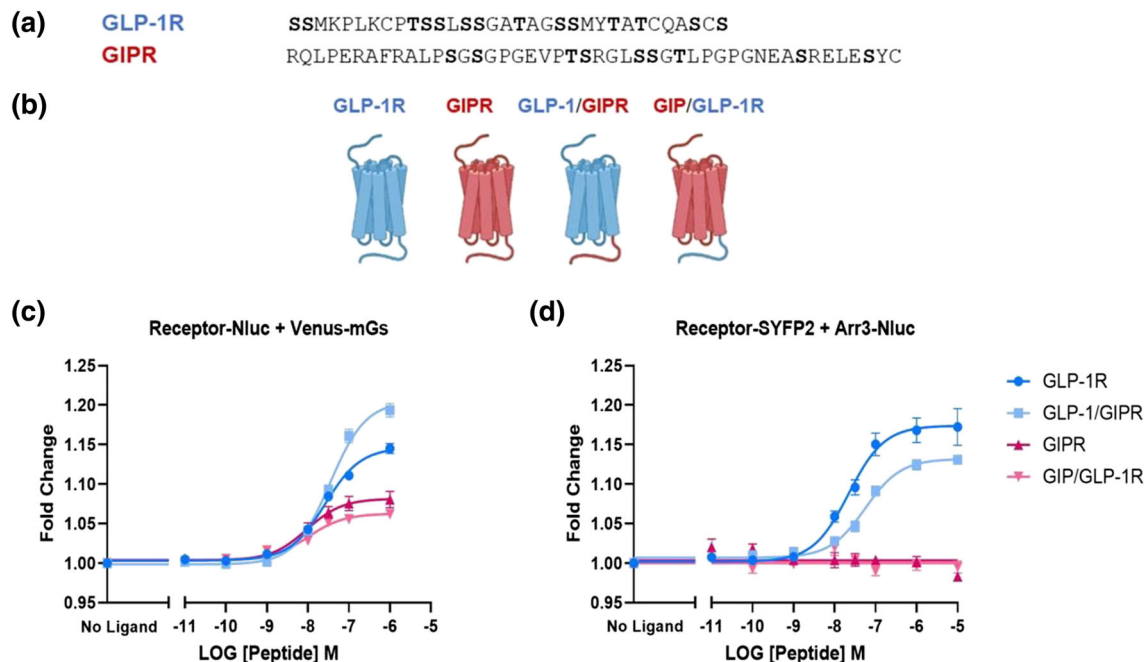


FIGURE 1 (a) The amino acid sequence of the C-terminal region of GLP-1R and GIPR with serine and threonine residues highlighted in bold. (b) A schematic representation of the wild-type and chimeric receptors generated for this study. (c) Venus-mGs recruitment to Nluc-labelled wild-type or chimeric receptor. (d) Arrestin3-Nluc recruitment to SYFP2-labelled wild type or chimeric receptor stimulated by either GLP-1 (for GLP-1R and GLP-1/GIPR) or GIP (for GIPR and GIP/GLP-1R)

Results/Discussion: Replacement of the C-terminal region of GLP-1R with that of GIPR caused an increase in E_{max} in the Gs recruitment assay although this was not significant when using ANOVA. The reciprocal substitution had no effect on Gs recruitment to GIPR (Figure 1C). No agonist stimulated recruitment of arrestin to GIPR was detectable using BRET. Substituting the C-terminal region of GIPR with that of GLP-1R did not promote arrestin recruitment, and the reciprocal substitution does not significantly inhibit arrestin recruitment to GLP-1R (Figure 1d).

Conclusion(s): The C-terminal region of the GLP-1 and GIP receptors is not the key determinant for their differential arrestin recruitment.

REFERENCE(S)

1. Al-Sabah, S., Al-Fulaij, M., Shaaban, G., Ahmed, H.A., Mann, R.J., Donnelly, D., et al. (2014). The GIP receptor displays higher basal activity than the GLP-1 receptor but does not recruit GRK2 or Arrestin3 effectively. *PLoS ONE* 9: e106890.

Oral communications—Neuropharmacology

OC011 | Mutant mice expressing an internalisation-resistant form of CB₁R display enhanced cannabinoid tolerance

Daniel Morgan; Angela Hendeson Redmond; Malabika Maulik; Mary Piscura; Kayla DeSchepper; Courtney Lulek

Marshall University

Introduction/Background & aims: Although cannabinoids such as delta-9-tetrahydrocannabinol (Δ^9 -THC) exhibit clinical efficacy in pain, tolerance to the antinociceptive effects develops with repeated treatment. The focus of our work is to investigate the mechanisms responsible for the acute response and tolerance to different cannabinoid agonists. We previously found that tolerance to cannabinoids is reduced in S426A/S430A mutant mice expressing a desensitisation-resistant form of cannabinoid receptor 1 (CB₁R) that disrupts the classic mechanism of G protein-coupled receptor kinase (GRK)/ β arrestin2-mediated CB₁R desensitisation [1]. The objective of our current work is to assess the role of CB₁R internalisation and trafficking on cannabinoid tolerance. This objective will be achieved using a novel six-point mutant mouse strain expressing an internalisation-resistant form of CB₁R that was recently produced in our laboratory.

Method/Summary of work: Knock-in mice were produced that express serine/threonine to alanine point mutations for six putative G protein-coupled receptor kinase (GRK) phosphorylation sites in the distal C-terminus of CB₁R that are required for the efficient internalisation of the receptor in transfected cells. The acute response to CP55,940 was assessed by performing cumulative dose response curves. Antinociception was measured using the tail-flick and hotplate tests, while cannabinoid-induced hypothermia was assessed by measuring core body

temperature. Tolerance to the antinociceptive and hypothermic effects of once daily injections of 0.6 mg/kg CP55,940 was determined.

Results/Discussion: We find that the maximal acute effect for CP55,940 on hypothermia and tail-flick antinociception is reduced in six point mutant mice relative to wild-type littermate controls. We also find a shorter duration for the acute hypothermic effects of CP55,940 in six-point mutant mice. Previous work has demonstrated that β arrestin2-mediated desensitisation of CB₁R modulates the magnitude and duration of acute responses for cannabinoids [1]. Six-point mutant mice also display enhanced tolerance to the antinociceptive and hypothermic effects of 0.6 mg/kg CP55,940 relative to wild-type littermate controls.

Conclusion(s): This work establishes six-point mutant mice as a novel model to study the role of CB₁R internalisation, trafficking and resensitization in vivo. Preliminary data show that cannabinoid tolerance is increased in six-point mutant suggesting that the normal processes of internalisation, traffickly and resensitization of CB₁R might play an important role in counteracting the development of cannabinoid tolerance.

REFERENCE(S)

1. Morgan DJ, Davis, BJ, Kearns, CS, Marcus DJ, Cook AJ, Wager-Miller J, Straiker AS, Myoga, MH, Stuart J, Sim-Selley LJ, Czyzyk, TA, Bradshaw, HB, Selley, DA, Mackie K. (2014) Mutation of putative GRK phosphorylation sites in the cannabinoid receptor 1 (CB1) confers resistance to cannabinoid tolerance and hypersensitivity to cannabinoids in mice. *Journal of Neuroscience*. 34: 5152–5163.

OC012 | Immunohistochemical evidence that paroxetine discontinuation in mice is associated with increased activation of 5-HT neurons

Helen M. Collins¹; Raquel Pinacho²; David Bannerman²; Trevor Sharp²

¹Department of Pharmacology, Oxford University; ²University of Oxford

Introduction/Background & aims: Abrupt cessation of selective serotonin reuptake inhibitor (SSRI) treatment is often associated with a discontinuation syndrome including symptoms such as high anxiety [1]. Recently, we detected increased anxiety-like behaviour in mice 2 days after discontinuation from repeated paroxetine treatment [2]. Since increased anxiety is associated with 5-HT neuron activation, here we investigated the effect of paroxetine discontinuation on the expression of the activity-dependent gene *c-Fos* in 5-HT neurons.

Method/Summary of work: Adult male C57BL/6 mice ($n = 12$ /group) were administered paroxetine (10 mg/kg s.c., once-daily) or saline vehicle for 12 days, then paroxetine was either continued or discontinued for 2 or 5 days. Mice were tested on the elevated plus maze (EPM) prior to collection of perfusion-fixed brains 90 min later. Cryostat-cut sections of the dorsal raphe nucleus (DRN) were immunohistochemically stained for *c-Fos*, tryptophan hydroxylase (TPH2; 5-HT neuron marker) and NeuN (neuron marker) ($n = 5-7$ /group). Mounted sections were imaged using epifluorescence microscopy, and

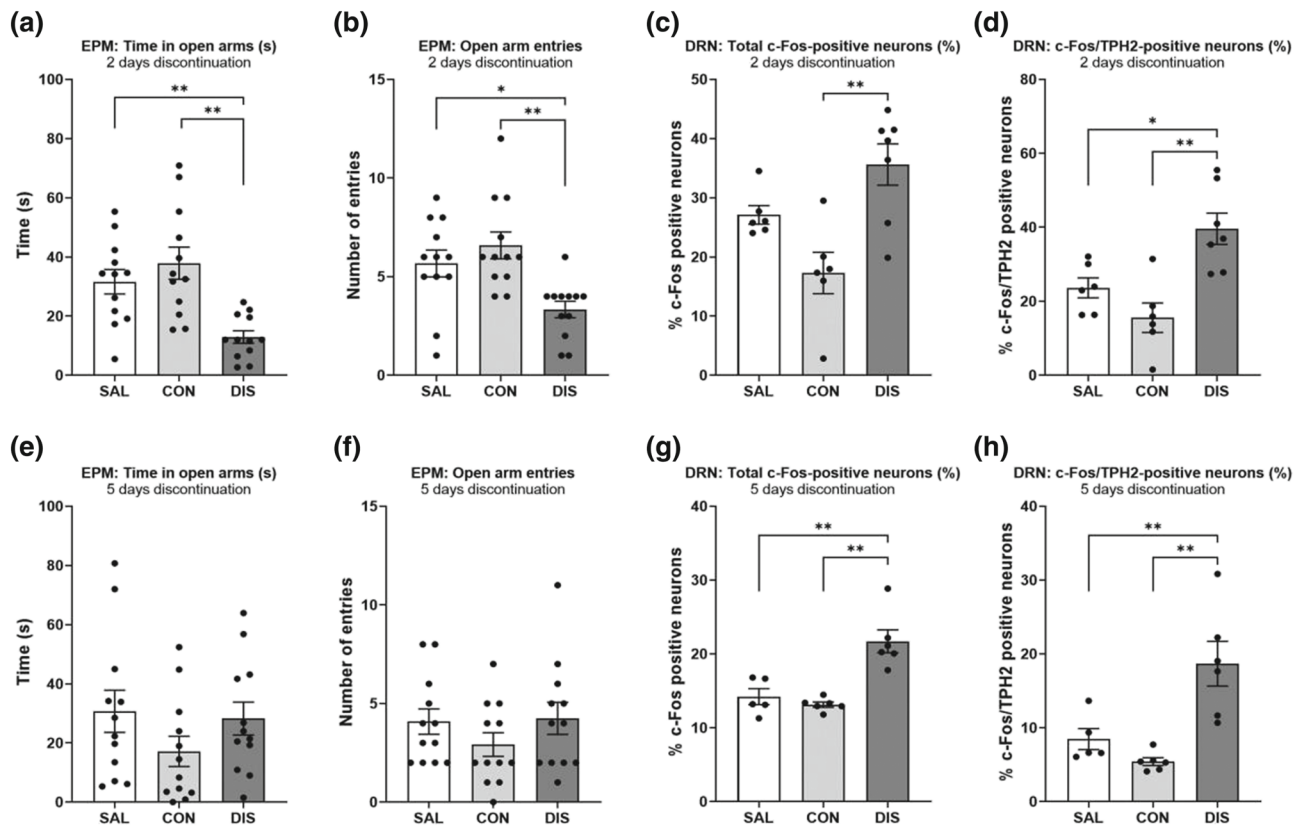


FIGURE 1 Effect of paroxetine discontinuation for either 2 days (a–d) or 5 days (e–h) on anxiety-like behaviour on the EPM ($n = 12/\text{group}$) and c-Fos immunoreactivity in the DRN ($n = 5\text{--}7/\text{group}$). For 2 days discontinuation: (a) time spent in open arms (main effect $F[2,33] = 9.902$, $p < .001$), (b) open arm entries (main effect $F(2,33) = 7.608$, $p = .002$), (c) percentage of c-Fos-positive neurons (main effect $F(2,16) = 9.089$, $p = .002$) and (d) number of c-Fos/TPH2-positive double-labelled neurons (main effect $F(2,16) = 10.85$, $p = .001$). For 5 days discontinuation: (e) time spent in open arms (main effect $F(2,33) = 1.451$, $p = .249$), (f) open arm entries (main effect $F(2,33) = 1.100$, $p = .345$), (g) number of c-Fos-positive neurons (main effect $F(2,14) = 18.17$, $p < .001$) and (h) number of c-Fos/TPH2-positive double-labelled neurons (main effect $F(2,14) = 12.40$, $p = .001$). Bars represent mean \pm SEM values for saline (SAL), continued paroxetine (CON) and discontinuation (DIS) groups, with dots representing individual mice. * $p < .05$, ** $p < .01$

c-Fos- and TPH2-positive neurons were quantified by an observer blind to treatment using ImageJ (NIH). Between-subject differences were assessed using one-way ANOVA with Tukey's post hoc test.

Results/Discussion: Two days after paroxetine discontinuation, mice exhibited increased anxiety-like behaviour on the EPM, evident as reduced time in the open arms and open arm entries (Figure 1a,b) compared with continued paroxetine and saline controls. Paroxetine discontinuation was associated with an increased percentage of c-Fos-positive neurons compared with continued paroxetine (Figure 1c) and increased c-Fos/TPH2-positive double-labelled neurons compared with continued paroxetine and saline controls (Figure 1d). Five days after paroxetine discontinuation, there were no effects of treatment on EPM performance (Figure 1e,f) but still an increased percentage of c-Fos-positive neurons (Figure 1g) and c-Fos/TPH2-positive double-labelled neurons (Figure 1h). Paroxetine discontinuation did not change the overall number of TPH2-positive neurons or the percentage of c-Fos-positive TPH2-negative neurons.

Conclusion(s): Two days of paroxetine discontinuation increased anxiety-like behaviour in mice, which was associated with c-Fos immunohistochemical evidence of increased 5-HT neuron activation.

While the latter effect remained 5 days after discontinuation, no change in anxiety-like behaviour was detected at this point. The current data therefore suggest a persistent increase in 5-HT neuron excitability following paroxetine discontinuation that is only partially tracked by measures of anxiety.

REFERENCE(S)

1. Davies J, Read J. A systematic review into the incidence, severity and duration of antidepressant withdrawal effects: Are guidelines evidence-based? *Addictive Behaviours*. 2019;97:111–121.
2. Collins HM, Pinacho R et al. Effect of SSRI discontinuation on anxiety-like behaviours in mice. *bioRxiv*. 2021.05.29.446266.

OC013 | The MIDAS motif of the voltage-gated calcium channel CACHD1 subunit contributes to protein trafficking

Maria Roznovcova¹; Paul Wright²; Graeme Cottrell¹; Gary Stephens¹

¹University of Reading; ²LifeArc Ltd

Introduction/Background & aims: Voltage-gated calcium channels (VGCCs) play a crucial role in the regulation of intracellular calcium. Dysfunction of such regulation is associated with different disease states, including pain. Moreover, auxiliary subunits of high-voltage-activated (HVA) VGCCs are targets for gabapentinoids, widely used as therapeutic agents in pain. There was little evidence of modulation of low-voltage-activated (LVA) VGCCs (T-type) by auxiliary subunits; however, we recently identified CACHD1 (calcium channel and chemotaxis receptor domain containing protein 1) as a modulator of Ca_v3, T-type LVA VGCCs [1]. α 2 δ (HVA VGCC subunit) and CACHD1 contain von Willebrand Factor A (VWA) domains. The α 2 δ VWA domain contains a MIDAS (metal ion-dependent adhesion site) motif (D¹¹²xSxS), shown to be essential for the trafficking and synaptic function of HVA VGCCs [2].

Method/Summary of work: Here, we examined the effects of MIDAS motif mutations on the expression and trafficking of CACHD1 in HEK293 cells stably expressing Myc-tagged CACHD1 constructs. For the CACHD1-AAA construct, the variant CACHD1 MIDAS motif (D²³⁴xGxS) was mutated by PCR at 3 key residues (D234A, G236A, S238A). For the CACHD1-G236S construct, a single mutation (G236S) generated the same MIDAS motif as in α 2 δ . Immunocytochemistry (ICC) was performed using rabbit anti-Myc (1:500, live cells), mouse anti-Myc (1:500, fixed cells) and AlexaFluor 488 and 546 (1:1000) antibodies ($n = 5$). Expression levels of CACHD1 were characterised by western blotting and densitometry ($n = 5$); statistical significance was determined using ANOVA followed by Tukey's post hoc tests on raw data.

Results/Discussion: ICC showed that CACHD1-wt and CACHD1-G236S were localised to the cell surface and intracellular vesicles, whereas CACHD1-AAA was largely localised to intracellular vesicles. In expression studies, a significant reduction in total CACHD1 levels was seen for CACHD1-AAA (27 \pm 6.8% vs. CACHD1-wt, mean \pm SEM, $P < .05$); there was no significant change for CACHD1-G236S (93 \pm 4.2% vs CACHD1-wt, mean \pm SEM).

Conclusion(s): We identify significant differences in our measured parameters for the 'AAA' MIDAS mutation, suggesting that the MIDAS motif contributes to expression pattern and trafficking of CACHD1, as also reported for the fully conserved MIDAS motif in α 2 δ subunits.

REFERENCE(S)

- Cottrell, GS, Soubrane, CH, Hounshell, JA, Lin, H, Owenson, V, Rigby, M, Cox, PJ, Barker, BS, Ottolini, M, Ince, S, Bauer, CC, Perez-Reyes, E, Patel, MK, Stevens, EB, Stephens, GJ (2018). CACHD1 is an α 2 δ -like protein that modulates Ca_v3 voltage-gated calcium channel activity. *The Journal of Neuroscience*, 38, 9186–9201.
- Hoppa, MB, Lana, B, Margas, W, Dolphin, AC, & Ryan, TA (2012) α 2 δ expression sets presynaptic calcium channel abundance and release probability. *Nature*, 486, 122–125.

OC014 | Reduced long-term motor impairment after delayed systemic amnion epithelial cell therapy in a mouse model of chronic stroke

Chris Sobey

La Trobe University

Introduction/Background & aims: Stroke is a major global health issue, especially in the aged, and yet has limited treatment options for long-term recovery. We have found that intravenous (i.v.) infusion of human amnion epithelial cells (hAECs) exerts beneficial effects when given within 2 h after stroke onset in mice, by limiting brain injury and inflammation, and reducing functional impairment [1]. Here, we tested the hypothesis that administration of hAECs at 1 day or 7 days after ischaemic stroke promotes long-term recovery of motor impairment in aged mice.

Method/Summary of work: Female C57Bl6 mice (13–16 months old, $n = 31$) received photothrombotic stroke in the left primary motor cortex under inhaled isoflurane anaesthesia (1%–5% in O₂). At 1 day or 7 days after stroke, mice received either vehicle (saline, $n = 15$) or 1×10^6 hAECs ($n = 16$) i.v. Motor function was assessed prior to surgery and at 1 week and 8 weeks poststroke as asymmetry of left versus right forepaw preference using the cylinder task. hAECs were isolated from placentas donated by healthy volunteers who underwent elective Caesarean section delivery. All procedures using animals and human tissues were approved by La Trobe University Ethics Committees in compliance with the National Health and Medical Research Council of Australia requirements.

Results/Discussion: Mice treated with hAECs at 1 day after stroke tended to exhibit milder motor impairment at 1 week ($n = 10$, 27 \pm 6%) than vehicle-treated controls ($n = 8$, 43 \pm 10%; $P = .09$, Student's paired t test), but by 8 weeks, there was clearly no effect of hAECs therapy (42 \pm 11% vs. 37 \pm 10%). By contrast, mice treated with hAECs at 7 days poststroke ($n = 6$) exhibited milder (~60%) motor impairment than vehicle-treated controls ($n = 7$) after 8 weeks (15 \pm 5% vs. 39 \pm 8%; $P < .05$).

Conclusion(s): These findings suggest that systemic administration of hAECs may reduce long-term motor impairment even when administered in the chronic phase of ischaemic stroke.

REFERENCE(S)

- Evans MA, Lim R, Kim H-A, Chu HX, Gardiner-Mann CV, Taylor KWE, et al. (2018). Acute or delayed systemic administration of human amnion epithelial cells improves outcomes in experimental stroke. *Stroke* 49:700–709.

OC015 | [Arg⁸]-vasopressin and adrenaline act in synergy to increase spontaneous myogenic contractile activity of human isolated stomach: Potential role in nausea

Raj Makwana¹; Ellie Crawley¹; Marilisa Straface¹; Armen Gharibans²; Kalpana Devalia³; John Loy³; Greg O'Grady²; Paul L. R. Andrews⁴; Gareth Sanger¹

¹Queen Mary University of London; ²University of Auckland; ³Homerton Hospital; ⁴St George's University of London

Introduction/Background & aims: Rhythmic electrical activity of human stomach, generated by interstitial cells of Cajal (ICC), becomes

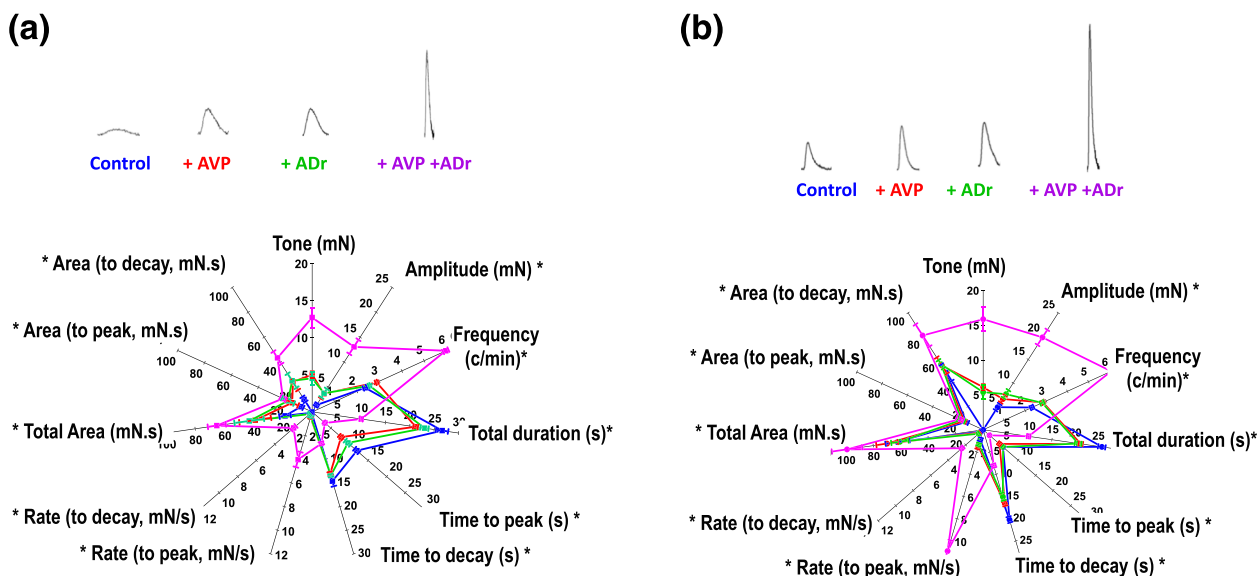


FIGURE 1 Spontaneous contraction waveform and its features of human (a) proximal and (b) distal stomach circular muscle before (baseline) and after AVP (10^{-9} M), ADR (10^{-9} M) or co-application of AVP (10^{-9} M), ADR (10^{-9} M). Also shown is the increase in muscle tone. $n = 4$. Concentrations of both hormones approximately equivalent to their EC_{75} . Data are mean \pm S.E.M. $n = 4$.

irregular during nausea¹, also associated with raised plasma [Arg⁸]-vasopressin (AVP) and adrenaline (ADr)². We hypothesised that AVP and ADr act on the stomach during nausea.

Method/Summary of work: Contractions of circular muscle from proximal (fundus-proximal corpus) and distal (distal corpus-antrum) human isolated stomach (3 male, 13 female; 23–67 years; sleeve gastrectomy; written informed consent) were recorded, quantified (custom software; <https://github.com/agheribans/GISMCA>) and displayed as RADAR plots. Changes in parameters were compared with baseline values. Data are mean \pm s.e.m. V_{1A} and α_1 -adrenoceptor co-localisation with c-Kit (ICC) and α -smooth muscle actin (muscle) was determined using immunofluorescence in paraffin-embedded sections of distal stomach (3:3 male: female; 40–59 years) using optimised primary-secondary antibody concentrations and DAPI nuclei counterstaining.

Results/Discussion: Spontaneous contractions of proximal and distal stomach were tetrodotoxin (10^{-6} M) insensitive ($n = 4$) of similar duration and frequency but $70.4 \pm 1.8\%$ smaller in proximal stomach ($P < .001$; $n = 8$; Figure 1a,b). Proximal stomach contractions developed and decayed with comparable rates, whereas those of distal stomach peaked $\sim 5\times$ faster, decaying more slowly. AVP (10^{-12} to 10^{-5} M; $pEC_{50} \sim 8.5$; $n = 4$) increased muscle tone, amplitude and frequency of contractions, respectively, increasing and decreasing the rate and duration of contraction development and decay (Figure 1a,b); these actions were antagonised by SR49059 (10^{-9} to 10^{-7} M; V_{1A} receptor antagonist; $pK_B \sim 9.5$; $n = 4$). ADr increased muscle tone ($pEC_{50} \sim 9.4$; reduced by prazosin: $pA_2 \sim 9.5$) followed by relaxation at $\geq 10^{-6}$ M (abolished by propranolol) and enhanced (10^{-10} to 10^{-5} M; $pEC_{50} \sim 8.6$) or reduced (10^{-4} M) amplitude and frequency of spontaneous contractions. AVP 10^{-9} M and ADr 10^{-8} M together (concentrations $\sim 75\%$ maximum) caused synergistic augmentation of muscle tone, amplitude, frequency and rate of contractions (Figure 1a,

b). The pattern of synergy was similar in both stomach regions, although magnitudes differed. V_{1A} and α_1 -adrenoceptor immunofluorescence was detected on, respectively, $69.4 \pm 12.5\%$ and $61.1 \pm 3.5\%$ of ICC (c-Kit+ with irregular processes from cell bodies, not stained by mast cell tryptase) and 100% and $44.5.1 \pm 18.1\%$ of muscle cells (α SMA+) (mean of three ICC or muscle cells, each; $n = 6$).

Conclusion(s): We hypothesise that low concentrations of AVP and ADr act together, creating a ‘tipping point’ at which stimulation of gastric contractions is signalled to the brain for interpretation as nausea.

REFERENCE(S)

- O'Grady G, Gharibans AA., Du P, Huizinga JD. The gastric conduction system in health and disease: A translational review. *The American Journal of Physiology* 2021;321:G527–G542.
- Stern RM, Koch KL., Andrews PLR. *Nausea: Mechanisms and management*. Oxford University Press, 2011, NY:USA.

Oral communications—Toxicology

OC006 | *In vitro* and *in silico* studies of interactions of cathine on 11 major human drug metabolising cytochrome P450 (CYP) enzyme activities

Sharoen Yu Ming Lim¹; Jason Siau Ee Loo²;
 Mustafa Ahmed Alshagga¹; Mohamed Abdullah Alshawsh³;
 Chin Eng Ong⁴; Yan Pan⁵

¹University of Nottingham; ²Taylor's University; ³Universiti Malaya;

⁴International Medical University; ⁵University of Nottingham

Introduction/Background & aims: We have identified that khat and its major compound, cathinone, showed *in vitro* inhibitory effects on human drug metabolising CYPs which suggested the possible khat-and/or cathinone-drug interactions when taken concurrently with medications [1–3]. We extended this research on cathine's (the stable-form of cathinone) inhibitory effects on CYP1A2, CYP2A6, CYP2B6, CYP2C8, CYP2C9, CYP2C19, CYP2D6, CYP2E1, CYP2J2, CYP3A4, CYP3A5 and *in silico* identification of their type of interactions and residues involved.

Method/Summary of work: Reversible inhibitory and time-dependent assays were performed in triplicate to determine all 11 CYPs enzyme activities via fluorescence-based assays using recombinant cDNA-expressed human CYPs in Vivid® P450 screening kits. The K_i values

were determined by secondary plots of cathine concentrations against slopes of Lineweaver–Burk plots and nonlinear regression using GraphPad Prism 9. Docking studies were performed on cathine with CYP2A6 and CYP3A4 following their inhibition *in vitro*. The top-ranked binding modes and protein-ligand interactions were visualised with PyMOL Molecular Graphics system.

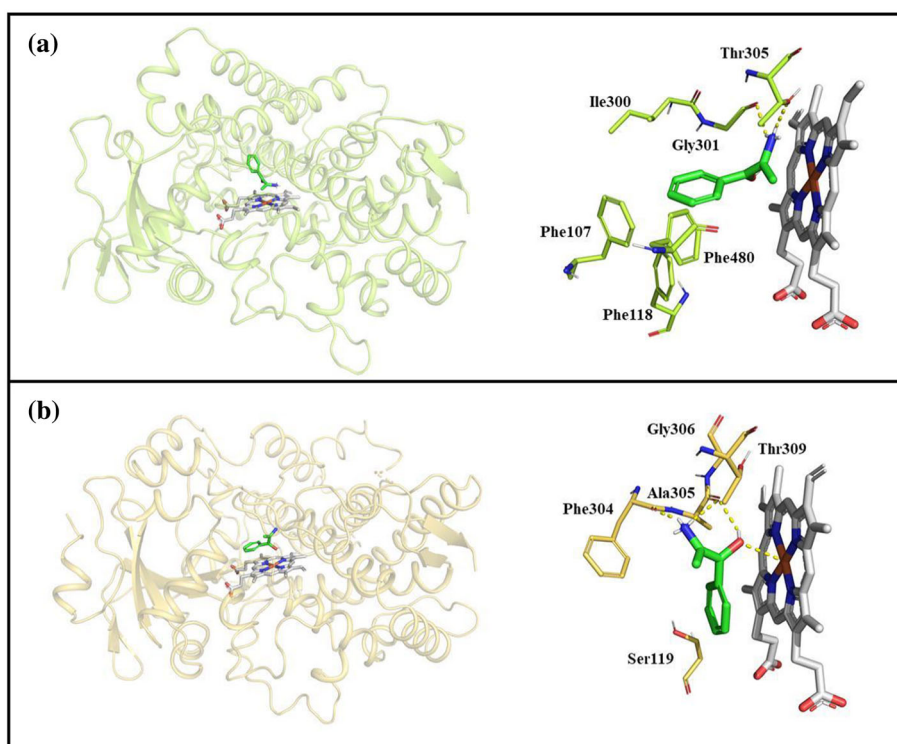
Results/Discussion: The half maximal inhibitory concentration (IC_{50}) values of cathine determined for CYP2A6 and CYP3A4 were 80 and 90 μM , while other nine CYPs showed no significant inhibition. IC_{50} less than 100 μM is considered as significant inhibition. Cathine reversibly inhibited CYP2A6 and CYP3A4 via noncompetitive modes with inhibition constant (K_i) values of 63 and 100 μM respectively. Cathine showed negligible time-dependent inhibition on all 11 CYPs.

TABLE 1 IC_{50} without/with NADPH in pre-incubation and IC_{50} shift of CYP1A2, CYP2A6, CYP2B6, CYP2C8, CYP2C9, CYP2C19, CYP2D6, CYP2E1, CYP2J2, CYP3A4 and CYP3A5 with cathine

CYP isoform	IC_{50} without NADPH (μM)	IC_{50} with NADPH (μM)	IC_{50} shift
CYP1A2	285	255	1.12
CYP2A6	80	70	1.14
CYP2B6	>100	>100	-
CYP2C8	>100	>100	-
CYP2C9	Not determined	Not determined	-
CYP2C19	Not determined	Not determined	-
CYP2D6	435	860	0.51
CYP2E1	Not determined	Not determined	-
CYP2J2	Not determined	Not determined	-
CYP3A4	90	Not determined	-
CYP3A5	>1000	Not determined	-

^aNot determined—the curve plateaus above the 50% half maximal inhibitory line.

FIGURE 1 Molecular docking demonstrating binding modes and key interactions of cathine (green) relative to the haem group (white) in the active sites of (a) CYP2A6 (PDB 2FDV) and (b) CYP3A4 (PDB 4D75). Hydrogen bonds are displayed as yellow dashed lines. Nonpolar hydrogens have been removed for visual clarity. Cathine interacted with CYP2A6 via three hydrophobic interactions with Ile300, Thr305 and Phe480; hydrogen bonding with Gly301 and Thr305; and π -stacking with Phe107 and Phe118. Cathine formed four hydrophobic interactions with Ser119, Ala305, Gly306 and Thr309 and hydrogen bonding with Phe304 and Ala305 with CYP3A4.



Further, *in silico* studies showed that cathine was bound to CYP2A6 via hydrophobic, hydrogen and π -stacking interactions and formed hydrophobic and hydrogen bonds with active site residues in CYP3A4.

Conclusion(s): We identify that khat consumption may result in inhibition of CYP2A6 and CYP3A4 through its stable active component, cathine, with potential clinically significant implications to users who may be taking prescribed medications that are metabolised by these CYPs. Both molecular docking prediction and *in vitro* outcome are in agreement, granting more comprehensive insights for envisaging CYPs metabolism and possible cathine–drug interactions. Therefore, it would be best for healthcare experts to be aware of the potential khat/cathine–drug interactions during their prescribing, either by advising abstinence or adjusting their prescribing accordingly.

REFERENCE(S)

1. Lim SYM, Binti Azidin AR, Ung YT, et al. Effect of 95% ethanol Khat extract and cathinone on *in vitro* human recombinant cytochrome P450 (CYP) 2C9, CYP2D6, and CYP3A4 activity. *European Journal of Drug Metabolism and Pharmacokinetics* 2019;44(3):423–431. <https://doi.org/10.1007/s13318-018-0518-2>
2. Lim SYM, Alshagga MA, Alshawsh MA, Ong CE, Pan Y. *In vitro* effects of 95% khat ethanol extract (KEE) on human recombinant cytochrome P450 (CYP) 1A2, CYP2A6, CYP2B6, CYP2C8, CYP2C19, CYP2E1, CYP2J2 and CYP3A5. *Drug Metab Pers Ther.* 2021;37(1). doi:<https://doi.org/10.1515/dmpt-2021-1000196>
3. Lim SYM, Loo JSE, Alshagga M, Alshawsh MA, Ong CE, Pan Y. *In vitro* and *in silico* studies of interactions of cathinone with human recombinant cytochrome P450 CYP(1A2), CYP2A6, CYP2B6, CYP2C8, CYP2C19, CYP2E1, CYP2J2, and CYP3A5. *Toxicol Reports.* 2022;9-(March):759–768. <https://doi.org/10.1016/j.toxrep.2022.03.040>

OC007 | Patients with naproxen-induced liver injury display T-cell memory responses towards an oxidative (S)-O-desmethyl naproxen metabolite

Paul Thomson¹; Laila Kafu¹; Nikolaos Fragkas²; Thomas Hammond³; Guruprasad Aithal⁴; Maribel Lucena⁵; Xiaoli Meng⁶; Munir Pirmohamed¹; Michael Kammüller²; Gerd Kullak-Ublick²; Dean Naisbitt¹

¹University of Liverpool; ²Novartis; ³AstraZeneca; ⁴Nottingham Digestive Disease Centre; ⁵Universidad de Málaga; ⁶University of Liverpool

Introduction/Background & aims: Naproxen is an NSAID commonly used in the treatment of mild to moderate pain. Similar to several other carboxylic acid drugs, naproxen is associated with rare but potentially serious immune-mediated hepatotoxicity. The intrinsic chemical stability and protein reactivity of acyl glucuronide metabolite has led to their postulated association as haptens, causal for these hepatic reactions. However, evidence for acyl glucuronidation as a metabolic pathway of immunological consequence is lacking.

Aim: The aim of this study is to investigate whether naproxen liver injury patients exhibit immunological memory towards naproxen and its major acyl glucuronide and desmethyl metabolites.

Method/Summary of work: Lymphocyte transformation test and IFN-g ELISpot were conducted on PBMCs of patients with naproxen-induced liver injury and alongside controls. Drug-responsive T-cell clones were generated to naproxen and its metabolites and tested for drug specificity, phenotype/function, and pathways of T-cell activation. Mass spectrometry was used to measure degradation of naproxen acyl glucuronide and characterise the generated drug modified albumin adducts.

Results/Discussion: Naproxen acyl glucuronide degraded spontaneously in buffer and albumin solution. Albumin binding was time- and concentration-dependent. CD4 + and CD8 + T-cells from patients expressing a range of different Vb receptors were stimulated to proliferate and secrete IFN-g and IL-22 when exposed to the desmethyl metabolite of naproxen but not the parent drug, the acyl glucuronide or acyl glucuronide adducts. Activation of the CD4 + TCC was MHC class II HLA-DQ-restricted and dependent on antigen presenting cells. Most T-cell clones with were activated with drug pulsed APC, while fixation of APC blocked the T cell response. Cross-reactivity was not observed with structurally-related drugs.

Conclusion(s): Our results show a T-cell memory response towards the stable desmethyl metabolite of naproxen thereby suggesting firstly, an overall immune-mediated basis for the adverse event and secondly, the oxidative desmethyl metabolite of naproxen to drive the T-cell antigenicity. While the FDA considers acyl glucuronide adduction of protein to be responsible for the liver reactions associated with carboxylic acid drugs, we found no evidence of this with respect to naproxen.

OC008 | Alpha-naphthylisothiocyanate (ANIT) induced changes of miR-200 family in serum and liver of CD-1 mice suggests potential as novel bile duct injury markers

Joseph Brown¹; Lawrence Howell²; Shiva Seyed Forootan¹; Christopher Goldring¹

¹University of Liverpool; ²GSK

Introduction/Background & aims: Joseph Brown, Lawrence Howell, Shiva Seyed Forootan, Christopher Goldring.

Introduction: Cholangiocyte damage is a common feature of mixed/cholestatic drug-induced liver injury (DILI). Progression to chronic liver injury is most likely with cholestatic DILI [1], which is diagnosed using R-value scores that rely upon poorly sensitive and nonspecific ALT/ALP. Novel DILI biomarkers include hepatocyte-enriched miR-122 [2]; however, fewer miRs have been proposed as markers of biliary injury. Our aim is to use an *in vivo* model of xenobiotic bile duct injury [3] to assess a panel of cholangiocyte-enriched miRs that could act as selective markers of biliary injury.

Method/Summary of work: Cholangiocytes and hepatocytes were isolated from CD-1 mice via two-step liver perfusion/digestion and

population purity was validated by immunofluorescence. Global profiles of extracted miRNA were evaluated through Microarray technology. CD-1 mice were later orally administered single-dose 75 mg/kg ANIT in corn-oil vehicle. miRNA was isolated from liver and serum of untreated and treated animals ($n = 5/\text{group}$) at four time-points, with serum ALP and ALT also measured. RT-qPCR was used to measure

candidate miR biomarkers in serum and liver. Western blotting was performed to assess biliary injury at the protein level. Haematoxylin and eosin staining provided phenotypic anchoring.

Results/Discussion: Microarray profiles facilitated identification of miRs more selectively expressed in cholangiocytes versus hepatocytes with relatively high abundance (Figure 1).

FIGURE 1 Healthy cholangiocytes and hepatocytes were isolated from CD-1 mice using a two-step liver perfusion and digestion method followed by cholangiocyte cell selection using Ep-CAM labelled magnetic beads. Global RNA profiles were evaluated by SurePrint Mouse miRNA Microarray (Release 21.0). Shared miRNAs with cholangiocyte enrichment were plotted as basal gene expression against their Log2 fold change expression in hepatocytes. This allowed selection of cholangiocyte-enriched miR-200 family –200a, –200b, –200c, –141 and –429 as candidate biomarkers.

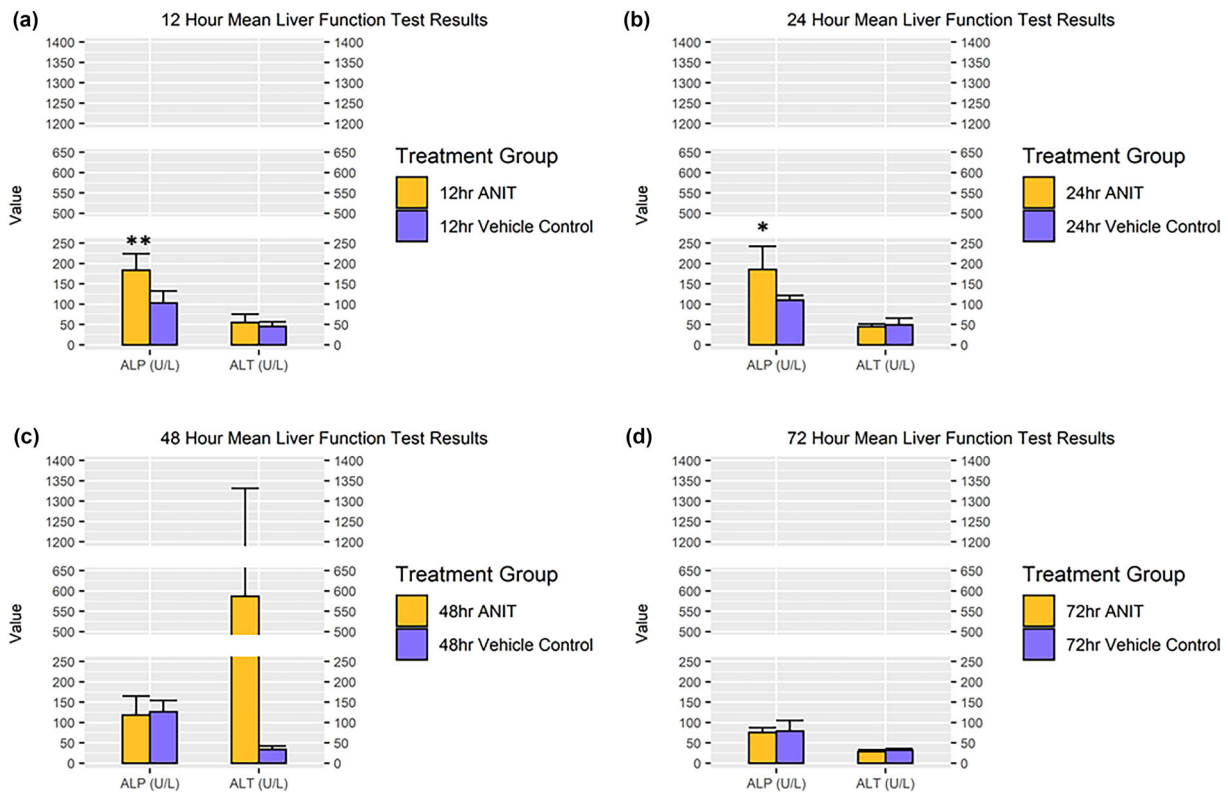
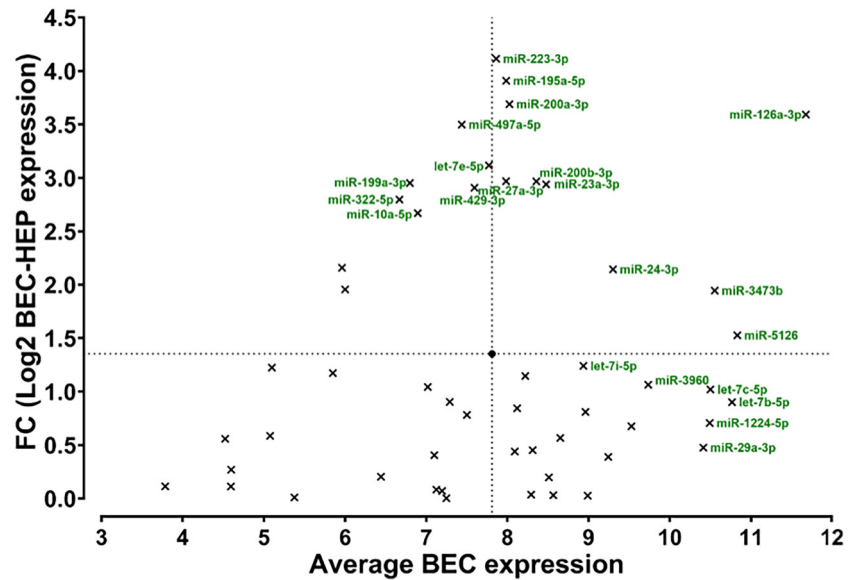


FIGURE 2 Following in vivo model optimization, CD-1 mice were treated with oral single-dose 75 mg/kg ANIT. Serum ALP and ALT were measured. group mean values in ANIT and corn oil groups are shown at (a) 12- (b) 24-, (c) 48- and (d) 72-h postdose. ALP is significantly increased in 12- and 24-h ANIT cohorts. * = $P \leq .05$, ** = $P \leq .01$. ALT is increased in the 48-h ANIT cohort, but large variability within the group is highlighted by high standard deviation.

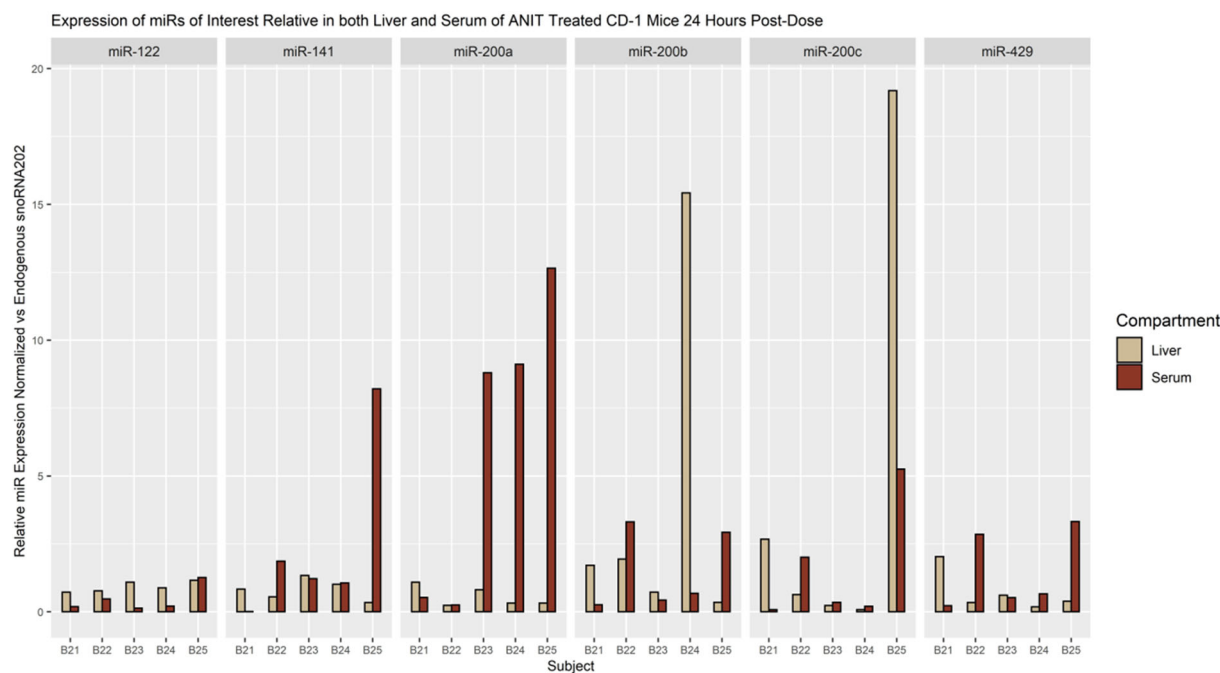


FIGURE 3 Each member of the 24-h treated cohort sees ≥ 2 -fold increase in at least one miR-200 family member in serum or liver.

ALP was significantly increased in serum of treated 12- ($P < .01$) and 24-h ($P < .05$) cohorts (Figure 2.). Significant upregulation of biliary-associated proteins in liver was evident for CFTR 12-h post-dose ($P < .01$) and FXR 24-h postdose ($P < .001$).

miR-200 family showed serum increases in members of treated cohorts within 24 h, with no major changes in miR-122 seen before 48 h.

The 24-h ANIT cohort animals all showed an increase in liver or serum for at least one miR of interest (Figure 3).

Conclusion(s)

- miR-200 family members increase in some CD-1 mice following single-dose ANIT, prior to hepatocyte-enriched miR-122.
- Increases are seen in some animals whose ALP < DILI threshold.
- Panel of cholangiocyte-enriched miRs could aid ALP in pre-clinical/clinical identification of mixed/cholestatic DILI.

REFERENCE(S)

1. Church RJ, Watkins PB. Serum biomarkers of drug-induced liver injury: Current status and future directions. *Journal of Digestive Diseases* 2019; 20(1):2–10.
2. Llewellyn HP, Vaidya VS, Wang Z, et al. Evaluating the sensitivity and specificity of promising circulating biomarkers to diagnose liver injury in humans. *Toxicological Sciences* 2021;181(1):23–34.
3. Li X, Liu R, Yu L, et al. Alpha-naphthylisothiocyanate impairs bile acid homeostasis through AMPK-FXR pathways in rat primary hepatocytes. *Toxicology* 2016;370:106–115.

OC009 | Differential effects of first- and second-generation nonnucleoside reverse transcriptase inhibitors efavirenz and rilpivirine on pancreatic β -cell mitochondria

Soulef Chahinez Maandi; Meriem Tinhinane Maandi; Jon Mabley
University of Brighton

Introduction/Background & aims: The nonnucleoside reverse transcriptase inhibitors (NNRTIs) are a central part surrounding the current guidelines on the management of HIV/AIDS. The first-generation NNRTI efavirenz and the second-generation NNRTI rilpivirine were both shown to increase intracellular oxidative stress in pancreatic β -cells, accompanied by mitochondrial toxicity [1]. Changes in mitochondrial membrane potential ($\Delta\psi_m$) were observed, as efavirenz was shown to decrease $\Delta\psi_m$, while rilpivirine increased $\Delta\psi_m$ in β -cells [1]. However, the mechanisms underlying the efavirenz- and rilpivirine-induced mitochondrial damage have not been elucidated yet. Therefore, the aim of this study was to investigate the effects of efavirenz and rilpivirine on central components of mitochondrial function in β -cells.

Method/Summary of work: The clonal rat β -cell line INS-1E was exposed to efavirenz (20 μ M) or rilpivirine (10 μ M) for 24 h before measuring mitochondrial ROS generation by flow cytometry following staining with mitoSOX and ATP levels by luminometry following reaction with luciferase. Uncoupling protein 2 (UCP2) mRNA expression

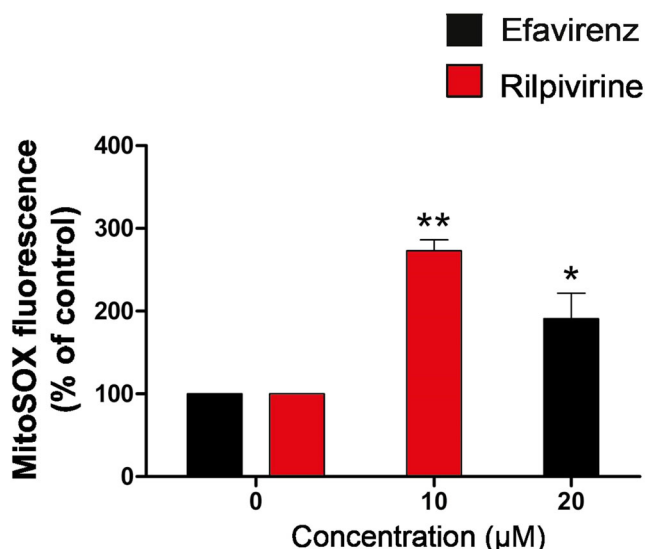


FIGURE 1 Efavirenz and rilpivirine increase mitochondrial ROS generation in INS-1E cells. INS-1E cells were exposed to efavirenz (20 μM) or rilpivirine (10 μM) for 24 h before quantifying mitochondrial ROS using the mitoSOX probe followed by flow cytometric analysis. MitoSOX fluorescence is proportional to the levels of mitochondrial ROS. Data are expressed as mean ± SD from n = 3 independent experiments. Statistically significant differences were determined using Kruskal–Wallis with Dunn's post hoc test. * p < .05, ** p < .01 significantly different from vehicle-treated control cells

levels were measured by RT-qPCR, and localisation of UCP2 was assessed by immunocytochemistry. Complex I activity was measured using spectrophotometry. Data are expressed as mean ± SD, and statistical analysis was carried out using one-way ANOVA and Bonferroni correction or Kruskal–Wallis with Dunn's post hoc test. P < .05 was considered as significant.

Results/Discussion: A 24-h exposure to efavirenz and rilpivirine increased mitochondrial ROS generation (Figure 1) and depleted ATP levels (Figure 2) in INS-1E cells. However, efavirenz, but not rilpivirine, directly inhibited complex I activity (Figure 3) and up-regulated UCP2 expression in INS-1E cells (Figure 4). UCP2 upregulation was previously associated with reductions in Δψm, a phenomenon previously seen with efavirenz [1] and potentially caused by its effect as a direct inhibitor of complex I activity in INS-1E cells. On the other hand, rilpivirine may directly inhibit another component of the electron transport chain, ATP synthase (complex V), hence directly inhibiting ATP generation in INS-1E cells.

Conclusion(s): In conclusion, both efavirenz and rilpivirine increased mitochondrial ROS generation and depleted ATP levels in pancreatic β-cells, likely via different mechanistic pathways. These differential mechanisms could shed light into potential pathological pathways involved in efavirenz- and rilpivirine-induced β-cell dysfunction and could help identify respective targets for protection against NNRTI-induced β-cell damage.

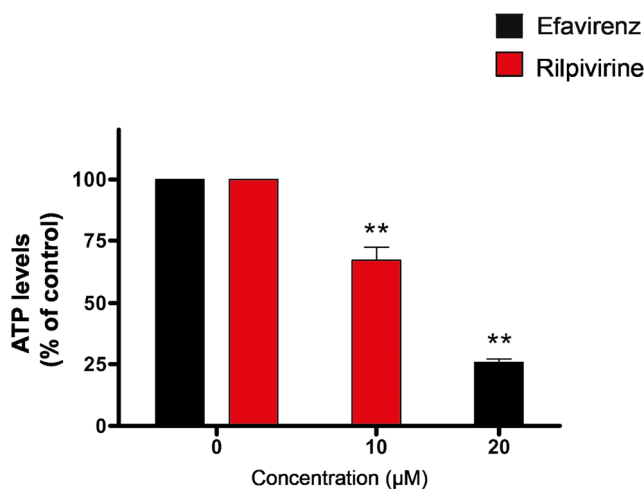


FIGURE 2 Efavirenz and rilpivirine decrease ATP levels in INS-1E cells. INS-1E cells were exposed to efavirenz (20 μM) or rilpivirine (10 μM) for 24 h before quantifying ATP levels using the luciferase reaction followed by luminometry. Data are expressed as mean ± SD from n = 3 independent experiments. Statistically significant differences were determined using Kruskal–Wallis with Dunn's post hoc test. ** p < .01, significantly different from vehicle-treated control cells

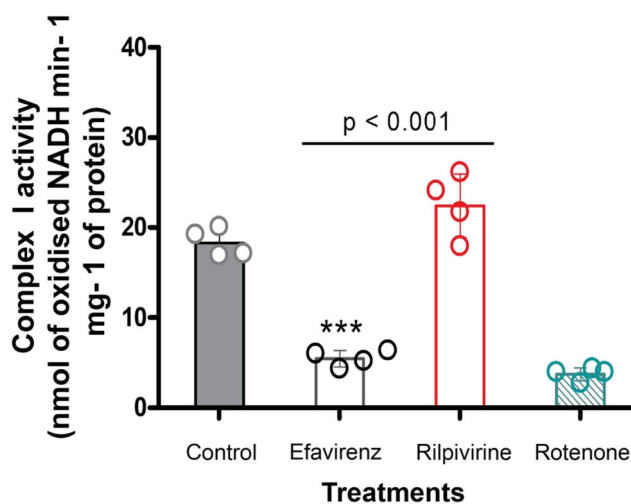


FIGURE 3 Efavirenz decreases complex I activity in mitochondria of INS-1E cells. Mitochondria were exposed to efavirenz (20 μM) or rilpivirine (10 μM) for 1 min before quantifying complex I activity using spectrophotometry. Rotenone (10 μM) was used as a positive control. Data are expressed as mean ± SD from n = 4 independent experiments. Statistically significant differences were determined using one-way ANOVA with Bonferroni post hoc test. *** p < .001, significantly different from vehicle-treated control cells.

REFERENCE(S)

1. Maandi, S. C., Maandi, M. T., Patel, A., Manville, R., & Mabley, J. (2022). Divergent effects of HIV reverse transcriptase inhibitors on pancreatic beta-cell function and survival: Potential role of oxidative stress and mitochondrial dysfunction. *Life Sciences*, [120329]. <https://doi.org/10.1016/j.lfs.2022.120329>

(a)

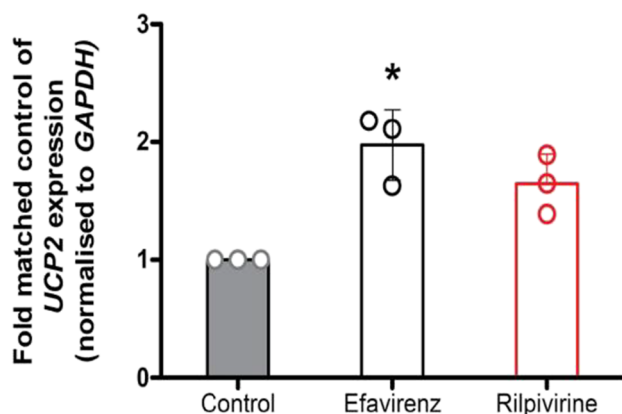
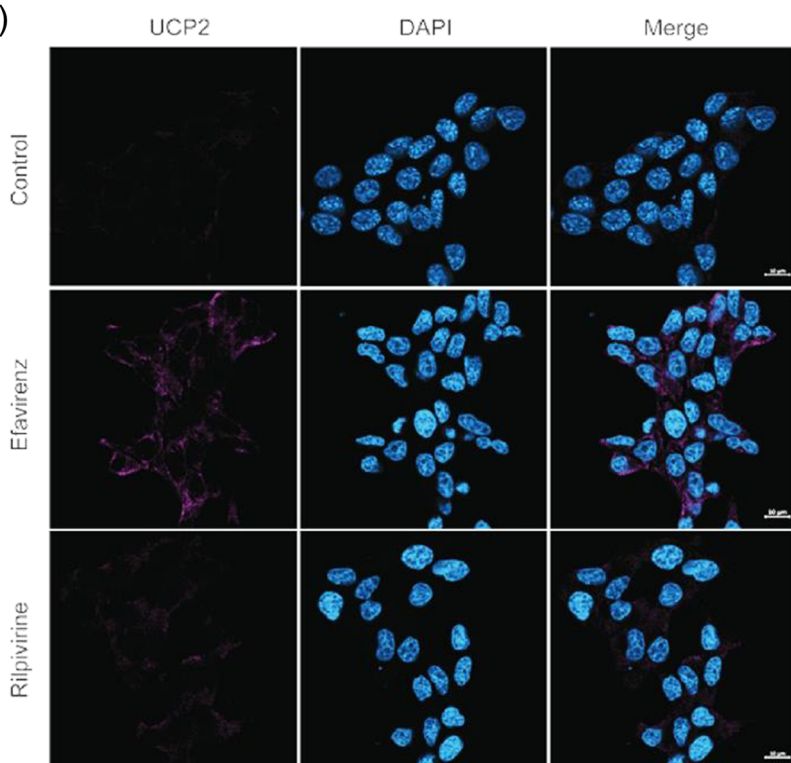


FIGURE 4 Efavirenz up-regulates UCP2 mRNA expression in INS-1E cells. INS-1E cells were exposed to efavirenz (20 μ M) or rilpivirine (10 μ M) for 24 h before quantifying UCP2 mRNA expression using qRT-PCR (a) and visualising UCP2 protein expression (violet) in INS-1E cells by immunocytochemical analysis (b). Data are expressed as mean \pm SD from $n = 3$ independent experiments. Statistically significant differences were determined using Kruskal-Wallis with Dunn's post hoc test. * $p < .05$, significantly different from vehicle-treated control cells. Scale bar, 10 μ m

(b)



OC010 | Investigating T cell responses to a major catechin found in green tea (epigallocatechin-3-O-gallate—EGCG) in healthy donors expressing HLA-B*35:01

James Line¹; Serat-E Ali²; Sophie Grice²; Dean Naisbitt²

¹The University of Liverpool; ²University of Liverpool

Introduction/Background & aims: Green Tea, derived from the *Camellia sinensis* plant, is a common constituent of many herbal supplements and is used globally. Green Tea extracts have been linked with immune-mediated idiosyncratic liver injury and associated with the expression of HLA-B*35:01. Epigallocatechin-3-O-gallate or 'EGCG' is the most abundant catechin found in green tea extracts and has been

implicated in the liver injury observed. This study utilises *in vitro* peripheral blood mononuclear cells (PBMC) and T-cell assays to investigate the immunogenicity of EGCG in healthy donors positive and negative for the HLA-B*35:01 risk allele.

Method/Summary of work: PBMC from HLA-B*35:01 positive and negative healthy donors were cultured with EGCG for 21 days. PBMCs were restimulated weekly with EGCG, IL-2 and irradiated autologous PBMCs before re-challenge and proliferative responses measured by [³H] thymidine incorporation. Naïve T cells and dendritic cells from random healthy donors were also cultured with EGCG for 12 days, rechallenged with EGCG in the presence of immune-checkpoint blockade in day 12 and a proliferative readout was taken on day 14. EGCG-responsive T cell clones (TCC) were generated from HLA-B*35:01 positive donors via serial dilution and repetitive mitogen stimulation. TCC were examined for specificity, phenotype, cytokine secretion and pathways of T cell activation.

Results/Discussion: Long-term PBMC cultures were interrogated for EGCG-specific priming. Significant proliferative responses were identified 2/4 donors from both allele positive and negative groups. EGCG-specific priming of naïve T cells was observed in random healthy donors in the presence of immune checkpoint inhibition; a marked increase in the number of wells demonstrating medium to severe proliferative responses was observed in the presence of PD-1 and PD-L1 but not CTLA-4 blockade. A number of EGCG-specific TCCs were identified from healthy donors expressing HLA-B*35:01. TCCs proliferated in a dose-dependent manner when stimulated with EGCG and secreted IFN γ , IL-5, IL-13 and Granzyme B. TCC had a CD4 + phenotype and demonstrated a chemokine profile (CCR9, CXCL3) which confers a Th2 subset. Activation of TCC was restricted to MHC Class II, more specifically HLA-DR.

Conclusion(s): These data suggest that EGCG has an intrinsic ability to be immunogenic and can effectively prime naïve T cells from both HLA-B*35:01 positive and negative healthy donors. Co-inhibitory signalling is likely to down-regulate an immune-response and blockade of this pathways potentiates the priming seen. EGCG is able to activate CD4 + TCC, stimulating the release of pro-inflammatory and cytolytic cytokines, driven through MHC Class II HLA-DR interactions.

Posters, Wednesday 14th September

Poster presentations—Cardiovascular and respiratory

P071 | TRPV2 and TRPV4, potential novel pharmacological targets for endothelial hyperpermeability in the diabetic eye

Adam Rollo; Josy Augustine; Peter Barabas; David Simpson; Tim Curtis

Wellcome-Wolfson Institute for Experimental Medicine, Queen's University, Belfast, Northern Ireland

Introduction/Background & aims: Diabetic macular oedema (DMO) is an ocular complication of diabetes, where retinal microvascular leakage leads to vision loss. It has previously been shown that transient receptor potential (TRP) channel mediated Ca²⁺ influx leads to endothelial permeability responses, outside of the retina [1]. Since multiple endogenous TRP channel agonists are up-regulated in the diabetic eye [2], we aim to determine whether aberrant TRP channel activation is implicated in DMO-related endothelial hyperpermeability and whether targeting these channels pharmacologically is a viable therapeutic target for DMO.

Method/Summary of work: In human retinal microvascular endothelial cells (HRMECs), TRP channel expression profiles were assessed with RT-qPCR. High-throughput Fura2 Ca²⁺ assays were then utilised to characterise Ca²⁺ mobilisation, in HRMECs. To demonstrate functional TRP channel expression, these assays were performed in cells treated with selective TRP channel agonists. Further Fura2 assays were performed to screen endogenous agonists, associated with diabetes, for potency and response magnitude. These assays were again performed, in combination with selective TRP channel antagonists, to assess the routes of Ca²⁺ mobilisation in response to the endogenous agonists. To characterise how the up-regulated endogenous agonists mobilise Ca²⁺ in diabetic conditions, assays were repeated under high D-glucose (30 mM), using an L-glucose osmotic control.

Results/Discussion: TRPV2 and 4; TRPC1,4 and 5; and TRPM7 transcripts were expressed in HRMECs. TRPV2 and TRPV4 were shown to be functionally active—with agonists Δ 9-THC (10 μ M) and GSK1016790A (0.3 μ M) leading to large Ca²⁺ responses. Histamine, thrombin, 4-oxo-nonenal (4-ONE) and lysophosphatidylcholine (LPC) gave rise to the most robust Ca²⁺ responses, out of 17 tested endogenous agonists, with EC₅₀ values in the nanomolar or low micromolar range. Ca²⁺ responses to thrombin was attenuated by TRPV2 and TRPV4 antagonism, whereas only TRPV2 antagonism effected the histamine response (Figure. 1). Under high D-glucose conditions, EC₅₀

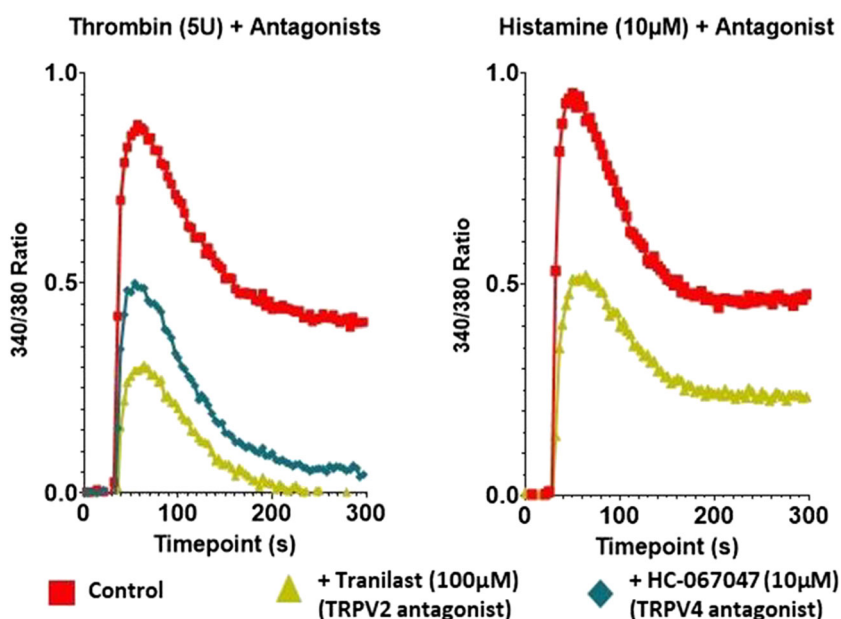


FIGURE 1 TRPV2 antagonist Tranilast (100 μ M) attenuates the Ca²⁺ response to both histamine and thrombin, whereas TRPV4 antagonism with HC-067047 (10 μ M) only attenuated the thrombin response but not that of histamine. Data are presented as mean 340/380 fluorescence ratios of the Fura-2 QBT dye, which correspond to [Ca²⁺]_i concentrations within the HRMECs.

value for thrombin underwent a substantial leftward shift (from 0.27 to 0.09 U/ml).

Conclusion(s): Endogenous molecules, up-regulated in the diabetic eye, activate TRPV2 and TRPV4 within HRMECs. Under high D-glucose, HRMECs show an increased sensitivity to thrombin. Investigation into how TRPV2 and TRPV4 activation and antagonism effects microvascular permeability in diabetes is ongoing.

REFERENCE(S)

1. Earley S, Brayden JE. Transient receptor potential channels in the vasculature. *Physiological Reviews* 2015;95(2):645–690. <https://doi.org/10.1152/physrev.00026.2014>
2. Patel JI, Tombran-Tink J, Hykin PG, Gregor ZJ, Cree IA. Vitreous and aqueous concentrations of proangiogenic, antiangiogenic factors and other cytokines in diabetic retinopathy patients with macular edema: Implications for structural differences in macular profiles. *Experimental Eye Research* 2006;82(5):798–806. <https://doi.org/10.1016/j.exer.2005.10.002>

P073 | Exploring the heteromerisation of the human P2X4 ion channel

Anna Fortuny-Gomez; Samuel J. Fountain

University of East Anglia

Introduction/Background & aims: P2X receptors are a family of seven ligand-gated cation channels activated by extracellular ATP. Their activation causes membrane depolarisation and an increase in cytoplasmic Ca^{2+} [1]. P2X1 and P2X4 subtypes are expressed in vascular smooth muscle cells and regulate vascular tone^[2]. Previous research shows evidence that rat P2X1 and P2X4 receptors can combine to form a heteromeric ion channel^[3]. This project aims to explore the multimeric assembly of human P2X4 receptors (hP2X4).

Method/Summary of work: A total of 1321 N1 human astrocytoma cells were transiently co-transfected with hP2X4 WT in combination with hP2X4 [K67A,K313A] or hP2X1 [K68A,K309A]. After 48 h, cells were stimulated with ATP, and receptor activity was measured as intracellular Ca^{2+} increase using a FlexStation3 instrument. Dose-response curves were fitted by a Hill1 equation and used to obtain potency (EC_{50}) and response maxima (E_{max}) values. Statistical analysis was performed with two-sample *t* tests. Western blot and co-immunoprecipitation assays were used to assess hP2X1 and hP2X4 protein expression and interaction. Data were expressed as mean \pm SEM and *N* represents the number of repeats.

Results/Discussion: ATP mediated a Ca^{2+} response in a concentration-dependent manner in 1321 N1 cells transiently expressing hP2X4 WT. When hP2X4 [K67A,K313A] and hP2X1 [K68A,K309A] double-dead subunits were co-transfected with hP2X4 WT, the ATP-induced E_{max} was significantly reduced by 43% and 24%, respectively ($p < .05$; $N = 5$), while the EC_{50} remained unchanged (1.1 ± 0.30 and 1.6 ± 0.26 μ M, correspondingly) compared with empty plasmid control (2.6 ± 0.73 μ M) (Table 1). Western blot and co-immunoprecipitation assays showed heterologous expression

TABLE 1 Effects of hP2X4 [K67A,K313A] and hP2X1 [K68A,K309A] double mutant subunits in hP2X4 WT ATP-evoked receptor activity

hP2X4 WT co-transfected with	EC_{50} (μ M)	E_{max} (%)
Empty plasmid control pcDNA3.1 (N = 5)	2.6 ± 0.73	67.2 ± 6.04
hP2X4 [K67A,K313A] (N = 5)	1.1 ± 0.30	24.2 ± 1.58^a
hP2X1 [K68A,K309A] (N = 5)	1.6 ± 0.26	43.0 ± 7.03^b

Note: Data were normalised to 100 μ M carbachol internal control.

^a $p = 0.0014$ versus empty plasmid control.

^b $p = 0.0310$ versus empty plasmid control.

of hP2X1 and hP2X4 and physical interaction between these subunits in 1321 N1 human astrocytoma cells ($N = 3$).

Conclusion(s): Data revealed that hP2X4 [K67A,K313A] and hP2X1 [K68A,K309A] exert a dominant negative effect on hP2X4 WT responses. Therefore, the use of double-dead subunits proves to be a good model to study the heteromerisation of P2X4 receptors. Data also confirmed a physical interaction between hP2X1 and hP2X4 when co-expressed in 1321 N1 human astrocytoma cells, suggestive of a possible human P2X1/4 heteromeric assembly. Unravelling the multimeric organisation of human P2X receptors will deepen our understanding of ATP signalling in health and disease and open new routes for more selective therapeutics.

REFERENCE(S)

1. Samways D *et al.*, (2014). *Frontiers in Cellular Neuroscience* 8: 1–18.
2. Nichols C *et al.*, (2014). *Purinerg Signal.* 10: 565–572.
3. Nicke A, Kerschensteiner D, and Soto F, (2005). *Journal of Neurochemistry* 4: 925–933.

P074 | Impaired perivascular adipose tissue-FGF-21 secretion in AMPK α 1 KO mice does not mediate the anticontractile function of PVAT

Ali AL-Ferjani; Simon Kennedy; Ian Salt

University of Glasgow

Introduction/Background & aims: Perivascular adipose tissue (PVAT) secretes a wide variety of substances which play a role in regulating vascular contractility. AMP-activated protein kinase (AMPK) is a ubiquitously expressed intracellular energy sensor and a key regulator of cellular and whole-body metabolism. Mice with a global knockout of AMPK α 1 have impaired adiponectin secretion from PVAT and a reduced anticontractile effect of PVAT in endothelium denuded aortic rings (1). However, the role of AMPK on PVAT-mediated regulation of endothelial function is still unknown. Fibroblast growth factor 21 (FGF-21) is also secreted by PVAT and previous studies have shown a relationship between FGF-21 and adiponectin in metabolic control and in prevention and amelioration

of atherosclerosis. Our initial work showed an alteration in the anticontractile effect of abdominal PVAT in AMPK α 1 KO mice and an impairment of PVAT-FGF21 secretion. So, the aim of this study was to evaluate the link between PVAT, FGF-21, AMPK and endothelial cell function.

Method/Summary of work: PVAT secretory profile was assessed using a Mouse Adipokine Array kit. FGF-21 secretion and expression in PVAT were investigated using ELISA and by immunoblotting and FGF-21 mRNA expression was assessed using reverse transcription polymerase chain reaction (RT-PCR). Endothelium-intact thoracic aortic rings from wild-type (WT; Sv129) mice were mounted on a wire myograph, preconstructed to phenylephrine (PE) (1 μ M), and dose-response curves to the AMPK-independent vasodilator cromakalim (1 nM to 10 μ M) or acetylcholine (1 nM to 10 μ M) were constructed in the presence and absence of recombinant mouse FGF-21 (100 ng/ml).

Results/Discussion: AMPK α 1 KO PVAT secreted less FGF-21 compared with WT PVAT ($P = .0013$; $n = 3-4$), and the level of FGF-21 in abdominal PVAT was higher in WT than in KO PVAT. FGF21 mRNA expression was not altered in KO abdominal or thoracic PVAT ($n = 3-4$, $P = ns$). In WT thoracic aortic rings with intact endothelium, FGF-21 had no effect on relaxation to cromakalim (66% vs. 46%; $n = 4-7$) or acetylcholine (39% vs. 44%; $n = 7$) compared with rings without FGF-21.

Conclusion(s): Deletion of AMPK α 1 significantly impaired the anticontractile effect of abdominal PVAT and FGF21 secretion, without altering FGF21 mRNA expression. However, as exogenous FGF-21 was unable to correct the impairment in AMPK α 1 deficient vessels, the impairment in anticontractile function of PVAT is unlikely to be mediated by reduced FGF-21 secretion.

REFERENCE(S)

1. Almabrouk, T.A.M., Ugusman, A.B., Katwan, O.J., Salt, I.P. & Kennedy, S. 2016, "Deletion of AMPK α 1 attenuates the anticontractile effect of perivascular adipose tissue (PVAT) and reduces adiponectin release: AMPK and PVAT function", *British Journal of Pharmacology*, vol. 174, no. 20, pp. 3398-3410.

P075 | Investigating the interaction between AMPK, NO synthase (NOS) and caveolin-1 in PVAT-mediated aortic relaxation

Abdmajid Hweji; Simon Kennedy; Ian Salt

University of Glasgow

Introduction/Background & aims: Perivascular adipose tissue (PVAT) surrounds blood vessels and releases a variety of bioactive molecules such as NO which may contribute to its anticontractile effect. Caveolin-1 (Cav-1) is the principal component of caveolae in plasma membranes, which negatively regulates eNOS activity via its scaffolding domain (amino acids 82-101). Structure-function analysis of Cav-1 has shown that phenylalanine 92 (F92) is critical for the

inhibitory actions of Cav-1 towards eNOS. We have previously shown that thoracic aortic PVAT produces significantly more NO compared with abdominal PVAT in WT, but not in mice lacking AMPK α 1[1]. In this study, we sought to investigate the role of AMPK α 1 in the regulation of CAV-1/eNOS coupling and PVAT-derived NO production using a mutant cell-permeable scaffolding domain peptide of CAV-1 fused to an antennapedia sequence (CAVAP).

Method/Summary of work: Wild type (Sv129) and AMPK α 1 knock-out (KO) mice were euthanised by a rising concentration of CO₂. About 20 mg of thoracic PVAT tissue from WT and KO mice was collected and incubated for 30 min in 1 ml oxygenated physiological buffer solution to produce conditioned media in which NO was analysed using a Sievers 280A NO analyser. CAV-1/eNOS binding in PVAT was assessed by co-immunoprecipitation and CAV-1 mRNA expression was assessed by RT-qPCR. Aortic rings with intact PVAT and endothelium-denuded from WT and AMPK α 1 KO mice were bathed in oxygenated and heated Krebs buffer (37°C) in a myograph chamber with CAVAP peptide (15 μ M for 6 h), or antennapedia peptides (control) before isometric tension responses to phenylephrine (200 pM to 10 μ M) were measured.

Results/Discussion: WT thoracic PVAT produced significantly more NO (300.2 nmol/mg/h $n = 8$), compared with KO PVAT (139 nmol/mg/h $n = 7$; $p < .05$). Co-IP and RT-qPCR data showed more CAV-1 expression in AMPK KO PVAT compared with WT PVAT. Incubation with CAVAP peptide increased basal NO release in AMPK α 1 KO thoracic PVAT (ACVAP = 485.24 nmol/mg/h) and (AP = 324.3028 nmol/mg/h) and reduced contraction in response to PE ($p = .0016$, $n = 3$).

Conclusion(s): This study has shown that CAVAP increased NO release from thoracic PVAT in AMPK α 1 KO, but not WT mice. This suggests that increased CAV-1/eNOS association in PVAT of AMPK α 1 KO mice contributes to reduced NO release, and this may account for reduced aortic relaxation in KO arteries with intact PVAT.

REFERENCE(S)

1. Hweji, A., Kennedy, S., and Salt, I.P. 2020. The role of AMPK in the regulation of nitric oxide synthesis by perivascular adipose tissue. Selected abstracts from pharmacology 2020. *British Journal of Pharmacology*, 178: 381-486. <https://doi.org/https://doi.org/10.1111/bph.15316>

P076 | Purine involvement in hypochlorous acid effects on vascular contractility of the porcine coronary artery

Ashwaq Baghdadi; Vera Ralevic; William Dunn

University of Nottingham

Introduction/Background & aims: Neutrophils are part of the body's defence mechanism against microorganisms [1]. Hypochlorous acid (HOCl), which is generated by neutrophils, plays a major role in killing pathogens in addition to being a mediator of the inflammation process [2]. High concentrations of purine nucleotides are present inside cells [3], but whether these participate in the vasomotor response to HOCl

is unclear. The objectives were to investigate purine nucleotide and receptor involvement in the vasomotor effects of HOCl in the porcine coronary artery (PCA) and the effect of HOCl on ATP release from cultured human coronary artery endothelial cells (HCAECs).

Method/Summary of work: A luminescent ATP detection assay kit (ab113849: Abcam, Cambridge, MA, USA) was used to measure ATP released by HCAECs. Segments of PCA were set up in organ baths for isometric tension recording. They were incubated in the absence and presence of suramin and pyridoxalphosphate-6-azophenyl-2',4'-disulphonic acid (PPADS) (100, 10 μ M, nonselective P2 receptor antagonists), MRS 2179 (10 μ M, P2Y1 receptor antagonist), probenecid (1 mM, pannexin 1 channel blocker), carbenoxolone (100 μ M, pannexin 1 and connexin channels blocker) and apyrase (10 units/ml, hydrolyses ATP) precontracted with U46619 (thromboxane A2 receptor agonist), then exposed to HOCl (100 and 500 μ M). Responses were expressed as a percentage of U46619-induced tone.

Results/Discussion: At 100 μ M, HOCl induced a transient initial endothelium-dependent relaxation which returned to baseline; thereafter, a second slow relaxation was observed for 60 min. A transient endothelium-dependent relaxation response was also induced by 500 μ M HOCl, followed by a contraction; following this, slow relaxation was observed over 60 min ($n = 7$). Suramin blocked the rapid relaxation observed at 100 μ M HOCl. In contrast, the rapid relaxation observed at 500 μ M HOCl was still evident in the presence of suramin. The contraction to 500 μ M HOCl was blocked by suramin. Slow relaxation responses were still evident in the presence of suramin for both 100 and 500 μ M HOCl ($n = 6$). MRS 2179, probenecid, carbenoxolone and PPADS did not alter the response to HOCl. Apyrase blocked the multiphasic responses to both concentrations of HOCl ($n = 6$). HOCl treated HCAECs showed higher ATP levels in the culture medium after 1 and 5 min when compared with untreated ones ($n = 4$).

Conclusion(s): HOCl produces a concentration-dependent multiphasic vasomotor response in the PCA. The use of apyrase and suramin shows a possible involvement of nucleotide release and actions at P2 receptors. Detection of HOCl-induced ATP release from HCAECs is consistent with an involvement of ATP in the rapid relaxation response to HOCl. Further work is needed to confirm P2 receptor involvement.

REFERENCE(S)

1. Rayner et al. (2014). *Free Radical bio Med*, 71, 240–255.
2. Zhang et al. (2001). *J Amer Med Assoc*, 286(17), 2136–2142.
3. Ralevic, V., & Dunn, W. R. (2015). *Auton Neurosci-Basic*, 191, 48–66.

P080 | Effect of combined antihypertensive treatments on blood pressure and vascular reactivity in SHR rats

Diego Lezama-Martinez; Víctor-Daniel Farías-Sánchez; Luis-Antonio Pimentel-Cuevas; Sofía-Lizbet Muñoz-Muñoz; Jazmín Flores-Monroy; Diana Ramírez-Hernández

Universidad Nacional Autónoma de México

Introduction/Background & aims: Combination treatments for hypertension can be with renin angiotensin system inhibitors, diuretics and β -blockers. In this regard, there are multiple and complex avenues to explain the antihypertensive mechanism of drug combinations [1]. While there are studies on some components of the renin-angiotensin system with individual treatments, it is still unknown what happens during the use of combination treatments. Therefore, in this study, different antihypertensive combinations were used to determine the antihypertensive effect and vascular reactivity in SHR rats.

Method/Summary of work: The animals (6-month old and body weight of 250 g) received rat chow and water ad libitum and were housed in acrylic boxes under standard laboratory conditions. The experiments followed the Official Mexican Norm NOM-062-ZOO-1999, and the Institutional Committee for the Care and Use of Experimental Animals approved the experimental protocol with the register number CICUAE-FESC C21_10. The male SHR rats were grouped into the following: (1) WKY, (2) untreated SHR, (3) SHR + captopril-hydrochlorothiazide, (4) SHR + losartan-hydrochlorothiazide, (5) SHR + captopril-amlodipine and (6) SHR + valsartan-amlodipine for 1 week. Blood pressure was measured by the Tail-Cuff method, and vascular reactivity was determined by angiotensin II, noradrenaline and acetylcholine concentration-response curves in aortic rings. PAPIIT-IN217122, CI2259, A1-5-8958.

Results/Discussion: Captopril-hydrochlorothiazide, losartan-hydrochlorothiazide, captopril-amlodipine and valsartan-amlodipine combinations reduced blood pressure after 1 week of treatment. Vascular reactivity to angiotensin II was reduced with losartan-hydrochlorothiazide and valsartan-amlodipine, while the response to noradrenaline remained unchanged, and the effect of acetylcholine was increased with the captopril-hydrochlorothiazide combination.

Conclusion(s): The combinations used were effective as antihypertensive treatment; in addition, polytherapy could modify vascular and neurohumoral hyperactivity.

REFERENCE(S)

1. Kalra, S., Kalra, B., & Agrawal, N. (2010). Combination therapy in hypertension: An update. *Diabetology & Metabolic Syndrome*, 2(1), 44. <https://doi.org/10.1186/1758-5996-2-44>

P081 | NO-induced Treg cell attenuates development of hypertension following inhibition of NOS in Dahl salt-resistant rat but not in Dahl salt-sensitive rat

Sungmin Jang; Inkyeom Kim

Department of Pharmacology, School of Medicine, Kyungpook National University

Introduction/Background & aims: Inhibition of nitric oxide synthase (NOS) by N (omega)-nitro-L-arginine methyl ester (L-NAME) is associated with several detrimental effects on the cardiovascular system. However, low-dose L-NAME increases NO synthesis, which in turn induces physiological cardiovascular benefits, probably by activating a

protective negative feedback mechanism. In a previous study, Dahl salt-sensitive (SS) and Dahl salt-resistant (SR) rats showed different blood pressure changes at specific concentrations of L-NAME. In addition, reducing ROS and increasing NO had a beneficial effect on ameliorating salt-sensitive hypertension. Therefore, we hypothesised that there would be significant differences in the degree of vasodilation and immune response to inflammation in both SS and SR rats when administered with an appropriate amount of L-NAME.

Method/Summary of work: A group of 6 SS and SR rats received L-NAME in the drinking water (10 mg/kg day) for 3–4 weeks. Systolic blood pressure was measured by the tail-cuff method. Expression of nitric oxide synthase (iNOS, nNOS) and T cell-related factors was measured by RT-qPCR. Dihydroethidium (DHE) and 2',7'-Dichlorofluorescein diacetate (DCFDA) were used to identify reactive oxygen species (ROS). Th17 cells and Treg cells population were quantified in splenocytes and peripheral blood mononuclear cells (PBMCs) by flow cytometry. Serum IL-17A and IL-10 were analysed by ELISA kit. Splenocytes were isolated from spleens of SS or SR rats. Total splenocytes were cultured in RPMI-1640 medium. To investigate the effect of nitric oxide synthase inhibitor, the splenic T cells were treated with additional GSNO concentrations: 0–2 mmol/L. The cultured cells and supernatant were collected for flow cytometry, qRT-PCR or ELISA.

Results/Discussion: In tail-cuff method studies, a significantly increased systolic blood pressure (SBP) was seen at weeks 1–4 in SS fed L-NAME ($P < .05$ vs. SS fed tap water); there were no significant changes at weeks 1, 3 and 4 in SR fed L-NAME compared with SR fed tap water. In flow cytometry, the population of Treg cells of PBMCs showed significant increase in SR fed L-NAME ($P < .05$ vs. SR fed tap water). However, there were no significant changes in the population of Treg cells of PBMCs in SS fed L-NAME ($P < .05$ vs. SS fed tap water). The population of Th17 cells of PBMCs has no significant changes in both SS and SR rats. In addition, Th17 cells and Treg cells of splenocytes had no significant differences in both SS and SR rats. Therefore, we will proceed with further studies of nitric oxide and ROS to elucidate the difference between SS and SR fed L-NAME. Furthermore, after culturing splenocytes and administering NO-generating drugs, we will check the changes in Th17 cells and Treg cells and infer the difference in SBP between SS and SR rats.

Conclusion(s): An adequate amount of L-NAME induces hypertension in Dahl salt-sensitive rats but not in Dahl salt-resistant rats. Thus, NO-induced anti-inflammatory Treg cell attenuates development of hypertension following inhibition of NOS in Dahl salt-resistant rat but not in Dahl salt-sensitive rat.

REFERENCE(S)

1. Ang P, Zhao X, Zhou L, Jin Y, Zheng X, Ouyang Y, Chen M, Zeng L, Chen S, Chen X, Tian Z. Protective effect of oral histidine on hypertension in dahl salt-sensitive rats induced by high-salt diet. *Life Sciences* 2021 Apr.
2. Gonzalez-Vicente A, Saez F, Monzon CM, Asirwatham J, Garvin JL. Thick ascending limb sodium transport in the pathogenesis of hypertension. *Physiological Reviews* 2019 Jan 1.

P082 | Increased production of contractile factors in perivascular adipose tissue during high-salt diet does not induce hypertension in Dahl salt-resistant rats

Choi Joonhuck; Lee Soyung; Kim InKyeom

Kyungpook National University

Introduction/Background & aims: Perivascular adipose tissue (PVAT) secretes various contractile and relaxing factors. Thoracic PVAT (tPVAT) is a kind of brown adipose tissue, and abdominal PVAT (aPVAT) is a kind of white adipose tissue that adiposity might be changed by high salt diet. We tested the hypothesis that increased production of contractile factors in thoracic PVAT and abdominal PVAT during high salt diet does not induce hypertension in Dahl salt-resistant rats.

Method/Summary of work: Dahl salt-sensitive (SS) and Dahl salt-resistant (SR) rats were fed high salt (4% salt) or normal salt (0.4%) for 4 weeks. Blood pressure was measured by the tail-cuff method. Vascular tension induced by phenylephrine, acetylcholine, and sodium nitroprusside in isolated aortic rings of SS and SR was measured in the absence or the presence of PVAT. The activity of contractile factors from tPVAT, aPVAT, or visceral adipose tissues of SS and SR were bioassayed using isolated thoracic aortic rings of Sprague–Dawley rats. Expression of tPVAT-derived factors were measured by reverse-transcription qRT-PCR.

Results/Discussion: In SS, a high-salt diet increases systolic blood pressure, and SR body weighs more than SS. In order to determine whether PVAT affects vessel contraction and relaxation ability, the results of vascular tension induced by phenylephrine, acetylcholine, and sodium nitrate in the separate aortic rings of SS and SR were measured in the absence or presence of PVAT, although PVAT-induced contraction inhibition was observed in SR. However, inhibition of relaxation by PVAT was observed in both NS and HS. Looking at the differences in mice of the same breed, both NS and HS were observed to inhibit PVAT-induced contraction in SS, but increased contraction due to PVAT was observed in SR. The difference in relaxation capacity showed the same tendency as salt with the same concentration.

Conclusion(s): High-salt diet produces more contractile factors in perivascular adipose tissues of Dahl salt-sensitive rats than in those of Dahl salt-resistant rats.

REFERENCE(S)

1. Andrea Grillo et al./*Nutrients*. 2019 Sep 11
2. (1962). *The Journal of Experimental Medicine*, 115, 1173, EFFECTS OF CHRONIC EXCESS SALT INGESTION, 1190. <https://doi.org/10.1084/jem.115.6.1173>
3. (2017). *British Journal of Pharmacology*, 174(20), 3496–3513, Perivascular adipose tissue inflammation in vascular disease. <https://doi.org/10.1111/bph.13705>

P084 | Gold nanoparticles inhibit steroid-insensitive asthma in mice preserving HDAC2 and Nrf2 pathways

Marco Aurélio Martins¹; Magda Serra²; Amanda Cotias¹;
Manuella Lanzetti³; Vinicius Carvalho¹; Patricia Martins²;
Emiliano Barreto⁴; Renato Cordeiro¹

¹Oswaldo Cruz Foundation; ²Fiocruz; ³Federal University of Rio de Janeiro; ⁴Federal University of Alagoas

Introduction/Background & aims: The clinical application of gold metallic compounds and their complexes for treating inflammation-related diseases has several thousand years of history, but some side effects limit its use. The innovative nanomedicine concept, which refers to biologically active molecules formulated as nanoparticles for improving bioavailability, pharmacokinetics, biodistribution and metabolism of drugs, has attracted growing interest. Prior study has provided evidence that gold nanoparticles (AuNPs) can inhibit pivotal pathological changes in distinct murine models of atopic asthma. Whether AuNPs can interfere with steroid-insensitive asthma is unclear. The current study was undertaken to assess the effectiveness of nebulised AuNPs in a murine model of GC-resistant asthma.

Method/Summary of work: A/J mice were sensitised to ovalbumin (OVA) and, subsequently, subjected to intranasal instillations of OVA once a week for nine consecutive weeks. Two weeks after starting allergen stimulations, mice were subjected to nebulised budesonide (7.5 mg/ml) or AuNPs (0.4 or 4 µg/ml) 1 h before stimuli. Airway hyperreactivity (AHR), leukocyte infiltration, airway remodelling, cytokine generation and oxidative stress were evaluated 24 h after the last allergen stimulation. Western blotting was used to assess Nrf2, PI3Kδ, AKT and HDAC2 expression in the lung tissue.

Results/Discussion: We found that mice challenged with OVA had airway hyperreactivity, eosinophil, and neutrophil infiltrates in the lung, concomitantly with peribronchiolar fibrosis, mucus production and proinflammatory cytokine generation compared with sham-challenged mice. These changes were inhibited in mice treated with AuNPs, but not budesonide. In the GC-resistant asthmatic mice, the oxidative stress was established, marked by a reduction in Nrf2 levels and catalase activity, accompanied by elevated values of TBARS, nitrotyrosine, PI3Kδ/AKT expression, as well as a reduction in the nuclear expression of HDAC2 in the lung tissue, all of which sensitive to AuNPs but not budesonide treatment.

Conclusion(s): These findings suggest that ovalbumin-sensitised A/J mice subjected to a long-term protocol of repeated intranasal ovalbumin provocations evolve to a chronic asthma-like condition that is unresponsive to corticosteroid treatment. All pathological changes reproduced in this model are sensitive to AuNPs given by nebulisation, in a mechanism associated with down-regulation of oxidative stress and rescue of HDAC2 levels. The data suggest that stimulation of antioxidative response through activation of Nrf2 may be a pharmacologically important part of the actions of AuNPs in this model,

providing novel perspectives for the treatment of steroid insensitive asthma and COPD at the interface of biological systems and nanomedicine. In summary, we conclude that AuNPs can improve GC-insensitive asthma by preserving HDAC2 and Nrf2, leading to a balanced redox environment.

P089 | The effect of AMPKα1 deletion on sphingosine kinase 1 protein expression in adipose tissue

Abdullah Alharethi¹; Simon Kennedy²; Craig Daly²

¹Glasgow University; ²University of Glasgow

Introduction/Background & aims: Perivascular adipose tissue (PVAT) surrounds most blood vessels and secretes factors involved in vascular reactivity under physiological conditions. Recently, it has been reported that deletion of AMPKα1 altered the secretory profile of PVAT and attenuated its anti-contractile effect on endothelium-denuded aortic rings. The molecular mechanisms by which PVAT AMPK regulates contraction and relaxation signalling in vascular reactivity is unclear. Several studies have shown that S1P treatment promotes relaxation in aortic endothelium suggesting that SK1 is involved in the regulation of relaxation signalling. Here we sought to study the effects of AMPK deletion on the protein expression of SK1 and how this influences vascular functions.

Method/Summary of work: Mice were euthanised with CO₂. PVAT was isolated from thoracic and abdominal arteries of wild-type (Sv129-WT) and global AMPKα1 knock-out (KO) mice (3–4 months old). For cellular studies, mouse embryonic fibroblast (MEF) was used. The MEF cells were grown in Dulbecco's modified Eagle medium (DMEM) supplemented with 10% foetal bovine serum (FBS). In some experiments, cells were treated with 10 µl of sphingosine-1-phosphate (S1P) for 1 h. The expression of SphK in PVAT and cultured cells was measured using Western blotting.

Results/Discussion: We have found in thoracic PVAT, isolated from mice lacking AMPKα1, had a significant increase in SK1 protein expression (~twofolds) when compared with the WT control group. No changes were observed in the SK1 protein level in the abdominal PVAT between AMPKα1 KO mice and WT mice. To further confirm this finding, MEF cells lacking AMPKα1 KO cells were used. Consistent with the thoracic PVAT data, we have found that deleting AMPKα1 in MEF cells resulted in 50% increase in SK1 protein expression.

Conclusion(s): This study has demonstrated that deletion of AMPKα1 in vitro and in vivo is associated with increased SK1 protein expression. The main mechanisms of SphKs/S1P regulation of PVAT are unclear. However, further studies will examine how the SphKs/S1P pathway could influence vascular functions in animals lacking the AMPKα1 enzyme.

P090 | Effect of early and late hormonal replacement therapy in old Wistar rats on vascular reactivity

Jazmin Flores-Monroy; Diana Ramirez-Hernandez;
Diego Lezama-Martinez

Universidad Nacional Autonoma de Mexico

Introduction/Background & aims: Cardiovascular disease is the leading cause of mortality in women. The most important age in the development of cardiovascular diseases in the female sex is the climacteric and menopause, where hormone replacement therapy (HRT) has been chosen; however, after large clinical trials, this therapy has not shown any cardiovascular benefit. In addition to this, the results on the effect of oestrogen therapy have been controversial since the dose or time of administration of the therapy has not been homologated and there seems to be a difference between early or late administration at the first symptoms of climacteric. Regarding the incidence of cardiovascular diseases (CVD) during this stage, an increase in vascular reactivity has been observed in the face of oestrogen depletion. This hyperreactivity to vasoconstrictor agonists and decreased vasorelaxant effect on vascular smooth muscle is important since it causes an increase in peripheral resistance that causes pressure overload that exacerbates the incidence and severity of CVD. Therefore, it is important to know if the effect of some agonists such as Angiotensin II in the vasoconstrictor axis or Acetylcholine in the vasorelaxant axis are affected by the administration of oestrogens in a model of menopause in rats.

Method/Summary of work: One-year-old female Wistar rats were randomised into several groups: (1) Sham; (2) 2-year-old Wistar rat with 10 weeks ovariectomy (OVX-10w); (3) Wistar rat 2 years old with 20 weeks ovariectomy (OVX-20w); (4) OVX-10w-early hormone therapy; (5) OVX-20w-late. Hormone therapy. The rats were anaesthetised with pentobarbital (55 mg/kg i.p.) and underwent bilateral oophorectomy. Oestradiol was administered orally at a dose of 5 µg/kg/day. Early hormone replacement therapy was administered 3 days after ovariectomy, and the rats were sacrificed after 10 weeks of surgery. Late therapy was administered after 10 weeks of oophorectomy and was administered daily for 10 weeks. Aortic rings were mounted in 10 ml chamber tissue baths filled with Krebs-Henseleit solution at 37°C (pH 7.4) and continuously aerated with 95% O₂/5% CO₂. The ring segments were adjusted to a tension of 3 g. The vasoconstrictor effect of Ang II was tested at 10⁻¹² to 10⁻⁶ M Ang II. Concentration-response curves were made to KCl (10⁻⁶ M) and the vasodilator effect was tested at 10⁻¹²–10⁻⁶ M Acetylcholine.

Results/Discussion: The availability of Ca²⁺ induced by KCl in the smooth muscle of the aortic rings, where it is shown that the availability of Ca²⁺ by the activity of the channels is not influenced by the administration of oestrogens but is dependent on the time of evolution of the surgery since both groups with 20 weeks as total time of evolution of ovariectomy present the same vascular reactivity as the sham group. Unlike the KCl curve, the vasoconstrictor effect of Angiotensin II is modulated by the administration or disposition of oestrogens since the groups that were not administered with hormonal

therapy showed an increase in vascular reactivity and those administered with therapy showed a contractile response similar to the sham group. The vasorelaxant effect of acetylcholine on vascular smooth muscle is not related to hormonal disposition but to the time of evolution of bilateral oophorectomy, with 10 weeks of oestrogen depletion being the time when there is a greater response to acetylcholine.

Conclusion(s): Hormone replacement therapy influences the modulation of the renin angiotensin system but not the parasympathetic nervous system or calcium channels activity.

REFERENCE(S)

- Newson, L. (2018). Menopause and cardiovascular disease. *Post Reproductive Health*, 24(1), 44–49. <https://doi.org/10.1177/2053369117749675>
- Honigberg, M. C., Zekavat, S. M., Aragam, K., Finneran, P., Klarin, D., Bhatt, D. L., Januzzi Jr J. L., Scott N. S., Natarajan, P. (2019). Association of premature natural and surgical menopause with incident cardiovascular disease. *Jama*, 322(24), 2411–2421. <https://doi.org/10.1001/jama.2019.19191>
- Reslan, M. O., & Khalil, R. A. (2012). Vascular effects of estrogenic menopausal hormone therapy. *Reviews on Recent Clinical Trials*, 7(1), 47–70. <https://doi.org/10.2174/157488712799363253>
- Iorga, A., Cunningham, C. M., Moazeni, S., Ruffenach, G., Umar, S., & Eghbali, M. (2017). The protective role of estrogen and estrogen receptors in cardiovascular disease and the controversial use of estrogen therapy. *Biology of Sex Differences*, 8(1), 1–16. <https://doi.org/10.1186/s13293-017-0152-8>
- Pan, M., Pan, X., Zhou, J., Wang, J., Qi, Q., & Wang, L. (2022). Update on hormone therapy for the management of postmenopausal women. *Bioscience Trends*, 16(1), 46–57. <https://doi.org/10.5582/bst.2021.01418>
- Paciuc, J. (2020). Hormone therapy in menopause. *Hormonal Pathology of the Uterus*, 89–120. https://doi.org/10.1007/978-3-030-38474-6_6
- Speth, R. C., D'Ambra, M., Ji, H., & Sandberg, K. (2018). A heartfelt message, estrogen replacement therapy: Use it or lose it. *American Journal of Physiology-Heart and Circulatory Physiology*, 315(6) H1765–H1778, <https://doi.org/10.1152/ajpheart.00041.2018>
- Dubey, R. K., Imthurn, B., Barton, M., & Jackson, E. K. (2005). Vascular consequences of menopause and hormone therapy: Importance of timing of treatment and type of estrogen. *Cardiovascular Research*, 66(2), 295–306 <https://doi.org/10.1016/j.cardiores.2004.12.012>
- Giordano, S., Xing, D., Chen, Y. F., Allon, S., Chen, C., Oparil, S., & Hage, F. G. (2015). Estrogen and cardiovascular disease: Is timing everything? *The American Journal of the Medical Sciences*, 350(1), 27–35. <https://doi.org/10.1097/MAJ.0000000000000512>

P092 | Endothelial TRPV4-mediated relaxation of mouse pulmonary artery requires oxidative activation of protein kinase G

Hala Alhabashneh; Adam Greenstein; Alison Gurney

University of Manchester

Introduction/Background & aims: Protein kinase G (PKG) is the end effector kinase in vasodilation mediated by the NO/cGMP pathway. PKG is also activated by oxidation of cysteine residues in the PKGI α subunit, which in smooth muscle induces relaxation [1]. PKG is also present in endothelium where its function is poorly understood. This

study investigated the role of oxidant activated, endothelial PKG in regulating pulmonary arterial tone.

Method/Summary of work: Endothelium-dependent relaxation evoked by carbachol or the TRPV4 agonist, GSK1016709A, was compared in intra-pulmonary arteries from wild type (WT) mice and PKG [C42S]^{KI} mice lacking the cysteine-based oxidant sensor [1], using wire myography. Endothelial Ca²⁺ signalling was compared in fluo4-loaded en face preparations using spinning-disc confocal microscopy. All procedures met the requirements of the Animals (Scientific Procedures) Act 1986/Amendment Regulations 2012. Data are given as mean ± S.E.M. and compared using two-tailed unpaired *t*-tests.

Results/Discussion: U46619 (30 nM)-contracted arteries from WT and PKG[C42S]^{KI} mice relaxed equally to carbachol, with pEC₅₀ values of 5.9 ± 0.1 (*n* = 9) and 5.8 ± 0.1 (*n* = 7), respectively, and maxima of 38 ± 9% and 40 ± 9%. Arteries from PKG[C42S]^{KI} mice were less sensitive to GSK1016790A (pEC₅₀ = 7.48 ± 0.08, *n* = 10) than WT arteries (pEC₅₀ = 8.0 ± 0.1, *n* = 8; *P* = 0.0005), but reached a similar maximum relaxation (WT = 91 ± 2%; PKG[C42S]^{KI} = 86 ± 3%). Endothelium removal suppressed relaxation to carbachol in both tissues, but inhibited responses to GSK1016790A only in WT arteries. Carbachol (10 μM) increased the frequency of Ca²⁺ pulsars from 0.6 ± 0.2 Hz to 1.5 ± 0.3 Hz (*n* = 11, *P* = 0.016) in WT endothelium, indicating enhanced Ca²⁺ release from the endoplasmic reticulum (ER). Pulsar frequency in PKG[C42S]^{KI} endothelium reached a similar level (1.3 ± 0.4 Hz, *n* = 7) after adding carbachol, from a baseline of 0.8 ± 0.2 Hz. Endothelial Ca²⁺ influx via TRPV4 channels (sparklets) was recorded in the presence of cyclopiazonic acid (1 μM) to block ER Ca²⁺ storage. The number of sites and frequency of sparklets recorded in the presence of 10 nM GSK1016790A was lower in the endothelium of PKG[C42S]^{KI} arteries (15 ± 2 sites/5 μm², 0.24 ± 0.02 Hz, *n* = 5) compared with WT arteries (92 ± 27 sites/5 μm², 1.5 ± 0.4 Hz, *n* = 5, *P* = 0.02).

Conclusion(s): The loss of GSK1016790A-induced Ca²⁺ sparklets and endothelium-dependent relaxation in PKG[C42S]^{KI} arteries indicates that oxidative activation of PKG facilitates TRPV4-mediated vasodilation. As carbachol retained its ability to stimulate Ca²⁺ pulsars and relaxation in PKG[C42S]^{KI} arteries, muscarinic vasodilation did not employ TRPV4 channels.

REFERENCE(S)

- Burgoyne, J. R., Madhani, M., Cuello, F., Charles, R. L., Brennan, J. P., Schroder, E., Browning, D. D., & Eaton, P. (2007). Cysteine redox sensor in PKG α enables oxidant-induced activation. *Science*, 317, 1393–1397.

P093 | Atomoxetine enhances the duration of noradrenergic vasoconstriction in porcine isolated renal arteries

Julian Benyamen

University of Nottingham

Introduction/Background & aims: Noradrenaline is the vasopressor agent of choice for managing blood pressure of patients with severe sepsis and evidence of vasoplegia⁽¹⁾. However, the beneficial vasoconstrictor actions mediated by noradrenaline on alpha-adrenoceptors is offset by the high infusion rates needed, that leads to appreciable activation of beta-adrenoceptors and subsequent immunosuppression⁽²⁾. One possible way to counteract this potential problem is to add selective uptake1 inhibitor with noradrenaline to enhance the vascular actions. Atomoxetine is a potent and selective noradrenergic uptake inhibitor currently used for treating ADHD, but has been reported to increase blood pressure in patient with autonomic failure⁽³⁾. The present study has examined the effect of atomoxetine on neurogenic contractions of porcine isolated renal arteries.

Method/Summary of work: Intralobular segments (1 mm diameter, 5 mm length) of porcine renal artery were prepared for isometric tension recording in 20 ml organ bath containing Krebs–Henseleit solution. After application of 5 g wt resting tension, segments were twice contracted with 60 mM KCl before commencement of electrical field stimulation (EFS)—16 Hz 0.3 ms, 200 mA for 10 s every 10 min for 2 h. After 60 min, the segments were exposed to 10 nM and 1 μM atomoxetine. The magnitude of the neurogenic contraction was measured, along with the time duration where the peak response relaxed by 50%. The changes of the vascular contractions after 60 min exposure to EFS were assessed by paired *t*-test and considered significant if *p* < 0.05.

Results/Discussion: The 60 mM KCl elicited a sustained contraction (6.33 ± 0.8 g wt., *n* = 5) of renal arteries, while responses to EFS (16 Hz, 10 s) were transient in nature and equivalent to 3.3 ± 0.8 g wt. The peak response was attained within 30 s of the onset of stimulation, relaxing by 50% after a further 60 s. Addition of 10 nM atomoxetine did not significantly alter the magnitude of neurogenic contractions after 60 min exposure, but the highest concentration (1 μM) of the drug significantly increased the contraction. Both concentrations of atomoxetine significantly increased the time for the neurogenic contractions by approximately 30% to attain the peak response and also increased the time required for response to wane to 50% of the peak response (Table 1). The addition of 100 nM prazosin at the end of the experiment abolished neurogenic contractions (*n* = 4).

Conclusion(s): This study demonstrates that low concentrations of atomoxetine enhances the vasoconstrictor effect of endogenously released noradrenaline in the porcine isolated renal artery. However, this effect is manifest mainly as an increase in the time to peak response and duration of the vasoconstrictor effect, rather than an overall increase in the magnitude of the response. The later observation may explain the beneficial effect of atomoxetine in patients who experience hypotension due to autonomic failure⁽⁴⁾. These findings also provide a basis for the examination of the effect of neuronal uptake blockers on neurogenic contractions in other vascular bed after exposure to lipopolysaccharide, to mimic vasoplegia encountered in septic shock.

TABLE 1 The effect of atomoxetine on the characteristics of neurogenic contractions (16 Hz 10s 0.3 ms 200 mA every 10 min) of the porcine isolated renal arteries. Responses are shown as the mean ± sem of 5 observations

	Control EFS response	Atomoxetine concentration	% change post 30 min	% change post 60 min
Contraction (g wt.)	3.3 ± 0.8	10 nM	11.4 ± 4.4	11.6 ± 5.7
Time to peak (s)	26.8 ± 4.8		14.6 ± 8.5	38.1 ± 10.8*
Time to 50% decline (s)	51.8 ± 20.1		63.2 ± 20.6	224.4 ± 79.5**
Contraction (g wt.)	3.4 ± 1.2	1 µM	-2.7 ± 5.6	-18.2 ± 4.9*
Time to peak (s)	31.1 ± 2.9		16.1 ± 7.3	37.1 ± 10.9*
Time to 50% decline (s)	78.6 ± 20.9		125.2 ± 28.0	169.8 ± 44.8*

Note: **p* < 0.05 and ***p* < 0.01 denotes a significant change after 60 min compared with control.

REFERENCE(S)

- Avni, T., et al. (2015). *PLoS ONE*, 10, e0129305, Vasopressors for the Treatment of Septic Shock: Systematic Review and Meta-Analysis. <https://doi.org/10.1371/journal.pone.0129305>
- Stolk, R. F., et al. (2020). *Am. Respir. Crit. Med.*, 202, 830–841, Norepinephrine Dysregulates the Immune Response and Compromises Host Defense during Sepsis. <https://doi.org/10.1164/rccm.202002-0339OC>
- Shibao, et al. (2007). *Hypertension*, 50, 47–53, Norepinephrine Transporter Blockade With Atomoxetine Induces Hypertension in Patients With Impaired Autonomic Function. <https://doi.org/10.1161/HYPERTENSIONAHA.107.089961>

P094 | Early and late oestrogen replacement therapy upon cardiovascular function in aged female Wistar rat

Diana Ramirez-Hernandez¹; Jazmin Flores-Monroy¹; Diego Lezama-Martinez¹; Pedro López-Sánchez²

¹Universidad Nacional Autonoma de Mexico; ²Instituto Politecnico Nacional

Introduction/Background & aims: Cardiovascular diseases are the leading death worldwide cause in women, the prevalence of these diseases has been associated with two important and directly related

processes, ageing and the decrease in oestrogens during menopause. Therefore, we aim to evaluate the effect of early and late therapy with 17-β oestradiol on the heart of adult female rats ovariectomized to determine whether early oestrogen replacement therapy improves cardiovascular function in aged female Wistar rat.

Method/Summary of work: All animal procedures were conducted according to Federal Regulation for Animal Experimentation and Care (SAGARPA, NOM-062-ZOO, 1999, Mexico), local ethics committee number C18_06 (CICUAE-FESC), and the National Institutes of Health Guide for the Care and Use of Laboratory Animals (NIH Publications No. 8023, revised 1978, USA). Randomised female Wistar rats were included in five groups with *n* = 7 of 18 months of age: sham, OVX-10 w-: 10 weeks of oophorectomy, OVX-20 w-: 20 weeks of oophorectomy, OVX-10w-eERT oophorectomy + early oestrogen replacement therapy, OVX-10w-IERT: oophorectomy + therapy late oestrogen replacement. After 3 days (OVX-10w-eERT) or 10 weeks (OVX-20w-IERT) of oophorectomy surgery, oestradiol was administered by oral route 5 µg/kg/day, 10 weeks after the initiation of therapy the cardiac function was evaluated using echocardiography, ECG and cardiac catheterization and Masson stain were performed. One-Way ANOVA followed by the Student–Newman–Keuls post hoc test was used for comparisons between groups. Statistical significance was established at *p* ≤ 0.05.

TABLE 1 Echocardiographic parameters in female Wistar rats with early and late oestrogen replacement therapy

Parameter	Sham	OVX-10 w	OVX-10w-eERT	OVX-20w	OVX-20w-IERT
IVSd (cm)	0.24 ± 0.01	0.24 ± 0.05	0.20 ± 0.02	0.19 ± 0.04	0.16 ± 0.02
LVIDd (cm)	0.64 ± 0.02	0.74 ± 0.04	0.75 ± 0.05	0.77 ± 0.05	0.77 ± 0.03
LVPWd (cm)	0.25 ± 0.02	0.26 ± 0.06	0.25 ± 0.04	0.18 ± 0.03	0.19 ± 0.01
IVSs (cm)	0.40 ± 0.01	0.36 ± 0.05	0.31 ± 0.02	0.41 ± 0.09	0.28 ± 0.02
LVIDs (cm)	0.30 ± 0.01	0.44 ± 0.02*	0.45 ± 0.03*	0.40 ± 0.05*	0.47 ± 0.03*
LVPWs (cm)	0.31 ± 0.01	0.34 ± 0.05	0.33 ± 0.04	0.54 ± 0.34	0.26 ± 0.01
EDV (ml)	0.60 ± 0.06	0.90 ± 0.12	0.96 ± 0.16	0.79 ± 0.07	1.03 ± 0.12
ESV (ml)	0.07 ± 0.01	0.21 ± 0.03	0.22 ± 0.03	0.34 ± 0.11*	0.26 ± 0.06
EF (%)	89 ± 1	76 ± 1	76 ± 3	68 ± 5 *	75 ± 4
SV (ml)	0.54 ± 0.06	0.69 ± 0.10	0.73 ± 0.14	0.68 ± 0.09	0.77 ± 0.09
FS (%)	54 ± 2	40 ± 1 *	40 ± 3 *	35 ± 4 *	40 ± 3 *
LVM (g)	1.6 ± 0.1	1.8 ± 0.1	1.7 ± 0.1	1.4 ± 0.1 #	1.4 ± 0.04

Note: These results are the mean ± standard error (*n* = 7). One-way ANOVA followed by a post hoc Student–Newman Keuls test, **P* < 0.05 vs. sham, #*P* < 0.05 vs. OVX-10w-eERT.

Results/Discussion: In the echocardiographic EF was lower in OVX-20w-IERT vs. Sham. Also, the FS was diminished in all the groups vs. Sham. Nonetheless, the LVDS was increased in all groups vs. sham. The ESV, was only increased in OVX-20 w vs. sham. In addition, in the ECG parameters, a significant decrease in P-wave was observed in OVX-20 w vs. sham, while, OVX-10w-eERT was increased vs. all groups, equally QRS segment was higher in OVX-10w-eERT. The diastolic and mean blood pressure was higher in the OVX-20w and OVX-20W-IERT vs. sham group. LVSP and LVDP do not show changes, however, the $-dP/dt$ was decreased in OVX-10w and OVX-20w. Finally, we found an increase in collagen deposition and myocytes hypertrophy in OVX-20w and OVX-20w-IERT vs. sham group.

Conclusion(s): Late ERT seems not to prevent the cardiovascular diastolic dysfunction in aged female rat with ovariectomy, while the early administration prevents changes in diastolic blood pressure and collagen deposition.

REFERENCE(S)

1. Young, L., & Cho, L. (2019). Unique cardiovascular risk factors in women. *Heart*, 105(21), 1656–1660. <https://doi.org/10.1136/heartjnl-2018-314268>
2. Al-Khatib, S. M., Hill, J. A., & Bozkurt, B. (2019). Third annual go red for women issue. *Circulation*, 139(8), 999–1000. <https://doi.org/10.1161/CIRCULATIONAHA.119.039778>

Poster presentations—Drug discovery, development & evaluation

P095 | Identification of a novel MrgprX1-selective inhibitor and its inhibitory effect on chloroquine-induced pruritus

Kunhi Ryu; Wan Namkung

Yonsei University

Introduction/Background & aims: Chloroquine (CQ) is an anti-malarial drug that has been widely used in treatment and prevention of malaria more than 70 years. One of the major adverse effects of chloroquine

in treatment of malaria is CQ-induced histamine independent pruritus. The side effects result in refusal of further treatment of drug leading emergence of CQ-resistant *Plasmodium falciparum*. Recently, Mas-related G Protein-coupled receptor X1 (MrgprX1) has been revealed to play pivotal role in CQ-induced pruritus [1]. Previously discovered MrgprX1 inhibitors lack selectivity and have limitation in application to mouse model.

Method/Summary of work: We have performed a high-throughput screening for the identification of novel potent and selective MrgprX1 antagonist in HEK-293T cells expressing MrgprX1. CQ, ATP, ionomycin, histamine, protease-activated receptors 2-activating peptide (PAR2-AP), deoxycholic acid (DCA)-induced intracellular calcium levels were measured using Fluo-4 NW calcium assay kit in HEK-293T and HT29 cells. YFP fluorescence quenching assay was performed in TGR5, CFTR and halide sensor YFP-F46L/H148Q/I152L expressing CHO-K1 cells as previously described [2]. Acute pruritogen-induced model was used to evaluate effect of MX1_{inh}-A01. MX1_{inh}-A01 was administered intraperitoneally after 30 min acclimatization. After 30 min, pruritogen compounds (i.e., CQ, histamine, PAR2-AP and DCA) were subcutaneously administered into the nape of the neck, and scratching bouts was recorded for 30 min. Continuous scratch movements with hind limbs was defined as a bout of scratching. All experiments were performed independently for a minimum of five times. Student's *t*-test was used to conduct statistical analysis. Statistical significance was considered at *p* values <0.05.

Results/Discussion: The most potent and selective antagonist, MX1_{inh}-A01, fully inhibited CQ-induced MrgprX1 calcium signalling with an IC₅₀ of 1.6 μM whereas showing little or no effect on ATP and ionomycin-induced calcium signalling. Moreover, MX1_{inh}-A01 significantly decreased CQ-induced extracellular signal-regulated kinase (ERK)-1/2 phosphorylation. MX1_{inh}-A01 also potently blocked CQ activated MrgprA3, a CQ-responsive mouse orthologue of MrgprX1, with an IC₅₀ of 2.87 μM. Notably, MX1_{inh}-A01 did not affect significantly on histamine, PAR2-AP and DCA mediated cellular signalling. In pruritogen-induced acute pruritus model, MX1_{inh}-A01 strongly blocked CQ-induced pruritus in a dose related manner and had no significant effect against histamine, PAR2-AP and DCA-induced pruritus in mice.

Conclusion(s): These results indicate that MX1_{inh}-A01 is a novel selective and potent MrgprX1 antagonist. Therefore, MX1_{inh}-A01

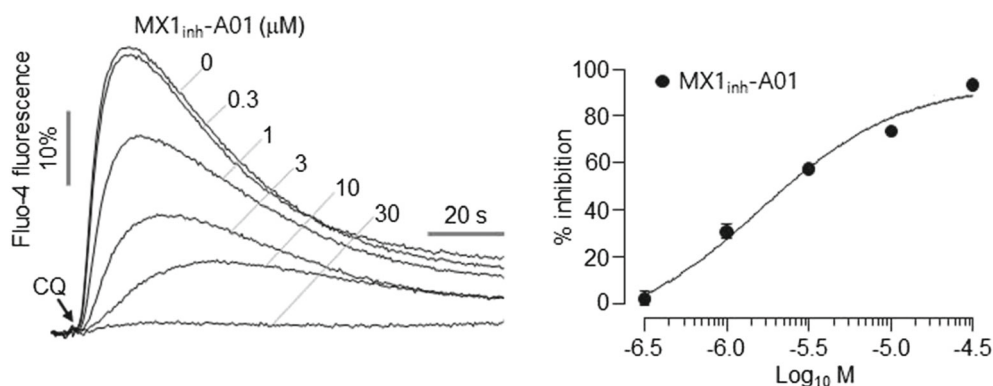


FIGURE 1 MX1_{inh}-A01 dose response of inhibition of CQ-induced MrgprX1 calcium signalling

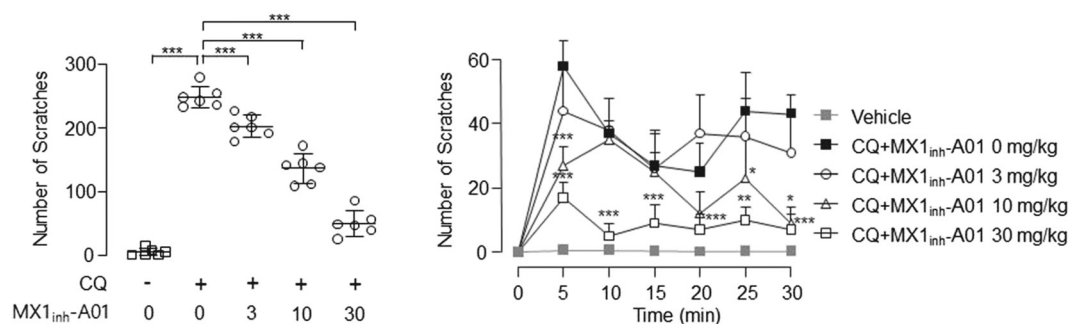


FIGURE 2 Effect of MX1_{inh}-A01 on total number and time-course of scratching induced by CQ. Mean ± SD, n = 6 mice per group, t-test, *p < 0.05, **p < 0.01, ***p < 0.001

may be useful as pharmacological tool and development of therapeutic agents for CQ-induced pruritus.

REFERENCE(S)

- Liu, Q., Tang Z., Surdenikova L., Kim S., Patel K.N., Kim A., Ru F., Guan Y., Weng H.J., Geng Y., Undem B.J., Kollarik M., Chen Z.F., Anderson D.J., Dong X. (2009). Sensory neuron-specific GPCR Mrgprs are itch receptors mediating chloroquine induced pruritus. *Cell*, 139(7), 1353–1365. <https://doi.org/10.1016/j.cell.2009.11.034>
- Lee, H. K., Park, J., Kim, B. R., Jun, I., Kim, T. I., & Namkung, W. (2021). Isorhamnetin ameliorates dry eye disease via CFTR activation in mice. *International Journal of Molecular Sciences*, 22(8), 3954. <https://doi.org/10.3390/ijms22083954>

P096 | Gas chromatography–mass spectrometry analysis and GnRH antagonist reversal activity of ethyl acetate fraction of *Caralluma dalzielii* N.E. Brown extract

Chinenye Ugwah-Oguejiofor¹; Charles Okoli²; Oguejiofor Ugwah³; Iyabo Adebisi⁴

¹Usmanu Danfodiyo University, Sokoto; ²University of Nigeria; ³Usmanu Danfodiyo University Teaching Hospital, Sokoto; ⁴Usmanu Danfodiyo University

Introduction/Background & aims: The reproductive system is governed by the hypothalamic–pituitary–gonadal axis (HPG), in which a pulsatile release of GnRH from the hypothalamus stimulates anterior pituitary gonadotropes to release LH and FSH, leading to steroid production from the ovaries [1]. Gonadotropin-releasing hormone (GnRH) antagonists have been used to suppress pituitary activity and to prevent premature surges of luteinizing hormone (LH) and ovulation [2]. Agents that are capable of reversing the blockade of GnRH may possess ovulation/fertility promoting properties. *Caralluma dalzielii* is a perennial cactus-like shrub that is used to treat infertility in Northern Nigeria. Previous study on the plant extract has validated its fertility promoting properties. The aim of the study was to determine the possible mechanism of the fertility promoting properties of *Caralluma dalzielii* N.E. Brown by determining the GnRH antagonist reversal activity of ethyl acetate fraction of the plant in Wistar rats.

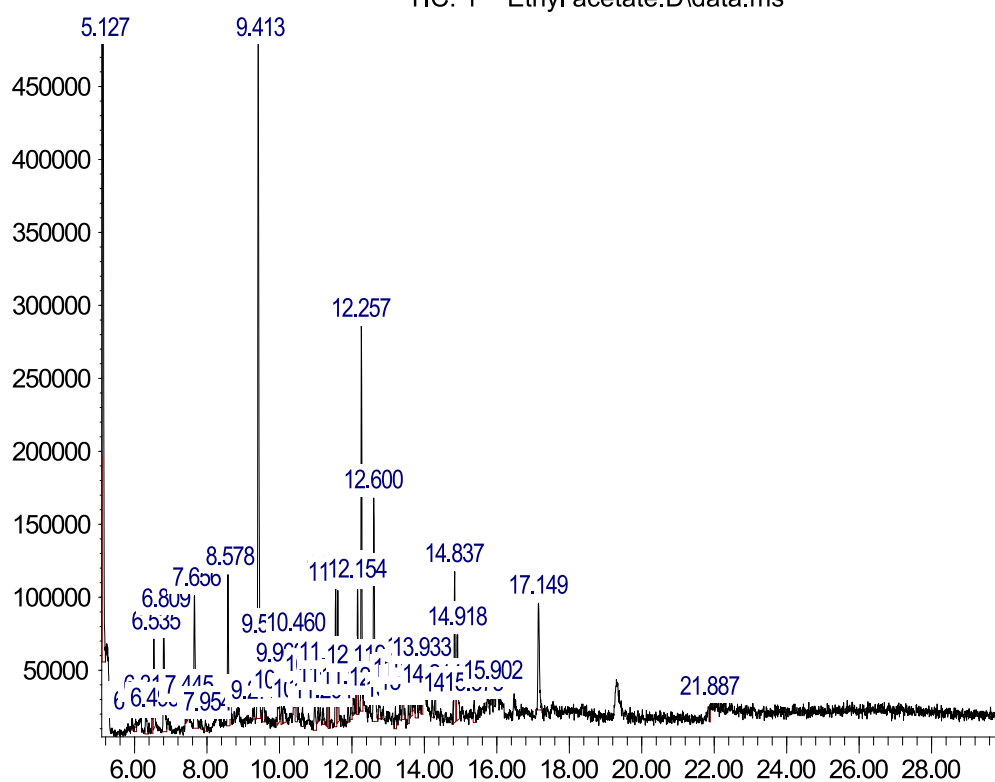
Method/Summary of work: Ethyl acetate fraction of *Caralluma dalzielii* was obtained by successive elution of dichloromethane/methanol (1:1) extract using petroleum ether first before ethyl acetate. The ethyl acetate fraction (EAF) was then concentrated over water bath at 50°C. Preliminary phytochemical analysis was carried out using standard procedures. The EAF was subjected to gas chromatography–mass spectrometry (GC-MS) analysis to identify its phytochemical constituents. Oral lethality test (LD₅₀) of EAF was determined in female Wistar rats using Lorke’s method. For the GnRH antagonist reversal activity, mature female virgin rats (200–220 g) with regular 4-day oestrus cycle were allotted into five groups (n = 6). At pro-oestrous phase of the oestrus cycle, the rats received a GnRH-antagonist (Cetorelix, 2 µg s.c.) at 1.00 p.m., which resulted in a 100% blockade of ovulation. At 3.00 p.m., all rats were treated with hCG (75 IU/kg/s.c.) as positive control, olive oil (negative control) or EAF (10, 25 and 40 mg/kg) orally. The following day, the oestrus cycles of the rats were determined. Blood samples were collected for LH and FSH assays. Ovaries were excised for histological evaluation.

Results/Discussion: The EAF contained alkaloids, flavonoids, steroids, tannins and steroids. GC-MS analysis of the fraction showed a total of 50 compounds (Figure 1) with cyclotrisiloxane, 1-dichloromethylsilyloxy-2-methylbenzene, 3'-amino-6-methoxyaurone, carbazole,1-,4,8-trimethyl, cyclotetrasiloxane, benzoic acid and 4H-1-benzopyran-4-one being the most abundant. The LD₅₀ of the fraction was calculated to be 70.71 mg/kg indicating that the fraction may be toxic to animals. Oestrus cycle of the rats in the groups treated with hCG and EAF (10, 25 and 40 mg/kg) showed oestrus phases. The groups significantly (p < 0.05) decreased LH but not FSH levels (Table 1). LH levels at pro-oestrous phase is highest, but at oestrus phase, the LH levels decreases implying that the fraction has reversed the GnRH antagonist blockade causing ovulation. This was evident in all groups except the negative control group. Histology of the ovaries in the EAF treated and positive control groups showed several fresh corpus lutea (Figure 2), which were absent in negative control group confirming the reversal.

Conclusion(s): Treatment of rats with EAF reversed blockade of ovulation caused by GnRH antagonist and caused the animals to reach oestrus phase. These findings reflect the potential ovulation induction effects of EAF and suggest that it could be used for the development

Abundance

TIC: 1 Ethyl acetate.D\data.ms



Time-->

FIGURE 1 GC-MS spectra of ethyl acetate fraction of *Caralluma dalzielii*

Treatment	Dose (mg/kg)	Ovary weight (mg/g)	LH (mIU/ml)	FSH (mIU/ml)
hCG (75 IU/kg)	-	30.38 ± 3.04*	4.01 ± 0.14*	1.22 ± 0.11
EAF	10	27.65 ± 2.55*	4.49 ± 0.2*	1.25 ± 0.07
	25	27.22 ± 3.94*	4.17 ± 0.12*	1.28 ± 0.08
	40	20.05 ± 3.53*	4.14 ± 0.11*	1.24 ± 0.06
Control (5 ml/kg)	-	35.42 ± 3.73	5.94 ± 0.13	1.13 ± 0.05

TABLE 1 Effect of ethyl acetate fraction on luteinizing and follicle stimulating hormones

Note: Values presented as mean ± SD; n = 6; *p < 0.05.

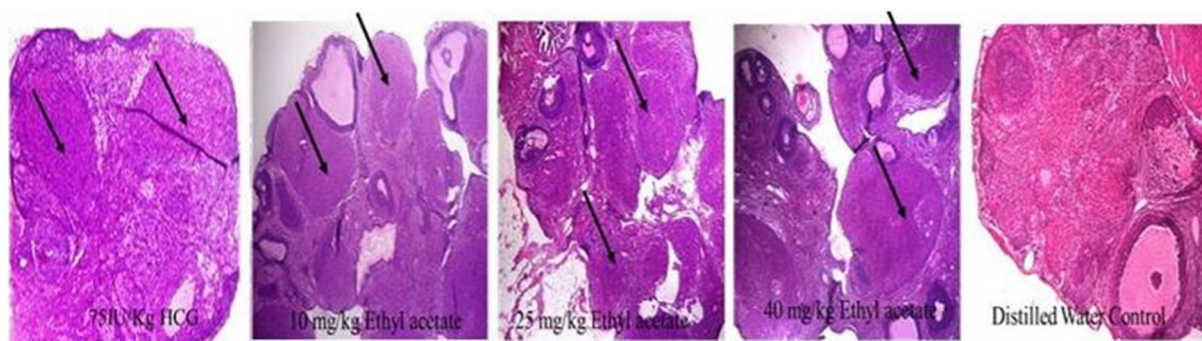


FIGURE 2 GC-MS spectra of ethyl acetate fraction of *Caralluma dalzielii*

effective drug in treatment of infertility. Further studies are needed to identify and isolate the active compound(s) present in the fraction.

REFERENCE(S)

1. Chaudhari, N., Dawalbhakta, M., & Nampoothiri, L. (2018). GnRH dysregulation in polycystic ovarian syndrome (PCOS) is a manifestation of an altered neurotransmitter profile. *Rep Biol Endocrinol*, 16(1), 1–13. <https://doi.org/10.1186/s12958-018-0354-x>
2. Wang, Y., Kuang, Y., Chen, Q., & Cai, R. (2018). Gonadotropin-releasing hormone antagonist versus progestin for the prevention of premature luteinising hormone surges in poor responders undergoing in vitro fertilisation treatment: Study protocol for a randomised controlled trial. *Trials*, 19(1), 1–6. <https://doi.org/10.1186/s13063-018-2850-x>

P098 | Gastroprotective activity of methanol extract of *Dioscorea prehendilis*

Iyabo Adebisi¹; Chinenye Ugwah-Oguejiofo¹; Kabiru Abubakar¹; Abdullahi Sulaiman¹; Sunday Fajobi²

¹Usmanu Danfodiyo University Sokoto, Nigeria; ²Specialist Hospital, Sokoto, Nigeria

Introduction/Background & aims: Peptic ulcer disease is a group of diseases that include gastric ulcers, duodenal ulcers, and gastritis. It is caused by an imbalance between the destructive and defensive factors in the stomach^[1]. *Dioscorea prehendilis* (DP) commonly called wild yam is used ethno botanically in the treatment of snake and scorpion bites. This study is aimed at investigating the gastroprotective effect of the methanol extract of DP in rat models of gastric ulcers.

Method/Summary of work: Rhizomes of DP were extracted by maceration in 80% methanol. The resulting extract was dried over a water bath maintained at 45°C. Phytochemical analysis of the extract was done using standard protocols. Acute oral toxicity was determined using the “Up and Down” procedure according to the Organization for Economic Development (OECD) guideline no 425. The

gastroprotective activity of DP was evaluated in ethanol and indomethacin-induced ulcer models in rats according to the methods of Ugwah^[2]. For the ethanol model, 25 Sprague–Dawley rats (160–180) g were allotted into five groups of five animals each. They were fasted for 24 h but had access to water for up to 2 h before the commencement of the experiment. Group 1 served as normal control and received distilled water (5 ml/kg). Group 2 received the standard drug omeprazole (20 mg/kg) while groups 3–5 received 125, 250, and 500 mg/kg of DP, respectively. An hour later, gastric lesions were induced with absolute ethanol (8 ml/kg). For the indomethacin-induced model, 25 Sprague–Dawley rats (160–180) were similarly treated as above but gastric lesions were induced with 100 mg/kg indomethacin. After 2 h for the ethanol-induced model and 4 h for the indomethacin model, rats were sacrificed and their stomach excised and opened along the greater curvature. The total length of all lesions for each stomach was designated as ulcer index and their percentage inhibition was calculated using the expression:

$$\% \text{Inhibition} = \frac{\text{Ulcer index of control} - \text{Ulcer index of the test}}{\text{Ulcer index of control}} \times 100$$

Results were expressed as mean ± standard error of the mean (SEM). Statistical analysis was performed by one-way analysis of variance (ANOVA) followed by Dunnett’s t-test for multiple comparisons. $p < 0.05$ was considered significant.

Results/Discussion: Phytochemical analysis of the methanol extract of DP shows the presence of saponins, tannins, flavonoids, steroids, carbohydrates, and proteins. At a limit dose of 2000 mg/kg, all the rats in the short and long-term observation survived hence the median lethal dose (LD₅₀) is >2000 mg/kg. The administration of absolute ethanol and indomethacin produced intense ulceration in the stomach of the rats. Oral administration of the extracts at doses of 125, 250, and 500 mg/kg exhibited a significant ($p < 0.01$) dose-dependent reduction in gastric lesions (Figure 1a) and percentage inhibition of 65.16, 68.20, and 79.64%, respectively (Figure 1b) in the

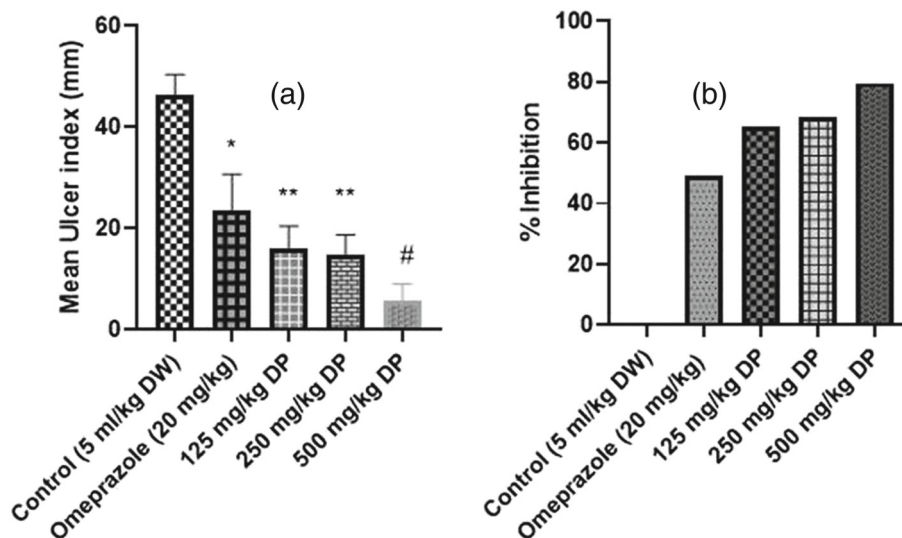


FIGURE 1 Effect of methanol extract of *Dioscorea prehendilis* on ethanol-induced ulcer showing mean ulcer index (a) and percentage inhibition (b). DW = Distilled water, DB = *Dioscorea prehendilis*. Data presented as mean ± SEM, N = 5 for all groups. * $p < 0.05$, ** $p < 0.01$, # $p < 0.0001$.

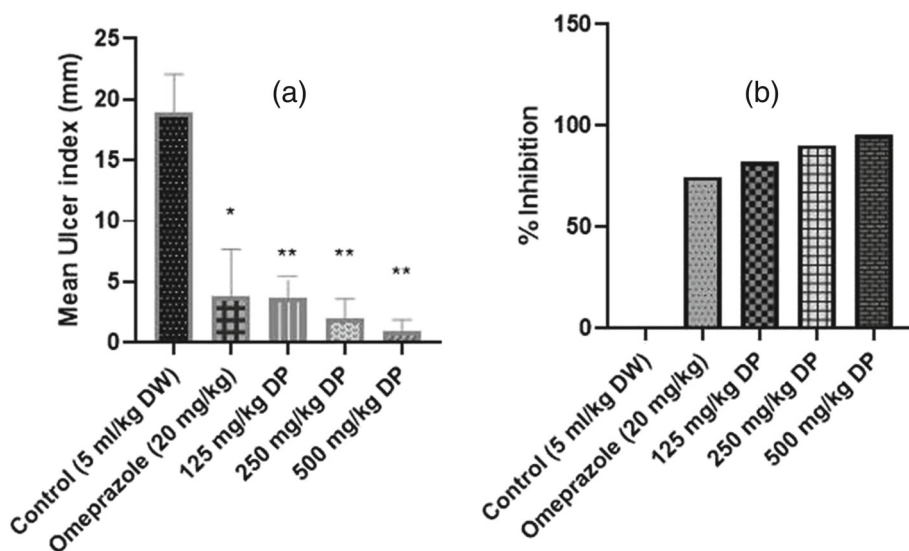


FIGURE 2 Effect of methanol extract of *Dioscorea prehendensis* on indomethacin-induced ulcer showing mean ulcer index (a) and percentage inhibition (b). DW = Distilled water, DB = *Dioscorea prehendensis*. Data presented as mean \pm SEM, N = 5 for all groups. * $p < 0.05$, ** $p < 0.01$.

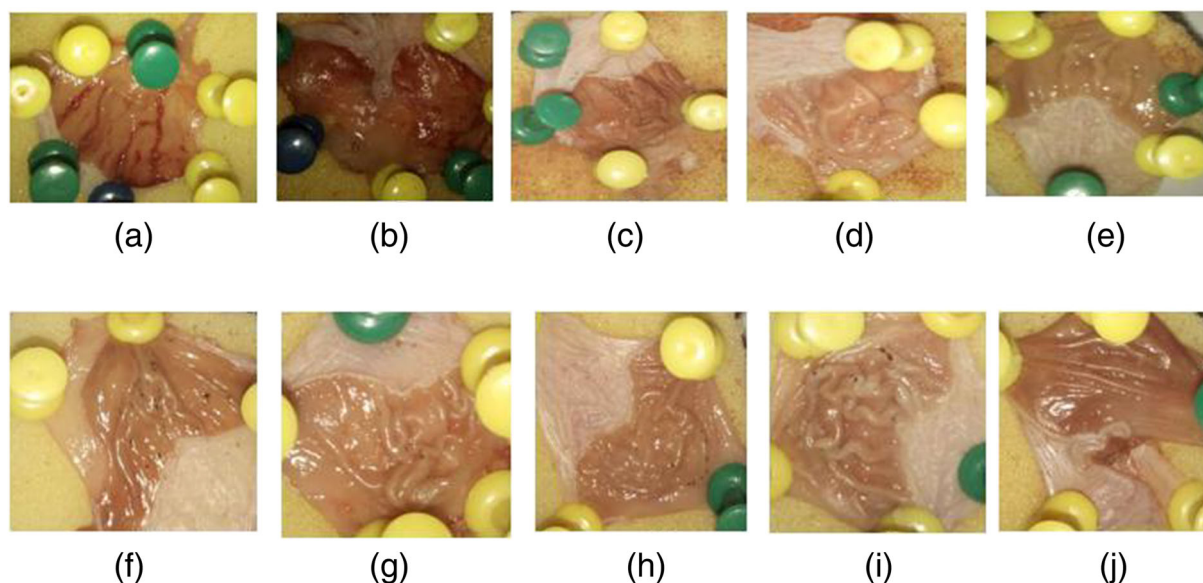


FIGURE 3 Pictures of gastric mucosa of rats showing areas of ulceration. a-e: For Control, omeprazole (20mg/kg), 125, 250, 500mg/kg *Dioscorea prehendensis* respectively in the ethanol-induced model. f-j: Control, omeprazole (20mg/kg), 125, 250, 500 mg/kg *Dioscorea prehendensis* respectively in the indomethacin-induced model

ethanol model. Similarly, in the indomethacin model, the extract at the doses of 125, 250, and 500 mg/kg offered significant ($p < 0.01$) gastroprotection against ulceration (Figure 2a). The percentage inhibitions were 81.89%, 90.44%, and 95.35%, respectively, compared with the control group (Figure 2b). Furthermore, the extract showed higher percentage inhibition than the standard drug (i.e., omeprazole, 20 mg/kg) at all doses in the two models.

Ethanol as an agent that induces gastric ulcers is usually employed in screening medicinal plants for antiulcer and cytoprotective properties. It produces severe damage to gastric mucosa by promoting a decrease in the secretion of bicarbonate and mucus

production, which ultimately leads to the development of haemorrhagic and necrotic lesions. Indomethacin on the other hand acts by inhibiting the activity of the cyclooxygenase enzyme leading to a reduction in prostaglandins production, thereby preventing the cytoprotective effect conferred by prostaglandins^[3]. Pretreatment with extract of DP conferred gastroprotection against these agents. The phytochemical analysis of the extract of DP shows the presence of some phytochemicals such as alkaloids, tannins, saponins, and flavonoids, all of which have been reported previously in literature to possess ulcer healing and gastroprotective effects.

Conclusion(s): In conclusion, methanol extract of *Dioscorea prehendilis* offered gastric protection against ethanol and indomethacin-induced gastric ulcers, with better protection in the indomethacin model. It may therefore be used in the development of new phytotherapeutic formulations for the treatment of peptic ulcer diseases.

REFERENCE(S)

1. Tytgat, G. N. J. (2011). Etiopathogenetic principles and peptic ulcer disease classification. *Digestive Diseases*, 29(5), 454–458. <https://doi.org/10.1159/000331520>
2. Ugwah, M. O., Ugwah-Oguejiofor, C. J., Etuk, E. U., Bello, S. O., & Aliero, A. A. (2019). Evaluation of the antiulcer activity of the aqueous stem bark extract of *Balanites aegyptiaca* L Delile in Wistar rats. *Journal of Ethnopharmacology*, 239, 111931. <https://doi.org/10.1016/j.jep.2019.111931>
3. Hiruma-Lima, C. A., Batista, L. M., de Almeida, A. B. A., de Pietro Magri, L., dos Santos, L. C., Vilegas, W., & Brito, A. R. M. S. (2009). Anti-ulcerogenic action of ethanolic extract of the resin from *Virola surinamensis* Warb.(Myristicaceae). *Journal of Ethnopharmacology*, 122(2), 406–409. <https://doi.org/10.1016/j.jep.2008.12.023>

P101 | Investigation of the pharmacology of the two isoforms of human GPR35

Amlan Ganguly; Tezz Quon; Amanda E. Mackenzie; Graeme Milligan
 University of Glasgow

Introduction/Background & aims: G protein-coupled receptor 35 (GPR35) is a poorly characterised receptor that has garnered increased attention as a therapeutic target through its potential contributions to a range of inflammatory and cardiovascular diseases, but many of its biological functions remain largely undefined. The human GPR35 gene can be transcribed and translated into three variants of which variant 1 represents a shorter isoform, GPR35a (309 amino acids), while variants 2 and 3 both encode the same longer isoform, GPR35b (340 amino acids) with 31 extra amino acids in the N-terminal domain [1]. Although they display highly similar pharmacology, agonist efficacy is almost 70% lower in the longer isoform compared with the shorter [2].

Method/Summary of work: Site directed mutagenesis generated mutants in various positions of both GPR35a and GPR35b to assess effects on both activation of the G protein G_{13} and β -arrestin-2 recruitment.

Results/Discussion: In GPR35a, a cysteine 8 within the N-terminus likely forms a disulphide bond with cysteine 248 of extracellular loop 3 as mutation of either of these residues nearly eliminates agonist function in both G protein and arrestin-based assays. In GPR35b, there is an additional cysteine at position 27. Mutation of this residue results in markedly increased agonist function, suggesting an additional disulphide bond limits agonist-induced activation of GPR35b. To further explore the role of the N-terminal extension of GPR35b, 10 additional mutants were generated in the backbone of Cys27Ser GPR35b in which various residues were replaced by cysteine. From

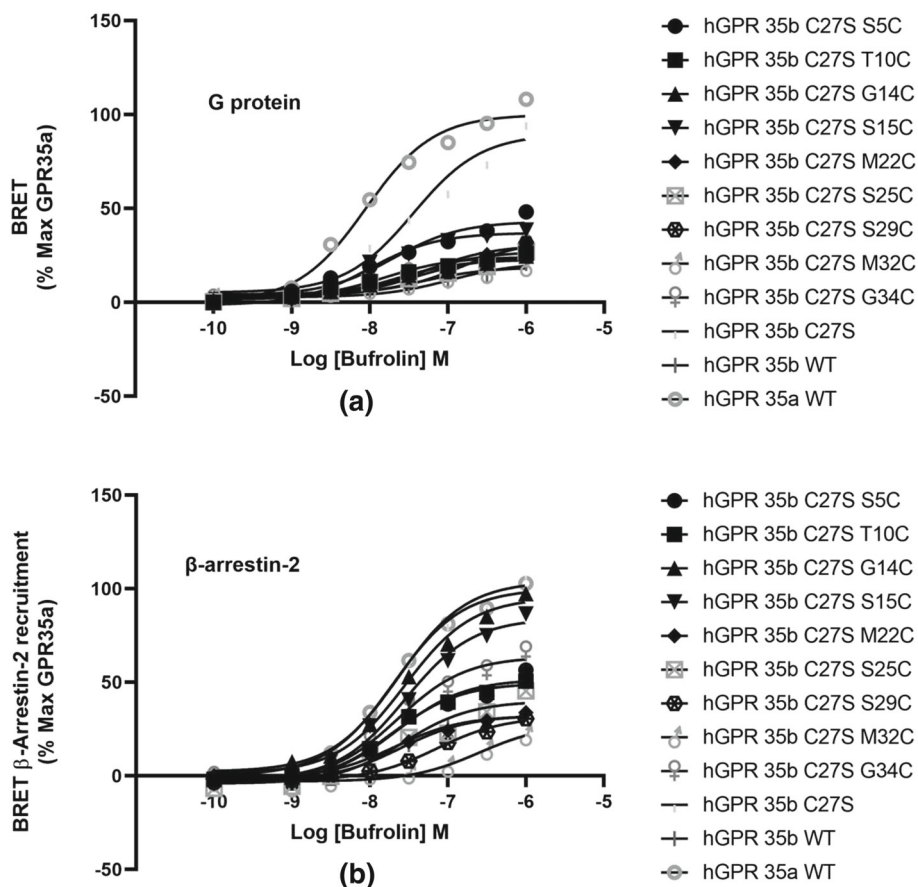


FIGURE 1 Comparison of effect of hGPR35 isoform mutants transiently expressed in HEK293T cells in (a) $G_{\alpha 13}$ SPASM sensors, (b) hGPR35 tagged with enhanced yellow fluorescent protein (eYFP) and β -arrestin-2 tagged with *Renilla* luciferase; (BRET) signals were monitored after treating with varying concentrations of Bufrolin for 5 min. hGPR35aWT, hGPR35bWT and hGPR35b C27S were used as control for each assay. Datasets represent the mean of three independent experiments \pm SEM, normalised to the maximum GPR35a response.

TABLE 1 Efficacy and potency of Bufrolin at different mutants of hGPR35-G α_{13} SPASM sensors and hGPR35 isoforms tagged with eYFP and β -arrestin-2 tagged with *Renilla* luciferase

	Efficacy (SPASM mutants)	Potency (log EC ₅₀)	Efficacy (mutants for Arrestin interaction)	Potency (log EC ₅₀)
hGPR35b C27S S5C	43.10 ± 0.34	-7.70 ± 0.01	51.63 ± 0.13	-7.65 ± 0.01
hGPR35b C27S T10C	24.23 ± 0.05	-7.82 ± 0.03	49.56 ± 0.01	-7.71 ± 0.01
hGPR35b C27S G14C	22.78 ± 0.36	-7.70 ± 0.01	95.36 ± 0.37	-7.55 ± 0.01
hGPR35b C27S S15C	37.03 ± 0.19	-8.01 ± 0.01	84.24 ± 0.32	-7.55 ± 0.01
hGPR35b C27S M22C	30.58 ± 0.27	-7.29 ± 0.01	32.18 ± 0.21	-7.68 ± 0.02
hGPR35b C27S S25C	23.98 ± 0.35	-7.45 ± 0.02	40.00 ± 0.13	-7.57 ± 0.01
hGPR35b C27S S29C	33.09 ± 0.45	-6.84 ± 0.02	31.64 ± 0.18	-7.15 ± 0.01
hGPR35b C27S M32C	18.79 ± 0.23	-7.36 ± 0.03	27.80 ± 0.17	-6.60 ± 0.01
hGPR35b C27S G34C	27.12 ± 0.38	-7.39 ± 0.05	63.69 ± 0.28	-7.64 ± 0.01
hGPR35b C27S	89.73 ± 0.66	-7.44 ± 0.01	103.9 ± 0.07	-7.63 ± 0.01
hGPR35b WT	21.21 ± 0.41	-6.97 ± 0.01	32.32 ± 0.25	-7.61 ± 0.01
hGPR35a WT	100.00 ± 0.00	-8.05 ± 0.01	100.0 ± 0.00	-7.69 ± 0.01

Note: Data represent the mean ± SEM from three independent experiments.

the data, we have found that with the introduction of cysteine almost all the mutants displayed G protein activation and β -arrestin-2 recruitment activity nearly similar to hGPR35b (wild type).

Conclusion(s): The observed results may be due to the formation of new disulphide bonds at different positions of the N-terminal region and can thus restrict activation of the long GPR35b isoform. Molecular modelling and, potentially, information from atomic level structures will be required to understand fully the importance of the organisation of the N-terminal domain of GPR35b.

REFERENCE(S)

1. Quon T, Lin LC, Ganguly A, Tobin AB, Milligan G. Therapeutic opportunities and challenges in targeting the orphan G protein-coupled receptor GPR35. *ACS Pharmacol Transl Sci*, 2020;3(5):801-812. <https://doi.org/10.1021/acspsci.0c00079>
2. Marti-Solano M, Crilly SE, Malinverni D, Munk C, Harris M, Pearce A, Quon T, Mackenzie AE, Wang X, Peng J, Tobin AB, Ladds G, Milligan G, Gloriam DE, Puthenveedu MA, Babu MM Combinatorial expression of GPCR isoforms affects signalling and drug responses. *Nature*, 2020;587(7835):650-656. <https://doi.org/10.1038/s41586-020-2888-2>

P102 | Multityrosine kinase inhibitor sunitinib has anti-inflammatory activity in macrophages mediated via inhibition of NF- κ B

Laura Chaffey; Amelia Bowman; Annabell Roberti; Gareth Purvis; Conan O'Brien; David R. Greaves

University of Oxford

Introduction/Background & aims: With reduced development costs and lower toxicity-associated failure risks, drug repurposing is an attractive strategy for the discovery of novel classes of anti-

inflammatory therapeutics. Macrophages are a driver of pathology in both acute and chronic inflammatory disease and are therefore an attractive therapeutic target. The aim of this study was to investigate previously unreported anti-inflammatory activity of FDA-approved medicines for repurposing in inflammatory disease.

Method/Summary of work: The murine macrophage RAW-Blue NF- κ B reporter cell-line was used to screen a library of 159 FDA-approved medicines for NF- κ B inhibitory activity ($n = 1$). NF- κ B-mediated anti-inflammatory effects of sunitinib were investigated in vitro in lipopolysaccharide (LPS; 100 ng ml⁻¹) stimulated bone marrow derived macrophages (BMDMs; $n = 7$) and IC₅₀ values for cytokine production were determined using a sigmoidal concentration-response model. To assess activity of sunitinib in inflammatory models in vivo, male C57Bl/6 mice (10-12 per group) were orally dosed with sunitinib (30 mg/kg) at 24 and 4 h prior to intraperitoneal injection with LPS (10 mg/kg) and then sacrificed at 1 and 24 h post-injection to determine cytokine production and organ dysfunction. To investigate effects of sunitinib in chronic inflammation, male *Ldlr*^{-/-} mice on a C57Bl/6 background were fed a high fat diet for 8 weeks. For the final 4 weeks, mice were orally dosed with either sunitinib (30 mg/kg; $n = 15$) or vehicle ($n = 14$) daily five times per week. Inflammatory markers and atherosclerotic plaque formation were assessed.

Results/Discussion: Initial screening identified 18 medicines with >25% inhibition of NF- κ B activity. Of these, the multityrosine kinase inhibitor sunitinib was further investigated and found to reduce proinflammatory mediator production in BMDMs (IC₅₀ values: TNF α = 0.97 μ M, IL-6 = 1.14 μ M, CCL2 = 1.19 μ M, NO = 0.59 μ M) without compromising cell viability at active concentrations. In vivo, sunitinib significantly reduces serum TNF α (41% reduction; $p < 0.05$; one-way ANOVA; $n = 10$) and p65 nuclear translocation (55% reduction; $p < 0.05$; T-test; $n = 6$) in endotoxemia at 1 h, and reduces plasma markers of organ damage (aspartate aminotransferase, alanine aminotransferase, creatinine, urea; $p < 0.05$; one-way ANOVA;

$n = 12$) at 24 h. In a chronic inflammatory model of high-fat diet-induced atherosclerosis, sunitinib significantly lowers serum TNF α compared with vehicle (55% reduction; $p < 0.001$; T -test; $n = 14-15$), with no effect on plaque size.

Conclusion(s): Sunitinib has underexplored anti-inflammatory activity in macrophages ex vivo and in vivo, mediated at least in part via an NF- κ B-dependent mechanism. These results justify the further characterisation of sunitinib in inflammatory disease and investigation into the feasibility of its repurposing as an anti-inflammatory therapeutic.

P105 | A fluorescent G protein mimetic peptide probe for high-throughput characterisation of intracellular allosteric modulator binding and GPCR activation

James Farmer; Nicholas Holliday; Shailesh Mistry; Charles Laughton
University of Nottingham

Introduction/Background & aims: G protein-coupled receptors (GPCR) are the most widely therapeutically targeted family of membrane receptors. GPCR intracellular allosteric modulators (IAMs) provide opportunities to develop more selective therapeutics with reduced side effects^[1]. However, a general method for identifying new IAMs is lacking. Here, we develop a fluorescent G protein peptidomimetic probe for the Gs-GPCR site. We show its use in a novel β_2 -adrenoceptor (AR) IAM binding assay, and as a receptor activation sensor.

Method/Summary of work: The abilities of G α S C-terminus peptides (G α S11, G α S24 and G α S19cha18, [cha = cyclohexylalanine]^{[1],[2]}) to modulate ligand affinity were explored in TR-FRET competition binding assays. Competition between BODIPY-FL-PEG8-propranolol (K_D :

16 nM) and orthosteric ligands determined effects of G α C-terminal peptides on ligand binding. Cold ligand was incubated with Terbium labelled SNAP- β_2 -AR HEK293 membranes (1 μ g/well), 20 nM BODIPY-FL-PEG8-propranolol and either buffer or 10 μ M G α peptide. The assay plate was incubated at 37°C and specific binding analysed to determine IC50s at regular timepoints. Nonspecific binding (NSB) was assessed with 10 μ M ICI118551.

Tetramethylrhodamine-G α S19cha18 (TMR-G α S19cha18) binding was determined using 1 μ g SNAP- β_2 -AR-Nanoluc HEK293 membranes preincubated with 1/960 diluted furimazine (from manufacturer stock). NSB was assessed with 10 μ M G α S19cha18. In recruitment/competition assays, 500 nM or 1 μ M tracer was incubated with corresponding concentrations of agonist/competing peptide. Competition studies included 10 μ M isoprenaline, promoting tracer recruitment. NanoBRET ratios were measured at 37°C every 1.16 min over 30 min post membrane injection.

Results/Discussion: Within BODIPY-FL-PEG8-propranolol TR-FRET studies, G α S19cha18 and G α S24 increased isoprenaline affinity by 12 and 15 times, respectively (Figure 1).

TMR-G α S19cha18 specific binding only occurred in the presence of 10 μ M isoprenaline (K_D : 588 \pm 19 nM, $n = 5$). TMR-G α S19cha18 in competition studies determined affinities of G α S24 (K_i 2.2 \pm 0.2 μ M, $n = 5$) and G α S19cha18 (K_i 249 \pm 0.1 nM, $n = 5$) at the intracellular site. Ligand stimulated TMR-G α S19cha18 binding derived potency and maximal responses of different agonists (Figure 2). TMR-G α S19cha18 binding further displays Gs receptor specificity, binding with Gs coupled EP $_2$ but not Gi coupled CXCR2.

Conclusion(s): We demonstrate G protein peptidomimetics can form the basis of GPCR-G protein binding site probes, broadly applicable for NanoBRET binding assays for IAM compound screening. TMR-G α S19cha18 recruitment also provides a homogenous readout for agonist activation in kinetic and endpoint assays.

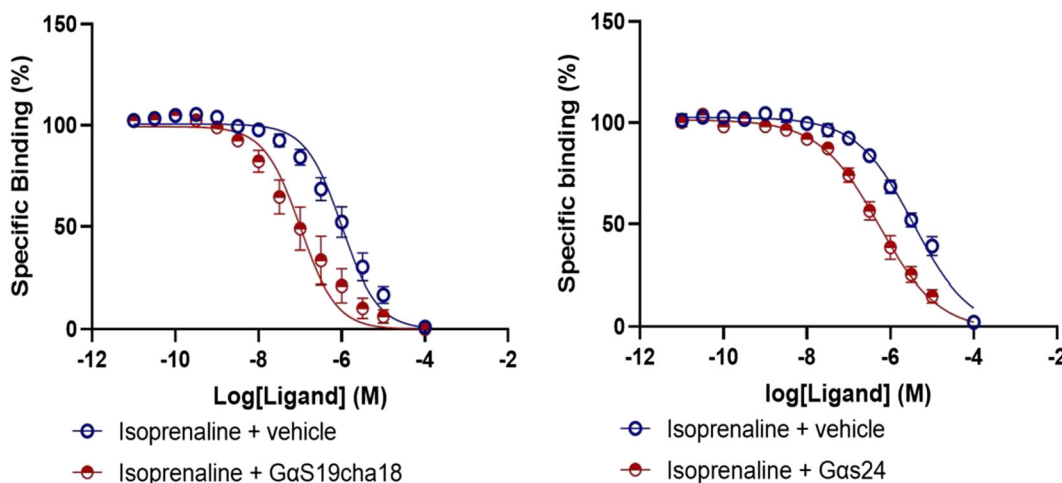


FIGURE 1 TR-FRET based competition between FI-propranolol and β_2 -AR agonist isoprenaline in the presence of 10 μ M G α S19cha18 or G α S24. Data are pooled and normalised ($n = 5$).

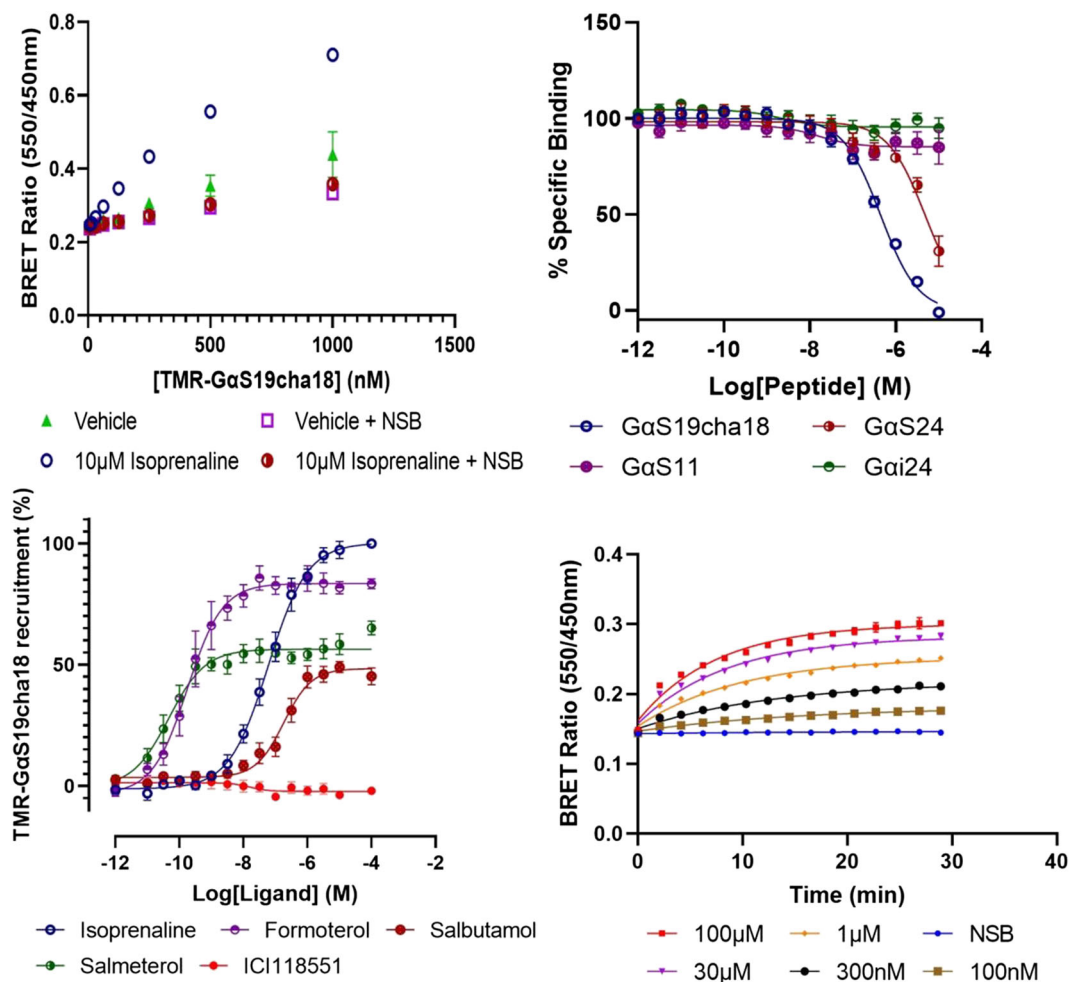


FIGURE 2 NanoBRET assays characterising the utility of TMR-GαS19cha18 as a fluorescent tracer of the β_2 -AR-Gs intracellular binding site. (top left) Saturation binding of TMR-GαS19cha18 in the presence of either buffer [vehicle] or agonist. (top right) Competition between unlabelled Gα peptides and TMR-GαS19cha18. (bottom left) Ligand dependant recruitment of a single concentration of TMR-GαS19cha18, identifying both full and partial agonism, for example, isoprenaline pEC50 7.25 ± 0.12 M, Rmax $100.59 \pm 1.26\%$ 10 μM iso response; salmeterol pEC50 10.32 ± 0.18 M, Rmax $57.09 \pm 3.54\%$. (bottom right) Kinetic analysis of isoprenaline concentration dependant recruitment of TMR-GαS19cha18. All data are either representative or pooled, normalised, data from 3–5 independent experiments.

REFERENCE(S)

- Mannes M, Martin C., Triest S., Pia Dimmito M., Mollica A., Laeremans T., Menet C.J., Ballet S. (2021). Development of generic G protein peptidomimetics able to stabilise active state Gs protein-coupled receptors for application in drug discovery. *Angewandte Chemie, International Edition*, 60, 10247, 10254. <https://doi.org/10.1002/anie.202100180>
- Gilchrist, A., Li, A., & Hamm, H. E. (2002). G COOH-terminal minigene vectors dissect heterotrimeric G protein signalling. *Sci Sig.*, 2002(118), pl1–pl1. <https://doi.org/10.1126/scisignal.1182002pl1>

P106 | *Zingiber officinale* inhibits angiogenesis and down-regulated vascular endothelial growth factor (VEGF) gene expression in the rat aortic ring model

Iyabo Adebisi; Oricha Bello; Constance Shehu; Musa Abdullahi; Nnaemeka Ndodo; Mohammed Umar; Chinenye Ugwah-Oguejiofor
 Usmanu Danfodiyo University Sokoto, Nigeria

Introduction/Background & aims: *Zingiber officinale* (ZO), common name ginger, is used extensively worldwide as a spice, flavouring agent, and herbal remedy. Several in vitro and in vivo studies have shown that its rhizome and several of its phenolic constituents have anticancer potential, although little is known about the mechanisms of action^[1]. The VEGF (vascular endothelial growth factor) pathway has emerged as an important target for cancer therapy. It promotes tumour angiogenesis by stimulating endothelial cells' proliferation and survival^[2]. This study is aimed at investigating the effect of methanol extract of rhizomes of ZO on vascular endothelial growth factor (VEGF) gene expressions in the rat aortic rings model of angiogenesis. **Method/Summary of work:** The rhizomes of ZO were extracted by maceration in 80% methanol. The resulting extract was dried over a water bath maintained at 45°C. Angiogenesis was studied using the rat aortic ring model. Isolated rat aortic rings from Sprague–Dawley rats (8–10 weeks) were sectioned into 1.0 mm thick rings and cultured in serum-free endothelial basal media-2 (EBM-2). ZO at a final

concentration of 1000, 500, 250, 125, and 75 µg/ml was added to the cultures and maintained for 8 days. Recombinant VEGF (5 µg/ml) was included as positive control while the untreated media was used as the negative control. Total RNA was extracted using Trizol (LS Invitrogen, USA), and the final total RNA quality was assessed by the spectrophotometric method (A_{260}/A_{280}). Complementary DNA (cDNA) was synthesised using QIAGEN one-step real-time polymerase chain reaction (RT-PCR) kit in a final volume of 20 µl according to the manufacturer's instruction. The following primers were used for VEGF-A: forward, 5'-CAGGCTGCTGTAACGATGAA-3' and reverse, 5'-TTTCTTGCCTTCGTTTTT-3'. Actin-B was used as the house-keeping/reference gene. Template RNA from untreated control aortic rings was used to generate a standard curve. Quantification of gene expression was calculated using the standard curve and cycle threshold of each sample. The results of gene expression were normalised to

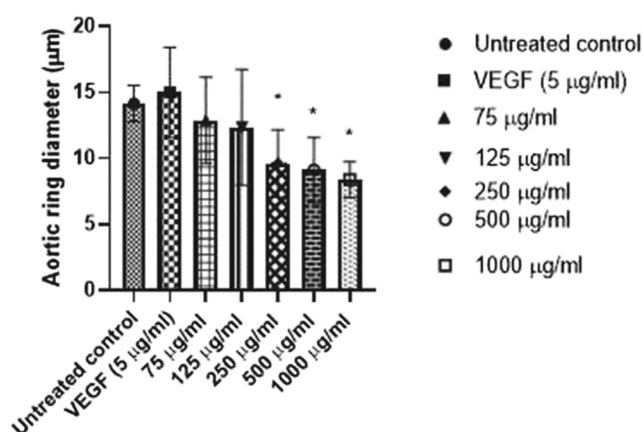


FIGURE 1 Mean diameter of rat aortic rings culture in methanol extract of *Zingiber officinale* incubated at 37°C, 5% CO₂. Pictures were captured on day 8 and the ring diameter was measured using a measuring gauge of a digital microscope. VEGF = Vascular endothelial growth factor, * is significant at p<0.05 compared to the untreated control. N = 2.

reference gene expression (actin -B) and the fold change was determined in comparison with untreated control. One-way ANOVA with Dunnet post hoc was used to assess the significant differences at ($p < 0.05$).

Results/Discussion: The ability of the extract of *Zingiber officinale* to inhibit angiogenesis was evaluated by measuring the diameter of the rat aortic rings cultured in its methanol extract. A significant dose-dependent decrease was observed in the diameter of aortic rings cultured in 250, 500, and 1000 µg/ml ZO extract compared with the untreated control as shown in Figure 1. Furthermore, ZO showed a dose-dependent down-regulation in VEGF expression compared with the untreated control. The relative VEGF gene expression in the aortic rings treated with ZO extract was found to be significantly lower ($p < 0.05$) than the untreated control in all the concentrations used as shown in Figure 2. The results demonstrate that ZO inhibits angiogenesis and may be useful in the treatment of tumours and other angiogenesis-dependent processes. *Zingiber officinale* extracts have been reported to inhibit growth and modulate secretion of angiogenic factors in a number of cancer cell lines^[3].

Conclusion(s): In conclusion, *Zingiber officinale* decreased microvessel formation and down-regulated the expression of VEGF in the rat aortic rings. This indicates that it possesses phytoconstituents that can inhibit angiogenesis and decrease VEGF gene expression. This may be a potential mechanism for its reported anticancer properties.

REFERENCE(S)

1. European Medicines Agency, 2012. Assessment report on *Zingiber officinale* Roscoe rhizome. EMA/HMPC/577856/2010
2. Yang, J., Yan, J., & Liu, B. (2018). Targeting VEGF/VEGFR to modulate antitumor immunity. *Front. Immunol.*, 9, 978. <https://doi.org/10.3389/fimmu.2018.00978>
3. Dongare, S., Gupta, S. K., Mathur, R., Saxena, R., Mathur, S., Agarwal, R., Nag, T. C., Srivastava, S., & Kumar, P. (2016). *Zingiber officinale* attenuates retinal microvascular changes in diabetic rats via anti-inflammatory and antiangiogenic mechanisms. *Molecular Vision*, 22, 599, 609.

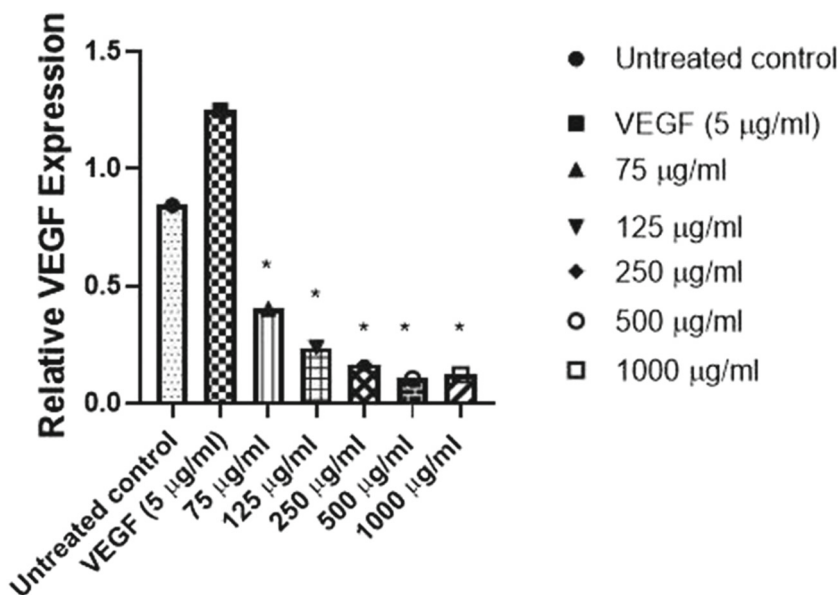


FIGURE 2 Expression level of VEGF in rat aortic ring treated with *Zingiber officinale* using primer design master mix precision plus qPCR. Data are shown as a fold change of VEGF levels in aortic rings. VEGF = Vascular endothelial growth factor, * is significant at p<0.05 compared to the untreated control. N = 2

P107 | Drug combination therapies effectively inhibit the dermonecrotic activity of cytotoxic venoms from geographically diverse snake species in vivo

Steven Hall; Edouard Crittenden; Charlotte Dawson; Keirah Bartlett; Adam Westhorpe; Laura-Oana Albulescu; Nicholas Casewell

Liverpool School of Tropical Medicine

Introduction/Background & aims: Snakebite is a neglected tropical disease (NTD) that kills approximately 138,000 and maims 400,000

people annually. Polyclonal antibody-based antivenoms, which are expensive and poorly efficacious against snake venom-induced tissue necrosis, are the only currently available treatments [1]. Inhibition of toxin families prevalent across diverse snake species by small molecule drug inhibitors offers a revolutionary new way of treating snakebite-induced necrosis, particularly when used in combination to target multiple toxin families [2]. Herein, we describe how the repurposed drugs 2,3-dimercapto-1-propanesulfonic acid (DMPS), marimastat, and varespladib inhibit the dermonecrotic activity of geographically diverse cytotoxic snake venoms and how their activity is improved when used in combination.

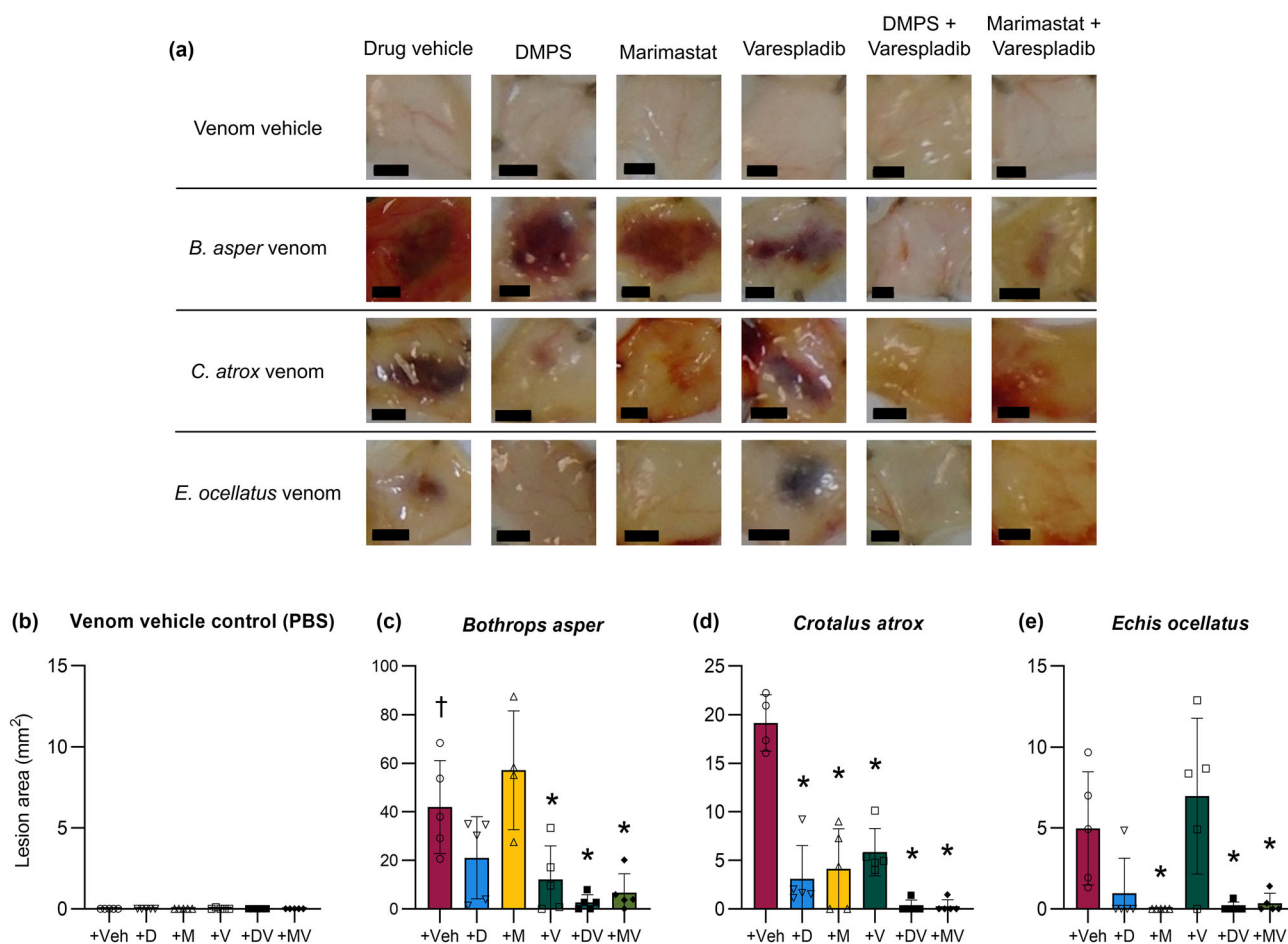


FIGURE 1 Dermal lesions induced by diverse cytotoxic snake venoms are inhibited by drug combinations containing either DMPS or marimastat with varespladib. Mice were intradermally injected with *B. asper* (150 µg), *C. atrox* (100 µg), or *E. ocellatus* (39 µg) venom or venom vehicle control (PBS) that had been preincubated with drug vehicle control (98.48% PBS, 1.52% DMSO; Veh), DMPS (110 µg; D), marimastat (60 µg; M), varespladib (19 µg; V), DMPS-plus-varespladib (110 and 19 µg, respectively; DV), or marimastat-plus-varespladib (60 and 19 µg, respectively; MV). After 72 h,† the mice were euthanised and their lesions excised, height and width measured with callipers, and photographed. (a) Representative images of the lesions resulting from each treatment group (black scale bar represents 3 mm). Bar graphs summarising the average total lesion areas for each drug treatment group when preincubated with (b) venom vehicle control (PBS), (c) *B. asper*, (d) *C. atrox*, or (e) *E. ocellatus* venom. † Signifies that these mice were culled at 24 h instead of the usual 72 h, due to their external lesions progressing to the maximum permitted size defined in our animal ethics licence, thus resulting in early euthanasia. * Signifies that value is significantly different than that of the drug vehicle control for that venom as determined by a one-way ANOVA followed by Dunnett's multiple comparisons test ($P < 0.05$, $n \geq 4$). ANOVA statistics for individual statistically analysed graphs are: (b) $F(5,24) = 1.000$, $P = 0.4389$, (c) $F(5,23) = 8.808$, $P < 0.0001$; (d) $F(5,23) = 28.80$, $P < 0.0001$; (e) $F(5,24) = 6.587$, $P = 0.0005$. Error bars represent standard deviation of at least four lesions, and the individual values for each lesion are shown as points within each of the bars.

Method/Summary of work: Mice ($n = 5/\text{group}$) were anaesthetised with inhalational isoflurane (4% for induction, 1.5–2% for maintenance) and intradermally injected in the shaved rear flank with 50 μl treatments consisting of (a) venom plus drug vehicle control (1.52% DMSO, 98.48% PBS), (b) venom plus drug (DMPS [110 μg], marimastat [60 μg], varespladib [19 μg], DMPS-plus-varespladib [DV], or marimastat-plus-varespladib [MV]), or (c) venom vehicle (PBS) plus drug. Venom treatments were from *Bothrops asper* (150 $\mu\text{g}/\text{treatment}$), *Crotalus atrox* (100 $\mu\text{g}/\text{treatment}$), and *Echis ocellatus* (39 $\mu\text{g}/\text{treatment}$). After 72 h, mice were euthanised using rising concentrations of CO_2 , the skin around the injection sites dissected, and internal dermal lesions measured with callipers and photographed.

Results/Discussion: Versus drug vehicle control, varespladib reduced dermonecrotic lesion formation caused by *B. asper* venom by 77%; DMPS, marimastat, and varespladib reduced that caused by *C. atrox* venom by 84%, 78%, and 69%, respectively; marimastat reduced that caused by *E. ocellatus* venom by 100%. Both MV and DV combination therapies significantly inhibited lesion formation induced by all three snake venoms by a minimum of 84%. Data and statistical details can be found in Figure 1.

Conclusion(s): The impressive inhibition of dermonecrosis induced by the venoms of three geographically diverse snake species suggests that the development of a pan-species effective drug therapy for snakebite-induced tissue cytotoxicity is feasible, warranting further translational research to develop such treatments as future treatments of snakebite in human victims worldwide.

REFERENCE(S)

- Harrison, R. A., Casewell, N. R., Ainsworth, S. A., & Laloo, D. G. (2019). The time is now: A call for action to translate recent momentum on tackling tropical snakebite into sustained benefit for victims. *Transactions of the Royal Society of Tropical Medicine and Hygiene*, 113(12), 834–837. <https://doi.org/10.1093/trstmh/try134>
- Clare, R. H., Hall, S. R., Patel, R. N., & Casewell, N. R. (2021). Small molecule drug discovery for neglected tropical snakebite. *Trends in Pharmacological Sciences*, 42(5), 340–353. <https://doi.org/10.1016/j.tips.2021.02.005>

P108 | Transdermal delivery of a hydrogen sulphide donor, AP39 using aqueous gel formulations in the treatment of neurological dysfunction

Mandeep Marwah¹, Shakil Ahmad¹, Hala Shokr², Irundika Dias¹, Lissette Sanchez-Aranguren¹

¹Aston University; ²University of Manchester

Introduction/Background & aims: Parkinson's disease (PD) is a neurodegenerative condition associated with mitochondrial dysfunction. AP39, a mitochondrial-targeted hydrogen sulphide (H_2S) donor, may

preserve the mitochondrial function due to its antioxidant activity. Although H_2S donors are promising therapeutic agents, translation to clinic requires an efficient delivery method, such as transdermal gels (1) given their potential to deliver drugs at low and sustained rates. This study investigated the feasibility of transdermal delivery of AP39, using ex vivo skin whilst exploring the ability of permeated AP39 to cross a blood–brain-barrier (BBB) microvasculature model, and to modulate parameters of mitochondrial function in PD-like environment.

Method/Summary of work: Hypromellose gels (5% w/v) were prepared with up to 10% v/v propylene glycol (PG) with 0.05% w/w AP39. AP39 permeation from formulations across excised murine skin was quantified using HPLC-UV detection. Collected media was applied to a barrier system mimicking the BBB to observe AP39 permeability and functionality. Mitochondrial oxygen consumption was evaluated using a Seahorse XF24 (2) in SHSY5Y (neuroblastoma cells) exposed to 6-hydroxydopamine (6OH-dop) for 24 h.

Results/Discussion: PG increased AP39 permeation across skin compared with gels without PG, from 28.38 ± 6.12 to $66.77 \pm 4.70\%$ thus was selected for further studies (Figure 1a). Upon application to the BBB model, the apparent permeability (P_{app}) was $0.018 \pm 0.001 \times 10^{-6} \text{ cm/s}$ in the influx direction and $0.014 \pm 0.001 \times 10^{-6} \text{ cm/s}$ in the efflux direction (Figure 1b) giving an influx ratio of 1.2. H_2S release was maximal at 25 μM within 0.5 h (Figure 1c).

Finally, we explored whether AP39 would preserve the mitochondrial respiration in SHSY5Y exposed to 6OH-dop. Whilst 6OH-dop significantly reduced respiration rates, coexposure with AP39 resulted in a significant restoration of these parameters, similar to nontreated cells (Figure 2).

Conclusion(s): These findings suggest that transdermal delivery of AP39 is a promising approach for the effective delivery of AP39 thus H_2S . Gels prepared with 10% v/v PG have the potential for immediate H_2S release whereas gels without PG may be useful for sustained H_2S release. Permeated AP39 sustained H_2S ability to protect the mitochondrial function in a model of PD in vitro, suggesting that transdermal delivery of AP39 is a potential therapeutic approach to further explore in the treatment of PD.

REFERENCE(S)

- Marwah, M. K., Shokr, H., Sanchez-Aranguren, L., Badhan, R. K. S., Wang, K., & Ahmad, S. (2022). Transdermal delivery of a hydrogen sulphide donor, ADT-OH using aqueous gel formulations for the treatment of impaired vascular function: An ex vivo study. *Pharmaceutical Research*, 39, 341, 352. <https://doi.org/10.1007/s11095-021-03164-z>.
- Sanchez-Aranguren, L. C., Espinosa-Gonzalez, C. T., Gonzalez-Ortiz, L. M., Sanabria-Barrera, S. M., Riano-Medina, C. E., Nunez, A. F., et al. (2018). Soluble Fms-like tyrosine Kinase-1 alters cellular metabolism and mitochondrial bioenergetics in preeclampsia. *Frontiers in Physiology*, 9, 83. <https://doi.org/10.3389/fphys.2018.00083>.

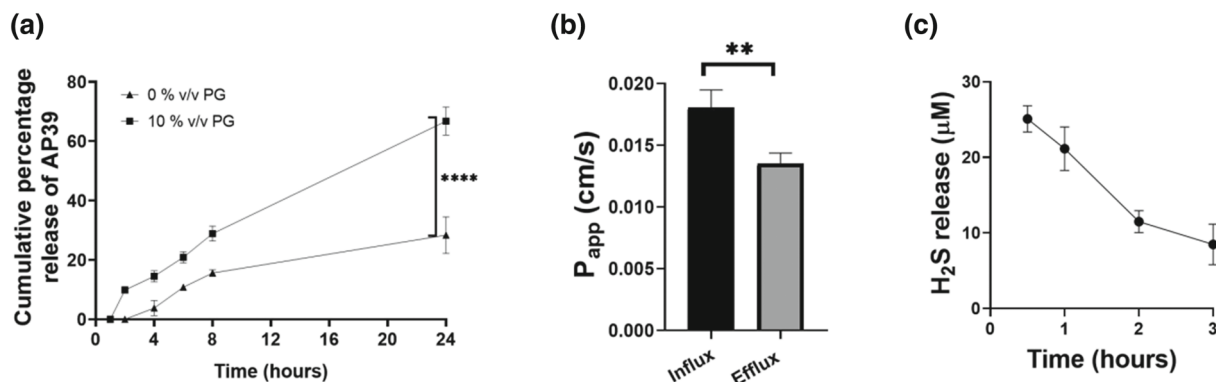


FIGURE 1 AP39 permeates across ex vivo murine skin and a microvasculature BBB model. (a) PG 10% v/v in gels increased AP39 flux across ex vivo murine skin samples up to 24 h compared with gels without PG. (b) P_{app} values in the influx and efflux direction for permeate of PG gels only. (c) H_2S release using a H_2S -specific microsensor in microvascular model. ** $p \leq 0.01$, **** $p \leq 0.0001$, $n = 6$, 3 independent experiments.

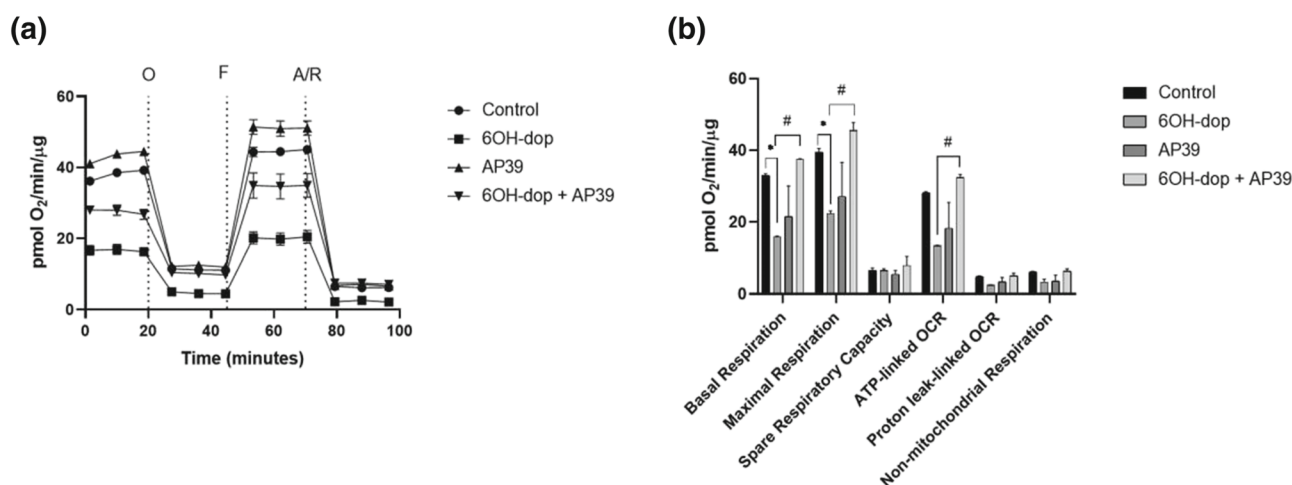


FIGURE 2 AP39 (0.3 μM) restored the mitochondrial oxygen consumption in SHSY5Y exposed to 6OH-dop (10 μM). Sequential injections of oligomycin (O), FCCP (F) and mixture of rotenone and antimycin A (A/R) allowed to calculate parameters of mitochondrial function: Basal and maximal respiration, spare respiratory capacity, oxygen consumption linked to ATP (ATP-linked OCR), proton leak (proton leak-linked OCR) and nonmitochondrial respiration. * $p \leq 0.05$ vs. control, # $p \leq 0.05$ vs. 6OH-dop. $n = 5$.

P109 | Trends in new drug approvals in 2021 and the GuidetoPharmacology.org database

Steve Alexander¹; Jane Armstrong²; Huayu Cao¹;
 Anthony Davenport³; Jamie Davies²; Elena Faccenda²;
 Simon Harding²; Chris Southan⁴; Michael Spedding⁵

¹University of Nottingham; ²University of Edinburgh; ³University of Cambridge; ⁴Medicines Discovery Catapult; ⁵Spedding Research Solutions SAS

Introduction/Background & aims: Four major new drug approval bodies report their activities in the English language: The Food and Drug Administration (FDA, via the Center for Drug Evaluation and Research) in the United States; the European Medicines Agency

(EMA); the Central Drugs Standard Control Organization (CDSCO) in India and the Pharmaceuticals and Medical Devices Agency (PMDA) in Japan.

Method/Summary of work: In 2021, the FDA approved 50 novel entities, including two diagnostic agents, four combinations and three anti-infective agents (to treat trypanosomiasis, candidiasis and cytomegalovirus). For the EMA, these figures were 58 novel entities, with six combinations, while the CDSCO and PMDA had fewer approvals (25 and 45, respectively). The table identifies the remaining novel drugs approved by the FDA, EMA, PMDA and CDSCO in 2021. Many of the FDA-approved drugs were also approved in other jurisdictions simultaneously or previously.

Results/Discussion

Of the antibodies, aducanumab, evinacumab, tezepelumab and isotumab vedotin are reported to address new targets (amyloid β , angiotensin-like 3, thymic stromal lymphopoietin and coagulation

Table: 2021 approved novel drugs (where appropriate, hyperlinked to the [GuidetoPharmacology.org](https://guidetoPharmacology.org) database)

Antibodies	Aducanumab-avwa, amivantamab-vmjw, anifrolumab-fnia, dostarlimab-gxly, efgartigimod alfa-fcab, evinacumab-dgnb, loncastuximab tesirine-lpyl, tezepelumab-ekko, tisotumab vedotin-tftv, tralokinumab-ldrm EMA/PMDA: bimekizumab, casirivimab, regdanvimab, sotrovimab
Enzymes	Asparaginase <i>erwinia chrysanthemi</i> -rywn, avalglucosidase alfa-ngpt
'Hormones'	Dasiglucagon, lonapegsomatropin-tcgd, ropeginterferon alfa-2b-njft
Kinase inhibitors	Asciminib, belumosudil, infigratinib, mobocertinib, sotorasib, tepotinib, tivozanib, trilaciclib, umbralisib EMA: abrocitinib
Receptor ligands	Atogepant, avacopan, difelikefalin, finerenone, ponesimod, vericiguat, vosoritide CDSCO: omidenepag PMDA: anamorelin, upacicalcet
Enzyme inhibitors	Voclosporin PMDA: difamilast, tucidinostat
Transporter inhibitors	Maralixibat, odevixibat, viloxazine
Nucleotides	Casimersen, inclisiran
Other targets	Belzutifan, fosdenopterin, imeglimin, melphalan flufenamide, pegcetacoplan

Factor III). The kinase inhibitors focus on previously targeted kinases, with the exception of sotorasib, which targets K-Ras (particularly the G12C mutant), although asciminib targets an allosteric myristoylated site on BCR-Abl.

One of the seven GPCR ligands addresses a previously untargeted GPCR (avacopan antagonizes C5a₁ receptors) while defelikefalin is a 'first-in-class' κ opioid peptide receptor peptide agonist. Anamorelin, atogepant, omidenepag, ponesimod and upacicalcet are described as a ghrelin receptor agonist, CGRP receptor antagonist, EP₂ prostanoid receptor agonist, S1P₁ sphingosine 1-phosphate receptor agonist and calcium-sensing receptor positive allosteric modulator, respectively. Vericiguat and vosoritide activate soluble and particulate (guanylyl cyclase-B receptors) members of the receptor guanylyl cyclase family, respectively.

Voclosporin targets calcineurin, while difamilast inhibits phosphodiesterase 4D. Tucidinostat and belzutifan target hypoxia-inducible factor-related proteins.

Maralixibat and odevixibat both target SLC10A2/IBAT ileal sodium-dependent bile acid transporter as first FDA approvals, while viloxazine targets both the SLC6A2/NET transporter and 5HT receptors.

Casimersen is an antisense oligonucleotide, which targets dystrophin exon skipping, while inclisiran is a siRNA targeting subtilisin expression.

Fosdenopterin is a precursor of molybdopterin. Imeglimin is reported to have multiple targets, while melphalan flufenamide is a DNA alkylating agent, and pegcetacoplan chelates complement C3.

Conclusion(s): Of the 52 novel drugs identified in the table, we have records in [GuidetoPharmacology.org](https://guidetoPharmacology.org) for the majority. As we would expect, our coverage is excellent for the antibodies (14/14) and small molecule drugs targeting conventional human proteins (27/29).

P110 | Elucidating the anti-malarial mechanism of action of primaquine and tafenoquine using in vitro hepatic metabolism models

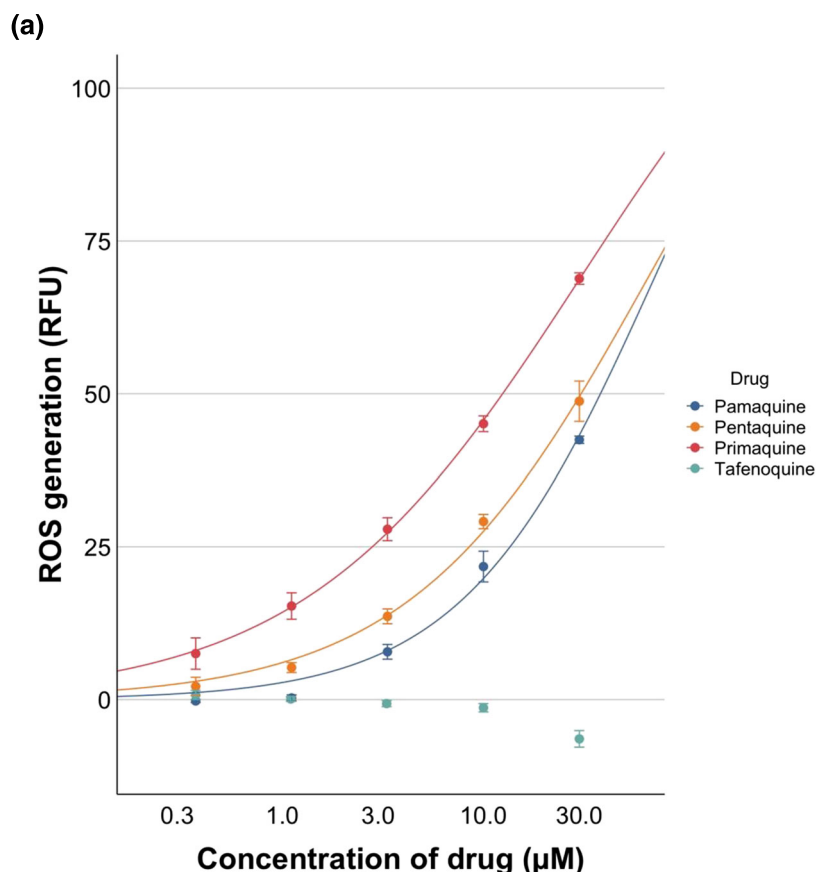
Jessica Jinks; Ghaith Aljayyousi; Giancarlo Biagini

Liverpool School of Tropical Medicine

Introduction/Background & aims: *Plasmodium vivax* presents a unique challenge to malaria eradication due to the persistence of dormant liver stages called hypnozoites. Two drugs: primaquine and tafenoquine show efficacy against hypnozoites and are licenced for use [1]. There is still limited knowledge into the mode of action and toxicity of these drugs, hindering the improvement of treatment regimens.

We have previously shown that primaquine functions via a two-step Cytochrome P450 (CYP) 2D6-mediated mechanism of action involving the generation of hydroxylated metabolites, which cause accumulation of anti-parasitic levels of reactive oxygen species (ROS) through redox cycling with Cytochrome P450 Reductase (CPR) [2]. Although established for primaquine, the link between CYP/CPR-mediated metabolism and tafenoquine activity is unclear. Tafenoquine's long half-life and high protein binding present significant challenges to in vitro research. Interestingly, clinical research shows no link between poor CYP 2D6 metaboliser status and treatment failure for tafenoquine but does for primaquine [3]. We hypothesise that tafenoquine's mode of action, while differing from primaquine via the routes and rates of its initial (Step 1) bioactivation step, ultimately elicits antimalarial activity via catalytic ROS generation (Step 2).

Method/Summary of work: To investigate drug mode of action, we measured ROS generation from primaquine and tafenoquine; and historical 8-aminoquinolines: Pamaquine and pentaquine using human liver microsomes incubated with fluorescent ROS probe:



(b)

	EC_{50} (μM)	Hillslope	Average ROS production at 3.33 μM (RFU)
Primaquine	30.99	0.63	27.88
Tafenoquine	NA	NA	-0.65
Pamaquine	71.89	0.91	7.82
Pentaquine	66.98	0.73	13.62

CM-H₂DCFDA. Microsomes (0.1 mg/ml) were pretreated with 2.5 μM CM-H₂DCFDA for 30 min at 37°C. A concentration range of each drug (0.041–30 μM) was incubated with CM-H₂DCFDA-treated microsomes for 2 h at 37°C and read on a fluorescence microplate reader (Ex/Em 500/527).

Results/Discussion: Results show that clinically relevant concentrations of primaquine, pamaquine and pentaquine generate ROS in a concentration-dependent manner (Figure 1). Primaquine, the current 'gold standard' treatment was most potent compared with older antimalarial agents. This is consistent with older treatments requiring a higher dose to elicit their efficacy [1]. Incubation of tafenoquine with microsomes caused a quenching of background ROS at higher concentrations. Tafenoquine's high microsomal binding is a likely explanation for lack of activity in this assay. However, ongoing work with CM-H₂DCFDA-treated Hep-G2 spheroids shows comparable ROS generation from primaquine and tafenoquine.

FIGURE 1 Reactive oxygen species generation by 8-Aminoquinoline compounds incubated with a hepatic microsomal metabolising system. Reactive oxygen species (ROS) generation from 8-Aminoquinoline compounds: Primaquine, pamaquine, pentaquine and tafenoquine were assessed using a microsomal metabolism-linked ROS detection assay with fluorescent ROS probe CM-H₂DCFDA. (a) Plotted ROS data with fitted concentration–response curves. Data are given as relative fluorescence units (RFU) normalised to the background RFU measured from the solvent control (0.45% Methanol). Data points are shown as the mean \pm SEM of three experiments ($n = 3$) with three technical replicates per plate. Data were fitted to a concentration–response model, where Emax was estimated for the drug with the highest activity (primaquine, $\text{Emax} = 138.82$ RFU); this value was then used as a fixed Emax value for the other drugs to ensure comparability of potency across the drugs within a clinically relevant concentration range. (b) Coefficients used to generate the concentration–response curves as well as the average ROS production (RFU) for all drugs at 3.33 μM are given. Primaquine, pentaquine and pamaquine show ROS production at clinically relevant drug concentrations, with primaquine the most potent. Tafenoquine does not produce ROS in this model; therefore, a concentration–response curve was not plotted.

Conclusion(s): These data suggest that tafenoquine produces ROS when investigated in more physiologically relevant models, identifying that more complex in vitro models are required to deconvolute tafenoquine's mode of action. To this end, ongoing work investigating tafenoquine's metabolism using a low clearance H μ REL[®] co-culture assay with liquid chromatography with tandem mass spectrometry will be presented.

REFERENCE(S)

1. Recht, J., Ashley, E., & White, N. (2014). *Safety of 8-aminoquinoline anti-malarial medicines*. World Health Organisation.
2. Camarda, G., Jirawatcharadech, P., Priestley, R. S., et al. (2019). Antimalarial activity of primaquine operates via a two-step biochemical relay. *Nature Communications*, 10(1), 3226. <https://doi.org/10.1038/s41467-019-11239-0>
3. Lacerda, M. V. G., Llanos-Cuentas, A., Krudsood, S., et al. (2019). Single-dose tafenoquine to prevent relapse of *Plasmodium vivax* malaria. *The New England Journal of Medicine*, 380(3), 215–228. <https://doi.org/10.1056/NEJMoa1710775>

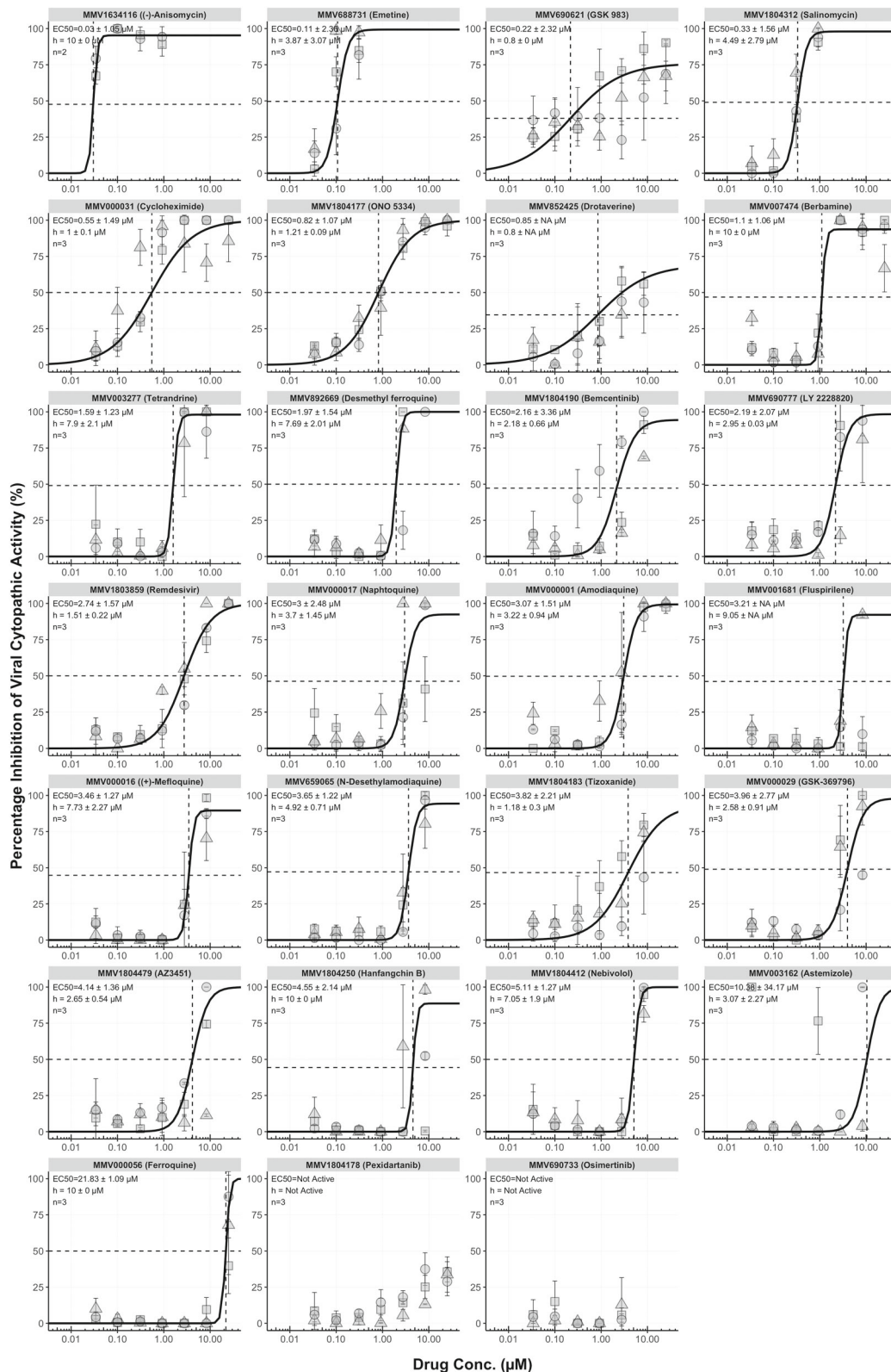


FIGURE 1 Concentration–effect relationship for the inhibition (%) of SARS-CoV-2 cytopathic activity for all compounds with >50% inhibition of viral cytopathic activity at either 0.5 µM and/or 5 µM. For each compound, activity was expressed relative to uninfected/untreated controls (100% inhibition of viral cytopathic activity) and infected/untreated controls (0% inhibition of viral activity). For a total of 29 compounds, we assessed activity at 25.00, 8.33, 2.78, 0.93, 0.31, 0.10 and 0.03 µM in triplicate. Data points impacted by drug toxicity were removed automatically. Nonlinear regression using an E_{MAX} model was performed on data taken from three independent biological replicates in order to generate concentration–effect predictions (solid black lines). For each compound, EC₅₀ values, hillslope and replicate number (n) are shown. Dashed lines represent the EC₅₀ of each compound.

P112 | An in vitro SARS-CoV-2 cytopathic activity screen of the 'MMV COVID box'

Shaun Pennington; Claire Caygill; Rose Lopeman; Laura Jeffreys; Jack Duggan; Alastair Breen; Jessica Jinks; Alison Ardrey; Ghaith Aljayoussi; Steve Ward; Giancarlo Biagini

Liverpool School of Tropical Medicine

Introduction/Background & aims: There remains a clear need for prophylactics and treatments with efficacy against SARS-CoV-2. Here, we describe a two-stage in vitro SARS-CoV-2 cytopathic activity screening method and apply it to assess the inhibitory activity of 160 compounds from the Medicines for Malaria Venture 'COVID Box'.

Method/Summary of work: Compound activity was assessed in Vero E6 and Calu-3 ACE2 cells inoculated with SARS-CoV-2 (MOI = 0.05). We performed a two-point screen for all compounds at 0.5 and 5 μ M in Vero E6 cells. For compounds with >50% inhibition of viral cytopathic activity at either concentration, 8-point concentration-response analysis was performed in Vero E6 cells. 'Active' compounds with a $C_{MAX}:EC_{90}$ ratio >1 were then assessed in Calu-3 ACE2 cells. Nonlinear regression was performed to generate concentration-effect predictions. EC_{50} , EC_{90} , E_{MAX} and hillslope were calculated for each compound that generated a robust, converged four-parameter fit.

Results/Discussion: 29/160 compounds demonstrated >50% inhibition of viral cytopathic activity at 0.5 μ M and/or 5 μ M. Compounds identified as 'active' demonstrated a broad range of potency against SARS-CoV-2—ranging from $EC_{50} = 0.03 \mu$ M (anisomycin) to $EC_{50} = 21.83 \mu$ M (ferroquine) (Figure 1). Six compounds were identified as having a $C_{MAX}:EC_{50}$ ratio >1, and 2 compounds (tizoxanide and mefloquine) were identified as having a $C_{MAX}:EC_{90}$ ratio >1. Of these, tizoxanide was not active against SARS-CoV-2 in Calu-3 ACE2 cells; however, mefloquine retained activity.

Conclusion(s): We describe a medium-throughput, two-stage in vitro screening method using Vero E6 and Calu-3 cells for the identification of compounds with activity against SARS-CoV-2. Whilst a relatively large proportion of compounds had activity, only two compounds had $C_{MAX}:EC_{90}$ ratio >1 and, of these, only mefloquine would appear to have a favourable profile. These data highlight the on-going challenge of identifying agents possessing tractable pharmacodynamic/pharmacokinetic profiles for treatment of SARS-CoV-2. Future experiments utilising multicell, dynamic flow models, such as lung-on-a-chip could help to overcome limitations of existing in vitro data and help accelerate drug discovery efforts.

P114 | Adrenomedullin as a possible biased ligand for CXCR4 and ACKR3

Pietro Cocchiara; Graeme Milligan; Gerard Graham

University of Glasgow

Introduction/Background & aims: The chemokine receptor 4 (CXCR4) is a G protein-coupled receptor (GPCR) widely expressed in immune response cells and the chemokine CXCL12 is its endogenous ligand. CXCL12 also binds to atypical chemokine receptor 3 (ACKR3) that may act as a scavenger receptor for CXCR4, hence preventing CXCL12 from binding to CXCR4 (1). ACKR3 can signal only through arrestin recruitment, while CXCR4 uses both arrestin recruitment and G-protein signalling (1). Both receptors are involved in HIV-1 infection, many (auto)immune diseases and several types of cancer pathogenesis, and they can form oligomers. The oligomerisation affects in many ways the receptors' life cycle and its functioning (2). Adrenomedullin (ADM), a nonchemokine peptide with proangiogenic effects, was proposed as a ligand for ACKR3, and may play a role in regulating the CXCR4-CXCL12-ACKR3 axis (1). Here, we aim to characterise the signalling and functional role of ADM on CXCR4 and ACKR3.

Method/Summary of work: [35 S]GTP γ S binding assays were performed using membranes from Flp In TReX 293 cells induced with doxycycline to express hCXCR4-mEGFP. Membranes were pretreated for 15 min with ADM before addition of CXCL12. cAMP accumulation assays were performed using same cells. β -arrestin-2 recruitment was assessed by bystander bioluminescent resonance energy transfer. HEK 293T cells were transfected transiently either with hCXCR4-eYFP or hACKR3-eYFP. For ADM or the CXCR4 antagonist IT1t, cells were pretreated for 15 min before addition of CXCL12. Western blots were performed on cell lysates. Gels were developed using the LI-COR system.

TABLE 1 [35 S]GTP γ S binding in membranes expressing hCXCR4-mEGFP is regulated by both CXCL12 and ADM

Ligand	EC_{50}
CXCL12 (n = 3) (mean \pm SEM)	-8.2 \pm 0.3
Ligand	IC_{50}
Adrenomedullin (n = 3) (mean \pm SEM)	-7.2 \pm 0.2

TABLE 2 cAMP accumulation assay for hCXCR4-mEGFP with CXCL12, ADM and IT1t

Ligand	EC_{50}
CXCL12 (n = 3) (mean \pm SEM)	-7.3 \pm 0.8
Ligand	IC_{50}
Adrenomedullin (n = 3) (mean \pm SEM)	-7.0 \pm 0.5
IT1t (n = 3) (mean \pm SEM)	-6.9 \pm 0.2

TABLE 3 β -Arrestin-2 bystander BRET assays show CXCL12 to promote interactions with both hCXCR4-eYFP and hACKR3-eYFP

Receptor	EC_{50}
hCXCR4-eYFP (n = 3) (mean \pm SEM)	-6.8 \pm 0.2
hACKR3-eYFP (n = 3) (mean \pm SEM)	-7.3 \pm 0.3

Results/Discussion: ADM prevents [³⁵S]GTPγS binding induced by CXCL12 in membranes expressing hCXCR4-mEGFP in a concentration-dependent manner.

In cAMP accumulation assays both ADM and IT1t displayed antagonist effects of CXCL12 function.

Immunoblotting studies using a pSer³²⁴/pSer³²⁵ hCXCR4 phospho-site specific antiserum indicated that ADM did not modulate these sites. Moreover, in bystander BRET assays of β-arrestin-2 proximity, ADM was also without activity.

Conclusion(s): These studies suggest that ADM may act as a potential biased ligand in regulating hCXCR4 and hACKR3 function physiology.

REFERENCE(S)

1. Szpakowska M et al, *Biochemical Pharmacology* 2018;153:299–309. <https://doi.org/10.1016/j.bcp.2018.03.007>.
2. Ward RJ et al., *The Journal of Biological Chemistry*. 2021;296:100139. <https://doi.org/10.1074/jbc.RA120.016612>.

P115 | Liposomes encapsulating hydrogen sulphide donor ADT-OH improves permeation in a placental microvasculature model and prolongs in vivo circulation time

Mandeep Marwah¹; Hala Shokr²; Sarah Hopkins¹; Lissette Sanchez-Aranguren¹; Keqing Wang¹; Shakil Ahmad¹; Raj Kumar Singh Badhan¹

¹Aston University; ²University of Manchester

Introduction/Background & aims: Hydrogen sulphide (H₂S) generated endogenously has been observed as a critical gasotransmitter involved in the modulation of vasodilation, angiogenesis, anti/proinflammation and cytoprotection. Manipulation of H₂S levels using H₂S-donors has revealed beneficial effects in vascular based disorders such as pre-eclampsia (1). However, delivery challenges such as rapid H₂S release, poor aqueous stability and short half-life pose a challenge. Liposomes present an exciting solution with the benefit of giving controlled release of drug (2). This study sought to determine the profile of liposomal ADT-OH, a H₂S donor, in cultured cells and in vivo.

Method/Summary of work: ADT-OH (0.01% w/v) loaded liposomes were formulated from phosphatidylcholine, DSPE-PEG(2000) and cholesterol. Release profile and ability of liposomal ADT-OH to promote angiogenesis was investigated. Liposomal or naked ADT-OH influx/efflux rates, permeability, and release profile of H₂S from the liposomes in cultured HUVEC cells was determined. Tube formation assays were performed as indicative of angiogenic potential. Liposomes or ADT-OH in PBS were intravenously injected in C57BL/6 mice and blood samples taken over 24 h to determine plasma drug concentration using HPLC-UV analysis.

Results/Discussion: Liposomes improved permeation of ADT-OH across the microvasculature model. The apparent membrane permeability (P_{app}) of naked drug was lower in both influx and efflux direction compared with liposomal drug (Figure 1). Furthermore, a controlled release of H₂S was observed from the liposomal formulation.

Liposomes provided a controlled release of ADT-OH thus H₂S. Application of formulation onto HUVEC's observed liposomal

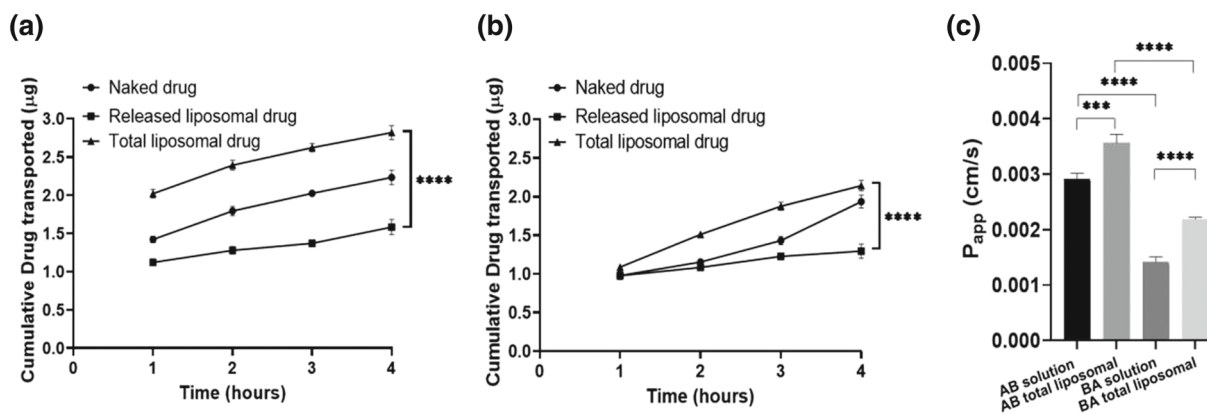


FIGURE 1 ADT-OH flux and H₂S release across HUVECs grown on permeable inserts. ADT-OH transport in (a) influx or (b) efflux direction with (c) associated apparent membrane permeability (P_{app}) values in the influx direction and (d) H₂S release as detected with a H₂S probe. **p ≤ 0.01, ***p ≤ 0.001 and ****p ≤ 0.0001 with appropriate ANOVA tests. n = 6, in three independent experiments.

TABLE 1 Pharmacokinetic parameters for naked and liposomal ADT-OH following injections into mice. Data represents mean ± SD. n = 12 independent batches.

Formulation	Half-life (h)	Area under the curve (mg/ml × h)	Clearance (ml/h)	Volume of distribution (ml)
Naked	20.6 ± 4.04	0.56 ± 0.075	0.018 ± 0.0022	0.53 ± 0.093
Liposome	93.08 ± 21.51	2.48 ± 0.46	0.0041 ± 0.001	0.54 ± 0.041

ADT-OH retained ability to enhance tubular network formation. Liposomes increased in vivo circulation time with the half-life increasing to 93 h resulting in a greater area under the curve, correlating to drug exposure for liposomal ADT-OH (Table 1). Clearance decreased to 0.0041 ml/h.

Conclusion(s): Liposomal delivery of ADT-OH could be a promising approach in the treatment of various vascular-related conditions associated with defective angiogenesis and vascular insufficiency such as preeclampsia. Using liposomes as a controlled release formulation may provide long-term low levels of H₂S to reduce toxicity and off targets effects as well as to reduce the need for repeated dosing when translated to clinical setting.

REFERENCE(S)

1. Wang, K., Ahmad, S., Cai, M., Rennie, J., Fujisawa, T., Crispi, F., et al. (2013). Dysregulation of hydrogen sulfide producing enzyme cystathionine γ -lyase contributes to maternal hypertension and placental abnormalities in preeclampsia. *Circulation*, 127(25), 2514–2522. <https://doi.org/10.1161/CIRCULATIONAHA.113.001631>
2. Marwah, M. K., Shokr, H., Sanchez-Aranguren, L., Badhan, R. K. S., Wang, K., & Ahmad, S. (2022). Transdermal delivery of a hydrogen sulphide donor, ADT-OH using aqueous gel formulations for the treatment of impaired vascular function: An ex vivo study. *Pharmaceutical Research*, 39, 341, 352. <https://doi.org/10.1007/s11095-021-03164-z>

P116 | Evaluation of the on-target dermal side effect profile of a retinoic acid receptor dual acting modulator NVG645 in vitro

Paul Chazot; Lilit Ghazaryan; Andy Whiting

Durham University

Introduction/Background & aims: Neurodegenerative diseases (NDDs) are a major global threat to human health. PD is the second most common NDD that is clinically defined as a progressive movement disorder that is often accompanied by nonmotor symptoms. There are currently no approved therapeutic interventions to modify

Capacity of NVG645 (10 nM) to protect in neuropathological pathways

Effect	Significance
Increases average neurite length at least 2-fold over ATRA in SH-SY5Y cells	Demonstrates ability to induce growth of mouse and human motor neurons at low concentrations
Increases the number of primary rat neurons in glutamate-induced excitotoxicity and upregulated AMPA receptor subunits (GluA1 and GluA2)	Protects against glutamate-induced excitotoxicity—a proposed mechanism of neuronal death in NDD
Potent neurotropic activity in iPSC derived motor neurons and human neural cell lines	Supports differentiation and neuronal repair
Supports neuromuscular function in ex vivo rat assay	Contributes to neuroprotection
Reduces number of sodium arsonate-induced induced stress granules, including large harmful (>100 mM size) SG	First time a RAR ligand has reduced number of stress-induced stress granules larger sizes
Activation of neuroprotective genes and inhibition of proinflammatory genes	Contributes to enhanced neurite growth, and anti-inflammatory effects

^a Following pretreatment with 10 μ M NVG645 for 24 h.

disease in PD; treatments are limited to providing symptomatic relief. Retinoids are vitamin A derived substances that are essential for normal neuronal cell function and have been implicated in PD pathogenesis [1]. In previous studies, we have shown that the lead synthetic retinoid, 4-[2-(5,5,8,8-tetramethyl-5,6,7,8-tetrahydroquinoxalin-2-yl) ethynyl] benzoic acid (NVG645), demonstrated clear neuroprotective, neuroplasticity, and neurorepair properties in neuronal cell lines and animal models of Parkinson's disease. However, NVG645 was shown to induce skin flaking and scaling in a rodent models after extended daily exposures.

Herein, we aimed to define the mechanistic bases for this on-target side effect of NVG645.

Method/Summary of work: This study investigates the proposed on-target side-effect profile of NVG645 in vitro using the HDF (dermal fibroblasts) and HaCaT (epidermal keratinocytes) cell model of human skin, at an administered NVG645 concentration of 10 nM. This concentration elicited the wide range of beneficial effects upon neurons in culture.

Functional, histological, and biochemical analyses were performed, using a range of assays, for example. MTT (oxidative stress), TNF α and IL-6 ELISAs (inflammation), senescence beta-GAL IHC, and immunofluorescence (expression of RAR α , β , γ proteins). In an attempt to assess the effects of NVG645 on autophagy for the first time, a proprietary fluorescent autophagosome marker was utilised within an autophagy assay kit in response to NVG645. This allowed visualisation of pre-autophagosomes, autophagosomes, and autolysosomes (autophagolysosomes) under normal and serum-starved conditions.

Results/Discussion: NVG645 significantly increased HaCaT cell number and decreased LPS-induced cytotoxicity, indicative of increased cell proliferation.

Biochemical studies suggested that NVG645 exacerbates inflammation (TNF α release) in HaCaT sensitised by LPS but also attenuated LPS-induced IL-6 release and inhibited senescence responses.

An additional role of NVG645 to promote autophagy responses was also demonstrated, which may correlate with the increased proliferation.

Finally, NVG645 appeared to increase both RAR β and RAR γ expression in both HDF and HaCaT cells.

Conclusion(s): Overall, these effects suggest that NVG645 shows a significant side-effect profile in skin cells, particularly epidermal skin cells that should be addressed to inform the safety and progression of future studies.

REFERENCE(S)

1. Clark, J. N., et al. (2020). Retinoic acid receptor-targeted drugs in neurodegenerative disease. *Expert Opinion on Drug Metabolism & Toxicology*, 16(11), 1097–1108, <https://doi.org/10.1080/17425255.2020.1811232>.

P121 | PSB-16671 acts as a ‘probe-dependent’ positive allosteric modulator at proinflammatory orphan receptor GPR84

Zobaer Al Mahmud¹; Laura Jenkins²; Brian Hudson¹; Graeme Milligan¹

¹University of Glasgow; ²University of Glasgow, Glasgow, UK

Introduction/Background & aims: Recently, allosteric modulation of GPCRs has attracted great interest for the development of drug

candidates with greater selectivity and higher safety profile, and as such, the actions of orthosteric agonists at G-protein coupled receptor 84 (GPR84) could potentially be substantially enhanced by positive allosteric modulators (PAM) to develop novel therapies against atherosclerosis [1]. Though di(5,7-difluoro-1H-indole-3-yl)methane (PSB-16671) has been identified as PAM of decanoic acid (C-10) at human GPR84 [2], information on the allosteric interaction of PSB-16671 with other orthosteric agonist is lacking. Moreover, no studies have been performed to assess the allosteric effects of PSB-16671 at other species orthologues of GPR84. Herein, we have performed detailed characterization of allosteric interactions between PSB-16671 and orthosteric GPR84 agonists at mouse monocytes RAW264.7 and human monocytes U937 cells.

Method/Summary of work: A series of [³⁵S]-GTP γ S binding assays were conducted according to Mancini et al. [3] using membranes prepared from LPS-treated RAW264.7 cells and U937 cells. Data were analysed using an operational model of allosteric modulation [3]. Data represent mean \pm SEM for three independent experiments.

Results/Discussion: PSB-16671 acted as a strong PAM of potency of C-10 and 6-OAU and PAM of potency and efficacy of embelin at RAW264.7 cells (Figure 1). PSB-16671 exhibited probe-dependence in modulating the binding affinity of orthosteric agonists for mouse GPR84 as evidenced from the findings that greatest magnitude of affinity modulation was observed for 6-OAU(α : 336) followed by for

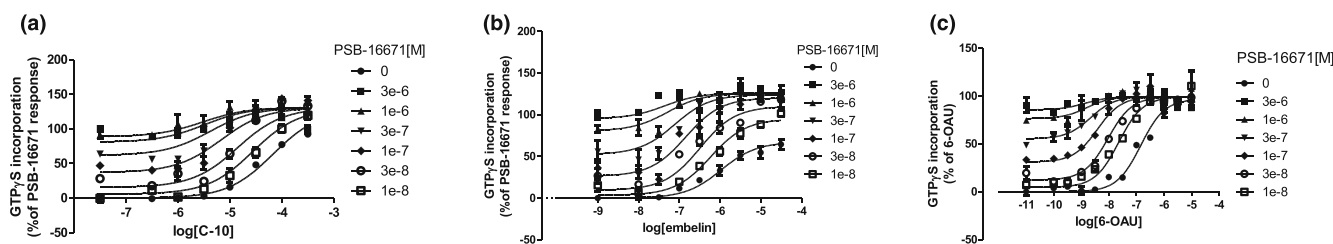


FIGURE 1 PSB-16671 displays high positive cooperativity in modulating function of C-10, embelin and 6-OAU in [³⁵S]-GTP γ S binding assays in RAW 264.7 cells. Increasing fixed concentrations of PSB-16671 were assessed for their ability to affect C-10 (a), embelin (b) and 6-OAU(c)-mediated [³⁵S]-GTP γ S incorporation into membranes purified from LPS-induced (100 ng/ml, 5 h) RAW264.7 cells. Curves drawn are from fitting the datasets with operational model of allosterism and the allosteric parameters quantified from these analyses are shown in Table 1.

TABLE 1 Operational model parameters of allosteric interactions between PSB-16671 and different orthosteric agonists at RAW 264.7 cells

Agonist ^a	6-OAU	PSB-16671	C-10	PSB-16671	Embelin	PSB-16671
Modulator ^b	PSB-16671	6-OAU	PSB-16671	C-10	PSB-16671	Embelin
log α	2.53 \pm 0.15	2.0 \pm 0.22	1.66 \pm 0.24	1.63 \pm 0.32	1.43 \pm 0.16	1.48 \pm 0.2
log β	0.04 \pm 0.06	0.34 \pm 0.09	0.06 \pm 0.14	0.47 \pm 0.10	0.76 \pm 0.06	0.3 \pm 0.07
pK _A ^c	6.3 \pm 0.1	6.23 \pm 0.15	3.6 \pm 0.20	6.5 \pm 0.17	5.7 \pm 0.1	6.6 \pm 0.13
pK _B ^d	6.2 \pm 0.07	6.50 \pm 0.1	6.5 \pm 0.08	3.63 \pm 0.2	6.0 \pm 0.1	5.5 \pm 0.10

^aAgonist is the compound used to generate concentration–response curve.

^bModulator is the compound used in defined concentrations.

^cpK_A are values estimated for the agonist.

^dpK_B are values estimated for the modulator.

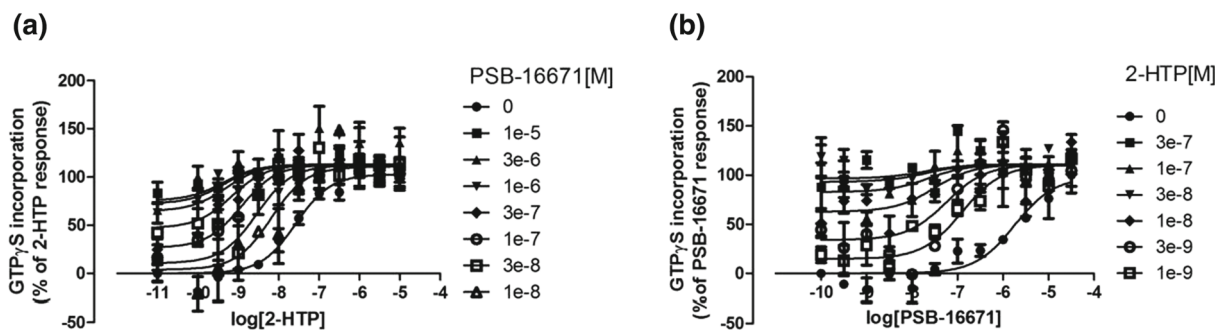


FIGURE 2 PSB-16671 acts as a strong PAM of potency of 2-HTP at GPR84 in LPS-treated human monocyte U937 cells. The ability of increasing fixed concentrations of PSB-16671 to affect 2-HTP-induced [35 S]-GTP γ S binding to membranes purified from LPS-treated U937 cells was evaluated (a). In reciprocal interaction studies, various concentrations of 2-HTP were evaluated for their capacity to modulate PSB-16671-promoted binding of [35 S]-GTP γ S (b). Curves displayed are from global fitting of experimental data with operational model of allosterism; the allosteric parameters are shown in Table 2.

TABLE 2 Operational model parameters of allosteric interactions between PSB-16671 and 2-HTP at LPS-treated U937 cells

Agonist ^a	2-HTP	PSB-16671
Modulator ^b	PSB-16671	2-HTP
log α	2.0 \pm 0.3	2.22 \pm 0.37
log β	0.13 \pm 0.1	0.13 \pm 0.14
pK _A ^c	7.1 \pm 0.2	5.4 \pm 0.3
pK _B ^d	6.4 \pm 0.17	7.9 \pm 0.12

^aAgonist is the compound used to generate concentration–response curve.

^bModulator is the compound used in defined concentrations.

^cpK_A are values estimated for the agonist.

^dpK_B are values estimated for the modulator.

C-10 (α : 46) and lowest binding affinity modulation (α : 26.7) was generated when embelin was used to probe the receptor function. Mathematical analysis of allosteric interaction revealed that PSB-16671 (K_A : 0.76 μ M) binds mouse GPR84 with 400-fold higher affinity than C-10 (K_A : 0.31 mM). PSB-16671 also displayed very high positive cooperativity with 2-(hexylthio)pyrimidine-4,6-diol (2-HTP) (Figure 2) at U937 cells, exhibiting affinity cooperativity factor, α , value of 100.

Allosteric parameters for interaction between PSB-16671 and GPR84 orthosteric agonists were extracted from the data generated from [35 S]-GTP γ S binding study using membranes prepared from LPS-treated RAW264.7 cells as described in Figure 1. Data are means \pm SEM.

Conclusion(s): PSB-16671 acted as a highly effective PAM of the function of orthosteric GPR84 agonists in RAW264.7 cells in a ‘probe-dependent’ manner.

REFERENCE(S)

- Gaidarov, I., Anthony, T., Gatlin, J., Chen, X., Mills, D., Solomon, M., Han, S., Semple, G., & Unett, D. J. (2018). Embelin and its derivatives unravel the signaling, proinflammatory and antiatherogenic properties

of GPR84 receptor. *Pharmacological Research*, 13, 185–198. <https://doi.org/10.1016/j.phrs.2018.02.021>

- Pillaiyar, T., Köse, M., Sylvester, K., Weighardt, H., Thimm, D., Borges, G., Förster, I., von Kügelgen, I., & Müller, C. E. (2017). Diindolylmethane derivatives: Potent agonists of the Immunostimulatory orphan G protein-coupled receptor GPR84. *Journal of Medicinal Chemistry*, 60(9), 3636–3655. <https://doi.org/10.1021/acs.jmedchem.6b01593>
- Mancini, S. J., Mahmud, Z. A., Jenkins, L., Bolognini, D., Newman, R., Barnes, M., Edye, M. E., McMahon, S. B., Tobin, A. B., & Milligan, G. (2019). *Scientific Reports*, 9(1), 1861. <https://doi.org/10.1038/s41598-019-38539-1>, On-target and off-target effects of novel orthosteric and allosteric activators of GPR84

P122 | Unravelling the structural mechanism for biased signalling at the formyl peptide receptors

Denise Pajonczyk

University of Münster

Introduction/Background & aims: The G protein-coupled formyl peptide receptor FPR1 is the founder member of the FPR family of pattern recognition receptors and senses predominantly shorter, formylated peptides. The bacteria-derived prototypic tripeptide agonist fMLF can activate FPR1 at very low concentrations, owing to its biological task of detecting bacterial infections. The evolutionary younger and highly conserved homologue FPR2 still reacts to formylated peptides, albeit with lower sensitivity. The pharmacological targeting of FPRs represents a novel therapeutic approach to treating inflammatory diseases. However, the molecular mechanisms of activation and action of FPR–ligand interaction are elusive.

Method/Summary of work: Here, we utilized fMLF and its methyl ester analogue fMLF-OMe as chemical leads to generate derivatives. Different functional groups (-NO₂, -NH₂, -N₃) were introduced to the phenylalanine moiety's phenyl ring in p-position (phenylalanine moiety). The dose–response curves of agonist-induced receptor internalization and the G protein-dependent cAMP signalling were

employed to perform bias calculations to estimate the pathway preference of each compound at FPR1 and 2.

Results/Discussion: The analysis of pathway preferences of fMLF and its derivatives showed that minor structural modifications were sufficient to significantly alter signal pathway preferences at FPR1 and FPR2. Together with mutagenesis data, our findings reveal potential interactions site of the peptides c-terminus with the ligand-binding pocket to activate FPRs leading to a favourable signalling preference towards receptor internalization.

Conclusion(s): These novel FPR agonists could serve as a starting point for the development of tailored agonists for pharmacological manipulation of FPRs. Agonists that preferentially induce internalization might be a suitable mechanism to address, that is, targeted cancer therapy via the design of FPR targeting cargo-peptides.

P123 | Functional insights into GPR84 signalling at low receptor expression levels using label-free impedance sensing

Vincent Luscombe; David Greaves

University of Oxford

Introduction/Background & aims: GPR84 is an immune-cell expressed orphan GPCR that is upregulated by inflammatory stimuli and enhances inflammation upon activation. The discovery of biased agonist DL-175 demonstrated that selective pathway activation can abrogate GPR84-mediated chemotaxis [1]. To make direct comparisons between assay modalities and time points, we sought to develop a single heterologous cell expression system in order to further interrogate differences between agonists 6-OAU and DL-175. In this study, we developed monoclonal GPR84 cell lines with different expression levels and compared them to primary bone-marrow derived macrophages (BMDMs) in a label-free impedance sensing system.

Method/Summary of work: BMDMs were prepared as described previously [1]. Cells were plated into RTCA 96 PET E-Plates at 50,000 cells/well and M1 polarised with 100 ng/ml LPS (BMDMs), or at 40,000 cells/well (CHO cells). Plates were incubated over 18–24 h and cell index measurements taken using the xCELLigence RTCA SP system. The impedance responses following agonist addition were first normalised to the cell index immediately prior to addition, and then normalised to baseline conditions. The average values from each experiment were pooled and analysed using GraphPad Prism (v9.3.1).

Results/Discussion: Agonist stimulation caused a rapid positive impedance response that peaked between 2 and 10 min and subsequently decayed over time (Figure 1). The BMDM response to DL-175 was characterised by a shallower slope of decay compared with 6-OAU. Only CHO-GPR84 clones with low receptor expression could recapitulate this phenotype. Conversely, high expressing cell lines exhibited a constitutively elevated signal. The subtle yet robust

differences between agonists were found to be independent of concentration, and consistently manifested in the slope of the decay phase. Furthermore, preincubation with the GRK2/3 inhibitor compound 101 augmented the positive impedance response elicited by 6-OAU in BMDMs and low expressing cell lines, but not in high expressing cell lines.

Conclusion(s): Receptor expression levels are a key determinant of cell impedance responses, and the ability of low expressing GPR84 cell lines to phenocopy BMDMs is consistent with a low receptor reserve and more physiological receptor-effector coupling. This study highlights the utility of kinetic and label-free readouts to discriminate between agonists that might otherwise share many signalling qualities and provides evidence for the fidelity of stable GPR84 cell lines for use in other high-throughput assays.

REFERENCE(S)

- Lucy, D., Purvis, G. S., Zeboudj, L., et al. (2019). A biased agonist at immunometabolic receptor GPR84 causes distinct functional effects in macrophages. *ACS Chemical Biology*, 14(9), 2055–2064. <https://doi.org/10.1021/acscchembio.9b00533>

P124 | Structure–activity relation of ivermectin: A positive allosteric modulator of the human P2X4 receptor

Jessica Meades; Samuel Fountain

University of East Anglia

Introduction/Background & aims: Ivermectin (IVM) is as a positive allosteric modulator of the P2X4 receptor, a ligand-gated ion channel activated by ATP. Various features restrict IVM as a viable pharmacological tool for P2X4 receptor modulation, including its ability to bind and modulate other mammalian ion channels. Lack of selective modulators for P2X4 channels has hindered research advancement, despite the growing evidence implicating P2X4 as a feasible therapeutic target in several cardiovascular and neurological disorders.

This study aims to investigate the structure–activity relationship of IVM using a library of structural analogues at the human P2X4 receptor. This information will be used to refine the SAR information for positive allosteric modulation of P2X4 and provide insight for developing drugs that can target this receptor with increased potency and selectivity.

Method/Summary of work: Fura-2 loaded 1321N1 astrocytoma cells stably expressing the human P2X4 receptor were used to assay ATP-evoked intracellular Ca^{2+} responses using a Flexstation III instrument. IVM analogues were tested for their ability to modulate maximal and potency of ATP. Data were expressed as mean \pm SEM and n represents the number of biological repeats. Dose–response curves were fitted to the Hill1 sigmoidal equation and used to determine EC50 and maximum response (Rmax). Statistical significance was determined using an unpaired two-sample t -test or Mann–Whitney test where appropriate.

Results/Discussion: ATP elicited intracellular Ca^{2+} responses in a concentration-dependent fashion ($\text{EC}_{50} = 0.45 \pm 0.032 \mu\text{M}$, $n = 5$). Concentration–response curves for IVM, together with most of the structural analogues, demonstrated a dose-dependent enhancement in ATP-evoked intracellular Ca^{2+} response. All compounds investigated were ranked in order of potency and efficacy, and the chemical features of IVM that produce effects at P2X4 were determined. Such features include redundancy of the large disaccharide moiety and positioning of carbon chains in the spiroketal group.

Conclusion(s): All structural analogues of IVM investigated potentiate the intracellular Ca^{2+} response through hP2X4 channels and can be ranked in terms of their potency and efficacy. Overall, the data suggest that IVM, and several structural distinct analogues investigated in this study, acts as positive allosteric modulators of human P2X4 and provide new chemical information.

P125 | Functional insights into GPR84 signalling at low receptor expression levels using label-free impedance sensing

Vincent Luscombe; David Greaves

University of Oxford

Introduction/Background & aims: GPR84 is an immune-cell expressed orphan GPCR that is upregulated by inflammatory stimuli and enhances inflammation upon activation. The discovery of biased agonist DL-175 demonstrated that selective pathway activation can abrogate GPR84-mediated chemotaxis [1]. To make direct comparisons between assay modalities and time points, we sought to develop a single heterologous cell expression system in order to further interrogate differences between agonists 6-OAU and DL-175. In this study, we

developed monoclonal GPR84 cell lines with different expression levels and compared them to primary bone-marrow derived macrophages (BMDMs) in a label-free impedance sensing system.

Method/Summary of work: BMDMs were prepared as described previously [1]. Cells were plated into RTCA 96 PET E-Plates at 50,000 cells/well and M1 polarised with 100 ng/ml LPS (BMDMs), or at 40,000 cells/well (CHO cells). Plates were incubated over 18–24 h and cell index measurements taken using the xCELLigence RTCA SP system. The impedance responses following agonist addition were first normalised to the cell index immediately prior to addition, and then normalised to baseline conditions. The average values from each experiment were pooled and analysed using GraphPad Prism (v9.3.1). **Results/Discussion:** Agonist stimulation caused a rapid positive impedance response that peaked between 2–10 min and subsequently decayed over time (Figure 1). The BMDM response to DL-175 was characterised by a shallower slope of decay compared with 6-OAU. Only CHO-GPR84 clones with low receptor expression could recapitulate this phenotype. Conversely, high expressing cell lines exhibited a constitutively elevated signal. The subtle yet robust differences between agonists were found to be independent of concentration and consistently manifested in the slope of the decay phase. Furthermore, preincubation with the GRK2/3 inhibitor compound 101 augmented the positive impedance response elicited by 6-OAU in BMDMs and low expressing cell lines, but not in high expressing cell lines.

Conclusion(s): Receptor expression levels are a key determinant of cell impedance responses, and the ability of low expressing GPR84 cell lines to phenocopy BMDMs is consistent with a low receptor reserve and more physiological receptor-effector coupling. This study highlights the utility of kinetic and label-free readouts to discriminate between agonists that might otherwise share many signalling qualities, and provides evidence for the fidelity of stable GPR84 cell lines for use in other high-throughput assays.

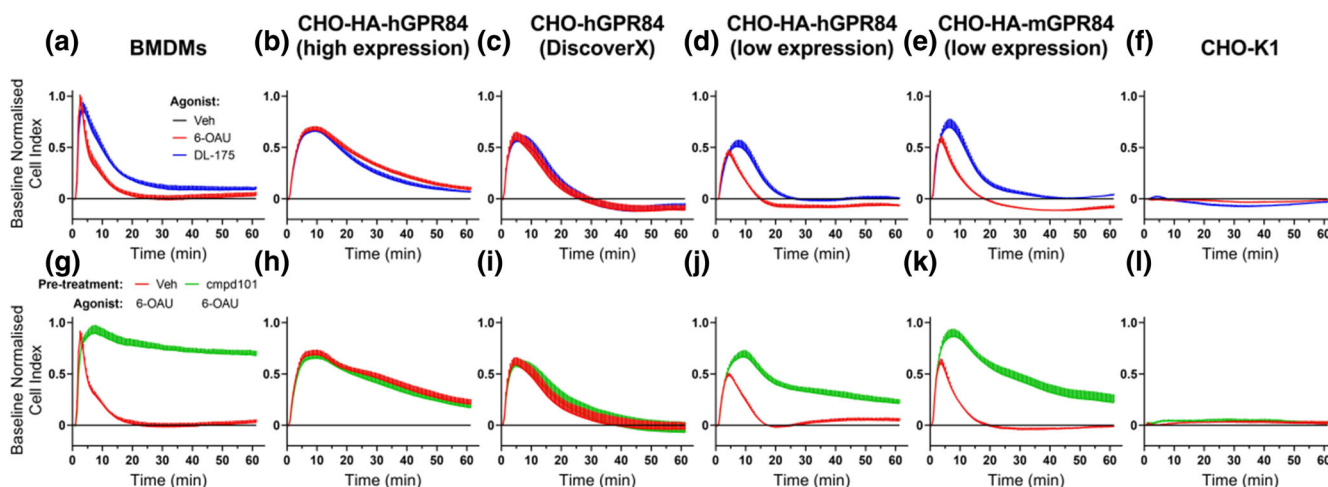


FIGURE 1 Impedance responses of BMDMs and CHO cell lines over time following stimulation with GPR84 agonists. Cells were plated 18–24 h prior to stimulation with $1 \mu\text{M}$ 6-OAU or DL-175 (A–F), or pretreated for 2 h with $30 \mu\text{M}$ compound 101 or Vehicle, followed by stimulation with $1 \mu\text{M}$ 6-OAU (G–L). Cell index values were normalised to baseline conditions (Veh, A–F; Veh–Veh, G–L). Lines depict mean \pm SEM of three independent experiments performed in duplicate.

REFERENCE(S)

1. Lucy, D., Purvis, G. S., Zeboudj, L., et al. (2019). A biased agonist at immunometabolic receptor GPR84 causes distinct functional effects in macrophages. *ACS Chemical Biology*, 14(9), 2055–2064. <https://doi.org/10.1021/acscchembio.9b00533>

Poster presentations - Education & Skills

P130 | Challenges and solutions for pharmacists starting their academic journey

Silvia Amadesi¹; Bozhana Stoyanova²; Joe Gunner²

¹University of Reading; ²School of Pharmacy, University of Reading

Introduction/Background & aims: Biology and physiology topics are the foundations of the Master of Pharmacy (MPharm) degree and for learning other disciplines including pharmacology, toxicology and therapeutics.

It was noticed that ~20% of year 1 MPharm students failed the biology and physiology-focused module that sets a basis for understanding diseases and their treatments in subsequent years of the MPharm.

Understanding what are the difficulties encountered by year 1 students when learning, and what type of support they need to improve their achievements, is essential to ensure academic success.¹

This study aimed to conduct focus group discussions with MPharm students and gain an in-depth understanding of students' difficulties and learning needs, as well as views and preferences in relation to learning tools required when learning biology and physiology topics.

Method/Summary of work: This study aligned with the core dimensions A1, A2 and A4, K2 and K3, and V1-3 of UKPSF. Two multiple-category design focus group discussions were organised with 3 year 1, 3 year 2 and 1 year 3 MPharm students. A 'topic guide', with prompting questions, was used to structure the discussions that were recorded, transcribed, synthesized and then analysed by thematic analysis.²

After coding the participants' responses, three major themes were identified: 'Year 1 challenges', 'Delivery of content', and 'Tools'.

The 'lack of pre-knowledge' on some of the topics, difficulties in 'appreciating the learning objectives' and adapting to the 'pace of delivery' of the lectures were among the major struggles experienced by students.

On the other hand, the use of lecture's screencasts, videos, tutorials and formative online assessments were highlighted as beneficial learning tools.

Results/Discussion: Adapting to different teaching approaches and managing workload seemed to be the major challenges encountered by students.

The use of technology and interactive sessions and the introduction of formative assessments should be considered to support students' learning and thus improve their academic achievements.³

Conclusion(s): Managing students' expectations, at the start of university journey may be important to support academic transition and improve students' engagement and thus their overall experience.

The results of this study were used to develop a Microsoft Forms-based survey aimed to further our understanding on the difficulties encountered by pharmacy students when learning biology and physiology topics and on the students' preferences for 'tools' to support learning and approaches to teaching.

The survey was distributed in Spring 2020 to year 1–4 MPharm students. Qualitative and quantitative analysis of the results are ongoing. It is anticipated that the outcomes of the survey will be transferable to other learning and teaching contexts including pharmacology, toxicology and therapeutics.

REFERENCE(S)

1. Brooker, A., Brooker, S., & Lawrence, J. (2017). First year students' perceptions of their difficulties. *Student Success*, 8(1), 49–62. <https://doi.org/10.5204/ssj.v8i1.352>.
2. Office of Institutional Research, Effectiveness, and Planning Guidelines for Conducting a Focus Group. 2005. https://irep.olemiss.edu/wp-content/uploads/sites/98/2016/05/Trinity_Duke_How_to_Conduct_a_Focus_Group.pdf. Accessed: 29 April 2022.
3. Gopal, T., Herronab, S. S., Mohnc, R. S., Hartseld, T., Jawore, J. M., & Blickenstaffa, J. C. (2010). Effect of an interactive web-based instruction in the performance of undergraduate anatomy and physiology lab students. *Computers & Education*, 55(2), 500–512.

P131 | Exploring the opinions of first-year medical students on the effectiveness of an interactive, online intervention for supporting pharmacology-based education

Mohammed Umar Pervez; Megan Chown; Laura Mongan

Hull York Medical School

Introduction/Background & aims: Pharmacology is an essential field for medical students to understand due to its role in safe prescribing. Most of pharmacology is learned during medical school, but students often feel underprepared to prescribe upon graduation [1]. Research shows that doctors regularly make prescribing mistakes, and a lack of knowledge may be a key reason [1]. Additionally, the prevalence of surface learning in medical schools could impact the frequency of such errors [2]. Our study aims to provide a solution via an e-learning tool (NOTEPAD- iNteractive Online iNtervention for supporting Pharma-cology eDucation) developed using the literature to promote deeper and active learning of pharmacology and prescribing.

Method/Summary of work: NOTEPAD builds upon a previously used noninteractive framework to support first-year medical students in studying essential medications through a curated list of drugs that follows the contemporaneous curriculum. The tool uses the Articulate

Rise 360™ software to create a user-friendly interface and is accessible through the VLE, with concurrent resources to further emphasise material integration.

NOTEPAD consists of two components, the first of which provides an overview of the drug containing weblinks to high-quality sources, which navigate to clinically relevant information. Feedback on the learning achieved is provided dynamically in the second component via a quiz consisting of four multiple-choice questions, with a fifth asking students to produce an example prescription.

Evaluation of the student experience is using a mixed methods approach with analysis of quantitative data from a survey offered to all users of the tool, and qualitative data from a focus group interview. **Results/Discussion:** In this study, we hope to evaluate the effectiveness of NOTEPAD for supporting pharmacology-based education, which implements the convenience and sustainability of self-directed, e-learning whilst implementing active engagement. Future longitudinal study is required to measure students' rating of preparedness for prescribing in clinical practice.

Conclusion(s): The approach taken offers a model for supporting education in the early years of an undergraduate programme in medicine that is low-cost to develop and adaptable to a variety of different curricula.

REFERENCE(S)

1. Brinkman, D., Tichelaar, J., Graaf, S., Otten, R., Richir, M., & van Agtmael, M. (2018). Do final-year medical students have sufficient prescribing competencies? A systematic literature review. *British Journal of Clinical Pharmacology*, 84(4), 615–635. <https://doi.org/10.1111/bcp.13491>
2. Piumatti, G., Guttormsen, S., Zurbuchen, B., Abbiati, M., Gerbase, M., & Baroffio, A. (2021). Trajectories of learning approaches during a full medical curriculum: Impact on clinical learning outcomes. *BMC Medical Education*, 21(1), 370. <https://doi.org/10.1186/s12909-021-02809-2>

P132 | Curriculum analysis—The what, where, how and why of pharmacology teaching in Phase 1 of the MBBS at QMUL

Eleanor Smith; Maimilian Michael Paley; Celia Woolf; Esther Murray; John Broad

Faculty of Medicine and Dentistry, QMUL

Introduction/Background & aims: Junior doctors feel underprepared to perform their responsibility of the prescribing of drugs safely and effectively in FY1 and FY2 [1], despite the addition of the prescribing skills assessment to the curriculum in 2014. This may be due to a misalignment between the pharmacology taught to students in Phase 1 of our MBBS programme (years 1 and 2), and what is required by students in their foundation years. Our aim was to produce a comprehensive curriculum review of the pharmacology teaching delivered to Phase 1 students and explore alignment between the drugs that are introduced to the students with the top 100 drugs most commonly prescribed by the National Health Service (NHS) [2].

Method/Summary of work: The learning materials in Phase 1 available to students on the university's online learning platform were reviewed over all 13 core modules (usually 3–4 weeks duration). The drugs and drug classes introduced in each module were tabulated. Data were analysed using Microsoft Excel and GraphPad Prism 9.0.

Four hundred nineteen lectures, 46 problem-based learning (PBL) scenarios, 58 supervised practical sessions and 31 self-directed activities were reviewed. Four lectures and one PBL scenario addressed the principals of pharmacology; 78% of the top 100 drugs were introduced to students. In total, 1084 drugs (mean (range) 123 (11–232) drugs/module) were introduced across the Phase 1 curriculum; 56% were mentioned only once. Most drugs were mentioned during the fundamentals of medicine, metabolism, and neuroscience modules.

Results/Discussion: This comprehensive review of teaching materials demonstrates the breadth, and relative lack of depth, of drugs taught to students in their first 2 years of their medical school career. There is a limited amount of dedicated teaching time for pharmacology in part due a more integrated curriculum and the loss of visibility of Clinical Pharmacology and Therapeutics as a discrete set of knowledge and competencies [3]. Whilst some of the drugs or drug classes that were mentioned once may still be important or relevant drugs, many of these drugs are not able to be prescribed in the NHS or even in use in the United Kingdom today.

Conclusion(s): This project provides evidence that pharmacology taught in Phase 1 of our MBBS programme is not well aligned with clinical practice, potentially compromising its basis for safe and effective prescribing. There is a focus on introducing students to drugs and drug classes rather than preparing students for clinical practice. We are currently investigating staff and student perceptions of pharmacology teaching.

REFERENCE(S)

1. Kennedy, M., et al. (2019). The role of undergraduate teaching, learning and a national prescribing safety assessment in preparation for practical prescribing: UK medical students' perspective. *British Journal of Clinical Pharmacology*, 85(10), 2390–2398. <https://doi.org/10.1111/bcp.14058>
2. Burrage, D., Baker, E., Lonsdale, D., & Hitchings, A. (2018). *The top 100 drugs: Clinical pharmacology and practical prescribing*. Netherlands: Elsevier Health Sciences.
3. Lerchenfeldt, S., & Hall, L. (2018). Pharm.D.s in the midst of M.D.s and Ph.D.s: The importance of pharmacists in medical education. *Medical Science Education*, 28(1), 259–261. <https://doi.org/10.1007/s40670-017-0520-3>

P134 | The award-winning IUPHAR/BPS guide to PHARMACOLOGY: Curating pharmacology for COVID-19, malaria and antibacterials

Simon Harding¹; Elena Faccenda¹; Jane Armstrong¹; Jamie Davies¹; Steve Alexander²; Anthony Davenport³; Michael Spedding⁴; Chris Southan¹

¹University of Edinburgh; ²University of Nottingham; ³University of Cambridge; ⁴Spedding Research Solutions SAS

Introduction/Background & aims: The IUPHAR/BPS Guide to PHARMACOLOGY (GtoPdb; www.guidetopharmacology.org) (1) is an open-access, expert-curated, online database that provides succinct overviews, key references and recommended experimental ligands for 3000 targets and includes 11,271 ligand molecules, including approved drugs, small molecules, peptides, and antibodies. Here, we report recent progress, particularly on COVID-19-related, antimalarial and antibacterial pharmacology, and provision of useful tools to explore and research pharmacology.

Method/Summary of work: The development of GtoPdb is overseen by NC-IUPHAR (2), data being selected by its subcommittees and expert curators covering established drug targets as well as those of emerging interest for drug discovery. Curation and database development is conducted by the GtoPdb Curation Team at The University of Edinburgh, with regular database updates.

Results/Discussion: In response to the COVID-19 pandemic, our page dedicated to COVID-19 pharmacological strategies continues to be updated weekly and now contains over 100 drugs, with a succinct expert commentary and links to the database for more detailed information. This work contributed to the published IUPHAR Review on a roadmap for SARS-CoV-2/COVID-19 pharmacotherapeutic research and development [3].

Our continuing collaboration with AntibioticDB (<https://www.anticbioticdb.com/>) through funding from the Global Antibiotic Research and Development Partnership (GARDP; <https://gardp.org/>) builds on the nearly 250 antibiotic ligands already curated and linked to AntibioticDB.

The Guide to Malaria Pharmacology (GtoMPdb) now includes the expansion of the Antimalarial Targets family to include subfamilies. GtoMPdb, produced with the Medicines for Malaria Venture, may be a prototype for other antibacterial/antiviral guides.

To improve data accessibility, we have extended our ligand downloads (<https://www.guidetopharmacology.org/downloads.jsp>) to include ligand data in SDF format and a ligand ID mapping file, which maps GtoPdb ligands to PubChem SID/CID, ChEMBL, ChEBI, UniProt, IUPAC, INN, CAS, DrugBank and DrugCentral identifiers. We also now provide a detailed download of endogenous ligated-target pairings. Our homepage layout has been revised to prioritise ways users can access the data.

Conclusion(s): GtoPdb is an expert-curated resource on drug targets and recommended ligands. With over 27,000 users per month, it is of great value to the research community and we continue to ensure the data are as widely accessible as possible.

Recognition of the value of the GtoPdb and acknowledgement of the contribution of all who have supported and developed the resource was made in September 2021 when it received a hidden REF award (<https://hidden-ref.org>).

REFERENCE(S)

1. Harding, S. D., et al. (2022). *Nucl. Acids Res.*, 50(Database Issue), D1282–D1294, The IUPHAR/BPS guide to PHARMACOLOGY in 2022: curating pharmacology for COVID-19, malaria and antibacterials. <https://doi.org/10.1093/nar/gkab1010>

2. Nomenclature and Standards Committee of the International Union of Basic and Clinical Pharmacology. (<https://www.guidetopharmacology.org/nciuphar.jsp>)
3. Alexander, S. P. H., et al. (2020). A rational roadmap for SARS-CoV-2/COVID-19 pharmacotherapeutic research and development: IUPHAR review 29. *British Journal of Pharmacology*, 177(21), 4942–4966. <https://doi.org/10.1111/bph.15094>

P135 | Student-led approaches to introducing animal research for first year biomedical science and pharmacology undergraduates

Sarah Bailey; Christine Edmead

University of Bath

Introduction/Background & aims: Animal research plays an essential role in biomedical research and the development of new medicines. The British Pharmacological Society's (BPS) curriculum for the use of research animals [1] outlines the knowledge, skills and attitudes that undergraduate and taught masters degree programmes should acquire. Here we describe two student-led approaches, with two different cohorts of first year undergraduates, to introducing core ethical principles and a caring attitude in animal research.

Method/Summary of work: For pharmacology students, we piloted the use of the Mouse Exchange Tool Kit [2]. This public engagement activity was created as part of the Animal Research Nexus project where participants can craft a felt mouse, engage in dialogue and reflection about the complexities of creating and caring for mice in research. We adapted this tool to explore student attitudes to research animals and consider the importance of a respectful and considerate attitude to research animals within the culture of care framework. In a 1-h workshop, small groups ($n = 6-8$) of students sat with a facilitator who initiated conversations that were developed by the students. For biomedical science students, we piloted a 1.5-h interactive workshop to consider the bioethics of research. Small groups of students ($n = 5-6$) were asked to draw, name and consider the welfare needs of a given organism (bacteria, HeLa cell, biopsy tissue, mouse, dog, Alzheimer's patient). Student-led class discussions comparatively explored the ethical issues associated with the use/involvement of each organism or subject in research and clinical trials. Qualitative comments were captured throughout the sessions and students asked to leave feedback using post-it notes.

Results/Discussion: Both approaches piloted really engaged the students, evidenced in qualitative comments. The nature of the workshops enabled facilitators to better understand where the students were starting from. The students demonstrated limited prior knowledge of, but much interest in, the origins of laboratory mice and the practices and processes of animal husbandry. The workshops provided a safe space for discussion of the role of different organisms in research, consideration of personal ethical viewpoints and opened up

conversations about care and respect for research subjects in a way that other introductory approaches had not previously done.

Conclusion(s): Instilling a respectful and considerate attitude to research animals and their tissues and a knowledge of the ethical principles underpinning the use of research animals are core learning outcomes of the BPS' curriculum for the use of research animals [1]. Previously, a more didactic approach focusing on formal ethics teaching of, for example, utilitarianism or the legal framework for animal research did not allow space for conversations about the care of animals. While the small group teaching approach delivers high quality engaged teaching, it is not suitable for large numbers of students. We will build on this student-led approach in first year teaching considering how peer-to-peer learning or how early career researchers might participate.

REFERENCE(S)

1. British Pharmacological Society's Curriculum for the use of research animals <https://www.bps.ac.uk/education-engagement/animal-research/curriculum-for-the-use-of-research-animals>
2. Crudgington B, Peres S, Hurley P and Roe E (2021) The Mouse Exchange Toolkit: tinyurl.com/MxToolkit

P136 | To game or not to game-that is the question: Evaluation of newly developed gamification elements in MSc pharmacology modules

Coen Wiegman¹; Laura Fedele¹; Margarita-Ioanna Koufaki¹; Graham Clarke²; Anne Burke-Gaffney¹

¹Imperial College London; ²AstraZeneca

Introduction/Background & aims: Gamification elements in higher education can increase students' interest, boosts competitive spirit, facilitate team building and motivate students to participate in the learning process [1,2]. Here, we evaluate the introduction of four gamification elements into two pharmacology modules (one core and one elective) of the Genes, Drugs and Stem Cells MSc, Imperial College, London. The aim of this study was to evaluate student's engagement with, enjoyment of, and learning through, gamification elements.

Method/Summary of work: Four gamification elements were developed. "Pharma Casino" explores challenges associated with the drug discovery process and "Movieceuticals" is a quiz designed to revise course content. The "Balloon Debate" is also revision of content, prepared individually but shared with other students. "Have I got DRUGS for you" draws on recent/relevant "pharmacology" news items in the form of a quiz. COVID restrictions forced re-designing from an in-person to an online format (Table 1). Fifty-six students took part in "Pharma Casino" and "Movieceuticals." Sixteen students took part in the "Balloon Debate" and "Have I got DRUGS for you" activity.

Evaluation was conducted using Qualtrics surveys. Five levels of word and numerical responses were recorded for questions on engagement, enjoyment, and learning. The combined survey response was 33% (expected level of response [3]); 70% of students said they engaged "a great deal" or "a lot" with the game activities in the core module and a majority (53%) enjoyed them. Over 75% of students thought the activities contributed to their learning. The elective module survey focused on preferences for team vs. individual and online vs. on-campus sessions. Most students (70%) learned best in teams, and 80% learned best during on-campus activities. In terms of enjoyment, all students who responded preferred the on-campus team games most.

Results/Discussion: The responses indicate that the gamification elements were well received, enjoyable, and enhanced learning. Limitations include the low survey response, and that this is a small, local, study designed to evaluate gamification elements in one MSc pharmacology course. Future educational research on the value of gamification across undergraduate and postgraduate pharmacology courses would be beneficial.

Conclusion(s): Introducing gamification elements in pharmacology education sessions increases engagement, enjoyment, and learning.

REFERENCE(S)

1. Çeker, E., & Özdamlı, F. (2017). What "gamification" is and what it's not. *European Journal of Contemporary Education*, 6(2), 221-228.
2. Wang, Z. (2021). Introduction to the Use of Gamification in Higher Education: Part 1. Instruction Design, Services.
3. How to increase survey response rates. (2022). Accessible at <https://www.qualtrics.com/uk/experience-management/research/improve-survey-response/>

TABLE 1 Game-based sessions and delivery

Session	Format	Module	Intended delivery	Actual delivery	Intended purpose
Pharma casino	Team	Core	On-campus	Online	Knowledge application
Movieceuticals	Team	Core	On-campus	Online	Recall/revision
Balloon debate	Individual	Elective	On-campus	Online	Recall/revision
Have I got DRUGS for you	Individual & team elements	Elective	On-campus	On-campus	Knowledge application

P137 | Comparison of student outcomes in laboratory, data or clinically based BSc research projects

Jennifer Stott; Fu Liang Ng

St George's University of London

Introduction/Background & aims: Within the Clinical Pharmacology BSc programme at St George's University of London, second year students undertake an eight-week, full time, research project. Projects are offered by supervisors in the following three categories: Laboratory, Clinical and Data. Laboratory projects are wet lab based, whilst Clinical projects involved patient-centred data. Data projects involve the secondary analysis of pre-extracted datasets that could be either from laboratory or clinical research. Students are assessed by both oral presentation and a written research report. We considered that different project types might result in different student outcomes. Therefore, this study investigated potential differences in student outcomes in the different categories of research projects.

Method/Summary of work: The student outcomes in overall project mark, presentation mark and report mark were analysed by one-way ANOVA with multiple comparisons for the three categories of project. In the 2020/21 cohort of students, 14 undertook laboratory projects, 15 undertook clinical projects and 24 undertook data projects. Students undertaking clinical projects had an overall project mark of 73.5% compared with students undertaking laboratory projects who had an average mark of 66.7% ($p = 0.08$). Analysis of the assessment components showed that clinical projects had an average written report mark of 69.3% compared with laboratory projects, which had an average mark of 65.1% ($p = 0.6$). Comparison of average oral presentation scores for the different categories were as follows: Clinical (76.1%) vs. Laboratory (66.8%) ($p < 0.05$). Data project marks were consistently in between those of clinical and laboratory projects (mean overall mark 72.6% [$p = 0.1$ vs. lab, $p = 0.9$ vs. clinical], mean oral presentation mark 74% [$p = 0.09$ vs. lab, $p = 0.8$ vs. clinical], mean written report mark 70.8% [$p = 0.4$ vs. lab, $p = 0.9$ vs. clinical]).

Results/Discussion: In our 2020/21 cohort, we identified a disparity in student outcomes in different project categories, which was disadvantageous to laboratory-based projects, particularly in oral presentation assessment. There are potential confounding factors that we are not able to account for, such as self-selection for projects, as well as supervision provided. However, clinical projects may be more accessible to a more general audience than lab projects. This discrepancy should be better characterised to consider the most appropriate method of standard setting across varied projects.

Conclusion(s): Whether student research projects have a clinical, data or laboratory basis can impact student outcomes in assessment, in particular in oral presentations.

P139 | Teaching and learning in Nigeria's only one hundred percent open and distance learning (ODL) university: 1—Perspectives on facilitation of pharmacology courses

Helen Kwanashie; Frank Ebhodaghe; George Ani; Elizabeth Joseph-Shehu

National Open University of Nigeria (NOUN)

Introduction/Background & aims: The National Open University of Nigeria (NOUN) is the only 100% open and distance learning (ODL) university in Nigeria although 12 other universities (out of a total of 170 universities in the country) have approvals to run some of their programmes via ODL. With over 600,000 students, it is the largest university in Nigeria, and the leading ODL institution in Africa. Course delivery is by a combination of 100–200 pages printed course materials and several other formats using the learning management system (LMS), *e-Learn*, which for each course involves deployment of twenty to thirty 5- to 10-min instructional videos, followed by minimum of eight 1-h online facilitation classes—with cloud recordings for repeated students' access. Pharmacology, as core courses at undergraduate level in all three departments in NOUN's Faculty of Health Sciences, and at the only postgraduate programme in the Faculty, is taught via online facilitation—introduced 3 years ago across the university to complement the existing mode of learning. Thus, like other responsible higher education institutions [1], NOUN is constantly evolving strategies to improve student engagement and the teaching-learning process as a whole [2]. The aim of this study was to determine students' perception of the online facilitation approach, particularly of pharmacology.

Method/Summary of work: Two courses were selected for the facilitation evaluation exercise, which utilised a 30-item Google form questionnaire, complemented by a key informant interview (KII) with the director in charge of NOUN's facilitation programme. The outcomes of both evaluations are summarised below.

The KII discourse largely supported the above findings and reiterated the university's commitment to seeing how the aforementioned challenges will be overcome by the university, staff and students.

Results/Discussion: The study objectives were met, and this is the first in a series of studies to be carried out by the authors in a bid to improve teaching and learning in ODL settings.

Conclusion(s): The study outcome has made significant contribution to scholarship and is expected to have generic application not only within Nigeria, but across the world.

REFERENCE(S)

- Rienties, B., Nguyen, Q., Holmes, W., & Reedy, K. (2017). A review of ten years of implementation and research in aligning learning design with learning analytics at the Open University UK. *Interaction Design and Architecture(s)*, 33, 134–154. <https://doi.org/10.55612/s-5002-033-007>
- Bello, L. K. (2021). Exploring the capabilities of online facilitation to bridge the instructional gaps in open and distance learning delivery in Nigeria. *Journal of Education and Practice*, 12(3), 174–184.

TABLE 1 Respondents' facilitation experiences, practices and perspectives

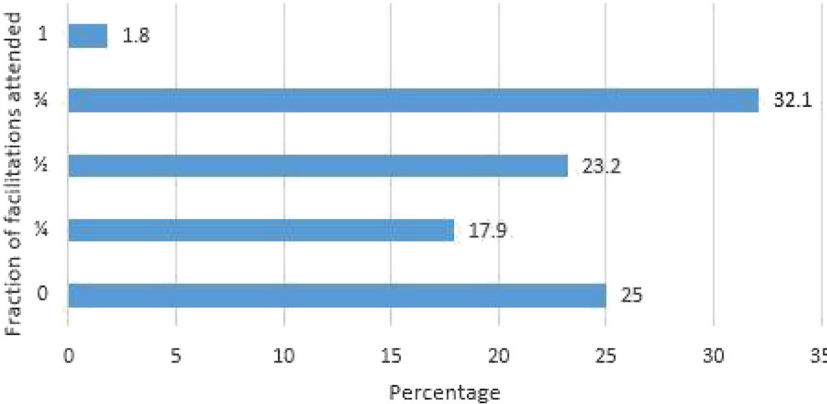
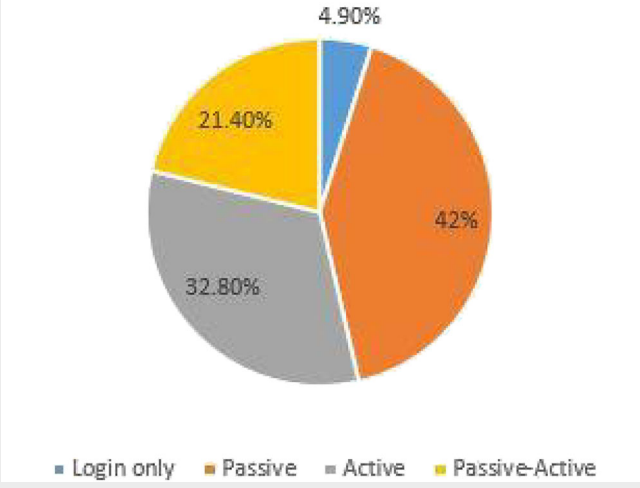
Item	Description and inference												
Socio-demographics	The respondents ($n = 63$), were mostly female (91.7%), aged between 30 and 44 years (65.1%), 100% employed, with self-acclaimed computer proficiency of good (41.0%), very good (34.4%) and excellent (9.8%). The most common electronic devices owned by the students and used by them during facilitations were smart phones (93.5%) and laptops (28.5%).												
Courses registered, facilitated and attended Total no. of courses registered by the respondents = 393 No. of courses offered for facilitation = 132 (33.59%) No. of facilitated courses students participated in = 59 (44.7% of those facilitated).	Thus, facilitation was found to be both under-offered and under-utilised.												
<p style="text-align: center;">Students' Participation in the facilitation</p>  <table border="1" data-bbox="140 646 970 1052"> <caption>Data for Students' Participation in the facilitation</caption> <thead> <tr> <th>Fraction of facilitations attended</th> <th>Percentage</th> </tr> </thead> <tbody> <tr> <td>0</td> <td>25</td> </tr> <tr> <td>1/4</td> <td>17.9</td> </tr> <tr> <td>1/2</td> <td>23.2</td> </tr> <tr> <td>3/4</td> <td>32.1</td> </tr> <tr> <td>1</td> <td>1.8</td> </tr> </tbody> </table>	Fraction of facilitations attended	Percentage	0	25	1/4	17.9	1/2	23.2	3/4	32.1	1	1.8	Again, facilitation was found to be under-utilised.
Fraction of facilitations attended	Percentage												
0	25												
1/4	17.9												
1/2	23.2												
3/4	32.1												
1	1.8												
<p style="text-align: center;">Nature of respondents' participation in facilitation</p>  <table border="1" data-bbox="140 1129 783 1619"> <caption>Data for Nature of respondents' participation in facilitation</caption> <thead> <tr> <th>Participation Type</th> <th>Percentage</th> </tr> </thead> <tbody> <tr> <td>Login only</td> <td>4.90%</td> </tr> <tr> <td>Passive</td> <td>42%</td> </tr> <tr> <td>Active</td> <td>32.80%</td> </tr> <tr> <td>Passive-Active</td> <td>21.40%</td> </tr> </tbody> </table>	Participation Type	Percentage	Login only	4.90%	Passive	42%	Active	32.80%	Passive-Active	21.40%	A higher proportion of the respondents reported being passive (listening only with no speaking), rather than active (both listening and speaking). Furthermore, cloud recordings of the facilitations were viewed by the respondents once (25.4%), twice (39.7%), thrice (11.1%), more than thrice (15.9%), or not at all (7.9%).		
Participation Type	Percentage												
Login only	4.90%												
Passive	42%												
Active	32.80%												
Passive-Active	21.40%												
Challenges to successful facilitation													
From students	From facilitators	From university											
Unstable internet connection (82.3%)	Facilitators not consistent with the facilitation schedule (86.0%)	Course materials were not always provided making it more difficult to prepare in advance for the facilitations (57.6%)											
Difficulties juggling work and facilitation schedule (56.6%)	Facilitators did not post cloud recordings at all or on time (18.0%)	Facilitations started too late into the semester leading to rushed programmes (44.1%)											

TABLE 1 (Continued)

Challenges to successful facilitation		
From students	From facilitators	From university
Inadequate data/Wi-Fi (32.3%)	Facilitators' poor skills (4.0%)	Discordance between the contents of courses and tutor-marked-assignments resulting in general frustrations and apathy towards facilitation, etc (39.0%)
Poor power supply to charge devices (29.0%)	Facilitators' poor mastery of the subject matter (2.0%)	The University's policy that facilitation and cloud recorded links should not be posted outside the e-learn course page, e.g., onto social media platforms (30.5%)
Boss/supervisors not giving time off work to participate (9.7%)		Online versions of the course materials were sometimes different from what the facilitators presented (18.6%)
Expectations, assessments and perceptions		
<ul style="list-style-type: none"> • Respondents' expectations of improved understanding of the courses (87.0%) were met fully (53.2%) or partially (43.5%); leading to their overall assessment that the facilitations were very worthwhile and helpful (69.8%) or averagely so (30.2%). • Respondents were satisfied with the timing (65.2%), quality (97.9%) and ease of the facilitations for students and facilitators (93.9%). • Respondents concluded 100%, that facilitation was a necessity and an acceptable medium for learning. 		

P140 | Teaching and learning in Nigeria's only one hundred percent open and distance learning (ODL) university: 2—Evaluation of virtual pharmacology laboratory

Helen Kwanashie; Elizabeth Joseph-Shehu; George Ani; Frank Ebhodaghe

National Open University of Nigeria (NOUN)

Introduction/Background & aims: This is the second instalment of our series to explore teaching and learning processes at the National Open University of Nigeria (NOUN), the only 100% open and distance learning (ODL) university in the country. As Nigeria's foremost university in terms of student population of more than 600,000 accessing quality education through 103 study centres spread across the country, the university and staff are constantly striving to improve on its service delivery. In line with this, online facilitation of some of its courses started 3 years ago and currently covers about a third of its courses. More recently, innovative virtual laboratories have been

TABLE 1 FGD data evaluating virtual pharmacology laboratory

Question	Consensus/reported comparisons of the VPL with face-to-face practicals
How does the virtual lab compare with the face-to-face lab during your undergraduate studies?	Probing for content, time spent and access, the students reported that both were comparable. VPL can be concluded in 1 h and yet was very effective in communicating the essence of the practical. In contrast, a typical face-to-face practical is usually scheduled for 3 h.
Considering that the usual manner in which practicals are organized, did the practical videos make sense?	Probing for YES or NO in relation to title, introduction, aim/objectives, results, discussion, etc., the consensus was YES for each. Students felt more content was covered in terms of information, corrections of routine misconceptions, clarifications, activities, etc.
What are your suggestions for enhancing or improving the learning experience of the student in the VPL?	One suggestion was that the videos could be edited to make them even shorter and more attractive for students to watch. The potential to keep on viewing the videos was considered a huge advantage. The fact that animals will not be sacrificed each time was a big bonus.
What are the possible implications of the VPL practical?	The group correctly identified implications in several areas including public health, environmental health, nursing and counselling.
Assess the VPL by awarding a score of 0 (lowest) to 10 (highest).	The scores given by the students ranged between 70 and 80, averaging 75% (all 'A's).
What was the worst aspect of the practical?	Inability to always observe some of the signs of organophosphate toxicity.
What was the best aspect of the practical?	Being able to post additional information on the screen throughout the duration of the practical plus the possibilities of repeat views of the videos.
Sample free quotes by the students	<p>“The virtual pharmacology lab was a new experience and it did impart knowledge too. I do not think I will forget it in a long time.”</p> <p>“My experience was insightful.”</p> <p>“My VPL experience was a remarkable experience and should be continued.”</p>

created by the Department of Nursing Science for the biomedical sciences, including virtual pharmacology laboratory (VPL). Thus, like other responsible higher education institutions [1], NOUN is constantly evolving strategies to improve student engagement and the teaching-learning process as a whole. The aim of this study was to test-run and evaluate the newly created VPL.

Method/Summary of work: A 1-h focus group discussion (FGD) followed by a half-hour surprise post-FGD oral test on a VPL titled 'Antidotal Therapy for Organophosphate Poisoning in Mice' was conducted by the researchers. The group was made up of six MSc Public Health student-participants (five females and one male) who, in addition to taking pharmacology as a core course within the MSc programme, had conventional face-to-face laboratory experiences during their undergraduate degree programmes from various universities outside NOUN, in nursing, pharmacology, biochemistry, physiotherapy and microbiology (two students). The VPL assessed was a pharmacology practical comprising of 3-parts-in-1 videos of approximately 15-min duration each. The students had access to the videos for 24 h during which they watched the videos two to three times. The FGD was guided by 10 structured lead questions with relevant probes while the post-FGD test was made up of 30 standard quiz questions based on the three videos. The outcome of the evaluation was based on notes and recordings of the FGD and scoring of the test by the researchers. The study (FGD and post-FGD test) were conducted virtually on zoom call platform.

Results/Discussion: The table below summarises the main outcome of the FGD.

The surprise test scores ranged from 55.56 to 70.37, averaging 57.41% (a "C" grade) showing reasonable grasping of the practical content.

Conclusion(s): The VPL represents an effective way to teach practical pharmacology to ODL students.

REFERENCE(S)

1. Anksorus, H. N., et al. (2021). The catalyst for change in teaching and assessing virtual laboratory skills. *Curr. Pharm. Teach. Learn.*, 13(12), 1550-1554. <https://doi.org/10.1016/j.cptl.2021.09.026>

Oral communications, Wednesday 14th September

Oral communications - Cardiovascular & Respiratory

OC021 | Divalent ligands of platelet GPVI and CLEC-2 function as agonists or antagonists depending on receptor density

Joanne Clark

University of Birmingham

Introduction/Background & aims: The platelet C-type lectin-like receptor 2 (CLEC-2) and glycoprotein VI (GPVI) receptor have been identified as targets for a new class of anti-thrombotic drugs due to their major role in driving occlusive thrombosis and their minor role in haemostasis. Activation of both receptors is mediated by clustering, but their membrane organisation is controversial and their dependency on ligand valency is not known. The aims were to determine whether CLEC-2 and GPVI are expressed as monomers or dimers in the membrane and investigate the dependency on ligand valency for activation of human platelets.

Method/Summary of work: We used fluorescence correlation spectroscopy (FCS) and photobleaching to determine the stoichiometry of CLEC-2 and GPVI in cell lines. HEK293T cells were transfected with GPVI-eGFP, CLEC-2-eGFP, CD86-eGFP and CD28-eGFP. FCS measurements were taken in the membrane, and subsequent autocorrelation and photon count histogram analysis was applied to determine diffusion coefficients and molecular brightness. For photobleaching, fixed cells were imaged in TIRF and automated spot and step detection algorithms were applied. We have investigated the ability of divalent and tetravalent ligands to CLEC-2 and GPVI (including novel crosslinked nanobodies) to induce activation of platelets with light transmission aggregometry. We tested whether the novel nanobody ligands cause clustering of CLEC-2 and GPVI and investigated the effect of Syk inhibition on CLEC-2 and GPVI clustering by FCS.

Results/Discussion: Contrary to previous reports, we show that CLEC-2 and GPVI are expressed as a mixture of monomers and dimers in cell lines with GPVI predominately monomeric ($n = 3-6$). Using human and mouse platelets, and cell lines transfected with low ($28 \pm 4\%$ transfection efficiency) and high ($73 \pm 3\%$ transfection efficiency) levels of CLEC-2, we report that divalent ligands serve as antagonists in human platelets (0% aggregation) and low-expressing cells lines (onefold increase in receptor signalling over basal) and as agonists in mouse platelets ($85 \pm 3.6\%$ aggregation) and high-expressing cell lines (threefold to ninefold increase in receptor signalling over basal) ($n = 3-5$). Likewise, divalent nanobodies to GPVI do not cause aggregation of human platelets (0% aggregation) ($n = 3$). Further, we show that tetravalent nanobodies cause aggregation of human platelets ($88 \pm 9.7\%$ aggregation) and using FCS that multivalent ligands cause clustering of CLEC-2 and GPVI in cell lines ($n = 3$). **Conclusion(s):** These results provide evidence that CLEC-2 and GPVI are present in both monomeric and dimeric forms with GPVI predominately monomeric. Divalent ligands can act as agonists and antagonists depending in part on receptor density. We therefore propose that divalent ligands should be considered as partial agonists.

OC022 | SGLT2 inhibitors induce vasorelaxation via a Kv7-dependent mechanism

Elizabeth Forrester¹; Geoffrey Abbott²; Johs Dannesboe³; Thomas Jepps³; Iain Greenwood¹

¹St George's University of London; ²University of California Irvine;

³University of Copenhagen

Introduction/Background & aims: Sodium-dependent glucose transporter 2 (SGLT2 or SLC5A2) inhibitors improve glycaemic control in diabetic patients, by preventing glucose reabsorption from the renal proximal tubule. In addition, SGLT2 inhibitors offer a cardio-protective benefit in diabetic and nondiabetic patients [1]. Whilst the mechanism is unknown, there is evidence that the SGLT2 inhibitor lowering of peripheral resistance and arterial relaxation is unlikely to be attributed to increased diuresis alone. Kv7 channels regulate arterial tone and contribute to receptor mediated relaxation [2]. This study aimed to identify if SGLT2 inhibitors relaxed resistance arteries and whether this occurred through activation of Kv7 channels.

Method/Summary of work: The effects of empagliflozin, dapagliflozin and ertugliflozin were determined via Wire-Myography on precontracted renal and second-order mesenteric arteries from male Wistar rats, in the presence of several potassium channel blockers. Concentration effect curves were generated with mean values plotted on a log(x) graph \pm SEM. Expression of SLC5 transporter and KCNQ genes in mesenteric and renal rat arteries was determined by RT-qPCR. In silico simulations of drug binding to the channel were performed.

Results/Discussion: *KCNQ1*, *KCNQ4* and *KCNQ5* (Kv7.1, Kv7.4 and Kv7.5) transcripts were expressed in mesenteric and renal arteries, however *SLC5A1* and *SLC5A2* (SGLT1 and SGLT2) were not ($N = 4$). The SGLT2 inhibitors empagliflozin, dapagliflozin and ertugliflozin relaxed precontracted mesenteric and renal arteries from male rats by $\sim 67\%$ ($N = 8$). The relaxation evoked by $30 \mu\text{mol L}^{-1}$ empagliflozin was attenuated by 46% upon preincubation with $10 \mu\text{mol L}^{-1}$ pan-Kv7 blocker linopirdine ($P < 0.001$), compared with 16% for both $30 \mu\text{mol L}^{-1}$ dapagliflozin and ertugliflozin. SGLT2 inhibitor concentrations above $100 \mu\text{mol L}^{-1}$ were linopirdine in-sensitive. Pharmacological inhibition of Kv7.1, BK_{Ca} , K_{ATP} or Kv1.1 and Kv1.2 channels did not attenuate said vasodilation. Using in silico docking empagliflozin, dapagliflozin and ertugliflozin are predicted to bind near the foot of the channel voltage sensor of Kv7.5.

Conclusion(s): This study is the first to demonstrate that SGLT2 inhibitors evoke vasorelaxation in renal and mesenteric arteries through an interaction with voltage-gated potassium channels. The data suggest that the molecular correlate is heteromeric Kv7.4/5 channels.

REFERENCE(S)

- Williams, D. M., & Evans, M. (2020). Are SGLT-2 inhibitors the future of heart failure treatment? The EMPEROR-preserved and EMPEROR-reduced trials. *Diabetes Therapy*, 11(9), 1925. <https://doi.org/10.1007/S13300-020-00889-9>, 1934
- Greenwood, I. A., & Ohya, S. (2009). New tricks for old dogs: KCNQ expression and role in smooth muscle. *British Journal of Pharmacology*, 156(8), 1196. <https://doi.org/10.1111/J.1476-5381.2009.00131.X>, 1203

OC024 | Oral nanotherapeutic formulations of insulin and liraglutide

Nicholas Hunt¹; Glen Lockwood¹; Scott Heffernan²; Jarryd Daymond¹; Zdenka Kuncic¹; Peter McCourt³; David Le Couteur¹; Victoria Cogger¹

¹University of Sydney; ²NSW Health; ³University of Tromsø

Introduction/Background & aims: Reformulation of injectable only medications to make them orally bioavailable is a growing area of research with the aim to improve patient compliance and quality of life. Insulin in particular is a diabetic medication that must be given three to six times a day and has a high risk of adverse events such as hypoglycaemia. Previously, we have shown orally administered nanomaterials rapidly cross the small intestine and are taken up by the liver in animal models [1]. A follow-up study showing this nanotechnology could be utilised to improve the bioavailability of orally available diabetic medications that have target sites of action in the liver (e.g., metformin) [2]. Currently, both insulin and liraglutide must be given via subcutaneous injection; however, these agents have distinct sites of action: Insulin acts on the liver, muscle and fat, and liraglutide acts almost exclusively on the pancreas and gut. This study aimed to develop and demonstrate a nanotechnology-based oral peptide delivery system for both these medications.

Method/Summary of work: Oral formulation was performed by conjugation of the peptide to Ag_2S quantum dots [1, 2] and encapsulation in a chitosan/glucose co-polymer. Following characterisation with TEM, SEM, FTIR, NMR, ICP-MS and SAXS, preclinical pharmacokinetic, pharmacodynamic and toxicity studies were performed in C57BL/6J mice utilising radiolabelling and Eliza's methods. We then examined our oral insulin formulation in animal models of type 1 diabetes (nonobese diabetic [NOD] mice and streptozotocin [STZ] treated rats) and in nonhuman primates (baboons) using insulin tolerance testing and 2–6 week continuous treatments. Biochemistry, lipids and haematology toxicity studies were performed in baboons. Our oral formulation of liraglutide was evacuated utilising C57BL/6J mice following similar PK and PD studies as our oral insulin in addition to 4 week continuous treatment in either high fat diet (65% fat) or aged (24 months) mice. All mice and rat studies were performed with $n = 5$ and baboon studies with $n = 20$. Statistical significance was determined using an ANOVA followed by a Tukey's post hoc test on raw data.

Results/Discussion: Oral insulin and liraglutide nanoformulations were 50–60 nm in size with a neutral charge in water. PK data demonstrated the bioavailability of oral insulin and liraglutide was 4% and 1.7%, respectively. Organ distribution of oral insulin was predominantly in the liver with injected insulin distributing to the liver muscle and fat. Oral liraglutide demonstrated localization to the pancreas and minimal expression in the liver and gut. PD data highlighted that both

oral insulin and liraglutide were effective at reducing blood glucose in a dose-dependent manner similar to injected insulin. Oral insulin did not induce hypoglycaemia at 300+ IU/kg dosages. Treatment in NOD mice and STZ rats demonstrated oral and injected insulin promoted similar effect sizes and time to onset of effect. Six-week treatment in STZ rats showed no weight gain with oral insulin. Baboons demonstrated a dose-dependent reduction in blood glucose of 10%, 20% and 30% with 2, 5 and 10 IU/kg oral insulin. No toxicity was observed in baboons following four treatment.

Conclusion(s): These studies demonstrate the application of our nano-technology to both liver acting and nonliver acting medications.

REFERENCE(S)

- Hunt, N. J., Lockwood, G. P., Le Couteur, F. H., McCourt, P. A., Singla, N., Kang, S. W. S., Burgess, A., Kuncic, Z., Le Couteur, D. G., & Cogger, V. C. (2020). Rapid intestinal uptake and targeted delivery to the liver endothelium using orally administered silver sulfide quantum dots. *ACS Nano*, 14(2), 1492–1507. <https://doi.org/10.1021/acsnano.9b06071>.
- Hunt, N. J., Lockwood, G. P., Kang, S. W., Westwood, L. J., Limantoro, C., Chrzanowski, W., McCourt, P. A., Kuncic, Z., Le Couteur, D. G., & Cogger, V. C. (2021). Quantum dot nanomedicine formulations dramatically improve pharmacological properties and alter uptake pathways of metformin and nicotinamide mononucleotide in aging mice. *ACS Nano*, 15(3), 4710–4727. <https://doi.org/10.1021/acsnano.0c09278>.

OC025 | Comparison of the effect of an IP receptor agonist and Kv7 activator in rat mesenteric and pulmonary arteries

Skye Lau¹; Elizabeth Forrester¹; Zena Wehbe¹; Samuel Badlwin²; Jennifer Stott¹; Iain Greenwood¹

¹St George's University of London; ²University of Copenhagen, Denmark

Introduction/Background & aims: KCNQ-encoded Kv7 channels play a key role in regulating vascular tone and have been implicated in prostacyclin (IP) receptor-mediated relaxations in rat mesenteric arteries [1]. Iloprost is a prostacyclin analogue used to treat pulmonary arterial hypertension. However, the involvement of Kv7 channels in iloprost-mediated responses in pulmonary arteries is unclear. Therefore, we performed a comparison of functional responses to Kv7 activators and IP receptor antagonist MRE-269 in rat pulmonary and mesenteric arteries.

Method/Summary of work: The relative expression of Kv7 channel (KCNQ1, 4) and prostanoid receptor (Ptger 1-4, PtgIR, Tbxr2) genes were determined by RT-qPCR in pulmonary and mesenteric rat arteries. The effect of Kv7 activators, iloprost and specific IP receptor agonist MRE-269 was determined through wire-myography on precontracted pulmonary and second-order mesenteric arteries from male Wistar rats in the presence of several potassium channel blockers or TASK-1 and Kv1.5 blockers. Concentration effects curves were plotted on a log (x) graph using values expressed as mean ± SEM.

Results/Discussion: The Kv7.2–7.5 activator ML213, relaxed precontracted mesenteric arteries but failed to relax precontracted pulmonary arteries. However, in the presence of TASK 1 and Kv1.5 blockers (1 μmol L⁻¹ ML365 and 1 μmol L⁻¹ DPO-1), a relaxation of ~44% was produced by ML213 in pulmonary arteries similar to previous reports [2] (n = 6). The TASK 1 and Kv1.5 blockers had no effect on relaxations to ML213 in the mesenteric artery. The IP receptor agonist MRE-269 was an effective inhibitor of precontracted rat mesenteric arteries (64% relaxation at 100 nM), which was attenuated by the pan-Kv7 blocker linopirdine and the Kv7.1 specific blocker HMR1556. In contrast, MRE-269 was an ineffective relaxant of pulmonary arteries up to 3 μM. KCNQ1, KCNQ4 (Kv7.1 and Kv7.4) and KCNE4 transcripts were expressed in pulmonary and mesenteric arteries. No PtgIR (IP receptor) transcripts were expressed in pulmonary arteries compared with mesenteric arteries (n = 3).

Conclusion(s): This study has shown differential Kv7 activator responses in mesenteric and pulmonary arteries, despite similar relative expression levels of KCNQ genes. The data suggest that Kv7 channel proteins are regulated differently in the two arteries.

REFERENCE(S)

- Baldwin, S. N., Forrester, E. A., McEwan, L., & Greenwood, I. A. (2022). Sexual dimorphism in prostacyclin-mimetic responses within rat mesenteric arteries: A novel role for Kv 7.1 in shaping IP receptor-mediated relaxation. *British Journal of Pharmacology*, 179(7), 1338–1352. <https://doi.org/10.1111/bph.15722>
- Mondéjar-Parreño, G., Barreira, B., Callejo, M., et al. (2020). Uncovered contribution of Kv7 channels to pulmonary vascular tone in pulmonary arterial hypertension. *Hypertension*, 76(4), 1134–1146. <https://doi.org/10.1161/HYPERTENSIONAHA.120.15221>

Oral communications—Drug discovery, development & evaluation

OC026 | Possible mechanism of antiulcer activity of phytochemical constituents of n-butanol fraction of *Balanites aegyptiaca*: An in silico approach

Chinenye Ugwah-Oguejiofor¹; Oguejiofor Ugwah²; Halilu Mshelia¹; Abayomi Adegboyega³

¹Usmanu Danfodiyo University, Sokoto; ²Usmanu Danfodiyo University Teaching Hospital; ³University of Jos

Introduction/Background & aims: Peptic ulcer disease (PUD) is a disease that arises due to an imbalance between defensive and destructive factors in the stomach [1]. Mucin secretion and prostaglandins are some of the defensive factors while hydrochloric acid and pepsin are some of the destructive ones. Many drugs are available for the treatment of PUD but not without side effects. Hence, there is a need to develop new antiulcer agents that are safe, affordable and readily available. *Balanites aegyptiaca* L. (Zygophyllaceae) is amongst the plant

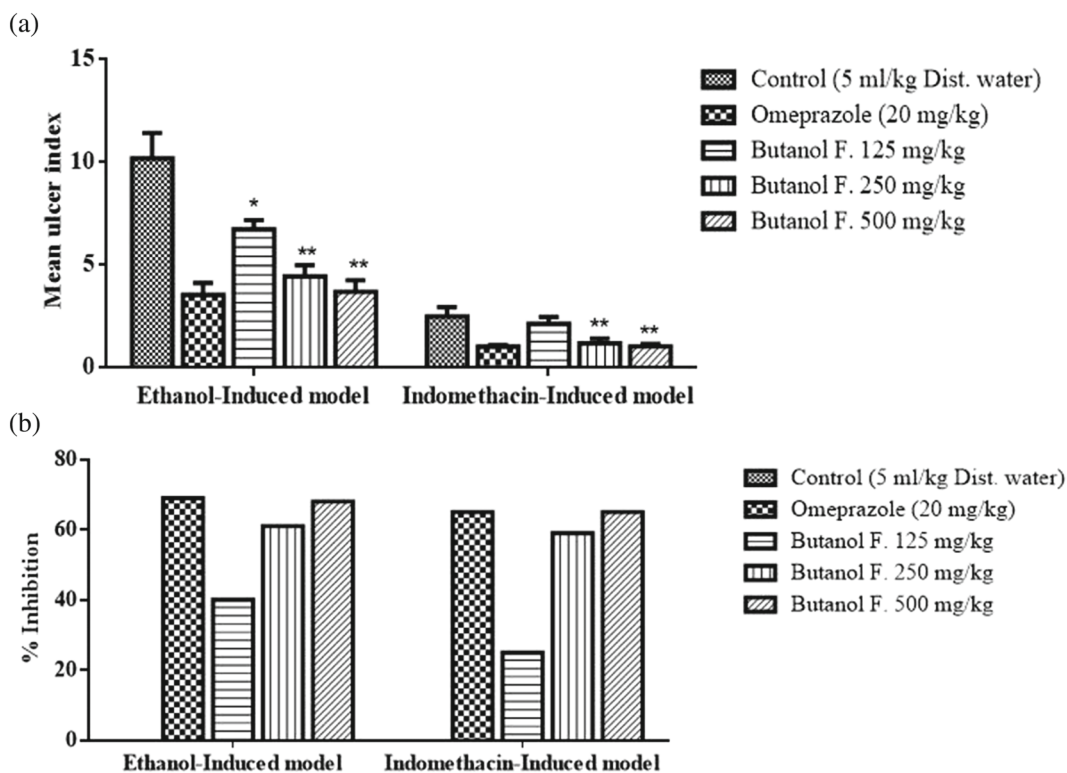


FIGURE 1 Effect of butanol fraction *Balanites aegyptiaca* on ethanol-induced and indomethacin-induced ulcers showing mean ulcer (a) and percentage inhibition (b). Data presented as means ± SD, n = 5 for all groups. **p < 0.01, *p < 0.05 compared with the distilled water control group analyzed using ANOVA followed by Dunnett's post hoc test

TABLE 1 Docking scores of the bioactive compounds from n-butanol fraction of *Balanites aegyptiaca* against muscarinic acetylcholine receptor

Compound name	PubChem CID	Docking score (kcal/mol)
Phenol, 4,4'-(1,2-diethyl-1,2-ethanediyl)bis-, (R*,S*)-	6,432,746	-9.026
Ethanone, 1-(4-hydroxy-3-methoxyphenyl)-	2214	-7.034
4,6-Bis(4-ethoxybenzylthio)-5-nitropyrimidine	585,037	-6.854
l-[-]-4-Hydroxy-1-methylproline	237,040	-6.837
Benzaldehyde, 3-hydroxy-4-methoxy-	12,127	-6.635
2H-Pyran-2-carboxylic acid, 5-ethylidene-5,6-dihydro-2,3-dimethyl-6-oxo-, [S-(E)]-	12,303,689	-6.092
1,2-Benzenedicarboxylic acid, bis(2-methylpropyl) ester	6782	-6.09
Octadecanoic acid, 2-methylpropyl ester	12,588	-5.934
Phenol, 2-methoxy-4-(1-propenyl)-	853,433	-5.89
Omeprazole	4594	-5.292
Heptacosane	11,636	-4.999
Heptasiloxane, hexadecamethyl-	10,912	-4.918
Dibutyl phthalate	3026	-4.47
3-Penten-2-ol	5,366,239	-3.996
Dimethylsulfoxide-D6	75,151	-3.863
1-Butanol	263	-3.198
n-Hexadecanoic acid	985	-1.786

TABLE 2 Docking scores of the bioactive compounds from n-butanol fraction of *Balanites aegyptiaca* against gastric H⁺K⁺-ATPase

Compound name	PubChem CID	Docking score (kcal/mol)
Phenol, 4,4'-(1,2-diethyl-1,2-ethanediyl)bis-, (R*,S*)-	6,432,746	-7.219
Ethanone, 1-(4-hydroxy-3-methoxyphenyl)-	2214	-6.837
Omeprazole	4594	-6.19
Benzaldehyde, 3-hydroxy-4-methoxy-	12,127	-6.087
l-[-]-4-Hydroxy-1-methylproline	237,040	-5.784
Phenol, 2-methoxy-4-(1-propenyl)-	853,433	-5.62
4,6-Bis(4-ethoxybenzylthio)-5-nitropyrimidine	585,037	-5.223
2H-Pyran-2-carboxylic acid, 5-ethylidene-5,6-dihydro-2,3-dimethyl-6-oxo-, [S-(E)]-	12,303,689	-5.143
Dimethylsulfoxide-D6	75,151	-4.19
1,2-Benzenedicarboxylic acid, bis(2-methylpropyl) ester	6782	-4.129
Octadecanoic acid, 2-methylpropyl ester	12,588	-3.998
3-Penten-2-ol	5,366,239	-3.864
Heptasiloxane, hexadecamethyl-	10,912	-3.796
Dibutyl phthalate	3026	-3.496
1-Butanol	263	-3.404
n-Hexadecanoic acid	985	-1.724

species reported in Nigeria with antiulcer activities [1]. It is a perennial tree that is mostly found in Africa, south Asia and most desert environments. The aim of the study was to determine the possible mechanism of antiulcer activity of phytochemical constituents of n-butanol fraction of *Balanites aegyptiaca* (BA) through in silico molecular docking studies.

Method/Summary of work: The n-butanol fraction of BA was got from successive fractionation of the aqueous stem bark extract of BA using petroleum ether, chloroform and finally n-butanol. Preliminary phytochemical studies were carried following standard procedures. Oral acute toxicity test was evaluated in female rats according to OECD 425 guidelines at a limit dose of 2000 mg/kg. The antiulcer activity of the fraction (125, 250 and 500 mg/kg, p.o.) was evaluated in ethanol and indomethacin-induced ulcer models in rats. The fraction was subjected to gas chromatography-mass spectrometry (GC-MS) analysis to identify its phytochemical constituents. The constituents were subjected to molecular docking studies against muscarinic acetylcholine receptor (MAR) and gastric proton pump, H⁺/K⁺-ATPase (HKA). Statistical significance was set at $p < 0.05$ determined using an ANOVA followed by a Dunnett's post hoc test.

Results/Discussion: The result of the phytochemical studies revealed the presence of alkaloids, tannins, flavonoids and saponins. The acute toxicity test at 2000 mg/kg produced neither mortality nor changes related to toxicity. In the ethanol and indomethacin-induced ulcer models, the fraction showed a dose-dependent decrease in mean ulcer inhibition, significantly ($p < 0.05$) lower than the control at all dose levels except at 125 mg/kg in the indomethacin-induced ulcer model (Figure 1). The GC-MS analysis revealed a total of 17 compounds. Molecular docking studies revealed that Phenol, 4,4'-(1,2-diethyl-1,2-ethanediyl)bis-(R*,S*) had the best binding affinity (-9.026 and -7.219 kcal/mol) to MAR and HKA respectively

amongst all the compounds (Tables 1 and 2). It was also found to be better than the positive control omeprazole (-5.292 and -6.19 kcal/mol) against MAR and HKA, respectively. The standard reference ligand, omeprazole, interacted with MAR by forming hydrogen bonds with THR 231, TYR 506 and a Pi-cation interaction with TRP 525. Phenol, 4,4'-(1,2-diethyl-1,2-ethanediyl)bis-, (R*,S*) interacted with the receptor by forming hydrogen bonds with ASP 147, ALA 238 and Pi-Pi stacking interactions with TYR 148, TRP 503 and TYR 529. Ethanone, 1-(4-hydroxy-3-methoxyphenyl) interacted by forming a Pi-Pi stacking interaction with SER 151 and ASN 507 while 4,6-bis(4-ethoxybenzylthio)-5-nitropyrimidine interacted by forming a Pi-Pi stacking interaction with THR 525. However, in the HKA interactions, phenol, 4,4'-(1,2-diethyl-1,2-ethanediyl)bis-, (R*,S*) interacted by forming a hydrogen bond with ASP 137 while ethanone, 1-(4-hydroxy-3-methoxyphenyl) and benzaldehyde, 3-hydroxy-4-methoxy interacted by forming a hydrogen bond with LEU 811. Omeprazole interacted by forming a hydrogen bond with ASN 369.

Conclusion(s): The study confirmed that the n-butanol fraction of *Balanites aegyptiaca* possesses antiulcer activity and contains various bioactive compounds that may be of phytopharmaceutical importance. Phenol, 4,4'-(1,2-diethyl-1,2-ethanediyl)bis-(R*,S*) and ethanone, 1-(4-hydroxy-3-methoxyphenyl) may be used to develop novel therapies for the management of peptic ulcer disease. Their possible mechanism of action could be through inhibition of gastric proton pump and muscarinic acetylcholine receptors.

REFERENCE(S)

- Ugwah, M. O., Ugwah-Oguejiofor, C. J., Etuk, E. U., Bello, S. O., & Aliero, A. A. (2019). Evaluation of the antiulcer activity of the aqueous stem bark extract of *Balanites aegyptiaca* L Delile in Wistar rats. *Journal of Ethnopharmacology*, 239, 111931. <https://doi.org/10.1016/j.jep.2019.111931>

OC027 | A9-301, a novel inhibitor of SLC26A9, completely and selectively blocked anion transport by SLC26A9

Sungwoo Cho; Wan Namkung; Jinhong Park

Yonsei University

Introduction/Background & aims: SLC26A9 (solute carrier family 26, member 9) is an epithelial anion transporter that is highly expressed in epithelial cells of the stomach, kidney, pancreas and respiratory tract. SLC26A9 contributes to Cl⁻ secretion and airway surface hydration, and emerging evidence suggests that SLC26A9 is a potential drug target for cystic fibrosis (CF), mucosal obstructive pulmonary diseases, and antacid [1]. In this study, we identified three novel SLC26A9 inhibitors in high-throughput screening (HTS). Then, we conducted structure-activity relationship studies on Class A Group and found A9-301, which is the most potent and selective inhibitor of SLC26A9.

Method/Summary of work: We conducted high-throughput screening (HTS) of 30,000 synthetic small molecules in LN-215 cells expressing SLC26A9 and halide-sensing YFP. LN215 cells expressing YFP-F46L/H148Q/I152L and SLC26A9 were plated at a density of 25,000 cells per well in 96-well microplates. Test compounds were applied to each well at 25 μM and plates were incubated for 10 min at 37°C.

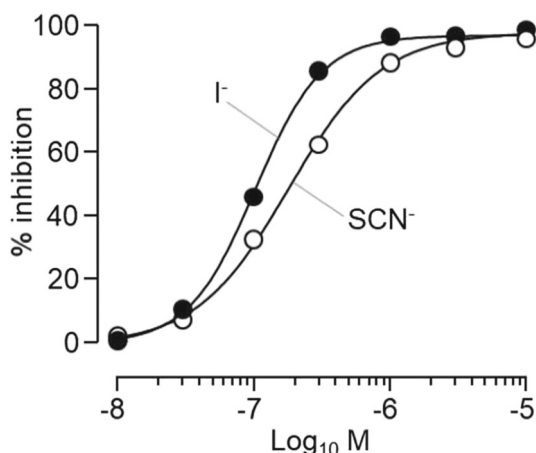


FIGURE 1 S9-A13 dose-response for the inhibition of SLC26A9-mediated Cl⁻/I⁻ and Cl⁻/SCN⁻ exchange activity.

YFP fluorescence was recorded by a microplate reader. The initial slope of YFP fluorescence was used to analyse SLC26A9 mediated I⁻ flux rate. YFP fluorescence quenching assay for assessment of SLC26A4, SLC26A6, SLC26A9, CFTR, ANO1 and VRAC activity were performed accordingly, as described in the previous study [2]. Student's t-tests (for paired or unpaired samples as appropriate) or ANOVA were used for statistical analysis.

Results/Discussion: The most potent inhibitor, A9-301, significantly inhibited SLC26A9 mediated Cl⁻/I⁻ and Cl⁻/SCN⁻ exchange activities with IC₅₀ of 90.9 ± 13.4 nM and 171.5 ± 34.7 nM, respectively (Figure 1). A9-301 did not inhibit other homologous anion exchangers including SLC26A3 (DRA), SLC26A4 (pendrin) or SLC26A6 (PAT-1) and chloride channel CFTR, ANO1 and VRAC (Figure 2).

Conclusion(s): These results revealed that A9-301 is the most potent and selective inhibitor of SLC26A9. Therefore, A9-301 could be used as a useful tool for the pharmacological dissection of SLC26A9 and could be a potential therapeutic candidate for airway inflammatory diseases and disorders that cause too much gastric acid.

REFERENCE(S)

- Bertrand CA, Zhang R, Pilewski JM, Frizzell RA. SLC26A9 is a constitutively active, CFTR-regulated anion conductance in human bronchial epithelia. *The Journal of General Physiology*. 2009;133(4):421-38. <https://doi.org/10.1085/jgp.200810097>
- Park J, Lee HJ, Song D, Gi M, Jo S, Jeon DK, Seo Y, Kim B, Lee H, Namkung W, Han G, Choi JY. Novel pendrin inhibitor attenuates airway hyperresponsiveness and mucin expression in experimental murine asthma. *The Journal of Allergy and Clinical Immunology* 2019; 144(5):1425-1428.e12. <https://doi.org/10.1016/j.jaci.2019.07.016>

OC028 | Genetic evidence for protective effects of angiotensin converting enzyme against Alzheimer's disease but not other neurodegenerative diseases

David Ryan¹; Ville Karhunen²; Bowen Su³; Matthew Traylor⁴; Tom G. Richardson⁵; Stephen Burgess⁶; Ioanna Tzoulaki⁷; Dipender Gill⁸

¹University College London; ²University of Oulu; ³Imperial College London; ⁴Queen Mary University of London; ⁵University of Bristol; ⁶University of Cambridge; ⁷University of Ioannina; ⁸St George's University of London

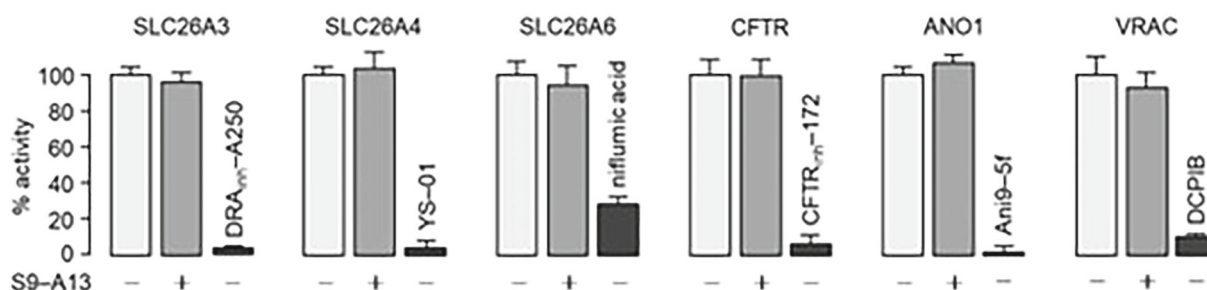


FIGURE 2 Effect of S9-A13 does not inhibit other SLC26 family members or chloride channels. Mean ± SEM (n = 4-5).

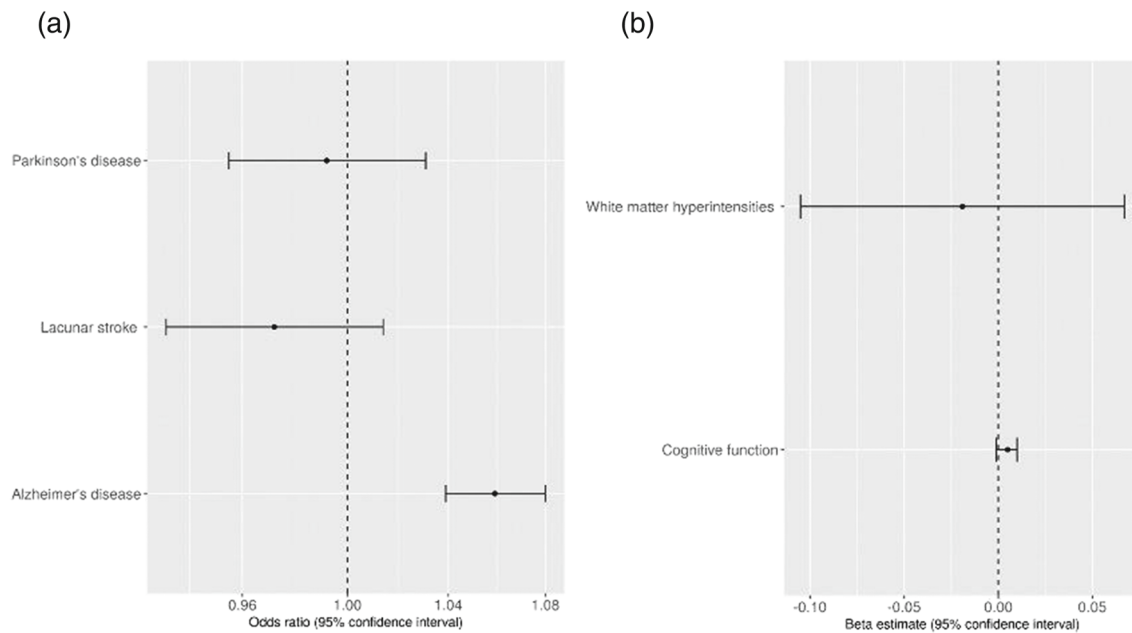


FIGURE 1 Associations between genetically proxied ACE inhibition and neurodegenerative traits. Forest plot showing associations between genetically proxied ACE inhibition (rs4291 effect allele A) with (a) disease outcomes and (b) continuous traits. In graph a, results reported as odds ratio per effect allele with 95% confidence interval. The x-axis is presented on the log10 scale. For graph b, results reported as beta estimate per effect allele with 95% confidence interval

Introduction/Background & aims: Observational studies have shown conflicting direction of association between angiotensin converting enzyme (ACE) inhibitors and risk of Alzheimer's disease (AD). [1] Genetic data can be leveraged using colocalization and Mendelian randomization (MR) techniques to explore associations between exposures and outcomes. These paradigms have advantages over observational methods as the random allocation of genetic variants at meiosis means that MR is less susceptible to reverse causality and confounding.[2] Therefore, in this study we leverage genetic data to assess whether (a) genetically proxied cortical ACE expression was associated with AD risk (b) any association extends to other neurodegenerative traits and (c) if any association was explained by changes in systolic blood pressure (SBP).

Method/Summary of work: Genetic data were obtained from publicly available genome-wide association studies. We conducted colocalization analysis of genetic associations for ACE gene expression in brain cortex tissue and AD liability using the Bayesian Coloc method [3]. This investigates whether cortical ACE expression and AD risk share a common causal variant. The variant with the greatest probability of colocalization represents the effect of cerebral cortex ACE modulation on AD risk. We then employ a MR paradigm to explore whether this variant is associated with other neurodegenerative traits (cognitive function, Parkinson's disease, white matter hyperintensity and lacunar stroke). Finally, two-sample MR was performed to investigate whether genetically proxied SBP or SBP lowering effect of ACE perturbation associates with risk of AD. Instruments to proxy SBP were selected as uncorrelated ($r^2 < 0.0001$) variants that significantly associated with

SBP ($p < 5 \times 10^{-8}$). Odds ratios were derived using inverse-variance weighted pooling of individual genetic variant Wald ratios.

Results/Discussion: Colocalization analysis provided evidence for a shared causal variant for cortical ACE expression on AD risk (posterior probability for colocalization = 0.98, A allele of rs4291 being the most likely candidate). The A allele of rs4291 that is associated with lower cortical ACE expression was negatively associated with SBP—thereby proxying the drug effect of ACE inhibitors. This same variant was positively associated with AD risk (odds ratio 1.06, 95% confidence interval 1.04–1.08 per effect copy) but no other neurodegenerative trait (Figure 1). Genetically predicted SBP was not associated with AD risk (OR 1.01, 95% confidence interval 1.00 to 1.01 per mmHg).

Conclusion(s): Genetic evidence supports a protective effects of cerebral ACE expression on AD, but not other neurodegenerative outcomes. Further work is required to investigate whether therapeutic inhibition of ACE increases risk of AD, particularly ACE inhibitors that more readily permeate the blood–brain barrier.

REFERENCE(S)

1. Quitterer, U., & AbdAlla, S. (2020). Improvements of symptoms of Alzheimer's disease by inhibition of the angiotensin system. *Pharmacological Research*, 154, 104230, <https://doi.org/10.1016/j.phrs.2019.04.014>.
2. Burgess, S., Butterworth, A., Malarstig, A., & Thompson, S. (2012). Use of Mendelian randomization to assess potential benefit of clinical intervention. *BMJ*, 345(nov06 1), e7325, <https://doi.org/10.1136/bmj.e7325>.

3. Giambartolomei, C., Vukcevic, D., Schadt, E., Franke, L., Hingorani, A., Wallace, C., & Plagnol, V. (2014). Bayesian test for colocalisation between pairs of genetic association studies using summary statistics. *PLoS Genetics*, 10(5), e1004383, <https://doi.org/10.1371/journal.pgen.1004383>.

OC029 | Histamine receptor 1: A potential therapeutic target for pancreatic cancer

Elena Tomas Bort¹; Cristina Salmeron Salvador²; Krishna Sriram²; Mehrak Javadi-Paydar²; Jane Smitham²; Richard Grose¹; Peter McCormick¹; Paul Insel²

¹Queen Mary University of London; ²University of California, San Diego

Introduction/Background & aims: Survival rates for pancreatic cancer (PC) are very poor (~11% over 5 years). Thus, new, safe and effective therapies are needed to treat PC patients. Pancreatic ductal adenocarcinoma (PDAC) is the most common and lethal type of PC. Patients taking antihistamines are protected from PDAC and have improved PDAC survival [1,2]. We hypothesised that histamine 1 receptor (HRH1) is protumorigenic and if so, HRH1 antihistamines might be repurposed to treat PDAC.

Method/Summary of work: We used data mining from The Cancer Genome Atlas (TCGA) and the Genotype-Tissue Expression (GTEx) database to define the expression of histamine receptors in PDAC tumours and normal pancreas. Additionally, we used compartmentalisation data from DECODER [3] and the TCGA-PDAC cohort to assess expression of histamine receptors in cell types in PDAC tumours. We validated the bioinformatic transcriptomic data in PDAC cell lines, testing the effect of histamine and HRH1 antihistamines on intracellular calcium (FLIPR-4) and migration (scratch wound) assays. Invasion

was analysed in 3D pancreatic tumour spheroids with fluorescently labelled human PDAC cells and stellate cells.

Results/Discussion: HRH1 had 20-fold higher expression in TCGA-PDAC samples compared with GTEx normal pancreas samples ($p < 0.01$). Cancer cell marker association analysis with cell type deconvolution of TCGA-PDAC tumours revealed that HRH1 was expressed mainly in PDAC cells. Moreover, TCGA-PDAC patients with high HRH1 expression displayed decreased survival (median survival: 16.6 vs. 23.4 months, log rank $p < 0.001$). Histamine treatment increased intracellular calcium in PDAC cells ($EC_{50} \sim 0.3 \mu M$), a response blocked by HRH1 antihistamines. Additionally, histamine increased migration and invasion of PDAC cell lines. 2-PEA (2-pyridylethylamine dihydrochloride), an HRH1-selective agonist, showed similar results to those with histamine. HRH1 antihistamines reduced histamine (Figure 1) and 2-PEA-induced migration and invasion.

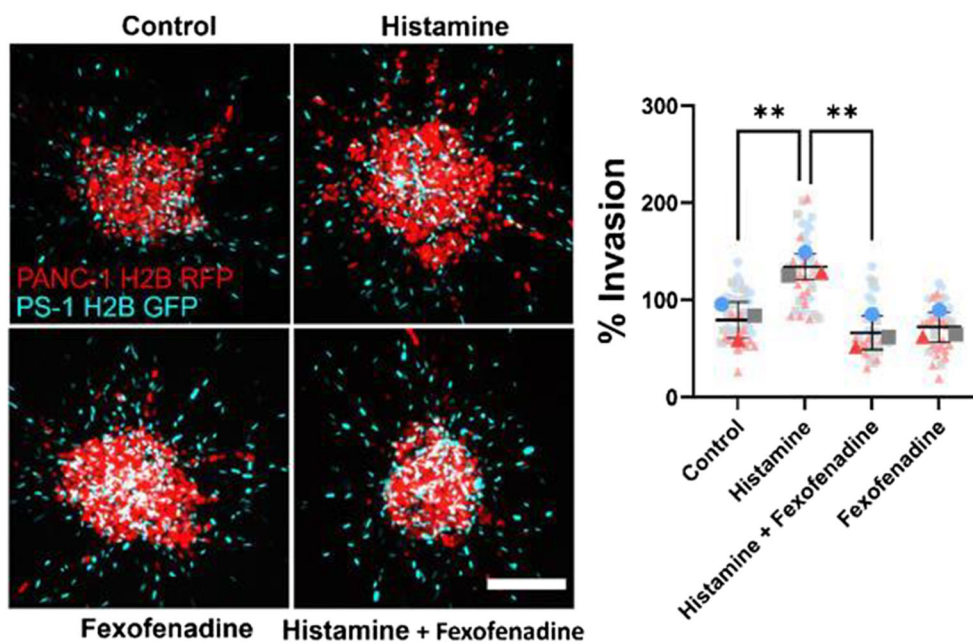
Conclusion(s): HRH1 has increased expression in PDAC tumours and cells and its activation increases calcium, migration and invasion in PDAC cells. Thus, HRH1 antihistamines are promising repurposing drugs for the treatment of pancreatic cancer.

REFERENCE(S)

- Huang, B. Z., Le Marchand, L., Haiman, C. A., et al. (2018). Atopic allergic conditions and pancreatic cancer risk: Results from the multiethnic cohort study. *International Journal of Cancer*, 142(10), 2019–2027. <https://doi.org/10.1002/ijc.31241>
- Fritz, I., Wagner, P., & Olsson, H. (2021). Improved survival in several cancers with use of H1-antihistamines desloratadine and loratadine. *Translational Oncology*, 14(4), 101029. <https://doi.org/10.1016/j.tranon.2021.101029>
- Peng, X. L., Moffitt, R. A., Torphy, R. J., Volmar, K. E., & Yeh, J. J. (2019). De novo compartment deconvolution and weight estimation of tumor samples using DECODER. *Nature Communications*, 10(1), 4729. <https://doi.org/10.1038/s41467-019-12517-7>

3D pancreatic cancer spheroids

FIGURE 1 HRH1 antihistamine reduces histamine-induced 3D PDAC spheroid invasion. Confocal images of 3D pancreatic cancer spheroids of the PDAC cancer cell line PANC-1 (labelled in red) and stellate cell line PS-1 (labelled in blue) embedded in a collagen and Matrigel mix. Spheres were treated with 10- μM histamine and/or 1- μM fexofenadine, an HRH1 inhibitor. Quantification of invasion (right panel) is shown in a SuperPlot, with biological replicates in different colours. Scale bar = 200 μm , one-way ANOVA with Bonferroni correction, $**p < 0.01$.



Oral communications—Education & skills

OC031 | The IUPHAR Pharmacology Education Project: A global site for educators and learners

Clare Guilding¹; Elena Faccenda²; Simon Maxwell²; John Szarek³

¹Newcastle University; ²University of Edinburgh; ³Gesinger Commonwealth School of Medicine

Introduction/Background & aims: The International Union of Basic and Clinical Pharmacology (IUPHAR) Pharmacology Education Project

(PEP; <https://www.pharmacologyeducation.org/>) is an online learning resource, initiated in 2013 with generous funding from ASPET (1). The PEP initiative was undertaken to meet the need for greater access to fundamental pharmacology information by making available free of charge content that describes the basic principles of pharmacology and guides the user to other sites that cover more specialised topics.

Method/Summary of work: PEP contains a range of resources, curated and reviewed by experts, including text, pictorial content, and embedded videos developed by the Editorial Board and contributors (Figure 1), links to other freely available content online, and links to the other IUPHAR initiatives, for example, Guide to Pharmacology, Immunopharmacology, and Malaria Pharmacology.

Results/Discussion: Established in April 2016, PEP now receives approximately 25,000 visits a month, with over 11 million page views

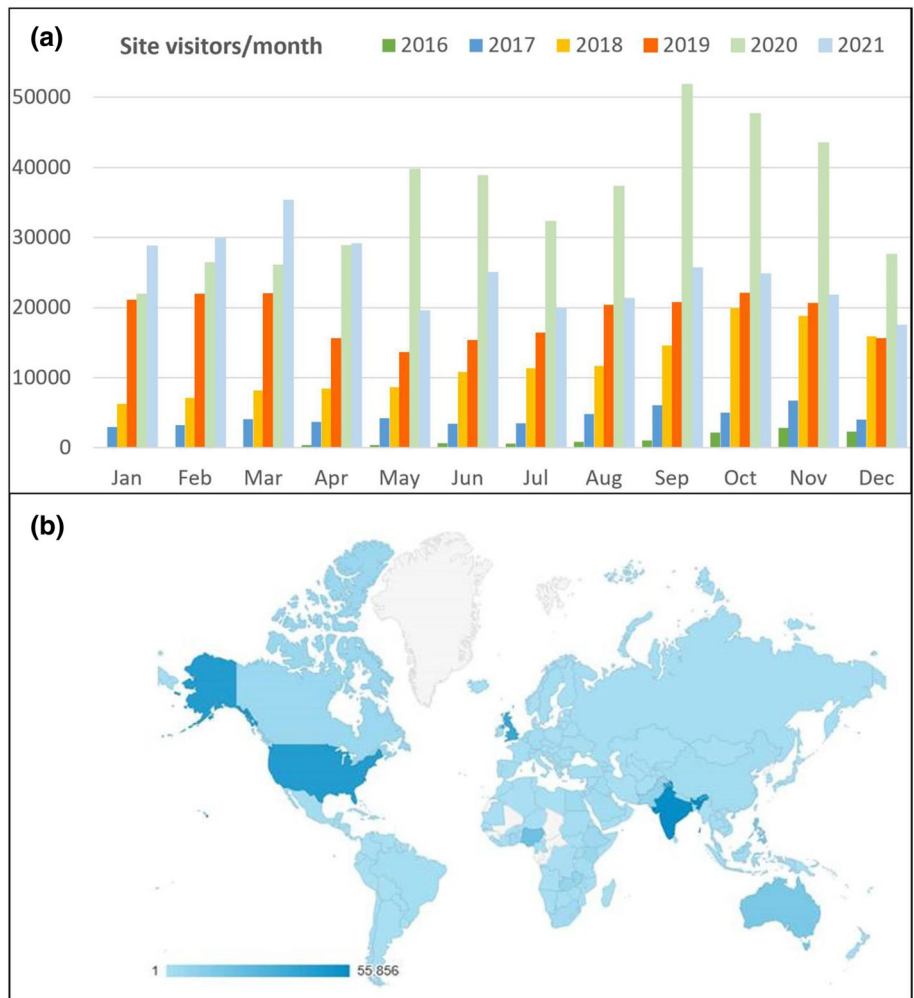
Sections



The screenshot displays the PEP website interface. At the top, a navigation bar includes 'Home', 'About', 'Pharmacology', 'Clinical Pharmacology', 'Drugs', 'Therapeutics', and 'Resources'. Below this, a sidebar on the left lists 'Modules' such as 'Introduction to clinical pharmacology', 'Clinical pharmacodynamics', 'Clinical pharmacokinetics', 'Individual variation in drug response', 'Adherence, compliance and concordance', 'Therapeutic drug monitoring', 'Adverse drug reactions', 'Drug interactions', 'Medication errors', 'Drug development and marketing', 'Clinical trials', 'Drug regulation', 'Medicines management', 'Evidence-based medicine', 'Prescribing', 'Complementary and alternative medicines', and 'Drug misuse'. The main content area is titled 'Clinical pharmacokinetics' and contains text explaining the study of 'what the body does to the drug'. Below the text are six video thumbnails, each with a title, duration, and a play button. The videos are: 'CPT-01-03-01 What is pharmacokinetics?' (07:45), 'CPT-01-03-02 How are drugs absorbed into the body?' (34:23), 'CPT-01-03-03 How are drugs distributed around the body?' (19:14), 'CPT-01-03-04 How are drugs metabolised?' (22:04), 'CPT-01-03-05 How are drugs excreted from the body?' (14:15), and 'CPT-01-03-06 What is the relationship between concentration and time (single dose)?' (16:23). Each video thumbnail also includes the name 'Simon Maxwell' and various interactive icons like a heart, a clock, and a play button.

FIGURE 1 Screenshot from the PEP website. The website is organized around four main sections: Pharmacology, clinical pharmacology, drugs and therapeutics. Under each section are a series of modules. Further resources including a glossary and links to pharmacology societies' curricula are found under 'resources'.

FIGURE 2 Visitors to the Pharmacology Education Project (PEP). (a) Month by month growth from 2016 to 2021, determined using Google's online tracking analytics. (b) Global user distribution from January to December 2021



since inception (Figure 2a). As much of the world moved to online learning during the initial states of the Covid-19 pandemic, usage peaked at over 50,000 sessions/month. PEP is used in most countries across the world (Figure 2b), and the results of an ongoing survey based on 71 responses from 30 countries shows 58%, 68%, and 62% rating the quality, quantity, and usability of the content as excellent.

PEP relies on input from international pharmacology educators, and we welcome contributions to any aspect of PEP that might be of value for learners, including learners developing resources for PEP as part of undergraduate education projects, for example, capstone projects. For more about the inception, management, format and goals of PEP, see our *Clinical Pharmacology and Therapeutics Practice* article (1).

Conclusion(s): PEP is an established resource that is well used, with around 300,000 visits/year in 2021, and over 400,000 in 2020 at the height of online learning. It is used in almost all countries across the world, and survey feedback from educators and learners is that it is an excellent resource. One challenge in creating a large-scale open educational website of this kind is continually engaging educators and students in building and maintaining the site. PEP has the potential to significantly enhance pharmacology knowledge across many disciplines worldwide, but this will only come about, however, with assistance and contributions from the international pharmacology community.

REFERENCE(S)

1. Faccenda, E., Maxwell, S., & Szarek, J. L. (2019). The IUPHAR pharmacology education project. *Clinical Pharmacology and Therapeutics*, 105, 45–48. <https://doi.org/10.1002/cpt.1278>

OC034 | Visibility matters: An inclusive learning and teaching resource for pharmacology/pharmacy. Patience Nimusiima, Jacob Wright, King's College London

Patience Nimusiima; Jacob Wright
King's College London University

Introduction/Background & aims: Lack of inclusive curriculum content and absence of role models were described as contributing factors to minority group attainment gap in HE (1). The aim of the project was to develop an inclusive teaching and learning resource, which not only highlight the achievements of self-identified BAME or LGBTQ researchers in pharmacology/pharmacy but also draw attention to the societal or scientific relevance of their work through student leadership and engagement.

Method/Summary of work: In the pilot work carried out in King's College London, the academics in department of pharmacology and pharmacy were asked to nominate self-identified scientists from BAME or LGBT community whose work inspired their teaching or research. The student researcher shortlisted the names of researchers who satisfied a set of given criteria and provide a brief citation for each researcher highlighting their contribution to pharmacology/pharmacy.

Results/Discussion: This learning and teaching resource is an innovative way of bringing inclusivity to pharmacology education. Using diverse role models and recognising their contribution while teaching pharmacology or pharmacy not only enriches teaching but also creates a sense of belonging (2) and provides a platform for decolonisation of curricula. Although students are likely to choose role models regardless of their ethnic background, it has been found that having role models of a background like their own could be seen as one means of tackling the attainment gap, as it promotes student empowerment (3). This work is an example of student-driven, teacher-supported co-creation of knowledge and underscore the fact that knowledge is created by people from all background, race, ethnicity, orientation, and ability.

The resource was reviewed by a number of pharmacology faculty members at King's College London after it was formulated and the majority welcomed the use of this resource in constructing teaching material.

“I was reading about Dr Surendra Nath Sehgal, I teach second-year Drugs and Disease immunology, and rapamycin is a drug that is important in this area” - Pharmacology Professor

“This sounds like a very credible project that you are working on. The British Pharmacological Society has a hall of fame on their website which showcases individuals, now deceased, who have made significant advances to Pharmacology. While including a few women, this has no BAME representation. Although I hope not, I wonder whether this means there are few known significant contributors from the BAME society.” - Professor/Head of Department of Pharmacology & Therapeutics.

Conclusion(s): In conclusion, with funding, the resource booklet could be made accessible to students. The current goal is that other departments would also use this incentive to incorporate diverse teaching material in their curriculums. The future of pharmacology is very diverse. To reach that point, we hope academia, publications, and awarding bodies continue to celebrate scientists of all backgrounds.

REFERENCE(S)

1. Frumkin, L. A., & Koutsoubou, M. (2013). Exploratory investigation of drivers of attainment in ethnic minority adult learners. *Journal of Further and Higher Education*, 37(2), 147–162. <https://doi.org/10.1080/0309877X.2011.644777>
2. Rattan, A., Savani, K., Komaraju, M., Morrison, M. M., Boggs, C., & Ambady, N. (2018). Meta-lay theories of scientific potential drive underrepresented students' sense of belonging to science, technology, engineering, and mathematics (STEM). *Journal of Personality and Social Psychology*, 115(1), 54–75. <https://doi.org/10.1037/pspi0000130>
3. Claridge, H., Stone, K., & Ussher, M. (2018). The ethnicity attainment gap among medical and biomedical science students: A qualitative study. *BMC Medical Education*, 18(1), 325. <https://doi.org/10.1186/s12909-018-1426-5>